

Palaeoenvironmental and sedimentological context for
dinosaurian assemblages in the Mussentuchit Member,
Cedar Mountain Formation, central Utah (USA)

by

Louis W. Jonk

Thesis presented in fulfilment of the requirements for the degree of Master of Science

(Geology) in the Faculty of Science at Stellenbosch University



UNIVERSITEIT
iYUNIVESITHI
STELLENBOSCH
UNIVERSITY

Department of Earth Sciences

100
1918 · 2018

Supervisor: Dr. Ryan Tucker

Co-supervisor: Dr. Lindsey Zanno

Date: December 2018

Declaration

By submitting this dissertation electronically, I declare that the entirety of the work contained herein is my own, original work, that I am the sole author thereof (except where explicitly otherwise stated), that reproduction and publication thereof by Stellenbosch University will not infringe any third-party rights and that I have not previously in its entirety or in part submitted it for obtaining any qualification.

Date: December 2018

Copyright © 2018 Stellenbosch University

All rights reserved

Abstract

The Cretaceous-aged sediments of the Western North America Interior preserve the geological and biological signatures of notable tectonic events in Earth's history, such as the formation of the Western Interior Basin and Beringian Land Bridge. The Mussentuchit Member of the Cedar Mountain Formation is a fossiliferous sedimentary succession that preserves a key portion of the geological and biological evolution of the North American Western Interior Basin. The geological and temporal context for this unit, however, remains limited. This study, therefore, attempts to place recently opened fossil quarries within the Mussentuchit Member near Cathedral Valley, Utah into a rigorous geological framework via stratigraphic, palaeoenvironmental, and temporal analysis.

This study identified fifteen facies and seven architectural elements, which were combined into six representative facies associations. Further, this study concludes that these sediments were deposited within a fluctuating, distal deltaic, or tidal mudflat. Stratigraphic reconstructions place the Mussentuchit Member near Cathedral Valley, Utah as the uppermost member of the Cedar Mountain Formation, with notable variations in sedimentation patterns between the lower and upper Mussentuchit. The change in sedimentation illustrates the gradation from a supra-tidal zone (lower Mussentuchit), to inter-tidal to sub-tidal zone (upper Mussentuchit) of the tidal delta. Geochronological results from radiometric dating of detrital zircon assemblages indicate that these environments developed in response to multiple tectonic events. Specifically, these include thin-skinned thrusting, subsequent internal breakup, and duplexing of the Pavant Sheet of the Sevier Orogeny. These tectonic events are respectively estimated to have occurred during the Albian (± 110.92 Ma), Cenomanian (± 96.00 Ma) and Turonian (± 93.00 Ma), with actual sedimentation of the member estimated to have occurred from the Cenomanian (± 98.00 Ma) to Turonian (± 93.00 Ma). This change in thrusting mechanisms resulted in the respective deposition of the lower

Mussentuchit and upper Mussentuchit within the late-underfilled stage and filled to overfilled stage of the Sevier Foredeep; the depositional low within the Western Interior basin closest to the orogenic highlands.

Results from this study added geological context to the fossil quarries on the western flank of the San Rafael Swell, near Cathedral Valley, Utah. Sediments from the lower Mussentuchit and quarries preserved there were dated at a maximum age of deposition of ± 105.00 Ma (Albian), though a younger depositional age of ± 98.00 Ma is suspected. The Fortunate Son fossil quarry, positioned within the lower Mussentuchit, was placed within the supra-tidal portion of a tidal delta. Detrital zircons from the Mini Troll and Suicide Hill fossil quarries of the upper Mussentuchit were radiometrically dated at a Cenomanian age of ± 93.95 Ma and ± 93.45 Ma, respectively, and placed within the intertidal to intertidal-subtidal transition zone of a tidal delta. This study provides a more robust understanding of the Mussentuchit sedimentation and enables more meaningful comparisons with regional-scale geological and faunal evolution.

Opsomming

Sedimentêre gesteentes in Innerlike Wes-Noord Amerika van die Kryt-tydperk preserveer die geologiese en biologiese tekens van belangrike tektoniese gebeurtenisse in die Aarde se geskiedenis, soos die formasie van die Westerlike Interne Kom en die Beringian Land Brug. Die Mussentuchit Lid van die Cedarberg Formasie is 'n fossielryke sedimentêre gesteente wat kerngedeeltes van die geologiese en biologiese evolusie van die Noord-Amerikaanse Westerlike Interne Kom preserveer. Tog is die geologiese en temporale konteks vir hierdie eenheid beperk. Hierdie studie poog dus om onlangs ontblote fossielsteengroewe in die Mussentuchit Lid naby Cathedral Valley, Utah in 'n samevattende raamwerk deur middel van stratigrafiese-, paleo-omgewings-, en temporale analise te beskryf.

Hierdie studie het vyftien fasies en sewe argitektoniese elemente identifiseer, wat kombineer was in ses verteenwoordige fasies assosiasies. Verder het die studie getoon dat hierdie sedimente deponer was in 'n wisselende, distale deltaïese of getyvlakte. Stratigrafiese herbouings plaas die Mussentuchit Lid naby Cathedral Valley, Utah, as die heel boonste lid van die Cedarberg Formasie, met opmerklike verskille in sedimentasiepatrone tussen die onderste en boonste Mussentuchit. Die verandering in sedimentasiepatrone illustreer die geleidelike verandering vanaf 'n fluviaal-gedomineerde, supra-gety sone (laer Mussentuchit) tot die gety-gedomineerde inter-gety tot sub-gety sone (hoër Mussentuchit) van die gety delta. Geochronologiese resultate van radiometriese datering van detrale sirkone toon dat hierdie omgewings ontwikkel het in respons tot verskeie tektoniese gebeurtenisse. Hierdie sluit in dunvellige stoting, gevolglike interne opbreek, en tyddeling van die Pavant Plaat van die Sevier Orogenie. Hierdie tektoniese gebeurtenisse word onderskeidelik beraam om plaas te gevind het gedurende die Albian (± 110.92 Ma), Cenomanian (± 96.00 Ma) en Tortonien (± 93.00 Ma), met werklike sedimentasie van die lid beraam om plaas te gevind het

vanaf die Cenomanian (± 98.00 Ma) tot die Tortonien (± 93.00 Ma). Hierdie verandering in stotingsmeganismes het gelei tot die onderskeidelike deposisie van die laer Mussentuchit en die hoër Mussentuchit binne die laat-onderge vulde stadium en gevulde tot oorgevulde stadium van die Sevier Voorland Trog; 'n strukturele element wat 'n deposisionele vermindering verteenwoordig in die Westerlike Interne Kom.

Resultate van hierdie studie het geologiese konteks bygedra tot die fossielgroewe op die westerlike flank van die San Rafael Swell, naby Cathedral Valley, Utah. Sedimente van die laer Mussentuchit en die steengroewe daarin is dateer teen 'n maksimum ouderdom van ± 105.00 Ma (Albian), alhoewel 'n jonger afsettingsouderdom van ± 98.00 Ma vermoed word. Die Fortunate Son-fossielgroef, geleë in die laer Mussentuchit, is in die opper-gety porsie van 'n gety-delta geplaas. Detrale sirkone van die Mini Troll en Suicide Hill fossielgroewe van die hoër Mussentuchit is onderskeidelik radiometries dateer op 'n Cenomaniaanse ouderdom van ± 93.95 Ma en ± 93.45 Ma, en is geplaas in die tussengety tyd tot subgety oorgangssone van 'n gety-delta. Hierdie studie bied 'n meer robuuste begrip van die Mussentuchit-sedimentasieprosesse en stel navorsers in staat om meer betekenisvolle vergelykings te maak met die streeksskaalse geologiese en faunale evolusie.

Acknowledgements

A thesis like this is not possible without the help of many people whose contributions range from everything from supervision, funding, analytical expertise, critiquing, proof reading, and coffee-aided psychotherapy. I will, therefore, most likely neglect to mention some; however, I would like to express my deepest gratitude to each and every person who contributed to this project irrespective of how small those contributions were.

Firstly, I would like to thank Dr Ryan Tucker, who initially brought this project to my attention. His supervision throughout this project and tireless revision of numerous drafts were instrumental both in completing this project and in making me the researcher I am today. Secondly, I would like to thank my co-supervisor, Dr Lindsay Zanno, for giving me the opportunity to join the 2016 field season, for organizing the project's analytical funding and for her helpful reviews on the thesis. Additionally, I would like to send a big thanks to the field crew of the 2016 field season, who made my stay there very memorable. I would also like to thank the staff at the Central Analytical Facilities at Stellenbosch for their expertise and patience in helping with all of the isotopic analysis. Furthermore, I would also like to thank the Department of Earth Sciences of Stellenbosch University for their partial funding of my tuition for this degree.

Many people also contributed to this project in a more personal way. As such, I would like to thank Schalk Walters, Robyn Symons, Zandri Rademan, and Tannie Loxie who listened to numerous of my half-baked theories and coffee-aided rants. I would also especially like to thank Llelani Coetzer, who remained my strongest support throughout both the exciting and difficult portions of this project, without you I would never have completed this project.

Finally, though the majority of them will probably never read this, I would like to acknowledge the researchers referenced in this thesis, as we will never be able to see past the horizon without standing on the shoulders of the giants who came before us.

Contents

Declaration.....	ii
Acknowledgments.....	vii
Contents	viii
List of Figures	x
List of Tables	xii
1. Introduction.....	1
2. Background.....	5
2.1 Tectonics.....	5
2.2 Basin Sedimentation	7
2.3 The Cedar Mountain Formation	10
2.4 Depositional Ages	14
2.5 Mussentuchit Member	15
2.5 Palaeontology	17
3. Methods.....	22
3.1 Sedimentological Analysis	22
3.2 Detrital Zircon Analysis	24
3.3 Youngest Detrital Zircon Age	26
4. Results.....	31

4.1 Facies Analysis	31
4.1.1 Facies Association 1 (FA1): Tidal Mudflats	34
Interpretation	35
4.1.2 Facies Association 2 (FA2): Palaeosols	37
Interpretation	38
4.1.3 Facies Association 3 (FA3): Crevasse Splays	40
Interpretation	41
4.1.4 Facies Association 4 (FA4): Abandoned Channels.....	43
Interpretation	44
4.1.5 Facies Association 5 (FA5): Channel Beds.....	46
Interpretation	47
4.1.6 Facies Association 6 (FA6): Ephemeral Ponds.....	49
Interpretation	50
4.2 Stratigraphy	52
4.2.1 Litho-stratigraphy	53
4.2.2 Facies Stratigraphy	59
4.2.3 Lower, middle and upper Mussentuchit	62
4.2.4 Palaeocurrents	66
4.2.5 Environmental Model.....	69
4.3 $^{206}\text{Pb}/^{238}\text{U}$ Detrital Zircon Analysis	70
4.3.1 Sample Descriptions.....	76
4.3.2 Detrital Zircon Age Population	97
4.3.3 KS Test.....	101
4.3.4 Youngest Maximum Depositional Ages for the Mussentuchit Member...	105

5. Discussion	107
5. Deposition of the Mussentuchit Member	107
6. Conclusion	116
References	119
Appendix: Stratigraphic columns of field transects	143

List of Figures

Figure 1: Map showing location of study area at Mussentuchit Wash	3
Figure 2.1: Diagram showing development of the Western Interior Basin in response to the Nevada and Sevier Orogeny	6
Figure 2.2: Figure showing the stratigraphy at Mussentuchit Wash	12
Figure 3.1: Map showing field transect locations and fossil quarries	24
Figure 4.1.1: Photomosaic showing sedimentological features of FA1	36
Figure 4.1.2: Photomosaic showing sedimentological features of FA2	39
Figure 4.1.3: Photomosaic showing sedimentological features of FA3	42
Figure 4.1.4: Photomosaic showing sedimentological features of FA4	45
Figure 4.1.5: Photomosaic showing sedimentological features of FA5	48
Figure 4.1.6: Photomosaic showing sedimentological features of FA6	51
Figure 4.2.1: Stratigraphic column of the Far Point field transect	55
Figure 4.2.2: Stratigraphic column of the Mini Troll field transect	56
Figure 4.2.3: Cross-section on Z1 to Z2 showing stratigraphic position of the Mussentuchit Member and lithological units therein	57
Figure 4.2.4: Cross-section on X1 to X2 showing stratigraphic position of the Mussentuchit Member and lithological units therein	58

Figure 4.2.5: Cross-section from Z1 to Z2 showing major facies associations within the Mussentuchit Member.....	64
Figure 4.2.6: Cross-section from X1 to X2 showing major facies associations within the Mussentuchit Member.....	65
Figure 4.2.7: Rose diagrams illustrating palaeocurrent directions within the lower and upper Mussentuchit. Photo line sketches highlight palaeocurrent indicators and directions	68
Figure 4.2.8: 3-D block diagram showing the depositional environment of the study area.....	69
Figure 4.3.1: Concordia diagrams of (A) GJ1 primary standard, (B) Plešovice secondary standard and (C) M127 secondary standard.....	70
Figure 4.3.2: Stratigraphic and geographic positions of detrital zircon samples.....	71
Figure 4.3.3 Cathode luminescence images of zircon assemblages.....	73
Figure 4.3.4a: Probability density plots of samples between 80 Ma and 2500 Ma with exploded views of youngest peaks	74
Figure 4.3.4b: Probability density plots of samples between 80 Ma and 2500 Ma with exploded views of youngest peaks	75
Figure 4.3.5: Pie diagram showing portions of grains in successive age populations per sample..	96
Figure 4.3.6: Evolution of North America with specific focus on the western margin.....	100
Figure 4.3.7: Cumulative probability plots for all sample zircon populations	98
Figure 4.3.8: Cumulative probability plots for only the youngest fractions of each sample.....	102
Figure 4.3.9: Graphical representation of youngest ages along with averaged youngest age.....	106
Figure 5.1: Diagram illustrating the development of the coastal embayment at the study area in response to various filled stages of the Western Interior Basin.....	115

List of Tables

Table 2.1: Historical nomenclature of the Cedar Mountain Formation	21
Table 3.1: LA-ICP-MS Specifications list, Central Analytical Facility, Stellenbosch University ..	29
Table 4.1.1: Bounding surfaces identified within Mussentuchit Member.....	31
Table 4.1.2: Facies codes identified within the Mussentuchit Member at Mussentuchit Wash ..	32
Table 4.1.3: Identified architectural elements and associated morphologies from the Mussentuchit Member.....	32
Table 4.1.4: Facies Association identified within the Mussentuchit Member of Mussentuchit Wash	33
Table 4.3.1: Pb/U data for sample 9B. $^{206}\text{Pb}/^{238}\text{U}$ ration used for age calculations	77
Table 4.3.2: Pb/U data for sample Suicide Hill. $^{206}\text{Pb}/^{238}\text{U}$ ration used for age calculations	79
Table 4.3.3: Pb/U data for sample Mini Troll. $^{206}\text{Pb}/^{238}\text{U}$ ration used for age calculations.....	72
Table 4.3.4: Pb/U data for sample Monollo-09-15. $^{206}\text{Pb}/^{238}\text{U}$ ration used for age calculations .	85
Table 4.3.5: Pb/U data for sample SCH-01-15. $^{206}\text{Pb}/^{238}\text{U}$ ration used for age calculations.....	88
Table 4.3.6: Pb/U data for sample ST-10-15. $^{206}\text{Pb}/^{238}\text{U}$ ration used for age calculations	90
Table 4.3.7: Pb/U data for sample SLF-08-15. $^{206}\text{Pb}/^{238}\text{U}$ ration used for age calculations.....	93
Table 4.3.8: Summary of youngest age matrices for the seven samples	95
Table 4.3.9: (A) Probability values of all samples following Kolmogorov-Smirnov test.....	102
(B) Shows table constructed from youngest age peaks	102
Table 4.3.10: Genetic probability values of samples following K-S test in age domains 2 and 3 showing high probability of genetic relationship	104

1. Introduction

Sediments from the Mesozoic Era record many of the earth's faunal evolutionary trends and migrations. This is especially true in western North America, where Mesozoic sediments preserve many of the faunal dispersion patterns occurring due to several tectonic reorganizations which characterize this timeframe (Kirkland & Madsen, 2007; Blakey & Ranney, 2017). These reorganizations include: (1) the separation of North America into Laurasia and Appalachia, (2) the flooding of Europe and Canada, (3) the formation of the Beringian Land Bridge, and (4) the formation of the Western Interior Foreland Basin (Kauffman & Caldwell, 1993; Cifelli *et al.*, 1997; Kirkland *et al.*, 1997; Kirkland, 2005; Dickenson, 2005; DeCelles & Coogan, 2006). Contextualizing the environmental, temporal, and geological frameworks for these events is crucial for our understanding of the local and global faunal evolution throughout the Mesozoic. The Jurassic to Cretaceous-aged sediments of western North America preserve world-class dinosaurian fossils such as *Triceratops*, *Tyrannosaurus*, and other species linked with the supposed Cretaceous Terrestrial Revolution (KTR) (Currie, 1998; Lockley & Matsukawa, 1999; Kirkland *et al.*, 2005; Kirkland & Madsen, 2007; Lloyd *et al.*, 2008; Kirkland *et al.*, 2017). Unfortunately, the limited preservation of these sediments has resulted in incomplete contextualization for this timeframe. The Cretaceous Cedar Mountain Formation is, however, one of the few sedimentary successions that preserve many of the tectonic and biological signatures associated with the Early Cretaceous portion of the KTR (Kirkland *et al.*, 2017).

Originally, Stokes (1944) described the Cedar Mountain Formation as drab, variegated mudstones notably void of faunal remains. However, this observation has been shown to be erroneous, as numerous fossil excavation programs since the early 1990's have yielded a wealth of Early to Late Cretaceous dinosaur specimens (e.g., Kirkland, 1997; Garrison *et al.*, 2007). Examples of these include specimens of the Neoceratopsia clade, the

Hadrosauromorph *Eolambia Caroljonesa*, and the Dromaeosaurid *Utahraptor Ostrommaysorum* (Kirkland *et al.*, 1993, 1999; Carpenter & Cifelli, 2016). Dr. Lindsay Zanno (Department of Biological Sciences at North Carolina State University and curator of Palaeontology at North Carolina Museum of Natural Sciences), in collaboration with Dr. Peter Makovicky (Associate Curator and Department Chair, Department of Geology at the Chicago Field Museum), have revealed an even greater diversity of fauna preserved within the Mussentuchit Member of the Cedar Mountain Formation. This is evident through their recent discoveries in the western flank of the San Rafael Swell, central Utah, which include the therizinosauroid *Falcarius utahensis* and the theropod *Siats meekerorum*, (Zanno, 2006; Zanno & Makovicky, 2013).

Localized and sporadic stratigraphy, geochronology, and taphonomy have, however, resulted in much dissension regarding the Mussentuchit Member's geological framework. This includes broad palaeoenvironmental interpretations associated with inconsistent temporal contexts. These discrepancies have led to uncertainties regarding the member's stratigraphic position in the Cedar Mountain Formation, suggesting a more complex deposition than previously thought (Sorenson, 2011; Holmes, 2017; Kirkland, 2017). Accordingly, much of the environmental, ecological, and temporal context of the Mussentuchit fossil assemblage remains unresolved.

The main objective for this project is to add relevant and useful context to a particular depo-centre by placing the sedimentary succession at Mussentuchit Wash, Central Utah within palaeoenvironmental, stratigraphic, and temporal frameworks (Fig 1). Located on the western flank of the San Rafael Swell, the focal area for this project lies 25 km due south of the town of Emery at 38°41'30.97" North and 111°15'00.58" West, at an altitude of approximately 1800 meters a.m.s.l. (Figure 1). The study area comprises approximately 25

km² with the outcrop representing stratigraphic units from the Morrison, Cedar Mountain, and Dakota Formations.

The study objective was achieved by addressing four main aims. The primary aim of this study focused on reconstructing a highly resolved, palaeoenvironmental model of the Mussentuchit Member at the field site, through the aid of a detailed sedimentological- and facies-based analysis of the Mussentuchit sediments. Secondly, this study focused on placing the sediments at the field site into a rigorous stratigraphic framework via detailed contextualization of the outcrop stratigraphy. Thirdly, a major facet of this project included erecting a temporal framework for fossil assemblages from specific Mussentuchit Wash sites via radiometric dating of detrital zircon crystals. Finally, this project utilized these isotope data sets to construct linkages to regional tectonic events, thereby constraining likely near-syn depositional environments.

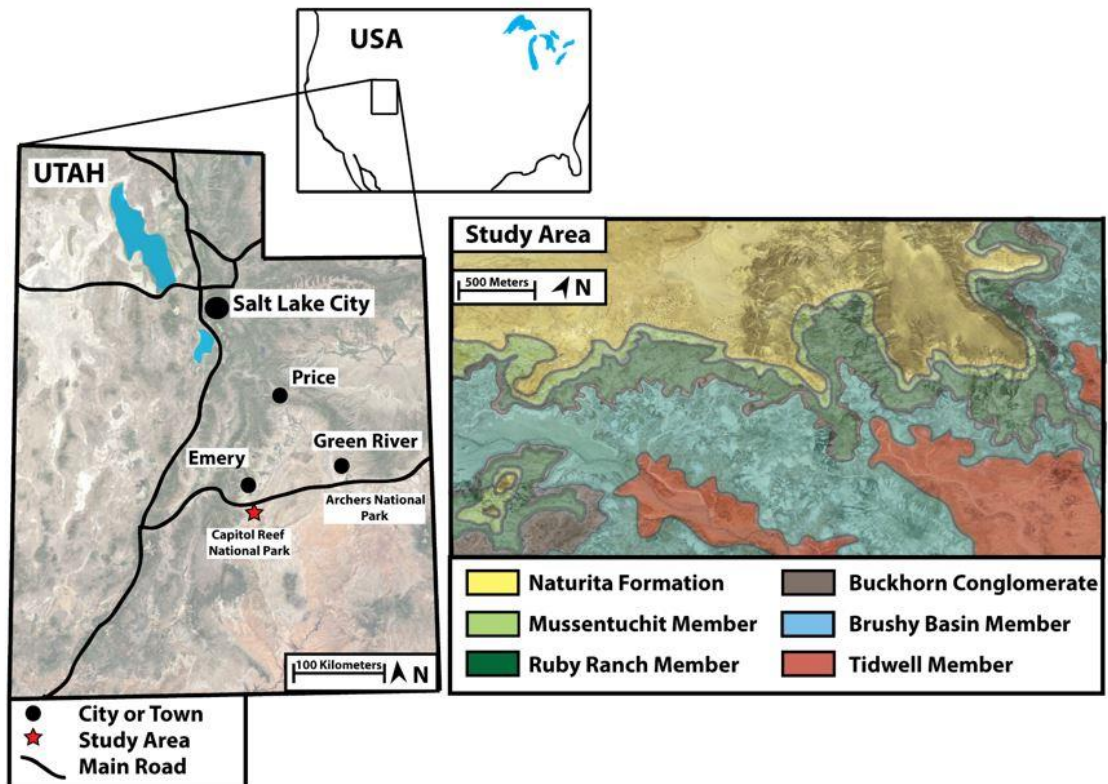


Figure 1: Map showing location of study area at Mussentuchit Wash, Cathedral Valley, denoted by red star. Backdrop modified from Google Earth ESRI Satellite Image

By placing key fossil sites at Mussentuchit Wash within temporal, stratigraphic, and detailed palaeoenvironmental frameworks, this study adds currently undescribed context to newly emerging assemblages of palaeofaunal remains found throughout the Mussentuchit. Additionally, information gained from this study will be invaluable for resolving much of the current inconsistencies regarding the Mussentuchit Member's depositional environment and stratigraphic context. By utilizing a combination of isotopic signatures and detailed sedimentological description, this study adds some much-needed resolution to the intricate drainage geometries within the complex depositional patterns of the Western Interior Basin (Kirkland, 2005; Miall, 2008; Suarez *et al.*, 2013). Ultimately, this study expanded on our understanding of the ecological and geological signatures characterizing the evolution of one of the most iconic times in evolutionary history.

2. Background

2.1 Tectonics

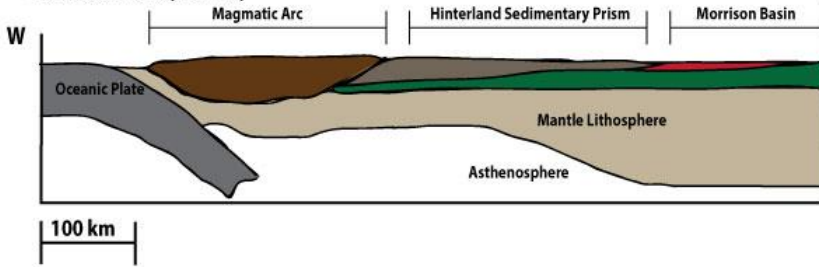
The North American Western Interior represents one of the world's most well-documented foreland basins, recording much of North America's western tectonic history. With initial thrusting starting between the Late Devonian and Early Triassic time, the Cordilleran Fold Belt records numerous orogenic events, such as the Late Devonian Antler Orogeny, the Permian/Triassic Sonoma Orogeny, the Jurassic Nevadan Orogeny, and the Cretaceous Sevier and Laramide orogenies (Dickenson, 2004). The later portion of the Cordilleran Fold Belt's orogenic history is exceptionally well preserved within the Late Jurassic Morrison Formation and Early Cretaceous Cedar Mountain Formation (DeCelles & Currie, 1996; DeCelles, 2004; Horton *et al.*, 2004; Miall *et al.*, 2008). These Jurassic and Cretaceous aged sediments reflect the formation of two retroarc Cordilleran Foreland Basin systems, associated with eastward subduction of the Farallon Plate during the final stages of the Cordilleran Fold Belt's construction (Currie, 2002; DeCelles, 2004; Miall *et al.*, 2008).

During the Late Jurassic, accretion of the Wrangellia and Angayuchan Terrains on the North American western margin led to the formation of the Nevadan Orogeny and the associated Jurassic Western Interior Foreland Basin, represented by the Morrison Formation (Brenner, 1983; Saleeby & Busby-Spera, 1992; Leckie & Smith, 1992; Stott, 1993; Bjerrum & Dorsey, 1995). This was followed by the Jurassic (?)/ Early Cretaceous thin-skinned thrusting of the Sevier Thrust Belt, resulting in the Sevier Foreland Basin, with a portion of the basin stratigraphically represented by the Cretaceous Cedar Mountain Formation (Fig. 2.1) (Armstrong, 1968; Cowan & Bruhn, 1992; Leckie & Smith, 1992; Pang & Nummedal, 1995).

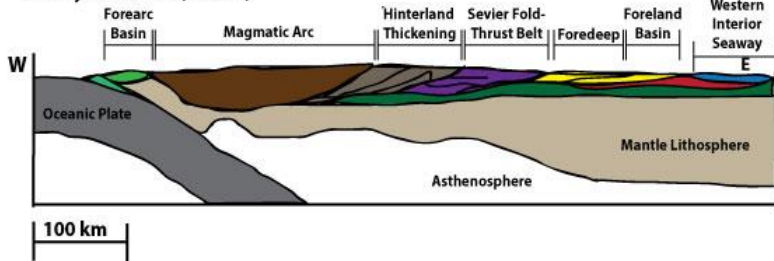
Tectonic Evolution of the Great Basin from L. Jurassic to L. Cretaceous

Cross sections on A1-A2

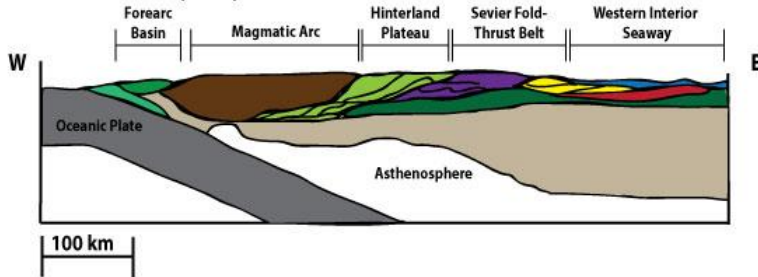
A: Late Jurassic (150 Ma)



B: Early Cretaceous (100 Ma)



C: Late Cretaceous (80 Ma)



Legend

- Western Interior Seaway
- Nevada Orogeny
- Sevier Orogeny
- Sevier Foreland Basin
- Morrison Basin

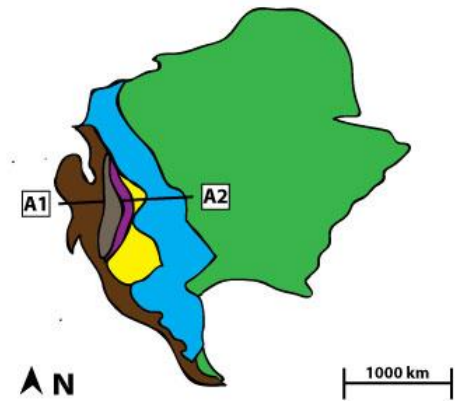
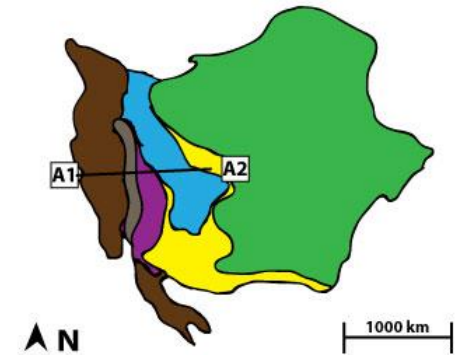
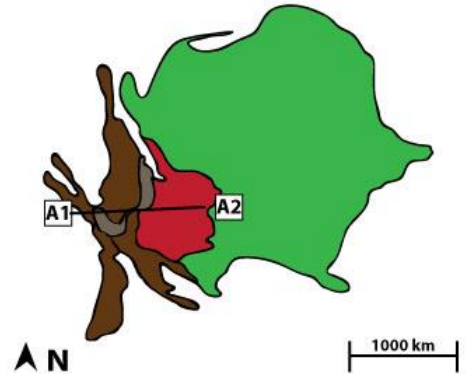


Figure 2.1: Diagram showing development of the Western Interior Basin in response to the Nevada and Sevier Orogeny. Modified after Yonkee and Weil (2015).

The Sevier Orogeny is a long-lived orogenic event; consisting of multiple, separate episodes of orogenic thrusting, leading up to, and forming part of the Laramide Orogeny (Dickenson, 2005; DeCelles & Coogan, 2006). These include the Canyon Range, Pavant, Paxton, and Grunning Thrust systems, of which the Canyon Range and Pavant thrust events are of special relevance to this project (Dickenson, 2005; DeCelles & Coogan, 2006). Consisting of multiple small-scale thrusting and duplexing events, the Canyon Range and Pavant orogenic events represent the main sediment provenance for the Cedar Mountain Formation. The Laramidian activity that followed resulted in extensive deformation of the Sevier Foreland Basin, forming numerous sub-basins including the Paradox Basin and the San Rafael Swell.

2.2 Basin Sedimentation

The ensuing depositional low of the Sevier Foreland Basin encompasses twelve (12) American states, including Arizona and New Mexico in the south and extending northwards into Montana, North Dakota, and Canadian Saskatchewan. Laterally, the basin extends from Utah and Idaho eastward into North and South Dakota, Nebraska, and Kansas (Turner & Peterson, 2004). Flexural subsidence is thought insufficient to accommodate the large geographic extent of these Jurassic and Cretaceous sediments. Researchers have therefore attributed the large accommodation space to associated dynamic subsidence (Lawton, 1994; Currie, 1998; DeCelles, 2004). Straddling the transition of the Morrison and Cedar Mountain formations is the basinwide K-1 unconformity, which constitutes an approximate 20 Ma gap in sedimentation (McGookey *et al.*, 1972; Pippingos & O'Sullivan, 1978; Imlay, 1980). Roca and Nadon (2007) suggested this unconformity might be associated with the change of deposition within a flexural forebulge/backbulge (Upper Jurassic Morrison Formation) to

deposition within a foredeep depozone (Lower Cretaceous Cedar Mountain Formation), (DeCelles & Currie, 1998; DeCelles, 2004; Roca & Nadon, 2007; Miall *et al.*, 2008). The K-1 unconformity marks this transition, which formed in response to renewed flexural subsidence and eastward migration of the flexural forebulge, accompanying the onset and duration of the Sevier Orogeny during Aptian to Maastrichtian time (Heller *et al.*, 1986; Yingling, 1987; Yingling & Heller, 1992; DeCelles *et al.*, 1995; Currie 1998, 2002). This resulted in much of the underlying rock-strata being deformed and incorporated in the Cordilleran Fold Belt. Accordingly, this fold belt is comprised of sediments from the Cordilleran miogeocline, deformed and added on by multiple tectonic events such as the Sonoma Orogeny, Antler Orogeny, Nevadan Orogeny, and Sevier Orogeny (Schweickert *et al.*, 1984; Albino, 1992; Prave, 1999; DeCelles, 2004; Dickenson, 2006; Blakey & Ranney, 2017). Rocca and Nadon (2007) characterized the deposition of the underlying Jurassic Morrison Formation within a predominantly terrestrial fluvial system forming within the Nevadan Foreland Basin. Moreover, Stokes (1952) and later Craig (1981), characterized the overlying Cretaceous Cedar Mountain Formation as depositing as a broad alluvial plain within the foredeep depozone of the Sevier Foreland Basin. Following these initial interpretations, Lawton *et al.* (1994, 2003) defined major southward and eastward flowing river systems depositing the Burro Canyon and Cedar Mountain formations respectively. He suggested that the sediments deposited within rapidly aggregating deltaic environments, corroborating Stokes' (1952) initial observations. Suarez *et al.* (2012) further expanded on these findings by identifying multiple, Cenomanian-timed northeast flowing river systems from the Sevier Mountains feeding into the developing Western Interior Seaway. The Cedar Mountain Formation also shows a notable marine influence, as this member deposited in response to the Kiowa-Skull Creek and Greenhorn transgressions, which occurred during the Mid to Late Cretaceous (Suarez *et al.*, 2012, 2013). Both the Kiowa-Skull Creek and

Greenhorn Transgressions have been linked to the elevated sea levels of the Zuni sequence, which occurred in response to the proposed Mid-Cretaceous Cratonic Superplume Event (Larson, 1991; 1995). During this event, sea levels showed an overall steady increase from approximately 170.0 m above modern sea levels to 250.0 m above modern sea levels (Haq *et al.*, 1987). Notably, the global sea level curve shows numerous smaller scale sea level fluctuations between 195.0 and 250.0 m above modern sea levels occurring throughout much of the Cretaceous (Haq *et al.*, 1987; Arthur & Sageman, 2004). These fluctuations have been interpreted as multiple small-scale regressions and depositional hiatuses occurring between and during the Kiowa-Skull Creek and Greenhorn Transgressions (Oboh-Ikuenobe *et al.*, 2008). As the rapid sea level rise outpaced the sediment input from the Sevier Orogeny, sediment was deposited in an overall retrogradational sequence stacking pattern (Arthur & Sageman, 2004).

A series of coarse-grained fluvial deposits of the Buckhorn Conglomerate, which stretch from southern Utah to western Alberta, define the K-1 transition from forebulge to foredeep deposition (Heller & Paola, 1989). Similar stratigraphic position and depositional environments have led researchers to believe a contemporaneous nature of these deposits, even though the geochronological and biostratigraphical information is limited (Stokes, 1944; Armstrong, 1968; Heller & Paola, 1989; Heller *et al.*, 2003). Due to the rough age bracket of these deposits, some controversy remains as to whether the Buckhorn Conglomerate constitutes the basal member of the Cedar Mountain Formation or the upper unit of the Morrison Formation (Rocca & Nadon, 2007). For consistency, all references to the Buckhorn Conglomerate herein assumes it as the basal member of the Cedar Mountain Formation as suggested by Kirkland *et al.* (1997).

2.3 The Cedar Mountain Formation

The Cedar Mountain Formation occurs throughout the central and western portions of Utah, with outcrops exposed along the Green River, Uinta Basin, Henry's Basin, and the San Rafael Swell. The sediments of the Cedar Mountain Formation have been stratigraphically correlated to the Burro Canyon Formation in Colorado, the Cloverly Formation in Wyoming, and the Willow Tank Formation in Nevada (Stokes, 1952; Noreiga, 1996; Kirkland *et al.*, 1999; Bonde *et al.*, 2008; Miller, 2016). The stratigraphy of the Cedar Mountain Formation is highly variable due to the complex depositional patterns associated with multiple depocentres (Fig. 2.2) (Kirkland *et al.*, 1999; Kirkland, 2005; Garrison *et al.*, 2007). As such, the complete Cedar Mountain stratigraphy is limited to only local occurrences, such as the type section at the San Rafael Swell (Kirkland *et al.*, 1997). Only three of the members of the Cedar Mountain Formation, therefore, are present at the study area at the western flank of the San Rafael Swell (Kirkland *et al.*, 2017). Most recent regional-scale revisions by Kirkland *et al.* (2017, and references therein) have subdivided the Cedar Mountain Formation into six members, described herein.

The lower three members of the Cedar Mountain Formation are represented by the Buckhorn Conglomerate, Yellow Cat, and Poison Strip Sandstone members. The basal Buckhorn Conglomerate unconformably overlies the Brushy Basin Member of the Morrison Formation and occurs within central Utah, ranging from 4.0 to 11.0 m in thickness (Kirkland *et al.*, 1997; Currie, 1998). The Buckhorn Conglomerate consists predominantly of a pebble- to cobble-sized ortho-conglomerate, with cherty clasts up to 20 cm in diameter. (Kirkland *et al.*, 1997). The Yellow Cat Member conformably overlies the Brushy Basin Member of the Morrison Formation and the Buckhorn Conglomerate where locally developed. The member

reaches a thickness of 24.0 meters at the type section found near the Gaston Quarry, west of the Yellow Cat Road, and consists of variegated mudstones, limestones, and palaeosols with sporadic to localized sandstone lenses (Kirkland *et al.*, 1997, 1999). The basal contact is commonly defined as a locally variable calcrete layer, while the contact between the Yellow Cat and the overlying Poison Strip Sandstone is interpreted as locally conformable (Aubrey, 1998; Kirkland *et al.*, 1999). The Yellow Cat is interpreted to represent an alluvial floodplain within a semi-arid monsoonal climate (Kirkland *et al.*, 1997). The Yellow Cat Member is overlain by the Poison Strip Sandstone Member, which occurs as a complex of several well-cemented sandstone layers (Kirkland *et al.*, 1999; Kirkland, 2005). The sandstone is composed of normally graded, fine- to medium-grained sand supporting black, grey, and white chert pebbles. Trough cross-bedding is prevalent throughout the sandstone with specific localities exhibiting large-scale epsilon cross-bedding. Kirkland *et al.* (1997) suggested the Poison Strip Sandstone represents a river system tracing from the San Rafael Swell across into Wyoming.

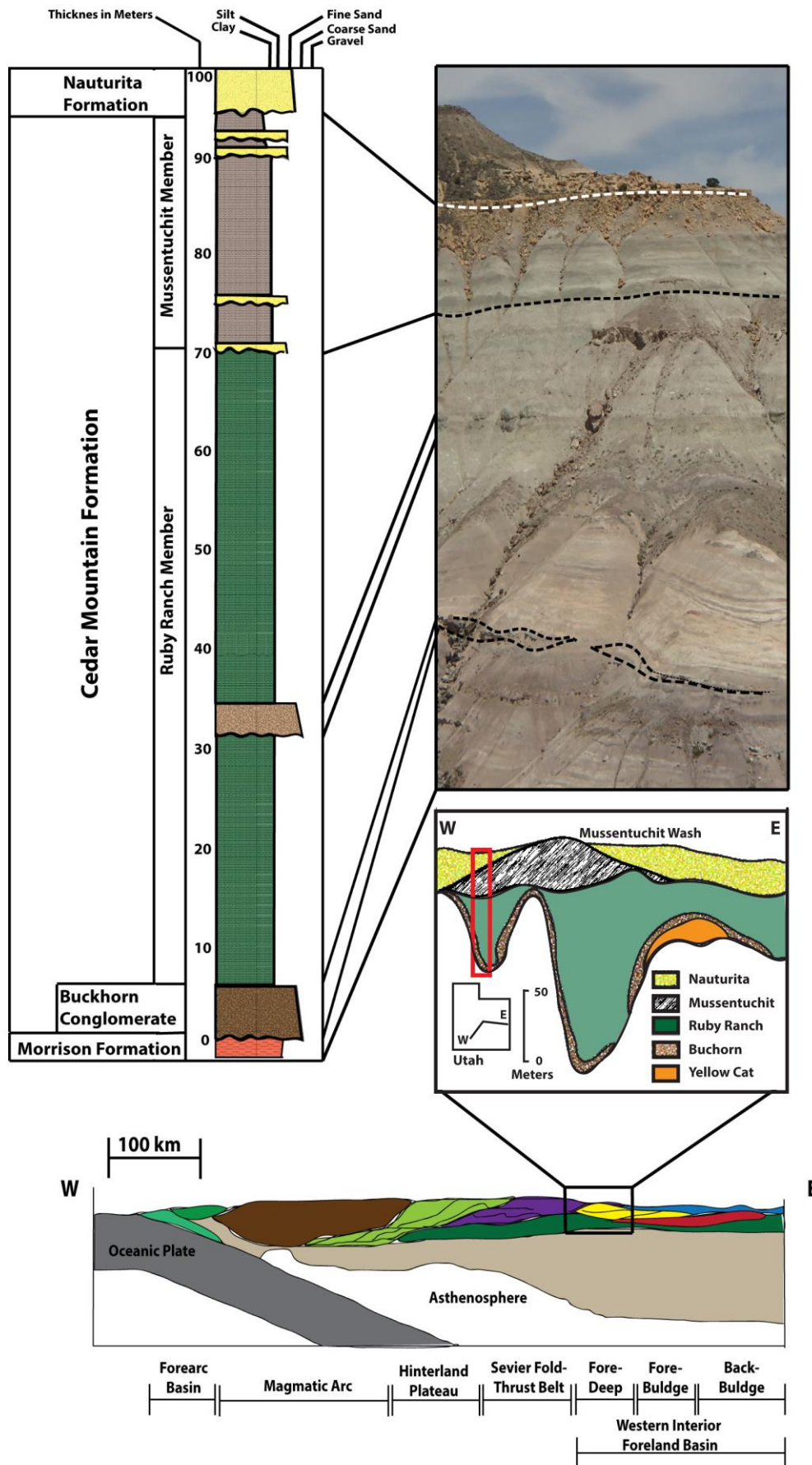


Figure 2.2: Figure showing the stratigraphy at Mussentuchit Wash, Cathedral Valley, Utah, modified after Yonkee and Weil (2015) and Kirkland *et al.* (2017). Photograph by Tucker (2016).

The upper three members of the Cedar Mountain Formation are represented by the Ruby Ranch, Short Canyon, and Mussentuchit members. The Ruby Ranch Member conformably overlies the Poison Strip Sandstone and outcrops from the Utah-Colorado border in the east to the west side of the San Rafael Swell with a maximum thickness of 33.1 meters. (Stokes, 1952; Young, 1960; Kirkland *et al.*, 1999). The member is composed of variegated mudstones with subordinate fine- to medium-grained sandstone layers locally preserving thalwegs and cross-bedding (Kirkland *et al.*, 1997, 1999; Garrison *et al.*, 2007). The most distinctive characteristic of the Ruby Ranch sediments is the abundance of carbonate nodules occurring throughout the member. This abundance of calcareous nodules indicates deposition within an alluvial floodplain within a semi-arid monsoonal setting (Kirkland *et al.*, 1997, 1999; Ludvigson *et al.*, 2002, 2006; Garrison *et al.*, 2007). The Short Canyon Member is a discontinuous series of conglomerate beds, with local occurrences unconformably overlying the Ruby Ranch Member. Though first identified by Kirkland and Madsen (2007), the Short Canyon Member was designated as an informal member of the Cedar Mountain Formation by Doelling and Kuehne (2013). The member ranges in thickness between 12.0 to 32.0 meters and shows the presence of distinctive quartzite clasts, distinguishing it from the Buckhorn Conglomerate Member. The Mussentuchit Member represents the uppermost member of the Cedar Mountain Formation and occurs locally throughout the Formation (Kirkland *et al.*, 1997; Kirkland *et al.*, 1999; Kirkland, 2005). The type section, located south of Mussentuchit Wash, shows a thickness of approximately 25.0 meters with a basal gradational contact characterized by either thin, discontinuous sandstones or the characteristic lack of carbonate nodules (Kirkland *et al.*, 1997). The Mussentuchit is primarily composed of interbedded mudstones (smectitic) and siltstones with minor occurrences of lenticular sandstones and localized development of a lignite horizon at the type section. The upper contact is defined as an erosive 6th order contact with the overlying,

thick Naturita Sandstone of the Dakota Formation, as per contact definitions by Vail (1977). The environmental interpretation for the Mussentuchit Member is that of a poorly drained floodplain to a floodplain-lacustrine setting with associated perennial lakes and vegetation (Currie, 1998; Garrison, 2007; Kirkland et al., 2017).

2.4 Depositional Ages

The age of the Morrison Formation has been placed as Late Jurassic through utilization of geochronological ages from bentonites (Kowallis *et al.*, 1991; Kowallis *et al.*, 1998; Trujillo *et al.*, 2006; Trujillo *et al.*, 2016), charophytes (Schudack *et al.*, 1998), palynomorphs (Litwin *et al.*, 1998), and magneto-stratigraphy (Steiner *et al.*, 1994; Steiner, 1998). Currently, the youngest ages of the Morrison Formation come from Hunt *et al.* (2011) and Trujillo *et al.* (2016) who used $^{206}\text{Pb}/^{238}\text{U}$ and $^{40}\text{Ar}/^{39}\text{Ar}$ ratios to define ages of 148.96 ± 2.54 Ma and 150 ± 0.52 Ma, respectively. Deposition of the overlying Cedar Mountain Formation is thought to have occurred from the Late Hauterivian (?)/ earliest Barremian to the Albian and Cenomanian boundary, from evidence of palynomorphs (Tschudy *et al.*, 1984), charophytes (Aubrey, 1998), dinosaur fauna (Kirkland, 1992), and bentonite dates (Cifelli *et al.*, 1997). The oldest age of sedimentation for the Cedar Mountain Formation comes from Hendrix *et al.* (2015), who used palaeosols collected from the Yellow Cat Member to define a $^{206}\text{Pb}/^{238}\text{U}$ youngest maximum age of deposition of 139.7 ± 2.2 Ma. Conversely, the youngest age of the Cedar Mountain Formation was reported as 98.37 ± 0.07 Ma, derived from radiometric dating of bentonitic tuff layers of the Mussentuchit Member (Cifelli & Muizon, 1997). These findings have subsequently been corroborated by multiple authors, including Cifelli *et al.* (1999) and Garrison *et al.* (2007), with ages of 96.7 ± 0.5 to 98.2 ± 0.6 Ma. Accordingly, these ages have been described as signifying the end of the Cedar Mountain sedimentation.

2.5 Mussentuchit Member

The Mussentuchit was first described by Stokes (1944) in the Cedar Mountain Shale as a green floodplain deposit with associated preserved channels. Stokes later revised this to the Cedar Mountain Formation in 1952 and included the Buckhorn Conglomerate as the basal member, Table 2.1. Initially, Stokes (1952) differentiated the Cedar Mountain Shale from the underlying Morrison and overlying Naturita Formations by its drably variegated colour, the presence of gastroliths (rounded chert pebbles) and an abundance of carbonate nodules (Stokes 1944, 1952). Possibly the most important distinguishing feature noted by Stokes was the apparent distinct absence of fossil elements, which led to a definite lack of interest in the Cedar Mountain Formation for the second half of the twentieth century (Stokes, 1944, 1952; Kirkland, 2005, 2007).

Later descriptive work was done by Young (1960), who correlated the Cedar Mountain, Burro and overlying Naturita formations into one laterally extensive formation within the Dakota group, Table 2.1. This assumption was however contested, (Graig *et al.*, 1961; Young, 1965; Craig, 1981) with later revisions resulting in the removal of the Cedar Mountain Formation from the Dakota Group. Young's definition of the overlying sandstones as the Naturita Formation has, however, gained popularity in more recent studies, as this interpretation limits confusion to the Nebraskan Dakota Formation (Carpenter *et al.*, 2008; Milán *et al.*, 2015; Cifelli *et al.*, 2016). Young's correlation between the southeastern Burro Canyon and northwestern Cedar Mountain Formations would later be corroborated by Craig (1981), lending value to Young's prototypical depositional model. This was further developed by Currie (1998, 2002), who characterized the Cedar Mountain Formation as depositing within a back-arc foreland basin setting with associated dynamic subsidence.

The Mussentuchit Member was first described by Kirkland (1997), along with the Yellow Cat, Poison Strip and Ruby Ranch members using diagnostic fossil assemblages, Table 2.1. The Mussentuchit has been defined as being a distinctively smectitic mudstone unit with a diagnostic absence of carbonate nodules and localized development of lignite beds and fine-grained sandy lenses (Kirkland *et al.*, 1997, 1999). An Early Cenomanian age of 98.37 ± 0.07 Ma was derived from radiometric dating of preserved volcanic ash beds and correlates well with the siliceous marine Mowry Shale north of the Cedar Mountain Formation (Obradovich, 1993; Gradstein *et al.*, 2004). Originally thought to be devoid of fossils, reported discoveries of preserved dinosaurian taxa during the early 1990's led to a massive amount of institutions attempting to describe the emerging wealth of fossil elements within the Mussentuchit Member (Kirkland *et al.*, 1997, 1999).

The first large-scale fossil reclamation campaign was conducted by the Oklahoma Museum of Natural History, which used wet screen-washing techniques to describe and categorize numerous examples of dinosaurian taxa (Cifelli *et al.*, 1997, 1999; Eaton & Cifelli, 2001). This, accompanied with a variety of fish, frog, bird, salamander, lizard, and even mammalian assemblages, not to mention a plethora of fossilized dental remains, have made the Mussentuchit one of the most fossiliferous sedimentary units throughout the Cretaceous (Kirkland, 2007). Furthermore, many Mussentuchit taxa represent the earliest definitive record of groups characterizing Late Cretaceous faunal assemblages, and others represent the last surviving examples of dinosaurian clades from the Early Cretaceous (Cifelli *et al.*, 1997; Kirkland & Madsen, 2007). Due to the hypothesized Asian ancestry of many of the recovered species (*Eolambia*, *Kokopellia*, and early tyrannosauroids), it is suggested that the Mussentuchit may have recorded the development of the Beringian Land Bridge. Accordingly, these sediments represent a view into the initial mass migrations from Asia into North America and subsequent competition-induced extinction of many of the fauna endemic

to North America during the Jurassic and Early Cretaceous (Cifelli *et al.*, 1997; Kirkland *et al.*, 1997, 1999; Kirkland, 2005, 2016).

The palaeoenvironment for the Mussentuchit was first noted by Kirkland *et al.* (1997) as being similar to that of the Ruby Ranch Member, save for overall wetter conditions due to the lack of carbonate nodules. This interpretation was later elaborated on by Garrison *et al.* (2007) who proposed a humid floodplain setting with associated perennial lakes instead of previously envisioned ephemeral lacustrine bodies. Currie (1998) reported a mixed floodplain/lacustrine environment for sediments within the upper portions of the Cedar Mountain Formation, which correlated well with findings by Garrison *et al.* (2007). Ludvigson *et al.* (2010, 2015) further corroborated the environmental interpretation by Garrison *et al.* (2007) of a perennial lacustrine setting, by noting that poorly formed palaeosols within the Mussentuchit and underlying Ruby Ranch members underwent pedogenesis within ponded environments. Further interpretations include those by Sorensen (2011) and Holmes (2017), who suggested deposition of the upper Mussentuchit occurring within a distal, terminal delta floodplain. Suarez *et al.* (2007a,b, 2012, 2014) added some of the much-needed climatic contexts by utilizing phosphate and water isotope proxies, which indicated high humidity levels and highland water sources during the Mussentuchit's deposition. Additionally, a study by Arrens and Harris (2015) suggested a possible temperature range of 16 to 26 degrees centigrade via leaf physiognomic methods. Currently, no geochemical-based temperature estimates have been determined (Kirkland, 2017).

2.5 Palaeontology

Utah is known globally for its wealth of preserved dinosaurian fossil specimens representing the Late Cretaceous, which is widely regarded as being one of the most complete fossil records known globally (Kirkland, 2005). It is, however, only relatively recently that sediments from the Early Cretaceous have yielded any meaningful faunal

remains (Galton & Jense, 1979; DeCourten, 1991; Kirkland *et al.*, 1997; Cifelli *et al.*, 1999; Kirkland *et al.*, 2005; Zanno & Makovicky, 2013). During the last two decades increased survey and collection efforts, coupled with improvements in geochronological dating technologies, have yielded a plethora of emerging dinosaurian taxa, as well as highly resolved temporal context to these discoveries (Kirkland *et al.*, 1999, Ludvigson., 2010; Hunt *et al.*, 2011). Accordingly, the emerging Cedar Mountain fossil specimens represent a uniquely well-preserved record of the Laramidian faunal dispersal patterns related to the oceanic transgressions across Cretaceous Europe and Canada (Kirkland *et al.*, 2005).

The most basal member, known as the Buckhorn Conglomerate, preserves few fossil remains save for reworked late Palaeozoic invertebrates (Kirkland *et al.*, 1999). Possibly the most notable fossil found within the Buckhorn is the discovery of ankylosaur remains, suggesting a Cretaceous age due to the proliferous nature of ankylosaur taxa within Cretaceous sediments (Kirkland, 2005).

Overlying the Buckhorn Conglomerate is the Yellow Cat Member. Dinosaurian taxa identified here include the polacanthine ankylosaur *Gastonia burgei* (Kirkland, 1998), advanced iguanodontians such as *Iguanodon ottingeri*, *Iguanacolossus fortis*, and *Hippodraco scutodens* (Galton & Jensen, 1979; MacDonald *et al.*, 2010), a brachiosaurid *Cedarosaurus weiskopfae* (Tidwell *et al.*, 1999), as well as a new titanosaurid and a possible camarasaurid (Britt *et al.*, 1997; Eberth *et al.*, 2006). Several theropod clades are also represented, such as the small coelurosaurian, *Nedcolbertia justinhoffmani*, (Kirkland *et al.*, 1998), a large dromaeosaurid *Utahraptor ostrommaysorum* (Kirkland *et al.*, 1993), and an unidentified allosaurian (Kirkland, 2005). The Yellow Cat also preserves the most basal and most complete theizinosauroid found to date, *Falcarius utahensis* (Kirkland *et al.*, 2005; Zanno, 2006).

At sections where the stratigraphy is best developed, the Poison Strip Member conformably overlies the Yellow Cat Member as a cliff-forming sandstone. Floral remains within this member commonly show petrified logs and cycads, such as *Cycadeoidea* and *Monathanasia* (Kirkland *et al.*, 1999; Dayvault & Hatch, 2005). Preserved faunal remains within the Poison Strip Member are similar to those of the Yellow Cat fauna and include *Gastonia* (Kirkland, 2005), the iguanodontian *Planicoxa venenica* (DiCroce & Carpenter, 2001), and a titanosaurimorph sauropod *Venenosaurus dicrocei* (Tidwell *et al.*, 2001).

Faunal elements from the Ruby Ranch Member are decidedly distinct from the assemblages found in the underlying strata. Dinosaurian remains found within the upper portions of the Ruby Ranch Member include a nodosaurid similar to *Sauropelta* (Warren & Carpenter, 2004), a giant nodosaurid, and a large ankylosaurid *Cedarpetta bilbyhalorum* (Carpenter *et al.*, 2001). Other herbivorous species are represented by the large ornithopod *Tenontosaurus* and a slender toothed brachiosaur (Bird, 2005; Chure *et al.*, 2006). Theropods are represented by small-bodied dromaeosaurs similar to *Deinonychus*, and a large-bodied allosaurian (DeCourten, 1991; Kirkland *et al.*, 1997).

The uppermost Mussentuchit Member represents the most fossiliferous unit of the Cedar Mountain Formation and has been subjected to multiple excavations and prospecting methods, such as wet-screening techniques at micro-fossil sites (Kirkland *et al.*, 1999). Presently, the Mussentuchit Member has yielded numerous fossilized remains representing different species of frogs, salamanders, lizards, snakes, crocodylians, birds, and even early mammals such as *Kokopellia* (Cifelli & Muizon, 1997; Kirkland *et al.*, 1997). Tooth fragments represent ankylosaurids, nodosaurid ankylosaurs, several ornithopod taxa, potential brachiosaurid sauropods, and pachycephalosaurs (Kirkland *et al.*, 1997; Cifelli *et al.*, 1999; Chinnery *et al.*, 1998; Kirkland *et al.*, 1999). Teeth representing troodontids, dromaeosaurids, as well as tyrannosauroids have also been excavated. Well-preserved skeletons are rare and as

of yet, only a few examples have been described. These include the advanced ornithomimid *Eolambia carljonesa* (Kirkland, 1998), the primitive nodosaurid ankylosaur *Animantarx ramaljonesi* (Carpenter *et al.*, 1999), and the carcharodontosaurian *Siats meekerorum* (Zanno & Makovicky, 2013).

Table 2.1 Historical Nomenclature of the Cedar Mountain Formation

Stokes, 1944		Stokes, 1952		Young, 1960				Kirkland <i>et al.</i> , 1997	
Dakota Formation		Dakota Formation		Naturita Formation				Dakota Formation	
	Cedar Mountain Shale		Cedar Mountain Shale		Upper Cedar Mountain		Unnamed Shale		Mussentuchit Member
	Buckhorn Conglomerate		Buckhorn Conglomerate		Middle Cedar Mountain Sand		Unnamed Shale		Poison Strip Sandstone
					Lower Cedar Mountain Sand				Yellow Cat Member
Morrison Formation		Morrison Formation		Dakota Group				Cedar Mountain Formation	
		Brushy Basin							Buckhorn Conglomerate
									Brushy Basin

3. Methods

3.1 Sedimentological Analysis

In-field analysis of the study area located at Mussentuchit Wash, Cathedral Valley, Utah, has been ongoing since 2014 with this particular study taking place during the August field season of 2016. This study primarily utilized facies and architectural element analysis following Miall (1977, 1985) and subsequent modifications by Eberth and Miall (1991), Fielding (2006), Miall (2016), and Tucker *et al.* (2017). Key methodology was gained from studies by Dalrymple (1992), Orton and Reading (1993), Bhattacharya (2002), Hori *et al.* (2002), Nichols and Fisher (2007), and Dalrymple and Choi, (2007), which enabled a more focused description of the specific environment at Mussentuchit Wash, Cathedral Valley. This approach focused on defining and characterizing: (1) outcrop lithology, (2) upper and lower unit bounding surfaces, (3) geometry and lateral extents of unit macroforms, (4) thickness of sedimentary units, and (5) sedimentary and biogenic structures (Miall, 1985). These features were then utilized to identify discrete, re-occurring codes, which were, in combination with distinct macroforms, used to identify and interpret several depositional facies.

Stratigraphic sections were constructed at decimetre scale, by way of Jacob Staff, Brunton Compass, and handheld Garmin GPS 60. The geodetic datum used in this study is the NAD 83 datum with the GRS80 map spheroid. Characterization of rock colour for both weathered and unweathered rocks follows the GSA Munsell Rock Colour Chart (1991). Depositional palaeocurrents from each transect were determined via the measurement of tractional derived structures, such as ripple cross-lamina, planar cross-beds, and parting lineations, with a Brunton Compass set at a magnetic declination of + 12.33⁰. In total, one

hundred and sixty-seven (167) palaeocurrent readings were taken from the base of the Mussentuchit up to the basal units of the overlying Naturita Sandstone beds. All palaeocurrents were plotted within rose diagrams using GeoRose software. Stratigraphic cross-sections were started in the underlying Morrison Formation (Tidwell and Brushy Basin members) and terminated in the overlying Naturita Sandstone. The cross-sections, therefore, encompass the entire Cedar Mountain Formation stratigraphy at Mussentuchit Wash. The outcrop is moderately to highly weathered; however, the extent of weathering is limited to surficial coverage with relatively fresh, *in situ* outcrop occurring between 0.5 and 1.5 meters below the surface. Seven transect sites were selected for their outcrop quality and relation to three fossil sites occurring at the Mussentuchit Wash field site including (1) the Mini-troll, (2) Suicide Hill, (3) and Fortunate Son fossil quarries, see Figure 3.1. The field transects include: (1) Mini Troll (**A**), (2) Suicide Hill (**B**), (3) Fortunate Son (**C**), (4) Far Point Front (**D**), (5) Far Point Back (**E**), (6) Prospect Point sections (**F**), and (7) Hummingbird Point (**G**), Figure 3.1.

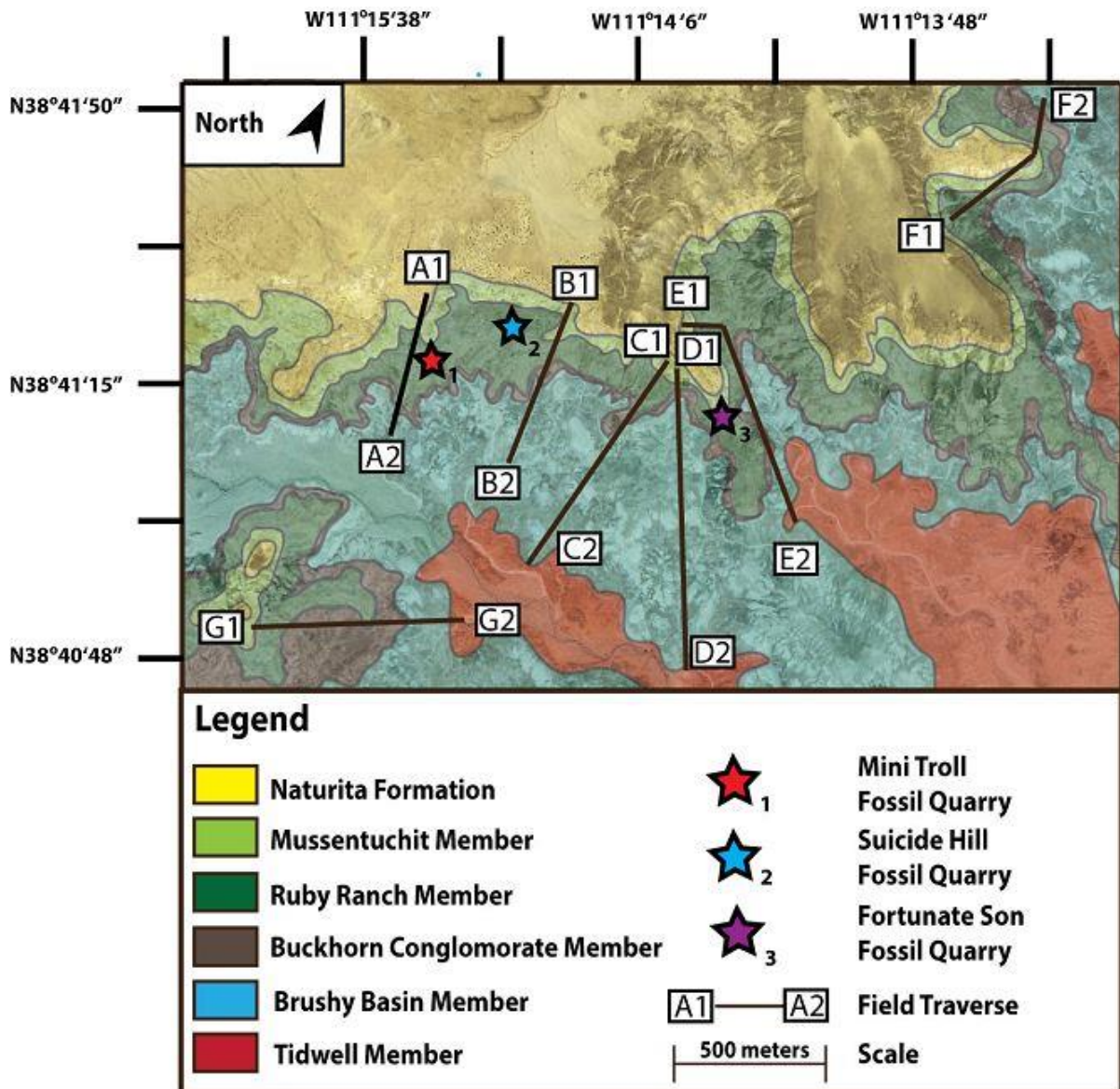


Figure 3.1: Map showing field transect locations and fossil quarries. Backdrop modified from Google Earth ESRI Satellite Image

3.2 Detrital Zircon Analysis

This study identified seven specific mudrocks and sandstones to assess the youngest maximum depositional ages of the sediments at Mussentuchit Wash. This was achieved via LA-ICP-MS analysis of the $^{206}\text{Pb}/^{238}\text{U}$ isotope ratios present within detrital zircon assemblages, commonly associated within sedimentary deposits (Gerdes & Zeh, 2006; Frei & Gerdes, 2009). This method of dating detrital zircons does not date the absolute age of

deposition, but rather of zircon formation, which is considered to be nearly synchronous with an associated magmatic event (Nelson, 2001; Lease *et al.*, 2007). Furthermore, radiogenic isotope ratios have been shown to be invaluable in identifying sediment provenance (Kosler *et al.*, 2002; Cawood *et al.*, 2003; Fedo *et al.*, 2003; Cluzel *et al.*, 2011). Accordingly, the isotope ratios of all samples were correlated to possible sediment source terrains. By combining these results with palaeocurrent data, these data sets will enable the study to recreate the palaeodrainage patterns characterizing the formation of the Cedar Mountain Formation.

All samples were cleaned, crushed, and milled in a tungsten carbide disc mill and then sieved to a 350- μm individual grain size. Clay fractions were liberated via repeated washing and decanting of the muddy sediment portion. Subsequent separation of heavy minerals was achieved through the use of a bi-directionally oscillating Superpanner. The heavy mineral fraction was separated into ferromagnetic, paramagnetic, and non-magnetic mineral fractions by using a permanent magnet and a Frantz Magnetic separator, incrementally stepped at charges of 0.5 A, 0.8 A, and 1.4 A charge. Non-magnetic, heavy mineral fractions were separated into minerals with densities higher and lower than 2.96 by funnelling the separate through a measure of Tetrabromoethane (TBE), which has an exact density of 2.96. For each sample, approximately 200 grains were handpicked and mounted onto an epoxy resin puck produced from SpeciFix Resin and SpeciFix-40 curing agent. A MD-Dac Satin Woven Acetate Polishing Cloth (3 μm) on a DiaPro-Dac3 Suspension was utilized to polish the puck for ten minutes. An MD-Nap Synthetic Short Nap Polishing Cloth (1 μm) with a DiaPro-Nap B1 Suspension was used to put the final polish on the puck. Samples were prepared for electron microscopy by coating the resin puck with a 10 nm thick layer of 23-carat gold by an Edwards S150A Gold Sputter Coater.

The Zeiss MERLIN Field Emission Gun Scanning Electron Microscope was used for image generation with the high energy beam operating at 20 kV accelerating voltage, 11nA probe current and the sample positioned at a 9.5 mm working distance. Detectors used for Cathode Luminescence (CL) and Back Scattered Electron (BSE) imagery were the Zeiss Cathode Luminescence Detector and Zeiss 5-diode Back Scattered Electron Detector respectively. Following this, samples were cleaned and subjected to trace elemental quantification through laser ablation - single collector - magnetic sectorfield - inductively coupled plasma - mass spectrometry (LA-SF-ICP-MS) via the Thermo Finnigan Element2 mass spectrometer and coupled ASI Resolution SE-S155 Excimer Laser Ablation system, Table 3.1. Spot diameter and depth were set to 25 μm and 10-15 μm respectively. All analysis was done with GJ-1 (602 Ma) (Jackson *et al.*, 2004) as a primary standard and Plešovice (337 Ma) (Sláma *et al.*, 2008) and M127 (527 Ma) (Nasdala *et al.*, 2016) as secondary standards. Finally, raw isotopic data was processed via the Iolite Data Processing Software extension in IgorPro. The resulting data sets were subsequently used in calculating and plotting relevant Concordia ages diagrams via ISOPLOT/Ex 4.15 (Ludwig, 2003). Discordancy of more than 10% was used as the main exclusion criteria, indicating that these grains have either undergone lead loss, common lead contamination, crystal fractionation, matrix interferences or gross analytical error resulting in inaccurate ages. Grains with ages of less than 90 Ma exhibited higher discordances along with intense micro-fracturing, indicating that these grains underwent structurally facilitated lead loss and are, therefore, considered excludable. All mineral separation and dating work was done in the Central Analytical Facilities at Stellenbosch University, Table 3.1.

3.3 Youngest Detrital Zircon Age

In the past, it has been common practice to utilize ages ascertained from the youngest detrital grains in a sample to constrain depositional ages of sediments (Rainbird *et al.*, 2001).

Recent studies have, however, found that different statistical integrations of the same grains resulted in different ages (Dickenson & Gehrels, 2009; Lawton & Bradford, 2011; Robinson *et al.*, 2012; Tucker *et al.*, 2013, 2016). This highlights the importance of utilizing and integrating multiple age calculation methodologies to produce a statistically robust depositional age of a sample. This study utilized the seven most commonly used methods for ascertaining youngest detrital zircon ages (Dickenson & Gehrels, 2009; Johnston *et al.*, 2009; Lawton & Bradford, 2011; Robinson *et al.*, 2012; Tucker *et al.*, 2013) The methods include: (1) youngest single grain age (YSG), (2) youngest graphical detrital zircon age (YPP), (3) youngest detrital zircon age (YDZ), (4) weighted mean average one sigma (YC1 σ), (5) weighted mean average two sigma (YC2 σ), (6) weighted average, and (7) TuffZirc age extractor.

The YSG method identifies the absolute youngest single detrital grain and interprets this as representing the youngest depositional age. Considering this method only uses a single value, it has no internal statistical robustness and is, accordingly, highly critiqued (Dickenson & Gehrels, 2009). The YPP method involves identifying the youngest graphical peak on an age distribution curve, generated with a graphical function within ISOPLOT (Ludwig, 2009). The YDZ age utilizes a Monte Carlo analysis function within ISOPLOT to extract the youngest subset of ages found within the overall sample data set (Dickenson & Gehrels, 2009; Ludwig, 2009). YC1 σ and YC2 σ were ascertained through the use of the AGE PICK program from the University of Arizona LaserChron Centre. This methodology determines the weighted mean averages of a group of three youngest zircons at 1 and 2 sigma respectively. Accordingly, this method incorporates both internal and external errors present within a specific sample set (Dickenson & Gehrels, 2009; Jones *et al.*, 2009). A weighted average of the youngest ten zircons was determined through a function within ISOPLOT. This method uses the ages and error values within each grain to construct an inverse

variance-weighted average, resultantly addressing age scatter and producing a more statistically robust age. The final method used to identify the youngest depositional age is the TuffZirc age extractor. This method uses an algorithm within ISOPLOT that calculates a mathematical age on the loss and inheritance of lead, and associated error, within each zircon (Ludwig, 2009). A large proportion of analysed zircons showed concentrated ages around the youngest age bracket, ten grains were included within this analysis to ensure the highest statistical robustness. These seven age matrices were evaluated and averaged to produce the most reliable and statistically robust youngest maximum depositional age for each sample.

Table 3.1: LA-ICP-MS Specifications List, Central Analytical Facility, Stellenbosch University

Laboratory & Sample Preparation	
Laboratory name	Central Analytical Facility, Stellenbosch University
Sample type / mineral	Detrital zircons, baddeleyite
Sample preparation	Conventional mineral separation, zircon: 2.54 cm resin mount and in-situ in thin section, 1 μm polish to finish
Imaging	CL MERLIN FE-SEM, 11 nA, working distance 9.5 mm
Laser ablation system	
Make, Model & type	Resonetics Resolution ME-S155, ArF Excimer ATL Atlex
Ablation cell & volume	Laurin Technology S155 dual volume cell
Laser wavelength	193 nm
Pulse width	< 5 ns
Fluence	2.0 J/cm ⁻² (measured with external energy meter above sample cell)
Repetition rate	9 Hz zircon
Spot size	25 μm
Sampling mode / pattern	25 μm single spot analyses
Cell carrier gas	100% He, Ar and N ₂ make-up gases combined into Nylon 10 tubing
Pre-ablation laser warm-up (background collection)	3 cleaning shots followed by 15 seconds background collection
Ablation duration	15 seconds
Wash-out delay	15 seconds
Cell carrier gas flows	325 ml/min He
ICP-MS Instrument	
Make, Model & type	Thermo Finnigan Element2 single collector HR-SF-ICP-MS
Sample introduction	Via Nylon 10 tubing
RF power	1350 W
Make-up gas flow	920 ml/min Ar & 4 ml/min N ₂
Detection system	Single collector secondary electron multiplier
Masses measured	202, 204, 206, 207, 208, 232, 233, 235, 238

Integration time per peak	4 ms
Total integration time per reading	0.1 sec <i>(represents the time resolution of the data)</i>
Sensitivity	30000 cps/ppm Pb
Dead time	6 ns
Data Processing	
Gas blank	15 second on-peak
Calibration strategy	GJ-1 used as primary reference material, Plešovice & M127 used as secondary reference materials (Quality Control)
Reference Material info	GJ-1 (Jackson <i>et al.</i> 2004), Plešovice (Sláma <i>et al.</i> 2008), M127 (Nasdala <i>et al.</i> 2008; Mattinson 2010)
Data processing package used / Correction for LIEF	Iolite data reduction software was used to process data
Mass discrimination	Standard-sample bracketing with $^{207}\text{Pb}/^{206}\text{Pb}$ and $^{206}\text{Pb}/^{238}\text{U}$ normalized to reference material GJ-1
Common-Pb correction, composition and uncertainty	204-method, Stacey & Kramers (1975) composition at the projected age of the mineral, 5% uncertainty assigned
Uncertainty level & propagation	Ages are quoted at 2 sigma absolute, propagation is by quadratic addition. Reproducibility and age uncertainty of reference material and common-Pb composition uncertainty are propagated.
Quality control / Validation	M127: Concordia age = 528 ± 6 Ma (2s, MSWD = 1.2) Plešovice: Concordia age = 340 ± 2 Ma (2s, MSWD = 1.03)
Other information	For detailed method description see Frei & Gerdes (2009)

4. Results

4.1 Facies Analysis

An outcrop-based analysis was conducted on the stratigraphy at Mussentuchit Wash, Capitol Reef National Park, Utah. The analysis was conducted in accordance to the lithological description as proposed by Reading (1996). Facies characterization was conducted in accordance with methods proposed by Miall (1977), with subsequent modifications by Miall (1985, 2016), Olariu and Bhattacharya (2006), Dalrymple and Choi (2007), Tucker *et al.*, (2017), and this study. A study by MacEachern and Bann (2008) was used to aid in the categorization of biological features preserved in the sediment. This study identified bounding surfaces varying from 0th to 5th following definitions by Vail (1977) and subsequent revisions by DeCelles *et al.*, 1991, and Miall (1985; 1996; 2010) (Table 4.1.1). In-field observations identified fifteen repeating facies codes (Table 4.1.2), along with multiple co-occurring architectural elements (Table 4.1.3). These were combined into six distinct facies associations (Table 4.1.4).

Table 4.1.1: Bounding surface orders. Modified after Vail, (1977)

Examples of processes	Fluvial, Deltaic depositional units	Rank and character of bounding surface
burst-sweep cycle	lamina	0 th -order, lamination surface
bedform migration	ripple (microform)	1 st -order, set bounding surface
bedform migration	diurnal/seasonal dune increment, reactivation surface	1 st -order, set bounding surface
bedform migration	dune (mesoform)	2 nd -order, co-set bounding surface
seasonal events, ten year flood	macroform growth increment	3 rd -order, dipping 5 ^o -20 ^o in direction of accretion
100-year channel and bar migration	macroform, immature palaeosol	4 th -order, convex up macroform top, minor channel scour, flat surface bounding floodplain elements
long term geomorphic processes	channel delta lobe, mature palaeosol	5 th -order, flat to concave-up major channel base
5 th order Milankovitch cycles	Channel belt, alluvial fan, minor sequence	6 th -order, sequence boundary: flat, regional extensive or base of incised valley

Table 4.1.2: Facies codes identified within the Mussentuchit Member at Mussentuchit Wash. Modified from Miall (1985, 2016) and Tucker *et al.* (2017).

Facies Code	Lithofacies	Sedimentary Structures	Interpretations
Gmx	Thin-lamina, matrix supported gravel	Grading-erosional surface interlaminated conglomerate	Basal contact of anastomosing channel or crevasse splay
St	Sand, fine to very coarse	Solitary (theta) or grouped (pi) trough cross beds	Dunes (lower flow regime)
Sp	Sand, fine to very coarse	Grouped planar crossbeds	Transverse bar (lower flow regime)
Sr	Sand, fine to very coarse	Ripple marks (crossbedding)	Lower flow regime ripples
Sh	Sand, fine to very coarse	Horizontal lamination, parting or streaming lineation	Planar bed flow (lower and upper regime)
Se	Erosional scours with intraclasts	Crude crossbedding	Scour fill
Fl	Sand, silt, mud	Fine lamination	Overbank or waning flood deposits
Fsc	Silt, mud	Laminated to massive	Backswamp deposits
Frip	Silt, mud	Rip-up clasts	Scour fill
VFc	Fine to very fine clay	Bedded to massive	Shallow lagoon, shore/delta
C	Silt, mud	Disseminated lignite	Salt marsh/preserved root(s)
P	Carbonate	Pedogenic features	Soil

Table 4.1.2: Identified architectural elements and associated morphologies from the Mussentuchit Member. Modified from Miall (1985, 2010) and Tucker *et al.* (2017).

Symbol	Facies	Geometry and relationship
CH	Any combination	Concave up, erosional base, bounded by 2 nd to 3 rd order surfaces
CH(OF)	Fsc, Fl, P	Concave up, erosional base, infilled by mds
LA/CW	St, Sp, Sr, Sh, Se	Wedge or sheet, characterized by internal lateral accretion
OF	Fl, Fsc	Deposits of overbank sheet flows or floodplain ponds
HO	Se, Gmx	Concave up, erosional base, bounded by 2 nd to 3 rd order surfaces
TS	Fsc, Fl	Thick successions of intercalated sand and mud units
CV	Sh, Si, Se, Ss	Crevasse splays

Table 4.1.3: Facies Association identified within the Mussentucht Member of Miaou (2010) and Tucker *et al.* (2017).

Facies association	Facies Codes													Architectural elements			Bounding surfaces		Morphology	Colour	Lithofacies	Environmental interpretation
	Gmx	St	Sp	Sr	Sh	Se	Fl	Fsc	Frip	VFc	C	Fr	P	Sediment size	Architectural elements	Bounding surfaces						
FA1 : Tidal Mudflat																0.003 mm (silty mud) - 0.0715mm (Silty sand)	TS	1st to 2nd order basal; 1st to 3rd order upper	3.0 - 6.0 meter thick, laterally continuous (900.0 meters) beds	UW: Medium grey to greenish grey (10GY 6/1) W: Light grey (10GY 8/1) to greenish grey (10GY 6/1)	Interbedded siltstone and silty mudstone with gypsum crystals	Tidal Mudflat deposits
FA2 : Palaeosols																0.003 mm (silty mud) - 0.0715mm (Silty sand)	OF	1st to 2nd order basal; 1st to 3rd order upper	0.5 - 0.7 meter thick, laterally continuous (600.0 meters) beds	UW: Dark Brown (5 YR 5/1) to Purple (5 RP 5/1) W: Light grey (10GY 8/1) to Purple (5 RP 5/1)	silty mudstone with gypsum crystals developing into paleosols	Muddy deposits developing into paleosols
FA3 : Crevasse Splay																0.03 mm (medium silt) - 0.71 mm (v. coarse sand)	CS	4th order basal; 2nd order upper	0.2 to 0.4 meter thick lenses extending between 6.0 to 30.0 meters	UW; Grey (N5) to dark grey (N3) W: Light grey (N7)	Silty to sandy gravel lenses	Crevasse splay deposits
FA4 : Abandoned Channel Deposits																0.003 mm (silty mud) - 0.0715mm (Silty sand)	CH(OF), LA/CW, HO	4th order basal; 2nd order upper	0.2 to 0.6 meter thick lenses extending between 5.0 to 10.0 meters	UW; Grey (N5) W: Light grey (N7)	Silty to sandy lenses	Abandoned Channel is infilled by muddy sediment
FA5 : Channel Deposits																0.03 mm (medium silt) - 0.71 mm (v. coarse sand)	CH, LA/CW, SB, HO	4th order basal; 3rd order upper	0.3 to 0.7 meter thick ribbons extending laterally up to 40.0 meters	UW : Moderate orange pink (5Y 8/4) W: Light yellowish grey (5Y 8/1)	Gravelly sand ribbons	Meandering fluvial channels
FA6 : Ephemeral Ponds																<0.002 mm (clay rich mud)	OF	1st to 2nd order basal; 3rd order upper	0.3 to 1.0 meter thick, laterally extensive (20.0 meters) beds	UW: Dark Grey (N3) to black (N1) W: Very light grey (N8) to Pale Yellowish Orange (10YR 8/6)	Finely laminated mudstone	Small, Ephemeral water bodies

4.1.1 Facies Association 1 (FA1): Tidal Mudflats

FA1 is comprised of identified facies codes Fsc and Fl in descending order. FA1 typically weathers to either light grey (10GY 8/1) or greenish grey (10GY 6/1), however, typical unweathered colour appears as medium grey (N5) and greenish grey (10GY 6/1) (Fig. 4.1.1). Additionally, FA1 forms a distinctive surficial popcorn weathering texture, due to volcanolithic bentonite muds forming a large component of the deposited sediments (Fig. 4.1.1).

Typical bounding surfaces exhibit gradational 1st to 2nd order basal and upper bounding surfaces, save for instances where other units undercut into FA1. Beds typically occur as laterally extensive units, ranging in thickness between 3.0 and 6.0 meters, and estimated to extend laterally up to 900.0 meters (Fig. 4.1.1.A).

Internally, FA1 shows medium bedded silt units, 5.0 to 20.0 centimetres thick, void of internal structures (Fsc), and intercalated with thinly bedded silty muds, typically 3.0 to 7.0 centimetres thick (Fig. 4.1.1.C). The silty mud units intermittently preserve occurrences of finely developed lamina (Fl), typically 0.1 to 0.3 centimetres thick (Fig. 4.1.1.B). Unit beds within FA1 exhibit normal grading from muddy silts to clay-rich muds, with grading especially prevalent within finer-grained unit beds. FA1 also preserves characteristic occurrences of bivalve shell fragments, 0.5 to 1.0 centimetres in diameter, sporadically forming minute lenses of shell hash within the finer-grained sediments. FA1 preserves a notable amount of distinctive acicular gypsum crystals, commonly 0.5 centimetres long and 0.1 centimetres thick, with rare occurrences of gypsum up to 3.0 centimetres long. FA1 additionally preserves fine precipitation of white anhydrite. The sediments of FA1 are predominantly comprised of volcanolithic, bentonite rich muddy silts (estimated at 5 to 15% silt), intercalated with sandy silts containing a litharenitic sand fraction (estimated at 10 to 20% fine sand).

FA1 is characterized by the tidal sequences (TS) architectural element. TS characteristically presents as a repeated sequence of intercalated sandy silt and silty mud couplets. These TS couplets are preserved as 5.0 to 15.0 centimetres thick beds, which are stacked vertically to form an intercalated unit up to 10.0 meters in thickness. The TS architectural elements show a highly variable lateral extent, ranging between 40.0 and 100.0 meters, with elements occurring side by side for up to 900.0 meters.

Trace fossils are preserved as small-scale, silty backfilled bioturbation of *Skolithos*, 0.5 centimetres thick and 9.0 centimetres in length, along with sporadic preservation of root traces, 0.01 centimetres thick and 2.0 centimetres in length.

Interpretation

The muddy units of FA1 are interpreted to represent sediments of an expansive tidal mudflat (Olariu & Bhattacharya, 2006; Dalrymple & Choi, 2007). The overall lack of ripples or other tractional features indicates deposition through suspension settling of fine-grained material. As such, the repeated sequence of muddy and silty tidal rhythmites is interpreted as representing a cyclical energy regime, associated with a tidally influenced system (Mazumder & Arima, 2005; Dalrymple & Choi, 2007; Caillaud *et al.*, 2017). Specifically, the coarser units represent deposition during hyperpycnal flow, while fine-grained sediments represent suspension settling during hypopycnal flow (Orton & Reading, 1993). This interplay between hypo- and hyperpycnal flow is associated with high and low tide influences respectively, with thickly deposited muddy units occurring due to the influence of spring tide (Wolanski *et al.*, 1995; Harris *et al.*, 2004). The notable green discolouration within these mudstones is attributed to the presence of glauconite, which indicates a constant flow of water through the system. This, coupled with the high prevalence of gypsum crystals, is interpreted to represent the chemical interplay of saline marine water (forming gypsum) and flowing fresh water (forming glauconite) (Groves *et al.*, 1981; Diez-Cansec *et al.*, 2014). This chemical

interaction is a feature typical of tidal mudflats at a coastal margin (Dalrymple & Choi, 2007; Garrison *et al.*, 2007; Tessier, 2012).

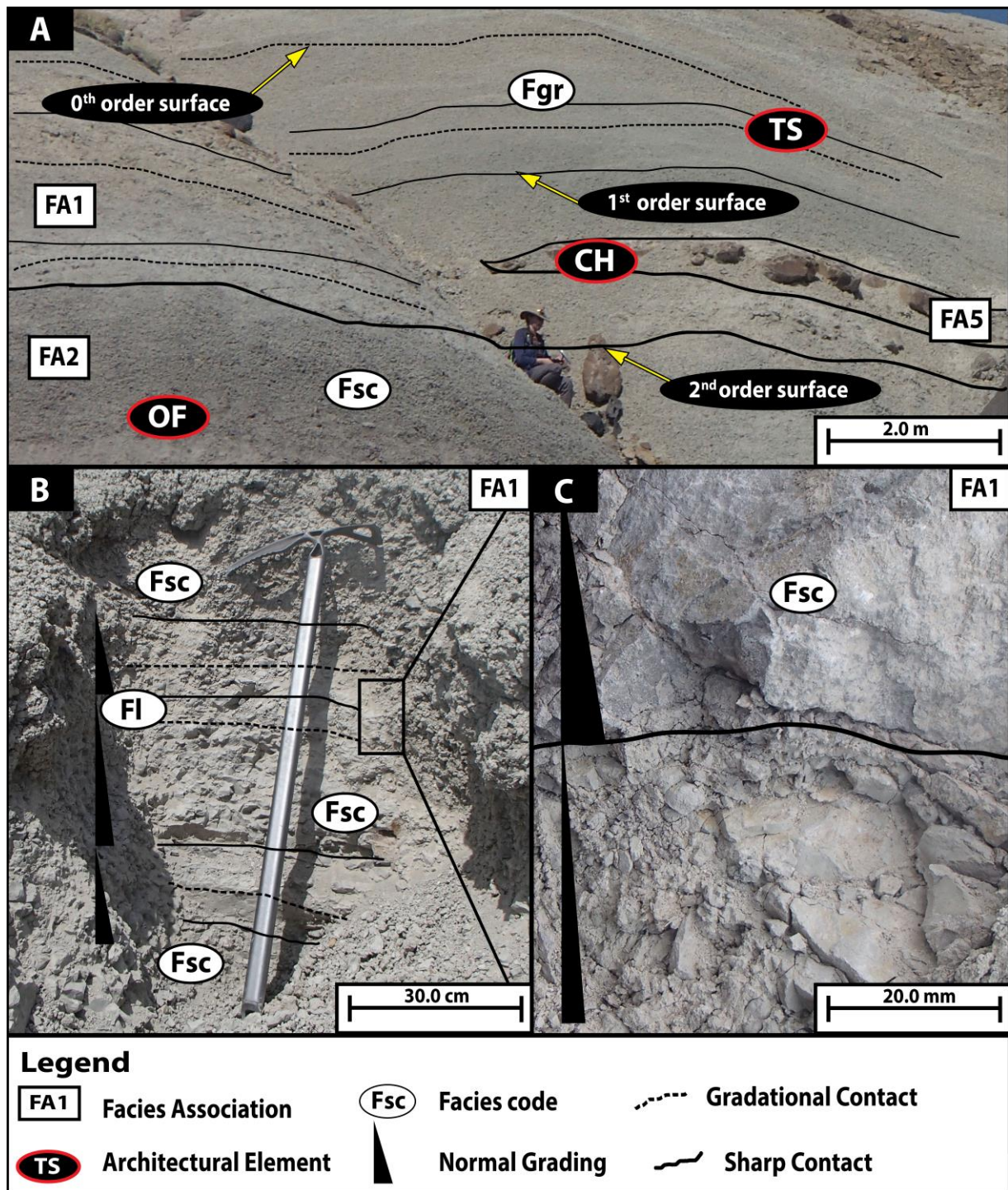


Figure 4.1.1: Photomosaic showing sedimentological features of FA1. (A) Shows typical thick, multi-story bed of repeated successions of normally graded silty to fine-grained units along with interbedded channel structures and basal 2nd order sharp contact with FA2. Note the faintly green coloration of the unit. (B) Shows magnified view of the sediment within FA1 with typical structureless silts and faintly laminated muds. Note repeated normal grading of silts into muds. (C) Illustrates the fine-grained muddy units overlain by silty units with a characteristically sharp contact. Photographs by Tucker (2016).

4.1.2 Facies Association 2 (FA2): Palaeosols

FA2 is comprised of identified facies codes P, Fsc, C, and Fr in descending order. FA2 typically weathers to either light grey (10GY 8/1) or purple (5RP 5/1), however, typical unweathered colour appears as dark brown (5YR 5/1) to purple (5RP 5/1) (Fig. 4.1.2). Additionally, FA2 exhibits a distinctive popcorn weathering texture, due to volcanolithic bentonite muds forming a large component of the deposited sediments.

Lower unit contacts exhibit gradational 1st order bounding surfaces. Upper bounding surfaces are characterized as 1st to 2nd order, with 3rd order surfaces occurring when FA2 is incised by an overlying unit. Beds typically occur as laterally extensive units, ranging in thickness between 0.5 and 0.7 meters and extending laterally for 50.0 up to 600.0 meters.

FA2 exhibits multiple pedogenic (P) features including: (1) well developed A and C horizons (Fig. 4.1.2.A), 0.3 meters and 0.2 to 0.4 meters thick respectively, (2) prominent, bowl-shaped intersecting slickenside structures, 2.0 to 17.0 centimetres across (Fig. 4.1.2.B, E), (3) formation of cubic soil peds, 1.5 to 3.0 centimetres in width, (4) nodular weathering, 3.0 to 7.0 centimetres in diameter (Fig. 4.1.2.B), (5) a high proportion of disseminated lignite fragments, commonly 0.1 to 0.3 centimetres in diameter, (6) rarely preserved root traces (Fr), 0.2 centimetres thick and 0.5 centimetres in length, and (7) variable degrees of bioturbation with a bioturbation index of 1 to 3. Additionally, FA2 exhibits distinctive occurrences of small gypsum crystals, 0.5 centimetres in length and 0.1 centimetres in thickness (Fig. 4.1.2.D). The basal portions of FA2 occasionally preserve instances of weakly developed normal grading, with graded units ranging in thickness from 10.0 to 20.0 centimetres. The sediments of FA2 consist predominately of bentonite rich, muddy silts (estimated at 60% silt), which grades upward to silty muds (estimated at 15% silt).

FA2 is characterized by the overbank fines (OF) architectural element and constitutes the only identifiable element within FA2. OF commonly presents as laterally extensive,

bedded units of fine-grained, muddy sediments, which range in thicknesses from 0.5 to 0.7 meters. FA2 shows a highly variable lateral extent ranging between 20.0 and 50.0 meters, however, erosional processes make accurate measurements difficult. Examples of FA2 periodically occur at similar stratigraphic heights, forming an almost continuous unit extending up to 600.0 meters, Fig. 4.1.2.

Interpretation

FA2 is interpreted as representing moderately to well-developed vertisols. The visibly developed, dark A horizon represents the organic nutrient-rich upper portions, while the light C horizon represents the lower, organic nutrient poor portions of the soil profile (Blockhuis, 1996). The absence of the B horizon is attributed to the shrinking and swelling nature of vertisols, which self-mulches the soil and impedes complete horizontal stratification (Grant & Blackmore, 1991). Disseminated plant remains (lignite) are attributed to the “self-mulching” shrinking-swelling action of vertisols, breaking up roots and other organic remains during pedogenesis (Grant & Blackmore, 1991). The notable dark purple discoloration is also indicative of a reducing environment, commonly associated with waterlogged soils. This horizontal development, coupled with pedogenic weathering (cubic and nodular) patterns, pervasive slickensides, a large organic fraction, and reducing redox conditions are characteristics of moderately to well-developed vertisols within a regularly flooded setting (Mack *et al.*, 1993; Retallack, 1988, 2001, 2008; Pal, 2017).

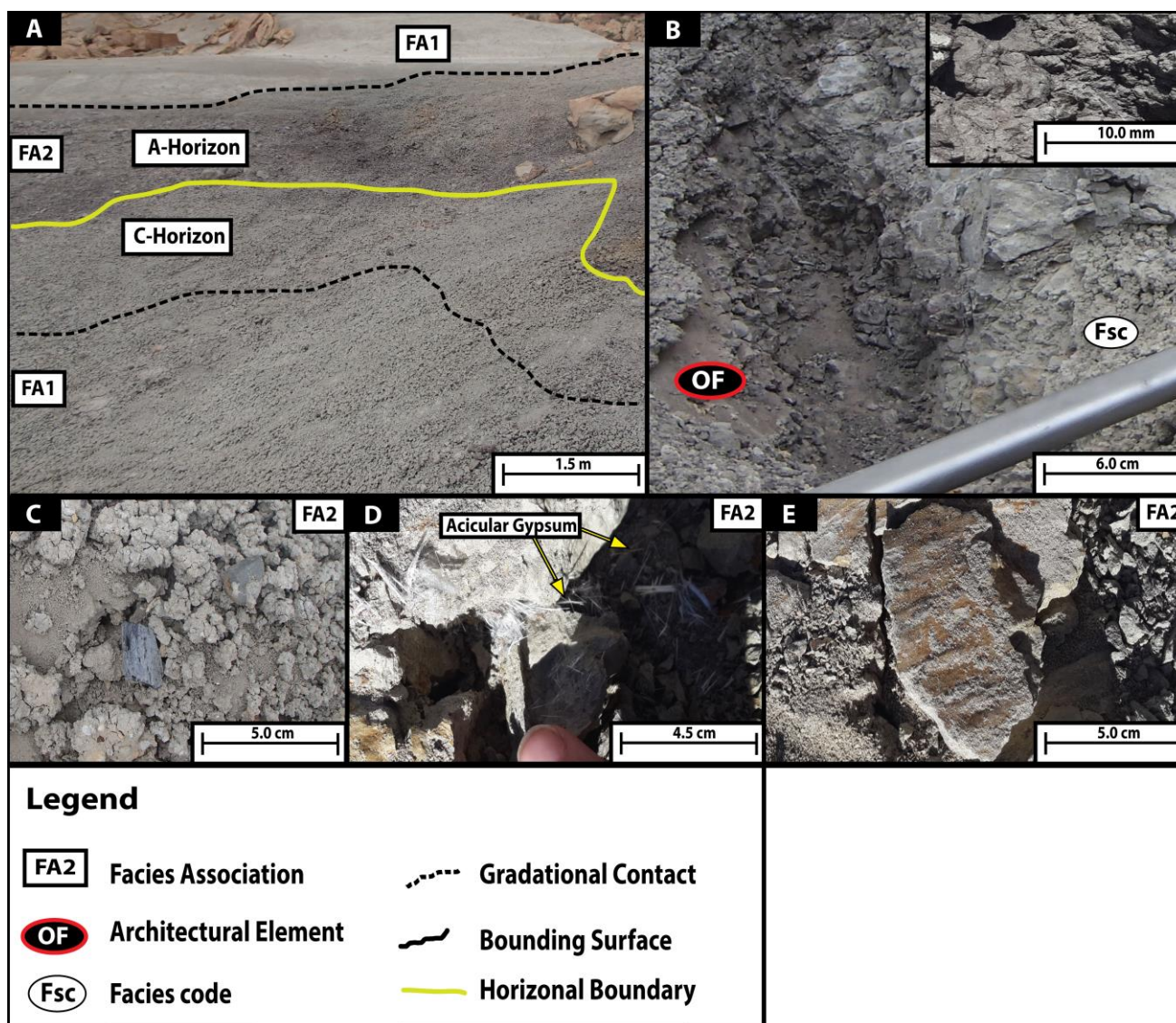


Figure 4.1.2: Photomosaic showing characteristic sedimentological features of FA2. (A) Shows outcrop of FA2 exhibiting purple weathering and horizontal development. (B) Shows typical, chaotic texture of FA2 with multiple bisecting slickensides. Magnified insert illustrates the fine-grained nature of the sediment with minor lignite fragments. (C) Shows typical collection of fossil fragments present within FA2. (D) Shows small, acicular gypsum crystals developed within FA2. (E) Shows planar view of slickenside surface exhibiting typical striated pattern. Photographs by Tucker (2016).

4.1.3 Facies Association 3 (FA3): Crevasse Splays

FA3 is comprised of identified facies codes Gmx, Se, Frip, and Sr in descending order. Typically, FA3 weathers to light grey (N7), forming stepped features, however, typical unweathered colour exhibits grey (N5) to darker grey (N3) (Fig. 4.1.3).

Typical lower bounding surfaces distinctly show 4th order erosive surfaces, characterized by upwardly concave erosional scouring. Upper bounding surfaces commonly exhibit 2nd to 3rd order bounding surfaces, including preservation of sandy bedform macroforms. Beds typically occur as lenticular bodies, ranging in thickness between 0.2 and 0.4 meters and laterally extend between 6.0 and 30.0 meters.

Internally, FA3 is predominantly characterized by homogeneously bedded to normally graded sediments (Fig. 4.1.3.C). Pockets of polymictal para-conglomerates (Gmx), with chert and quartzite clasts 0.2 to 0.5 centimetres in diameter, occur throughout the lower portions of FA3. These conglomerate pockets show a high prevalence within erosional scours (Se), which typically incise 3.0 centimetres deep and 5.0 to 10.0 centimetres across into the underlying units. Platy rip-up clasts (Frip), 0.2 centimetres in diameter, consisting of muddy sediment from the underlying units occur throughout the facies, with a higher prevalence near the basal erosive surface (Fig. 4.1.3.C-D). The uppermost portions of FA3 intermittently exhibit asymmetrical, fine ripple cross-lamination (Sr), with foresets showing an angle of repose of 20°, foreset thickness of 0.5 centimetres, and a toe-to-crest height of 3.0 centimetres. These cross-laminations are similar to the cross-laminations made by 2D ripples. FA3 is characterized by either litharenitic, medium-grained sands (0.031 centimetres), which grade into sandy silts (estimated at 60% silt), or by fine- to medium-grained sandy silts (estimated at 70 -90% silts), with a litharenitic sandy component.

FA3 is characterized by one major architectural element, namely crevasse splays (CS). CS commonly presents as 0.2 to 0.4-meter-thick sheets with lateral extents of 6.0 to 20.0 meters, typically showing massive to graded bedding.

Interpretation

FA3 is interpreted as representing crevasse splays, associated with high-energy flood events and channel bank failure. Coarse sand to sandy silt units showing moderate to high lateral extents, erosive contacts, and basal rip-up and gravelly clasts provide evidence for rapid deposition associated with crevasse splays (Miall, 1985; Lang *et al.*, 2004; Fielding, 2006). Furthermore, certain sandy units intermittently preserve minor occurrences of ripple cross-laminations, indicating minor current deposition as the depositional energy wanes. The variation between splays with fine and coarse sediments is interpreted to represent a variable flood energy regime. Specifically, fine sediments represent lower energy overbank splays and coarse sediments represent higher energy bank failure splays (Lang *et al.*, 2004; Nichols & Fisher, 2007).

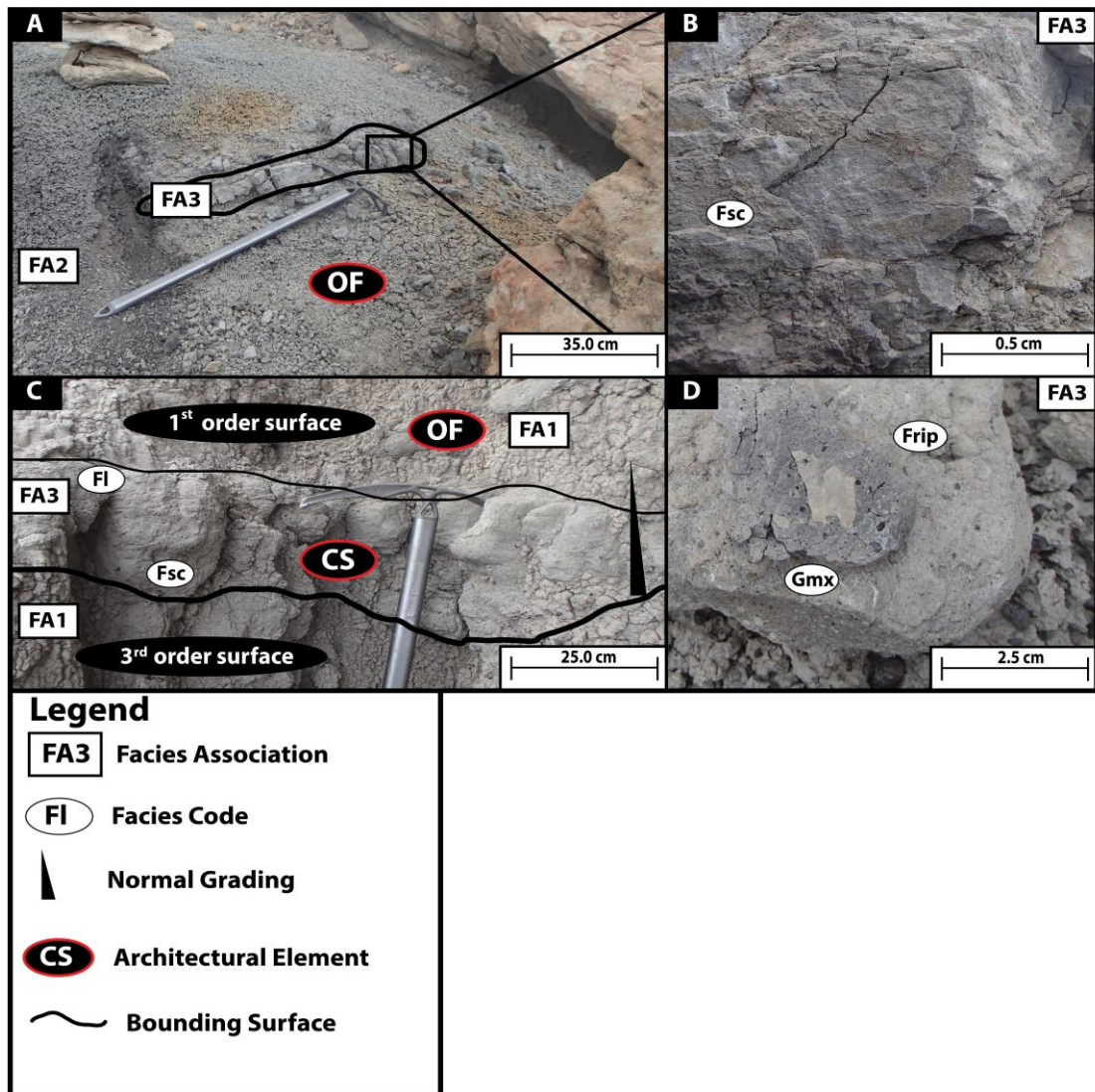


Figure 4.1.3: Photomosaic showing typical sedimentary characteristics of FA3. (A) Shows FA3 occurring as a small, lenticular silty body within FA2. (B) Shows an exploded view of the silty lens, illustrating the moderate fraction of sand within the silty matrix. (C) Shows an enlarged view of a silty unit illustrating the basal, erosive bounding surface with an upper, 1st order contact with the overlying FA1. (D) Shows a magnified view of the basal sediment illustrating both large amount of fine-grained rip-up clasts and floating gravel clasts. Photographs by Tucker (2016).

4.1.4 Facies Association 4 (FA4): Abandoned Channels

FA4 is comprised of identified facies codes Fsc, P, Fl, Sm, St, Gmx, and Sp in descending order. Typically, FA4 weathers to light grey (N7), forming stepped weathered units, however, typical unweathered colour is characterized as grey (N5) to darker grey (N4) (Fig. 4.1.4).

Typical lower bounding surfaces distinctly show 4th to 5th order erosive surfaces, including channel scours and concave up macroforms. Upper bounding surfaces commonly exhibit 2nd and 3rd order bounding surfaces, including preservation of the channel macroform and limited lateral accretion (Fig. 4.1.4.A). Beds typically range in thickness between 0.2 and 0.6 meters, and laterally extend between 5.0 and 10.0 meters, characteristically pinching out laterally.

The Internal structure is dominated by massively bedded silty mud units (Fsc), commonly exhibiting pedogenic (P) features, such as weathering into blocky to nodular peds with a width of 1.0 to 2.0 centimetres, and diameter of 3.0 to 30.0 centimetres, respectively (Fig. 4.1.4.B). Upper portions of the facies typically preserve fine laminations (Fl), 0.1 to 0.3 centimetres thick. Massively bedded silts (Sm) are prevalent within the lower portions of the facies. These silts commonly form the infill of macroscale troughs (St), which incise 0.1 to 0.2 meters deep and 3.0 to 6.0 meters across into the underlying sediments (Fig. 4.1.4.A, B). Fine-grained, polymictal gravels (Gmx), 0.2 centimetres in diameter, of quartzite and shale occur at the base of the facies, concentrating at the 3rd order bounding surface of the macroscale trough. Planar crossbeds (Sp) are identified at the lateral boundaries of FA4, and are typically characterized by interbedded silts and clays. These units typically exhibit asymmetrical cross-bedding with toe-to-crest heights of 10.0 to 20.0 centimetres, foreset thicknesses of 1.5 to 2.0 centimetres and foreset angles of repose of 15⁰ to 20⁰. The sediments

of FA4 are typified by muddy silts, with an estimated silt proportion of 25%, which grades to silty muds with an estimated 10% silt proportion near the upper contact.

FA4 preserves three identifiable architectural elements, including channels with overbank fines (CH (OF)), scour hollows (HO), and channel wings/lateral accretion (CW/LA). CH (OF) is recognized as massively bedded silty units, ranging in thickness from 0.1 to 0.4 meters and extending laterally for 3.0 to 6.0 meters (Fig. 4.1.4.A). HO elements are preserved as scoop-shaped hollows with asymmetrical fill, 0.1 to 0.2 meters deep with a lateral extent of 3.0 to 6.0 meters. CW/LA elements are identified as wedges or small sheets, tapering out to one end. CW/LA exhibits toe-to-crest heights of 0.1 meters with widths of 0.2 to 1.0 meters.

Interpretation

FA4 is interpreted to represent abandoned channels and oxbow lakes, resulting from channel avulsion. The architectural elements, HO, CW/LA, and CH (OF) are macroforms typically associated with fluvial channel facies (Allen, 1963; Nadon, 1994; Fielding, 2006; Gibling, 2006; Nichols & Fisher, 2007; Miall, 2014). HO macroforms are interpreted to represent channel erosion associated with the initial high-energy pulse during channel formation. CW/LA elements are only moderately developed and, as such, are interpreted to represent the very earliest stages of channel migration, preceding avulsion of the channel. CH (OF) is unique, as the channel macroforms are infilled by fine-grained, silty sediments, which indicate a departure from a typical fluvial dominated sediment deposition to a low energy suspension settling (Erskine *et al.*, 1992; Wolfe *et al.*, 2006). Accordingly, CH (OF) is interpreted as representing abandoned channel infill from overbank fines, derived from other proximal active fluvial channels (Erskine *et al.*, 1992). Pedogenesis indicates a break from fluvial sedimentation and stabilization of the sediment after deposition.

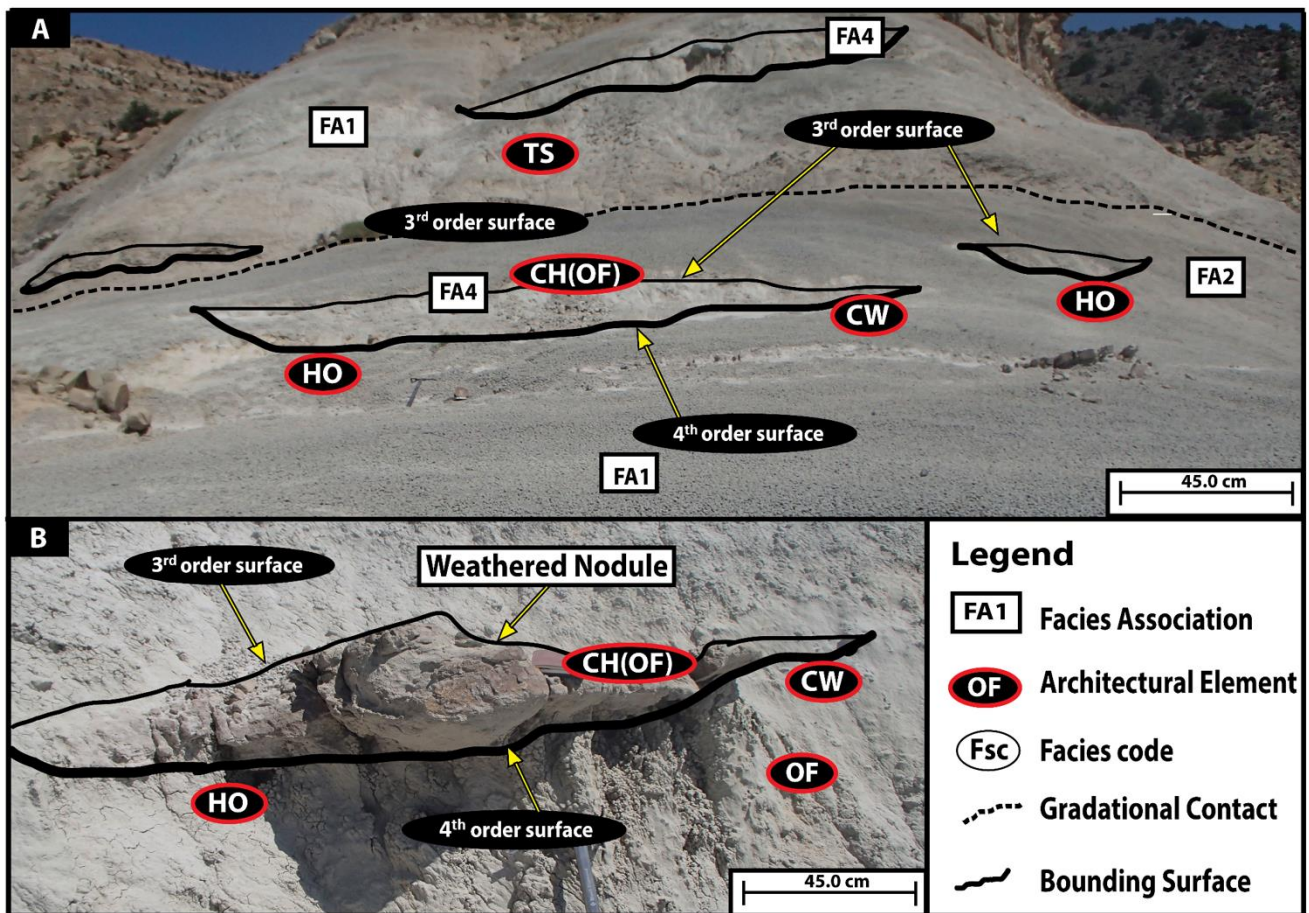


Figure 4.1.4: Figure showing typical features of FA4. (A) Shows occurrence of FA4 in outcrop, highlighting overall morphology and architectural element morphology. (B) Shows exploded view of one silt lens, illustrating erosive basal surface and diffused upper bounding surface. Note nodular weathering indicating incipient pedogenesis. Photographs by Tucker (2016).

4.1.5 Facies Association 5 (FA5): Channel Beds

FA5 is comprised of identified facies codes Sm, Gmx, St, Se, Sr, Sh, Fl, and Sp in descending order. Typically, FA5 weathers to yellowish grey (5Y 8/1), forming characteristic, positively weathering stepped features, with typical unweathered colour characterized as moderate orange pink (5Y 8/4).

The basal bounding surface of FA5 typically exhibits a 4th to 5th order erosional bounding surface, including channel scours and concave up macroforms. The upper bounding surface is characterized by 3rd to 4th order surfaces, including the growth of the channel macroform and lateral accretion development. Beds typically range in thickness between 0.3 and 0.7 meters, and laterally extend between 5.0 and 30.0 meters, commonly pinching out (Fig. 4.1.5.A-D).

Internally, the lower portions of FA5 preserve instances of massively bedded, medium-grained sand units (Sm), 5.0 to 20.0 centimetres thick, infilled by matrix supported, polymictal gravels (Gmx) of quartzite and shale, typically 0.5 to 2.0 centimetres in diameter. Gravels and sands commonly infill macroscale troughs (St), 0.1 to 0.3 meters deep and 1.0 to 5.0 meters across. Troughs also typically exhibit erosional scouring (Se) at the basal bounding surface, with scours incising 1.0 to 5.0 centimetres deep and 5.0 to 15.0 centimetres across. FA5 exhibits well-preserved, asymmetrical, ripple cross-lamination (Sr), angled at 20° to 25°, with foreset thicknesses of 0.5 to 0.8 centimetres, and toe-to-crest heights of 3.0 to 5.0 centimetres. Ripple laminations are commonly interbedded with horizontally bedded units (Sh), exhibiting 1.0 to 4.0 centimetre thick beds (Fig. 4.1.5.C-D). The uppermost portions of FA5 occasionally preserve laminated, muddy silts with lamina 0.3 to 0.6 centimetres thick. The terminal edges of FA5 characteristically exhibit planar cross-bedded units (Sp), presenting with a foreset angle of repose at 15° to 20°, a toe-to-crest height of 10.0 to 20.0 centimetres, and a foreset thickness of 2.0 to 4.0 centimetres (Fig. 4.1.5.C-F). The sediments

of FA5 consists of normally graded coarse sandy litharenites (estimated at 0.03 millimetres), which grade into sandy silts (estimated at 30% sand), with sporadic occurrences of fine silt within the upper portions of the unit (Fig. 4.1.5.C-E).

FA5 preserves four identifiable architectural elements, including scour hollows (HO), channel structures (CH), sandy bedforms (SB), and channel wings/lateral accretions (CW/LA). HO occurs as scoop-shaped hollows downcutting 0.1 to 0.4 meters into the underlying sediment with a lateral extent of 1.0 to 5.0 meters (Fig. 4.1.5.B). CH structures are preserved as planar features, with a maximum thickness ranging from 0.2 to 0.5 meters, and extending laterally for 3.0 to 25.0 meters. SB elements present as 0.2 to 0.4 meter, flat-lying units, typically extending laterally between 2.0 to 10.0 meters. CW/LA are commonly identified as wedge-like structures 0.1 to 0.3 meters thick, with lateral extents of 1.0 to 5.0 meters (Fig. 4.1.5.D).

Interpretation

FA5 is interpreted as representing laterally extensive, meandering channel deposits. The architectural elements preserved within this association, including CH, HO, and CW/LA, are concurrent with the interpretation of meandering channels (Allen, 1963; Nadon, 1994; Fielding, 2006; Gibling, 2006; Nichols & Fisher, 2007; Miall, 2014). HO elements are interpreted as channel erosion associated with the initial high energy pulse, leading to channel development (Cowan, 1992). Extensive LA elements preserved within the channel wings of FA5 are interpreted to represent point and scroll bars, developing with channel migration. CH elements are representative of the actual palaeoriver channel, with the complex interbedded relationships of CH and SB elements indicative of a notable degree of channel sinuosity (Tucker *et al.*, 2017). The complex, yet thinly bedded deposition of many of the elements is indicative of the relatively rapid waxing and waning of energy regimes within FA5.

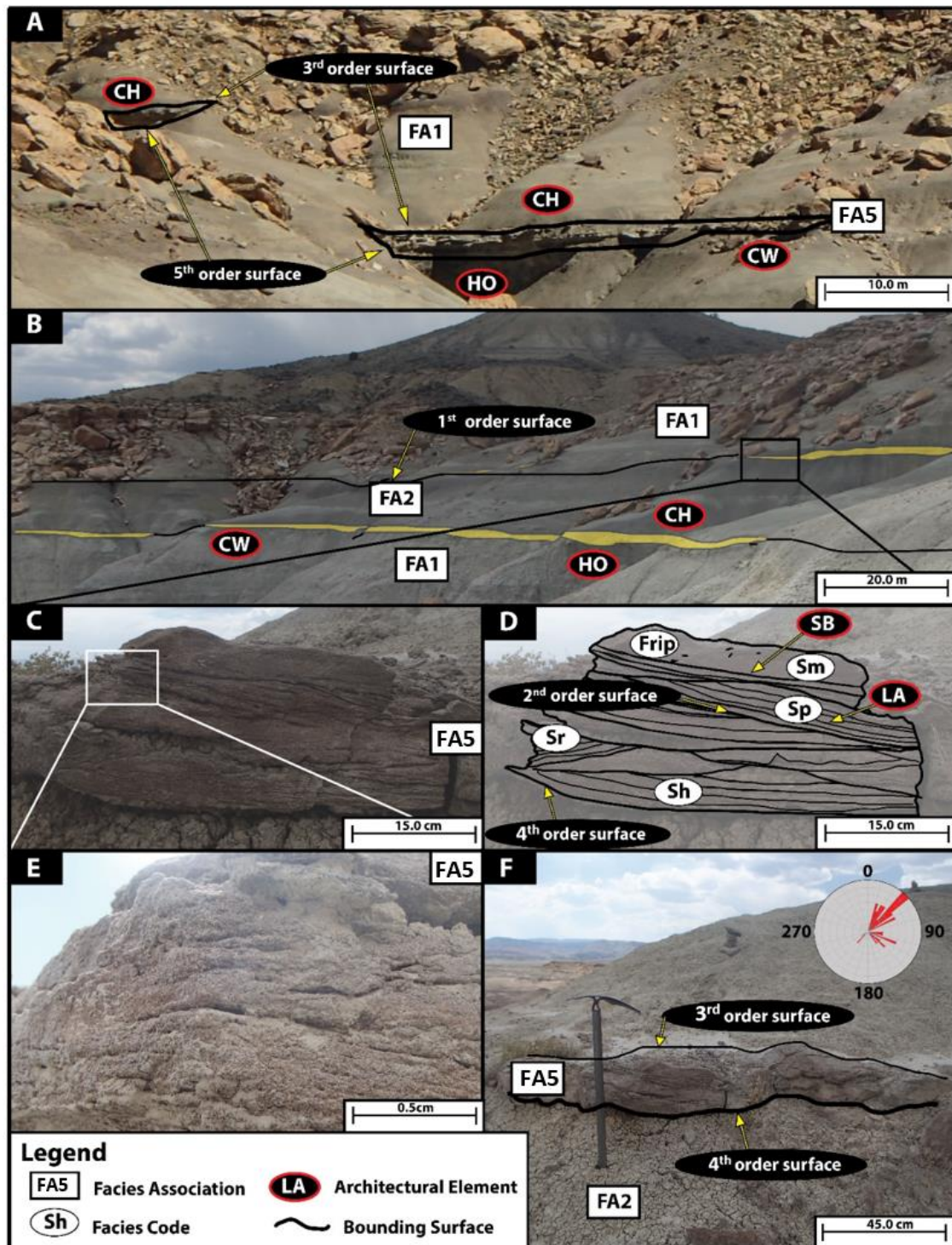


Figure 4.1.5: Photomosaic showing sedimentary features of FA5. (A) Shows strongly developed channels interbedded within the muddy substrate. (B) Shows the massive lateral extents of this facies at specific, stratigraphic intervals, associated with initial channel bifurcation over an extensive channel belt. (C) Shows a well-preserved outcrop of FA5 exhibiting planar cross-bedding, ripple beds, horizontal bedding, and massive bedding. Architectural elements identified include lateral accretions and sandy bedforms. (D) Shows line drawing of the intricately structured facies highlighting internal structure and bounding surfaces. (E) Shows magnified view of the sediment within FA5, illustrating the coarse-grained nature of these deposits. (F) Shows a zoomed-out image of the outcrop, illustrating the basal 4th order and upper 3rd order bounding surfaces with the hosting sediment. Inserted rose diagram represents palaeoflow indicators within FA5. Photographs by Tucker (2016).

4.1.6 Facies Association 6 (FA6): Ephemeral Ponds

FA6 is comprised of identified facies codes Fl, VFc, P, Fr and Fgr in descending order. Typically, FA6 weathers easily to light grey (N8), along with instances of orange (10YR 8/6) discoloration, however, unweathered colour exhibits dark grey (N3) to black (N1) (Fig. 4.1.6).

The basal bounding surface of FA6 commonly exhibits a 1st order gradational bounding surface. The upper bounding surface is commonly 6th order erosive surfaces, demonstrating the characteristic, highly erosive nature of the overlying unit. Beds occur as lenticular bodies, ranging in thickness between 0.2 and 0.6 meters, and laterally extending between 0.6 and 5 meters.

FA6 exhibits an internal structure typified by fine laminations (Fl), ranging in thickness from 0.01 to 0.03 centimetres (Fig. 4.1.6). The topmost portions of the facies preserve characteristically fine clay (VF) units, 3.0 to 7.0 centimetres thick. FA6 exhibits pedogenic features (P), such as (1) the formation of cubic peds, with widths of 2.0 to 3.0 centimetres, (2) nodular weathering, with nodules ranging in diameter of 3.0 to 5.0 centimetres (Fig. 4.1.6.C), and (3) preserved root traces of actinorhizal plants (Fr), showing symbiotic nodules, interpreted to have formed via the bacterium *Frankia* Brunchorst. The internal structure is, however, difficult to accurately contextualize, as the facies commonly exhibits intense soft sediment deformation features, such as pipes, balls, sand volcanoes, and pillar structures, ranging in size from a few millimetres to decimetre scale (Fig. 4.1.6.B, C). FA6 is characterized by basal silty muds (estimated at 25% silt), which typically grade (Fgr) into more clay dominated muds (estimated at 5% silt).

Architectural elements identified within FA6 are limited, with overbank fines (OF) forming the defining architectural element. OF commonly presents as concave up lenticular beds, 0.2 to 0.6 meters thick, and extends laterally for 0.6 to 5 meters before pinching out.

Interpretation

FA6 is interpreted to represent ephemeral wetland ponds. The lack of tractional features within FA6 is indicative of suspension settling within a still standing water body (Erskine *et al.*, 1992; Cooper, 2001; Wolfe *et al.*, 2006). The concave-up morphology of FA5 is indicative of deposition occurring within depositional hollows or lows, forming ponded features. The dark colour associated with orange staining indicates highly reducing, sulphur rich environments, leading to deposition of organic-rich clays (Curtis, 1980). High concentrations of sulphur have long been associated with marine systems due to the formation of dimethylsulphide from the degradation of marine planktonic species (Andreae *et al.*, 1983). The high sulphur content within these ponds is, therefore, interpreted to be derived from oceanic sulphur, indicating a proximal marine system (Love, 1967; Curtis, 1980; Chen *et al.*, 2015). Pedogenesis is evident from the formation of both soil peds and preserved roots, however, the presence of *Frankia* nodules is interpreted to indicate short-lived pedogenesis, as *Frankia* occurs predominantly in young, nitrate poor soils (Jangid *et al.*, 2013). This, along with the limited depositional extent of FA6, is interpreted to represent the relatively short-lived and sporadic nature of these pools. Furthermore, *Frankia* has been shown to preferentially grow in soils with a temperature of 30⁰ to 35⁰ centigrade, indicating an overall warm climate during deposition (Burggraaf & Shipton, 1982).

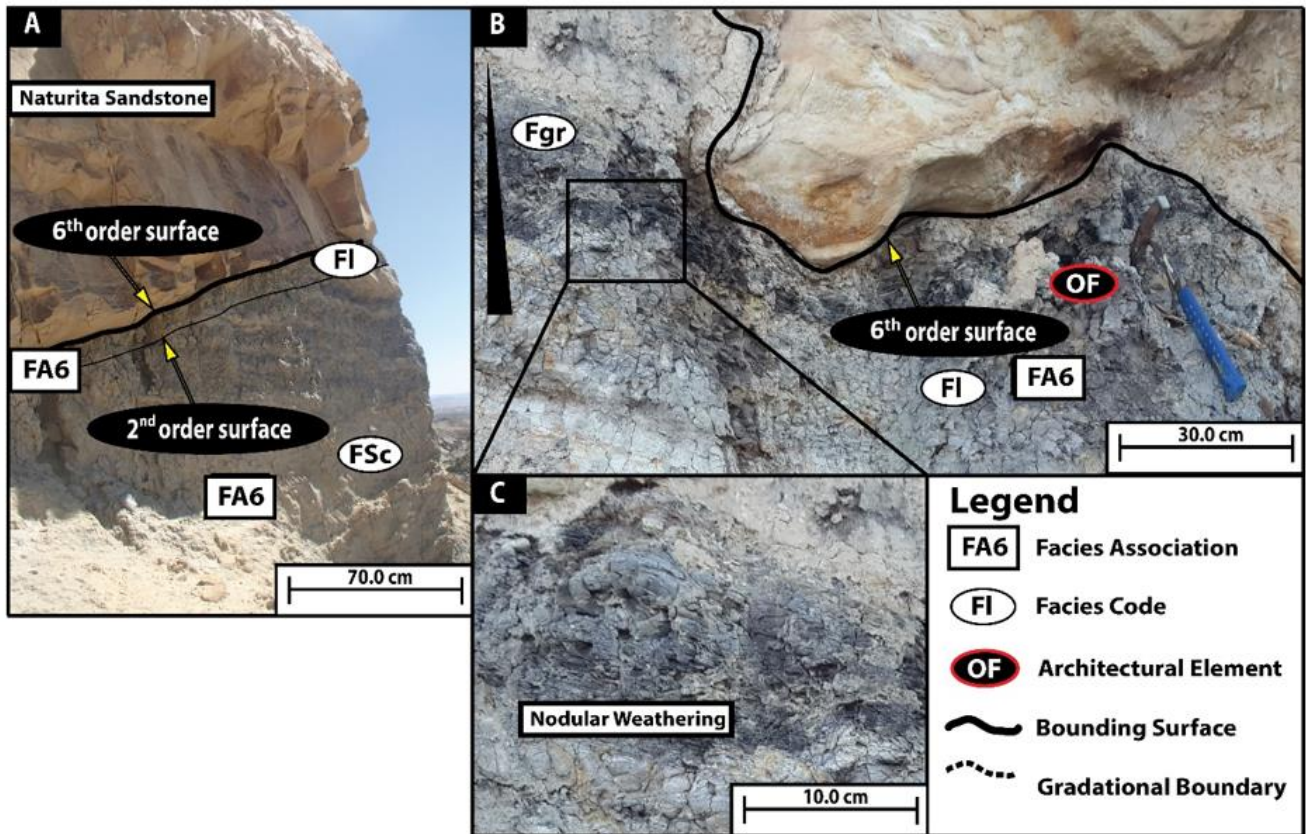


Figure 4.1.6: Figure showing typical features of FA6. (A) Shows typical 2nd order contact with underlying facies associations, along with a shift from massive to laminated structure. (B) Shows laminated structure along with black sediment color and orange discoloration. Note the extremely erosive 6th order upper bounding surface. (C) Shows example of nodular weathering within FA6. Photographs by Tucker (2016).

4.2 Stratigraphy

The Cedar Mountain Formation has been previously described as following typical layer cake stratigraphic sedimentation patterns (Kirkland *et al.*, 1999; Kirkland, 2005). This has, however, been shown to be erroneous, specifically with the Mussentuchit Member exhibiting notable lateral variations in sediment type and depositional patterns (Sorensen, 2011; Holmes, 2017; Kirkland *et al.*, 2017). To contextualize the Mussentuchit Member specifically, seven transects representing the upper Ruby Ranch until the contact with the overlying Naturita Sandstones were analysed in-field via lithological and facies analysis, as prescribed by Reading (1996) and Miall (1985, 2016), respectively. See Appendix for stratigraphic columns of field site transects.

4.2.1 Litho-stratigraphy

The Ruby Ranch Member of the Cedar Mountain Formation directly underlies the Mussentuchit Member. The member commonly forms a gradational to sharp, 2nd to 3rd order contact with the overlying unit. The Ruby Ranch Member typically presents in outcrop as steeply dipping slopes of fine-grained sediments, with the surface littered with numerous, red weathering carbonate nodules. Coarse-grained, sandy lenses are common, forming step-like features at regular intervals throughout the member. The Ruby Ranch Member shows a highly variable thickness throughout the stratigraphy of Mussentuchit Wash, ranging in thickness from 20.0 to 40.0 meters (Fig. 4.2.1; 4.2.2).

The Short Canyon Member is only locally developed within the study area, unconformably overlying the Ruby Ranch with a 5th order basal bounding surface where developed. The Short Canyon Member is, in turn, locally conformably overlain by the Mussentuchit Member with a 4th order boundary. The Short Canyon Member consists predominantly of litharenitic sands with pebble-sized clasts of quartzite and chert. The unit occurs as discontinuous, lenticular beds with thicknesses ranging between 0.4 and 1.0 meters and lateral extents of 5.0 to 10.0 meters (Fig. 4.2.1).

The Naturita Formation directly overlies the Mussentuchit Member, forming a characteristic 6th order erosive bounding surface with the underlying Cedar Mountain Formation. The Naturita Formation presents in outcrop as a highly competent, cliff-forming bed of interbedded, coarse- to fine-grained quartz litharenites and polymictal gravel lags. The upper contact of the Naturita Sandstone has been eroded, however, the unit shows a minimum thickness of 3.5 meters (Fig. 4.2.1; 4.2.2).

The Mussentuchit Member is well developed throughout the study area, with member thicknesses ranging from 25.0 meters in the southwest to 20.0 meters in the northeast. The member shows little variation within the study area, save for a slight thickening towards the

northeast from 20.0 to 25.0 meters (Fig. 4.2.3). One exception to this are the units in the western portions of the study area, which are positioned approximately 10 meters lower than the units in the rest of the study area (Fig. 4.2.4). This change in stratigraphic height is interpreted to represent a westerly dipping monocline accompanied with minor faulting. Due to the fine-grained nature of the sediments and intense surficial weathering, no actual folded or accompanying fault structures were identified in the sediments. The lateral position of the inferred monocline, however, corresponds to a series of minor, northeast trending faults, which were identified within the southernmost transect. At this transect, a normal fault was identified cross-cutting the Buckhorn Conglomerate Member. This was evident through the co-occurrence of prominent slickenside structures and a notable repetition of the member at two, stratigraphically close exposures.

Greenish grey, interbedded units of silts and muds (FA1) predominantly characterize the sediments of the Mussentuchit Member. These muds host various sedimentological features including: (1) purple vertisol beds (FA2), 0.5 to 0.7 meters thick, extending laterally for 50.0 to 600.0 meters, (2) finely cross-laminated silty lenses (FA3), 0.2 to 0.4 meters thick, extending laterally for 6.0 to 30.0 meters, (3) fine- to coarse-grained, massively bedded silt lenses (FA4), 0.2 to 0.6 thick, extending laterally for 5.0 to 10.0 meters, (4) sandy ribbons (FA5), 0.2 to 0.6 meters thick, extending laterally for 5.0 to 30.0 meters, and (5) black, carbonaceous mud lenses (FA6), 0.2 to 0.6 meters thick, extending laterally for 0.6 to 5.0 meters. Both sandy ribbons and palaeosols are especially prevalent within the lower portions of the Mussentuchit Member. Conversely, the upper portions show a prevalence of light green to grey interbedded mudstones and siltstones, along with multiple occurrences of gravely, silty lenses (Fig. 4.2.3; 4.2.4).

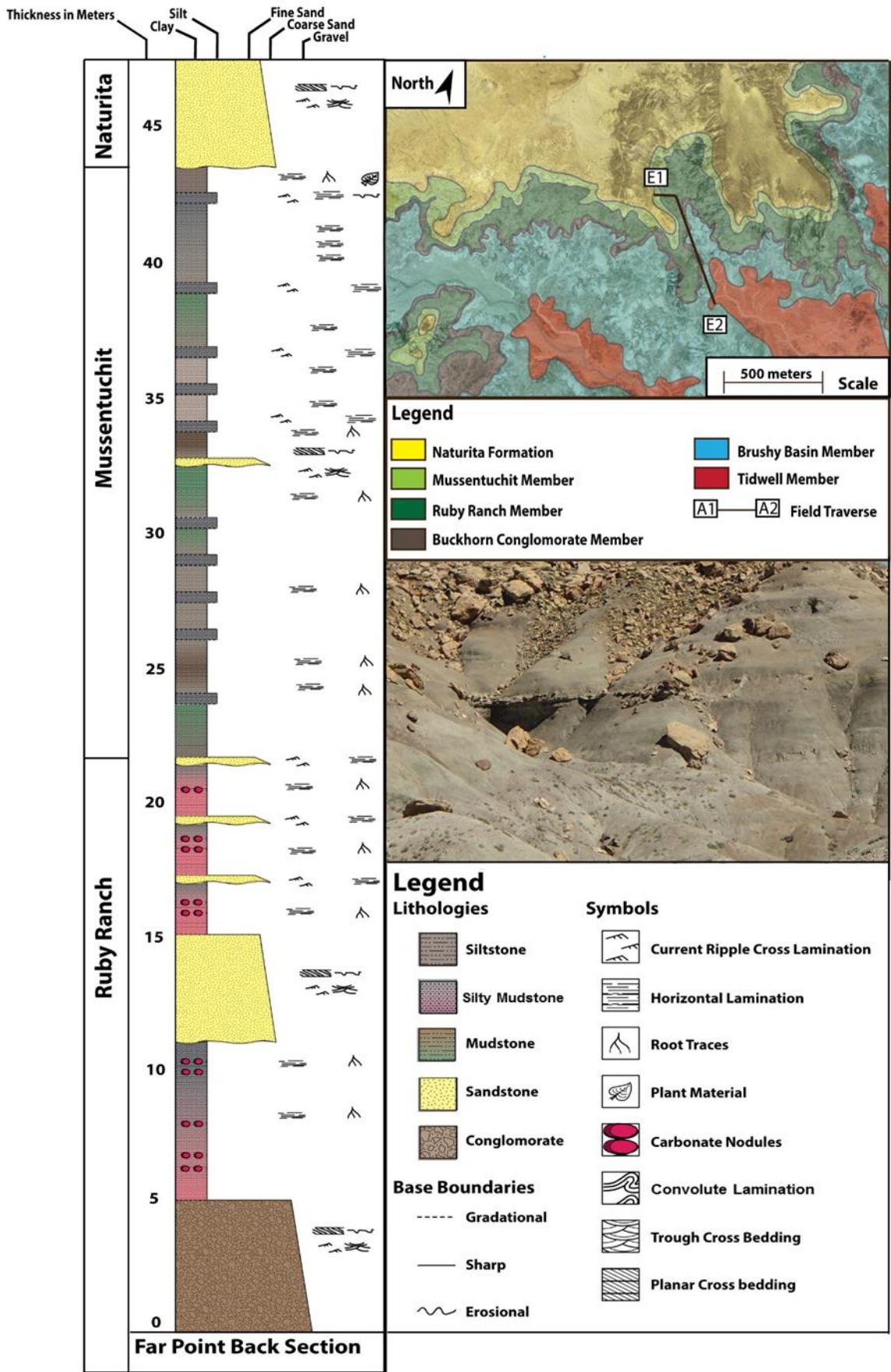


Figure 4.2.1: Figure showing stratigraphic column of the Far Point field transect. Photo insert illustrates coarse sandy units interbedded within silty muds. Photograph by Tucker (2016). Map modified from Google Earth ESRI Satellite Image

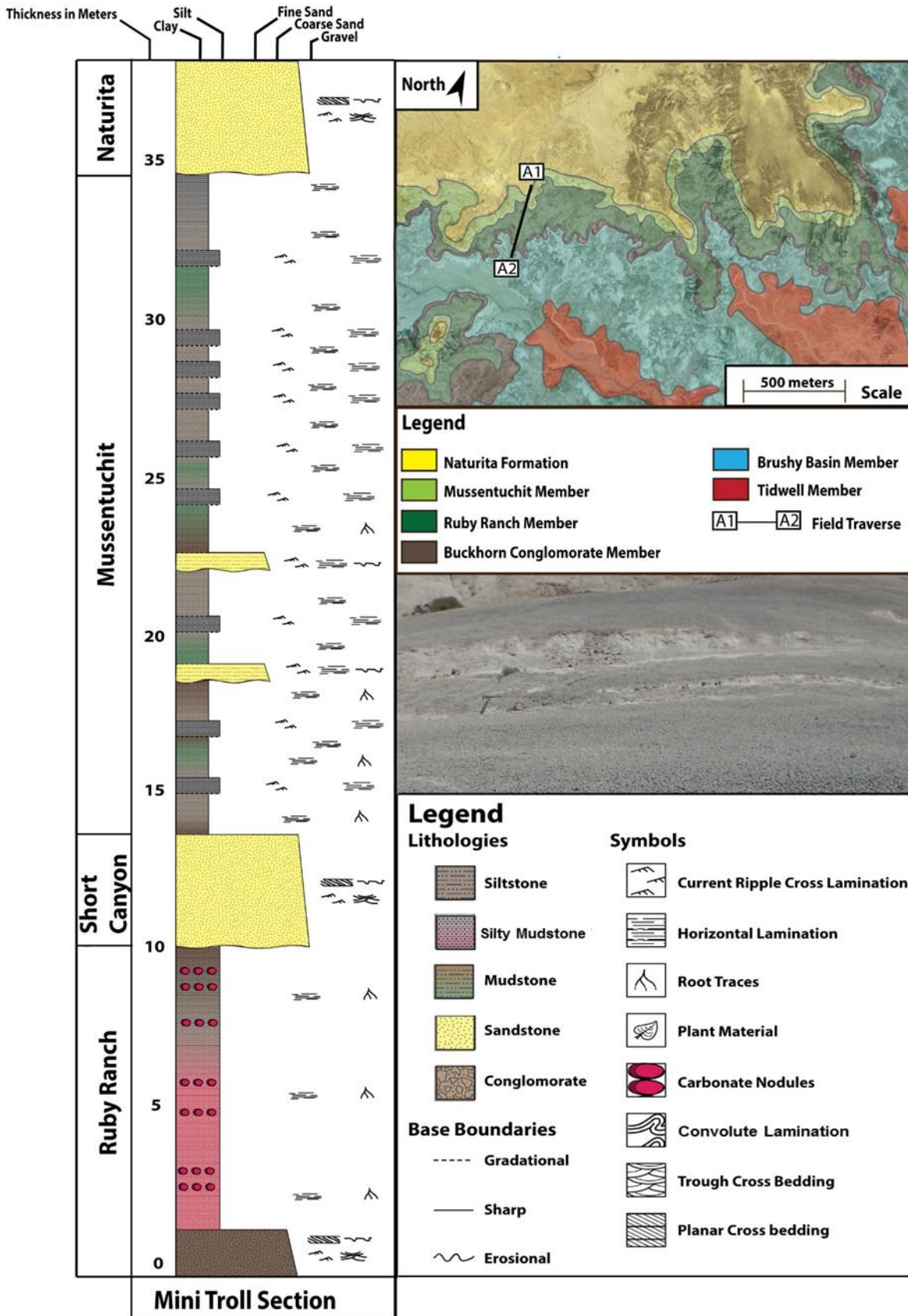


Figure 4.2.2: Stratigraphic column of the Mini Troll field transect. Note singular occurrence of the Short Canyon Member. Photo insert illustrates coarser silty lenses interbedded within the muddier succession. Photograph by Tucker (2016). Map modified from Google Earth ESRI Satellite Image.

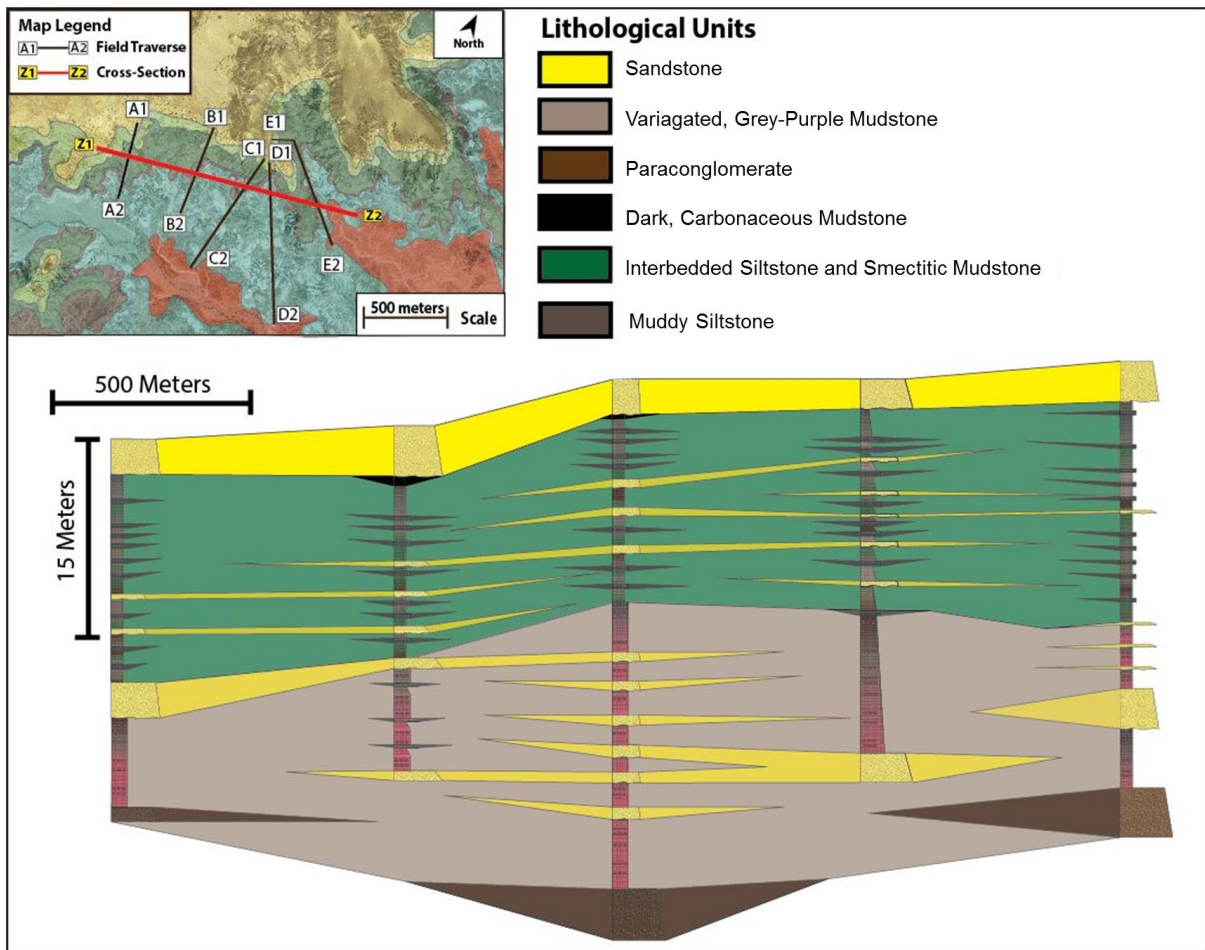


Figure 4.2.3: Cross-section on Z1 to Z2 showing position of the Mussentucht Member and lithological units therein. Note overall increase in elevation of units within the mid-western portions of the study area. Map modified from Google Earth ESRI Satellite Image.

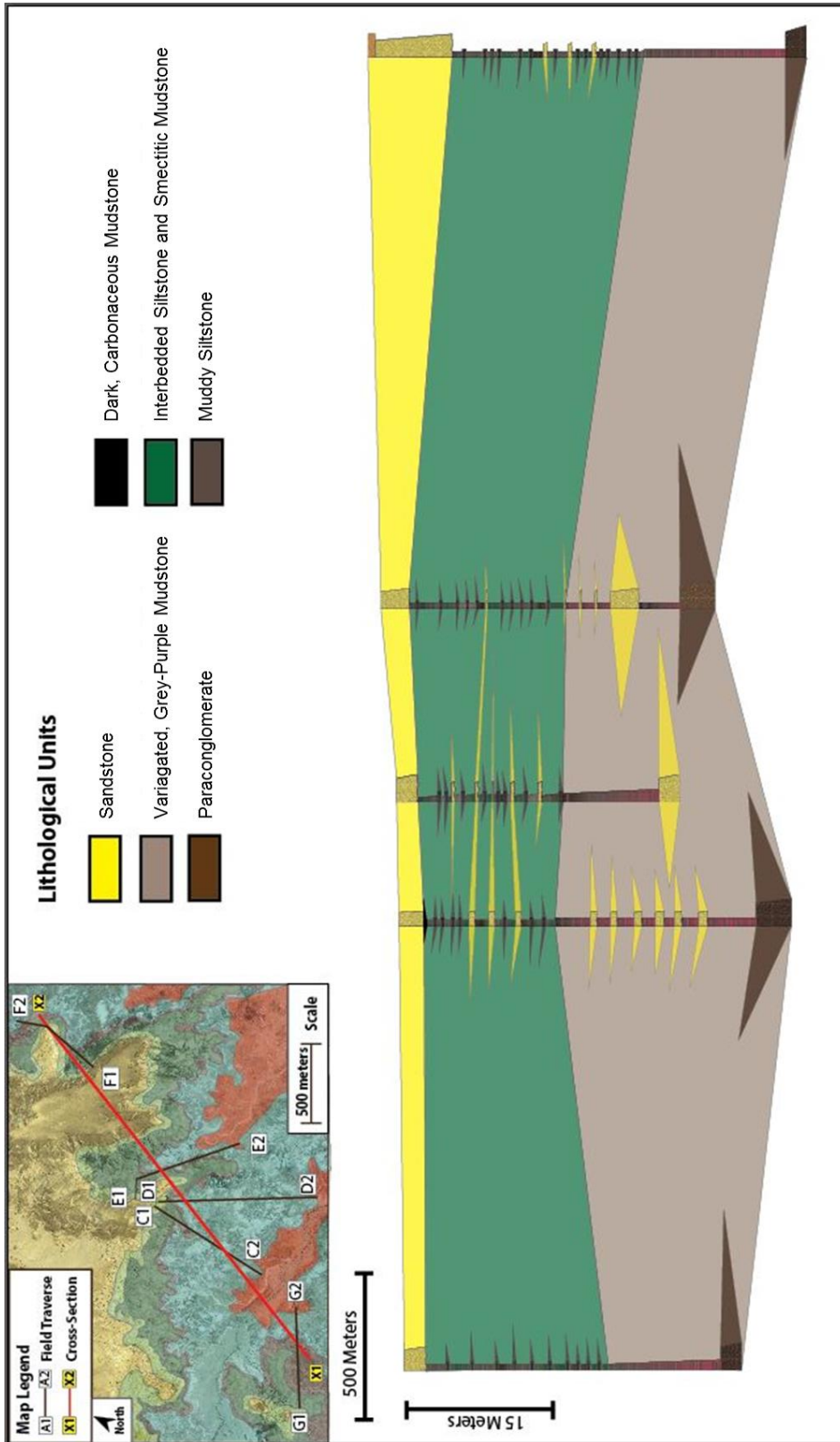


Figure 4.2.4: Cross-section on X1 to X2 showing stratigraphic position of the Mussettuchit Member and lithological units therein. Note overall increase in elevation of units within the mid-southern portions of the study area, as well as the decrease in stratigraphic elevation in the northern portions of the study area. Note the increased thickness of the Mussettuchit in the northern portions of the study area. Map modified from Google Earth ESRI Satellite Image.

4.2.2 Facies Stratigraphy

FA1 consists of vertically stacked, repeating couplets of muddy silts and silty muds representing tidal mudflats. This unit is especially well-developed within the upper portions of the Mussentuchit stratigraphy and around the southwestern and northeastern portions of the study area. FA1 is only moderately-well developed within the lower portions of the Mussentuchit stratigraphy, with units reaching thicknesses of 3.0 to 6.0 meters. FA1 is interbedded with other lithological units within the lower Mussentuchit, resultantly limiting the lateral continuity of the unit to 50.0 to 100.0 meters (Fig. 4.2.6; 4.2.7). Occurrences of FA1 within the middle portions of the Mussentuchit show a slightly higher level of pedogenesis, as evident from a notable greenish discoloration as well as more pronounced pedogenic fracturing. FA1 is slightly less developed within the middle Mussentuchit, only reaching thicknesses of 3.0 to 6.0 meters and lateral extents of 30.0 to 60.0 meters. FA1 is best developed within the upper portions of the Mussentuchit, with couplet successions reaching thicknesses of 6.0 to 10.0 meters. Most notable is the lateral extent of this facies association within the upper Mussentuchit, as stratigraphically co-occurring units can form laterally continuous successions extending from 100.0 to 900.0 meters (Fig. 4.2.6; 4.2.7).

FA2 consists of purple vertisol successions and is best developed within the lower to middle portions of the Mussentuchit Member. The southern- and western-most sections of the study area show the highest occurrence of FA2, while the central portions show the lowest occurrence (Fig. 4.2.6; 4.2.7). FA2 commonly occurs in association with channel deposits showing thicknesses of 2.0 to 4.0 meters and limited lateral extents of 20.0 to 50.0 meters, especially within the lower portions of the Mussentuchit. Units of FA2 within the lower Mussentuchit are also commonly down-cut by other, coarser-grained sediments, resulting in limited preservation of the actual palaeosol surface. FA2 is best developed within the middle portions of the Mussentuchit stratigraphy, with units of FA2 typically occurring with a

thickness of 2.0 to 5.0 meters. The most notable feature, however, is the many vertisol sequences occurring adjacent to each other, which form a continuous horizon which extends laterally for 100.0 to 600.0 meters. The upper portions of the Mussentuchit stratigraphy show the lowest developmental prevalence of FA2, with only localized occurrences of 2.0 to 3.0 meters thick and 10.0 to 30.0 meters wide present here (Fig. 4.2.6; 4.2.7).

FA3 is defined by gravely silt lenses, typically associated with crevasse splays, and is best developed within the geographical central portions of the study area. FA3 is moderately to well developed within the lower portions of the Mussentuchit stratigraphy, commonly occurring in close lateral proximity to sandy lenses or ribbon sandstones (Fig. 4.2.2; 4.2.6; 4.2.7). The number of occurrences of FA3 increases further up section; however, the overall unit thicknesses decrease from 4.0 - 6.0 meters to 2.0 - 3.0 meters, along with decreasing lateral extents of the units from 15.0 - 20.0 meters to 10.0 - 15.0 meters. FA3 is moderately to poorly developed within the middle portions of the Mussentuchit, typically occurring within the uppermost portions of the palaeosol sequences of FA2 or directly above them. The upper Mussentuchit shows the highest developmental prevalence for FA3; however, in addition to smaller unit geometries, the sediment size fines from sandy silts to muddy silts and shows a notable decrease in gravel content. Overall, instances of FA3 do not show a visible developmental pattern, save for a slightly higher concentration at specific stratigraphic intervals and around coarser-grained units (Fig. 4.2.6; 4.2.7).

Finely laminated silty lenses associated with abandoned channel deposits define FA4. FA4 is best developed within the upper portions of the Mussentuchit Stratigraphy and shows little to no geographically controlled deposition patterns across the study area (Fig. 4.2.6; 4.2.7). Though moderately-well developed within the lower portions of the Mussentuchit, occurrences of this unit are moderately scarce and typically form units 0.2 to 0.4 meters thick, which extend laterally for 3.0 to 6.0 meters. FA4 occurs predominantly at random intervals,

however, the unit does show a slight developmental preference around sandy ribbons and sandy to gravely lenses. FA4 is notably absent within the middle portions of the Mussentuchit and re-occurs above the well-developed palaeosol horizon of FA2. Though FA4 occurs more frequently within the upper Mussentuchit, the unit shows an overall decrease in size and coarseness, with occurrences limited to muddy silt units, 0.2 to 0.3 meters thick with lateral extents of 2.0 to 4.0 meters (Fig. 4.2.6; 4.2.7).

FA5 is defined by litharenitic sandy bedforms, which preserve numerous current induced structures and represents preserved palaeochannels. FA5 is best developed within the lower portions of the Mussentuchit stratigraphy and in some areas, forms the basal contact with the underlying Ruby Ranch Member (Fig. 4.2.6; 4.2.7). Though the occurrence of this basal sandy layer is common in the area, it is not the quintessential member contact. The southern- and western-most portions of the study area show a notable lack of FA5, while the central portions of the study area show the highest prevalence of this facies assemblage. Occurrences within the lower portions of the Mussentuchit commonly range in thickness from 4.0 to 7.0 meters with lateral extents of 20.0 to 30.0 meters. Units of FA5 additionally occur at similar stratigraphic positions, with laterally co-occurring units forming ribbon-like units extending up to 800 meters (Fig. 4.2.6; 4.2.7). FA5 is still present within the middle portions of the Mussentuchit Member, commonly forming directly above, and incising into, the notably developed palaeosols of FA2. FA5 rarely occurs within the upper Mussentuchit and when present, only occurs as thin, fine-grained sandy beds showing a maximum thickness of 0.4 meters. The lateral co-occurrences of FA5 units are also limited within the middle and upper portions of the Mussentuchit. Resultantly, the laterally extensive, ribbon-like sandstone units are notably scarce within the upper Mussentuchit (Fig. 4.2.6; 4.2.7).

FA6 is defined by darkly coloured, organic rich muddy lenses and is representative of ephemeral water bodies. FA6 is only developed within the uppermost portions of the

Mussentuchit Member and is notably absent within the northeastern portion of the study area (Fig. 4.2.6; 4.2.7). FA6 is only partially preserved, as the overlying Naturita Sandstone deeply incises into the upper portions of the Mussentuchit, deeply eroding exposures of FA6. Consequently, preservation of FA6 is limited, precluding accurate measurements of this facies association. There appears to be no change in FA6 across the study area where developed.

4.2.3 Lower, middle and upper Mussentuchit

The Mussentuchit Member exhibited slight differences in both modal proportions and the co-occurrence of certain facies assemblages at specific points within the member stratigraphy. This study, therefore, separated the Mussentuchit Member within three discrete portions, identifiable through the different proportions and occurrence of key lithological features. This enabled this study to further constrain the multiple fossil preservation sites located throughout the Mussentuchit stratigraphy.

The lower Mussentuchit is comprised of facies assemblages FA1, FA2, FA5, FA3, and FA4 in order of abundance, and ranges in thickness from 5.0 to 8.0 meters (Fig. 4.2.6; 4.2.7). The basal contact of the lower Mussentuchit is characterized by 3rd order bounding surfaces, where FA1 and FA2 are present, and 5th order bounding surfaces, where FA5 incises into the underlying Ruby Ranch Member. Though FA1 comprises the dominant facies assemblage within the lower Mussentuchit, it only forms approximately one-third of the stratigraphy. More notable than the silty sequences of FA1, is the presence of the sandy ribbons of FA5, which extend laterally for up to 600.0 meters. Facies associations FA3 and FA4, commonly concentrated near the sandy beds of FA5. FA2 occurs at random stratigraphic intervals within the lower Mussentuchit, however, shows a slight tendency to concentrate around occurrences of FA4 and FA5. The upper stratigraphy of the lower Mussentuchit shows a slight increase in the proportion of FA1, before being conformably

overlain by a notably well-developed palaeosol horizon (Fig. 4.2.6; 4.2.7). The lower Mussentuchit is host to the Fortunate Son fossil quarry, which forms one of the basal-most fossil preservation sites within the area.

The middle Mussentuchit is characterized by a well-formed palaeosol horizon and consists of FA2, FA4, FA1, FA5, and FA3 in order of abundance. The middle Mussentuchit ranges in thickness between 1.0 and 3.0 meters and shows a 2nd order basal bounding surface with the lower Mussentuchit. FA2 comprises approximately two-thirds of the lithologies presents within the stratigraphy, clearly making it the dominant facies assemblage. Though FA4, FA1, and FA3 are present at certain intervals throughout the middle Mussentuchit, they are predominantly developed within the uppermost portions of the middle Mussentuchit. FA5 is present only within the uppermost portions of the middle Mussentuchit, and typically marks the contact with the overlying upper Mussentuchit.

The upper Mussentuchit is characterized by a distinct dominance of FA1 and is comprised of FA1, FA2, FA4, FA3, FA6, and FA5 in order of abundance. The upper Mussentuchit ranges in thickness between 5.0 and 10.0 meters and shows a 3rd to 5th order basal contact with the underlying middle Mussentuchit (Fig. 4.2.6; 4.2.7). FA1 comprises approximately two-thirds of the stratigraphy of the upper Mussentuchit, with the other facies assemblages, save for FA6, occurring at random stratigraphic points throughout the upper Mussentuchit. FA1 is best developed within the lower to middle portions of the upper Mussentuchit, while FA2, FA3, and FA5 become more prominent within the topmost portions of the upper Mussentuchit. FA6 is only present within the topmost portions of the upper Mussentuchit and typically occurs near the upper 6th order bounding surface with the overlying Naturita Formation (Fig. 4.2.6; 4.2.7). The Mini Troll and Suicide Hill fossil quarries are preserved within the upper Mussentuchit.

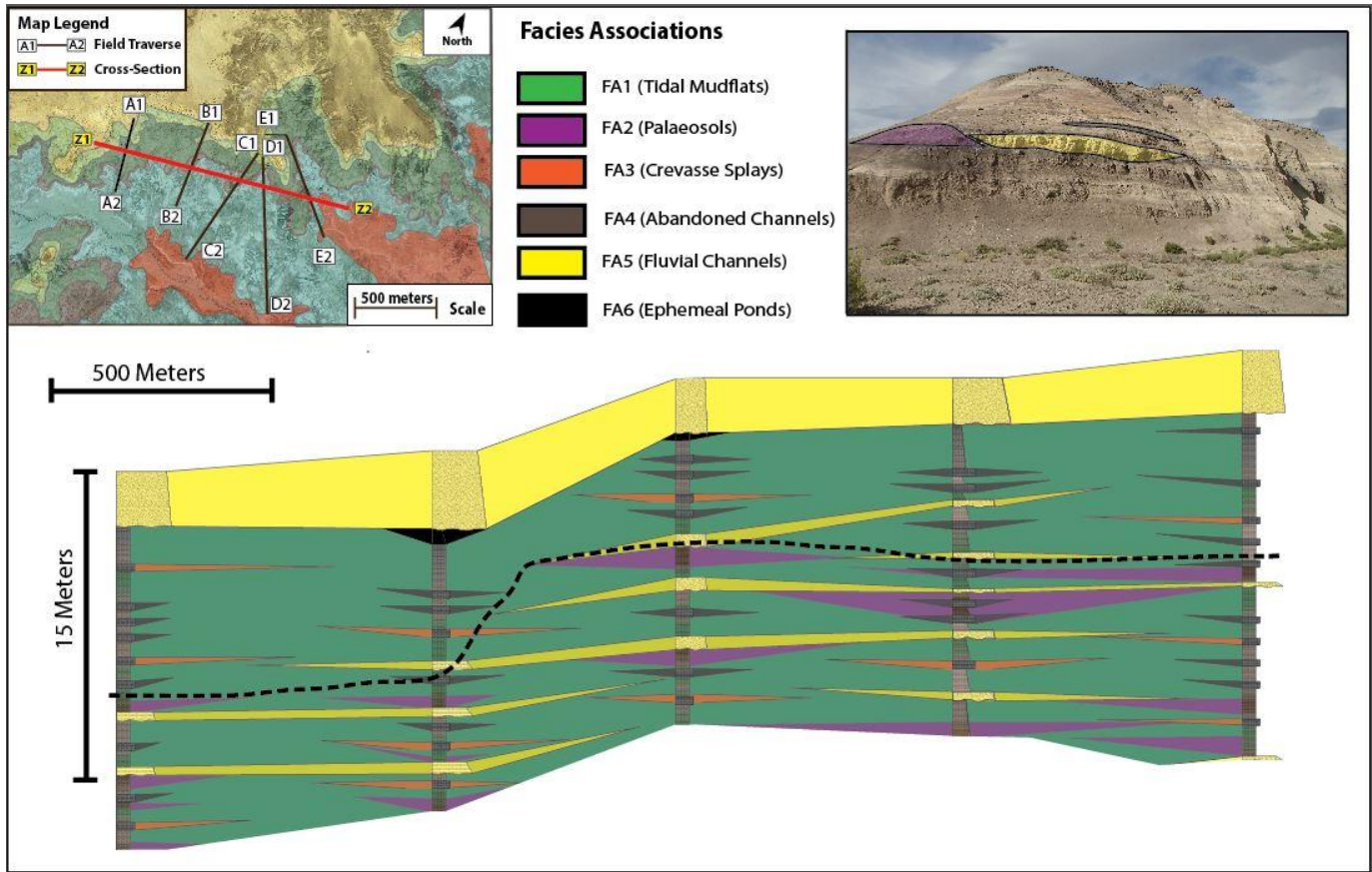


Figure 4.2.5: Cross-section from Z1 to Z2 showing major facies associations within the Mussentuchit Member. Note black, dashed line representing the border between the lower and upper Mussentuchit. Photographs by Tucker (2016). Map modified from Google Earth ESRI Satellite Image.

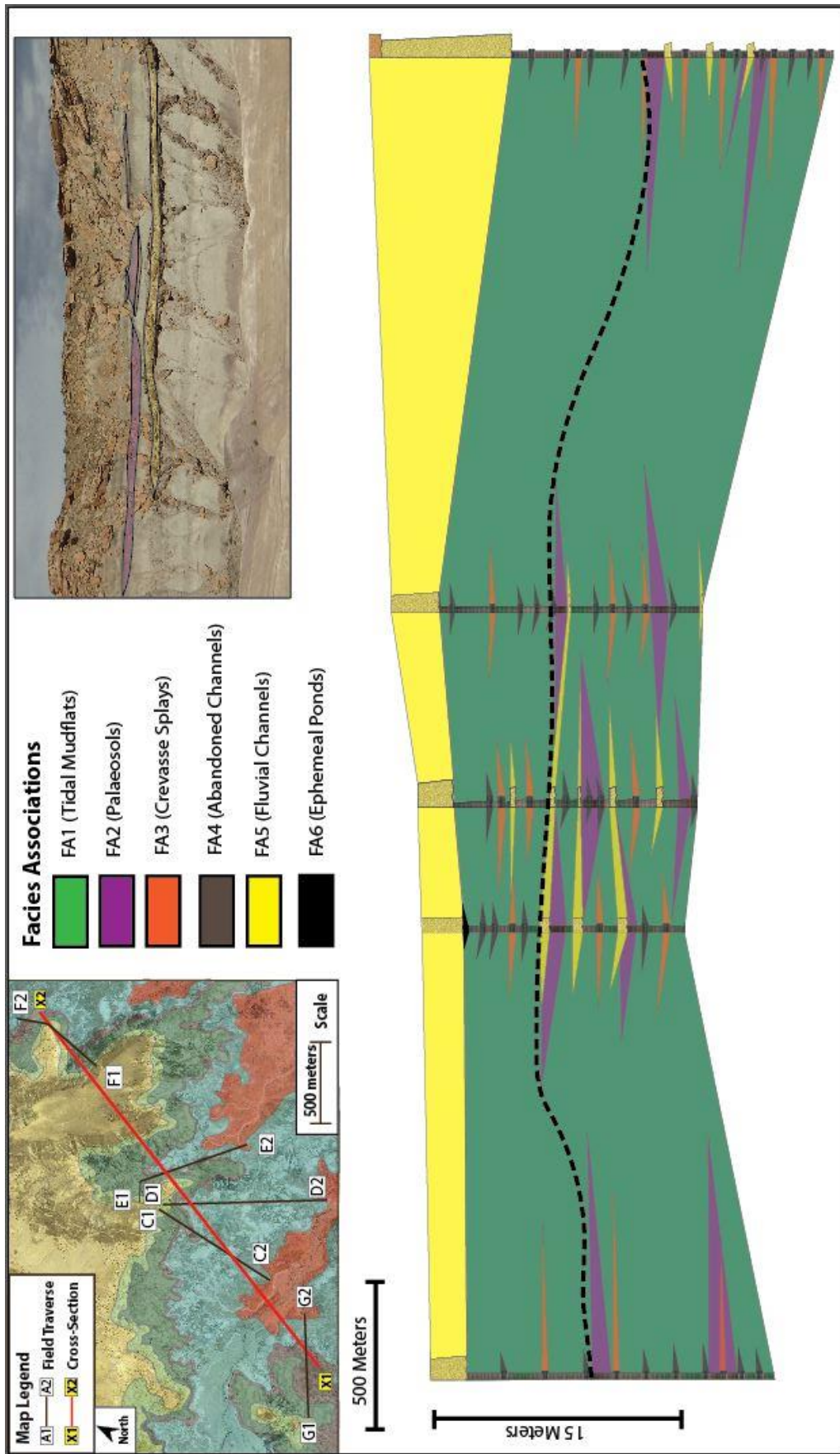


Figure 4.2.6: Cross-section from X1 to X2 showing major facies associations within the Mussentuchit Member. Note the black, dashed line denoting the border between the lower and upper Mussentuchit. Photographs by Tucker (2016). Map modified from Google Earth ESRI Satellite Image.

4.2.4 Palaeocurrents

Throughout the study area, depositional palaeocurrents were determined via the measurement of tractional derived structures such as ripple cross lamina and planar cross-beds. This was undertaken to determine the depositional flow patterns as they changed with the environmental evolution of the Mussentuchit. In total, one hundred and sixteen (116) palaeocurrent readings were taken from the base of the Mussentuchit up to the basal units of the overlying Naturita Sandstone beds (Fig 4.2.7).

Multiple sandstone ribbons, each yielding many palaeocurrent indicators, characterize the basal and lower portions of the Mussentuchit Member. These include planar cross-beds, cross-laminations, and parting lineations. This led to the identification of 5 main current trends including (1) a 5° - 55° north-easterly trend, (2) a 95° - 130° south-easterly trend, (3) a 210° - 250° south-westerly trend, (4) a 265° - 270° westerly trend, and (5) a 285° - 315° north-westerly trend. The dominant directional trend points north-east, indicating that this is the primary depositional direction with approximately 50° of directional swing. The north-westerly and south-easterly trends represent the lateral accretions associated with the main palaeoflow direction. The south-easterly trend also constitutes a secondary palaeoflow direction, with some of the north-eastern flow indicators and the south-western flow indicators representing the lateral accretion associated with the south-eastern palaeocurrent. The trend pointing west represents the apparent dips of the north-western and south-western flow indicators when measured on outcrop facing due south.

Conversely, the upper portions of the Mussentuchit show fewer occurrences of sandstone bodies with limited palaeocurrent indicators, including poorly developed planar cross-bedding and cross-laminations. Palaeocurrent readings derived from these structures showed deposition occurring in a predominantly southeast-easterly (95° - 115°) direction. Multiple subordinate directional trends are also present including (1) a 15° - 25° north-north-

easterly trend, (2) a 285°-300° northwest-westerly trend, (3) a 165°-210° southern trend, (4) a 260°-275° westerly trend, and (5) a 325°-335° north-north-westerly trend. The north-north-easterly and southern palaeocurrent trends represent the lateral accretions associated with the primary easterly palaeocurrent. A portion of the current indicators from the southeast-easterly trend and those from the east-north-easterly trend represent lateral accretion indicators for palaeoflow in the north-easterly direction. The western and north-north-western palaeocurrent trends represent apparent palaeocurrent indicators on rock outcrops facing due south and north-east respectively. (Fig 4.2.7).

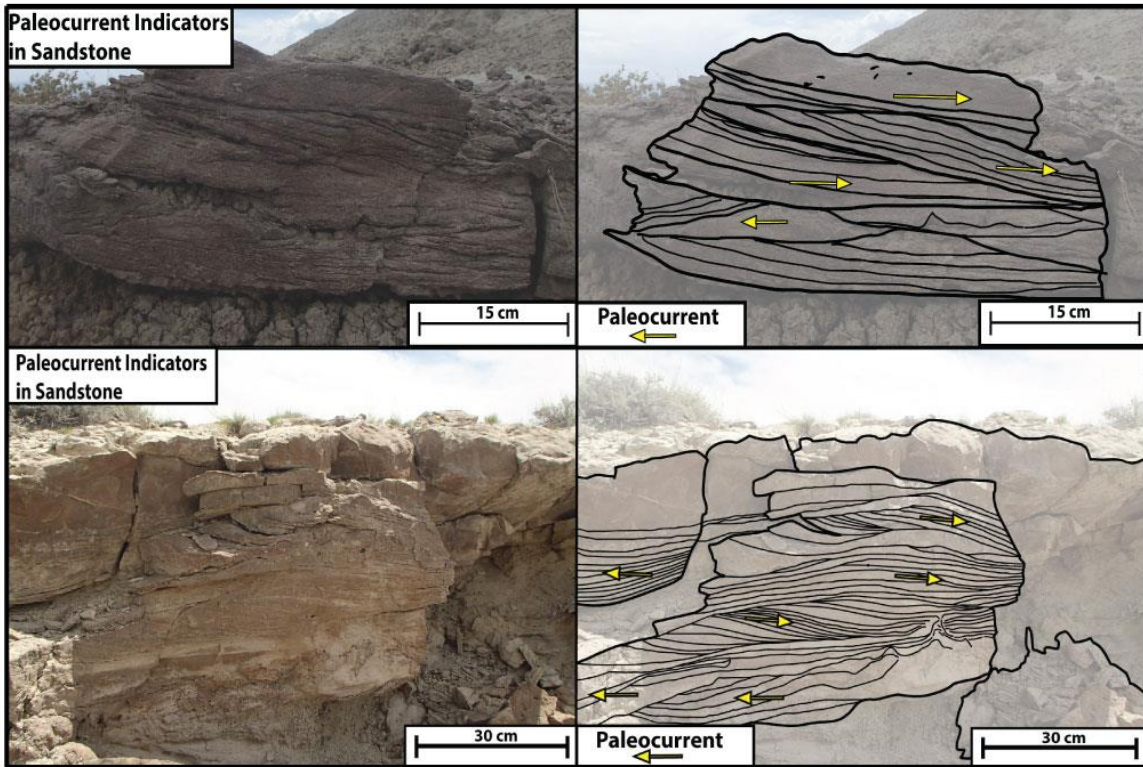
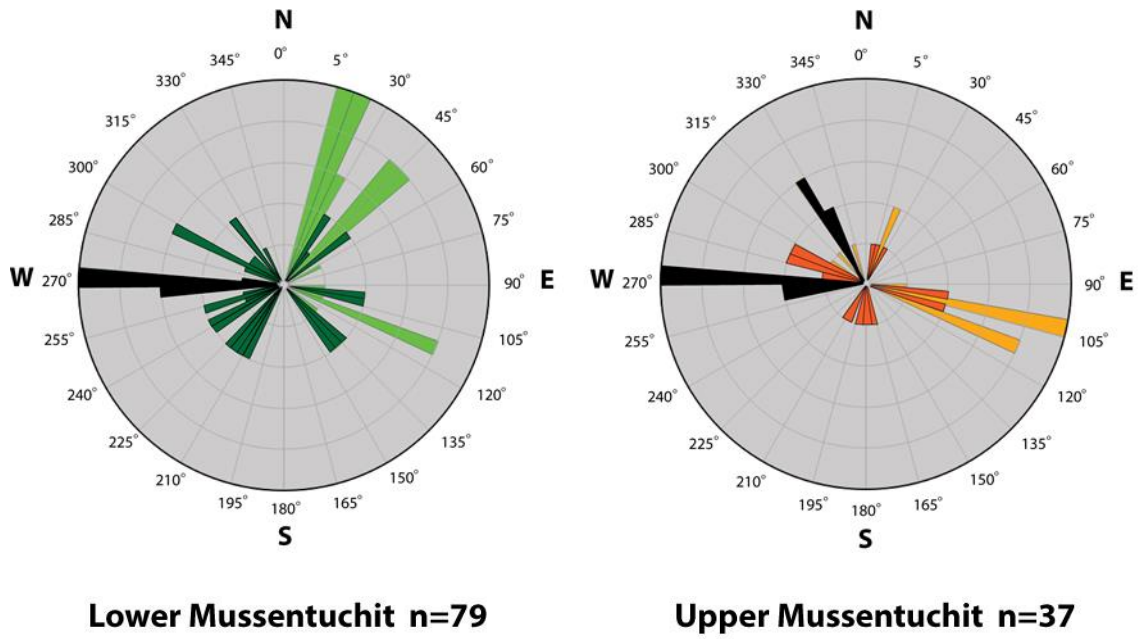


Figure 4.2.7: Rose diagrams illustrating palaeocurrent directions within the lower and upper Mussentuchit. Photo line sketches highlight palaeocurrent indicators and directions. Photographs by Tucker (2016).

4.2.5 Environmental Model

The stratigraphic results show that the Mussentuchit Member is comprised of numerous distinct lithological units. These units do not only vary laterally, but also vertically, indicating a change in depositional environment with time. These vertical changes are especially notable within the distinction between the lower and upper Mussentuchit. To visualize and better contextualize this variable environment, this study created a 3-dimensional block illustration of the environment (Fig. 4.2.8). This illustration shows the overall change in depositional environment with stratigraphic height, as well as incorporating the different lithological elements into a single depositional environment. Considering the dominant tidal facies in the stratigraphy, the environment is envisioned to represent a tidal delta. Accordingly, the Changjiang river delta was chosen as a depositional proxy for this reconstruction as it represents a flooded tidal delta with interchannel tidal flats, stable interchannel mounds, and channelized features. The fossil localities at the study area were placed within their respective environmental positions within the overall depositional area.

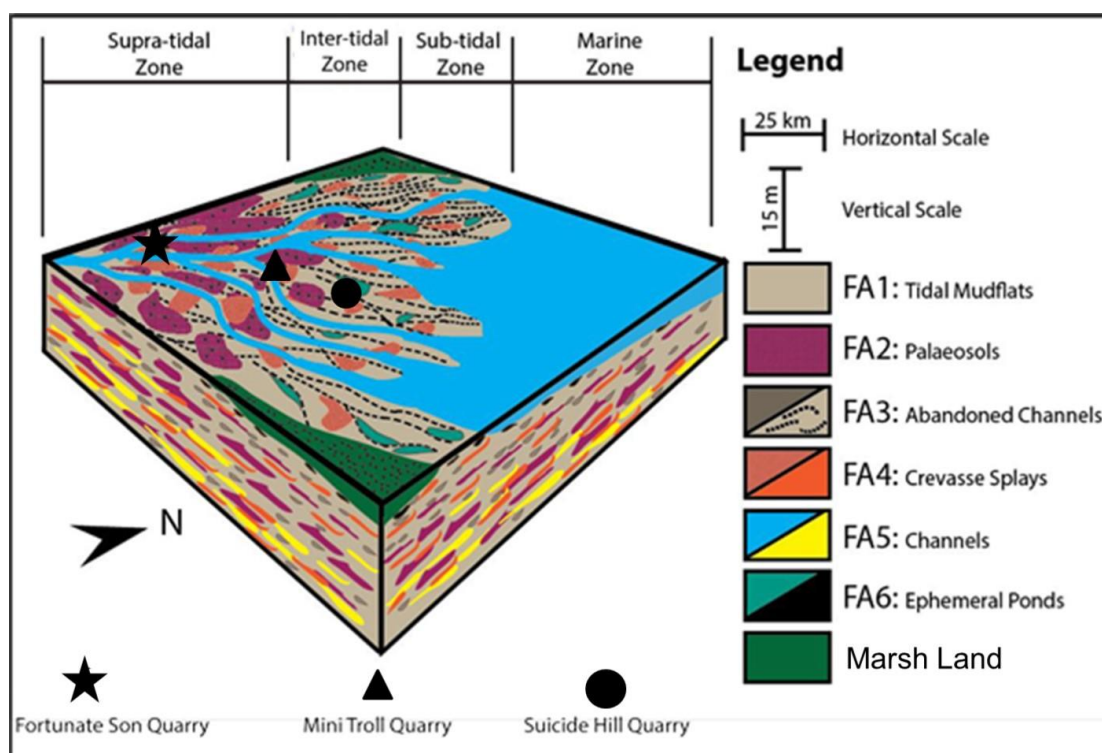


Figure 4.2.8: 3-D block diagram showing the depositional environment of the study area, modeled after a tide dominate river delta as described by Dalrymple & Choi (2007).

4.3 $^{206}\text{Pb}/^{238}\text{U}$ Detrital Zircon Analysis

During this project, seven sediment samples were collected throughout the Mussentuchit Member at key stratigraphic and fossiliferous localities (Fig. 4.3.2). These samples yielded 760 zircon grains suitable for analysis, with 663 of these grains generating ages within the 15% discordance between the $^{206}\text{Pb}/^{238}\text{U}$ and $^{207}\text{Pb}/^{235}\text{U}$ ages. Age populations were identified via the presence of three or more grains ($n \geq 3$) within a weighted mean average. Reliability of the analysis was determined using two secondary quality control standards, with 52 shot analyses on the Plešovice standards yielding an age of 338.77 Ma, while analysis of 30 shots on the M127 standard yielded an age of 530.6 Ma (Fig. 4.3.1). As these ages are close to the published ages of the standards, the data is interpreted to be reliable (Sláma *et al.*, 2008; Nasdala *et al.*, 2016).

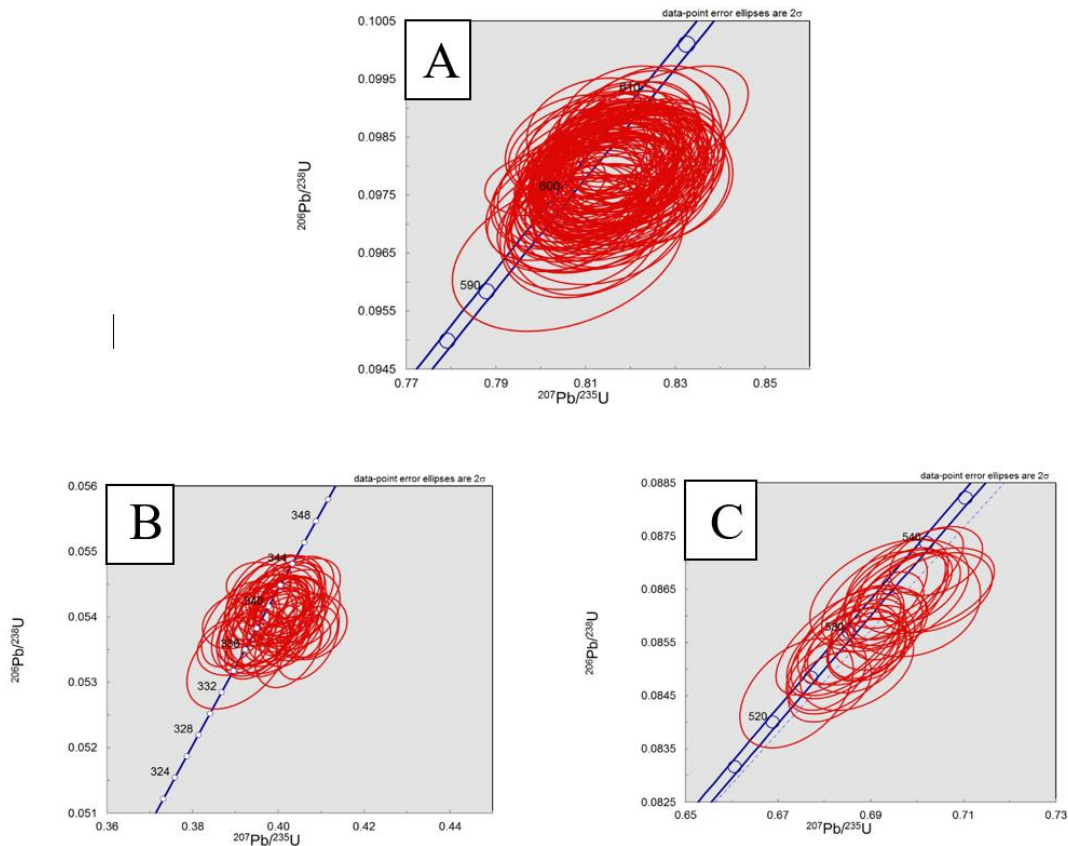


Figure 4.3.1: Concordia diagrams of (A) GJ1 primary standard, (B) Plešovice secondary standard and (C) M127 secondary standard.

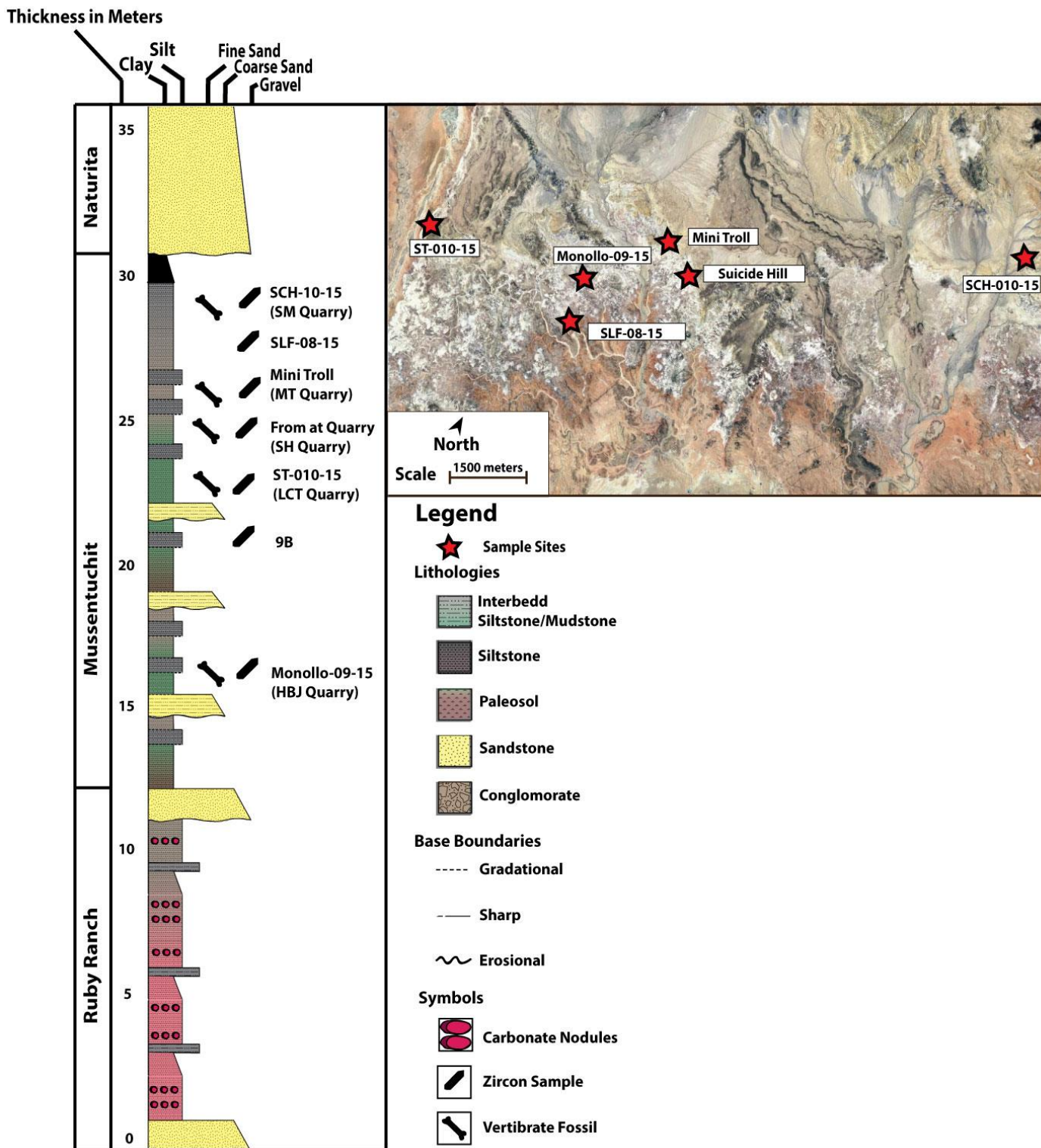


Figure 4.3.2: Stratigraphic and geographic positions of detrital zircon samples.

Detrital zircon samples were characterized by angular to rounded zircon grains, with the grains of different samples showing slight variations in degree. Through secondary electron backscatter (BSE) imaging, zircon grains also exhibited different degrees of microfracturing, varying from few to many microfractures between each sample (Fig. 4.3.3). Zircon grains under a reflected light binary microscope, show morphologies consisting of (1) elongated, doubly terminated crystals, (2) long, singularly terminated acicular crystals (typically fractured at one terminus), and (3) short, equal axis, doubly terminating crystals. Based on Pupin's (1980) Zircon morphology system, zircon morphologies ranged between S6 to S12 (50%), P1 to P3 (30%), and R1 to R3 (20%). Internal grain structures (Fig. 4.3.3) are discernible through the use of cathode luminescence (CL) imaging and is shown to be predominately comprised of magmatic oscillatory zoning, with metamorphic zoning present in a limited amount of grains ($\pm 15\%$ of all grains). Approximately 20% of zircon grains contained relict core textures, identified by irregular internal structure within the core (Corfu *et al.*, 2003). A very limited number of grains (10%) exhibited convolute zoning from fluid leaching between microfractures (Corfu *et al.*, 2003).

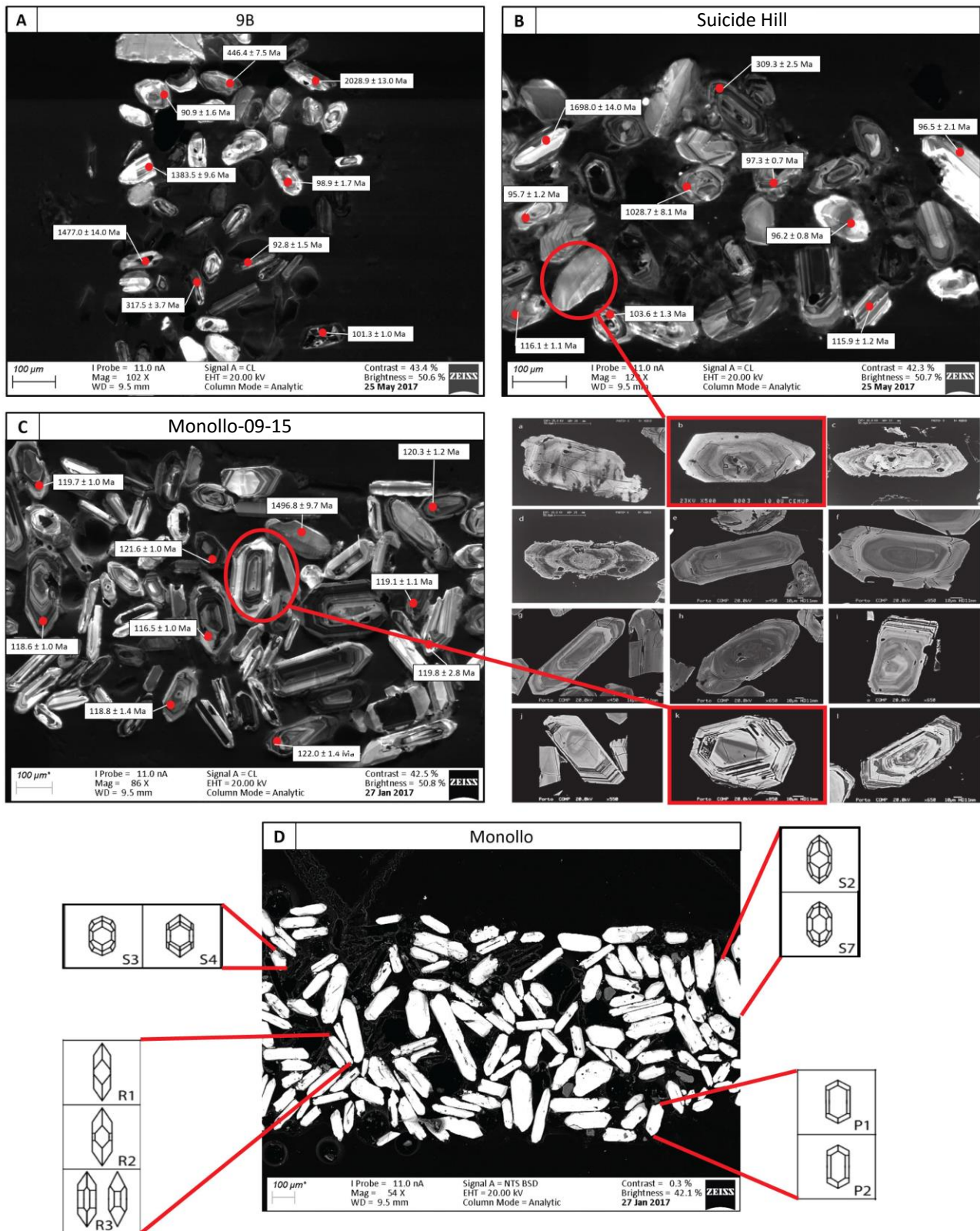


Figure 4.3.3 Cathode Luminescence images of zircon assemblages (A; B; C). Insert from Corfu *et al.* (2003) illustrates the presence of metamorphic zoning (A) and magmatic oscillatory zoning (C). (D) Shows electron back scatter images with inserts illustrating morphological characterization, following Pupin (1980).

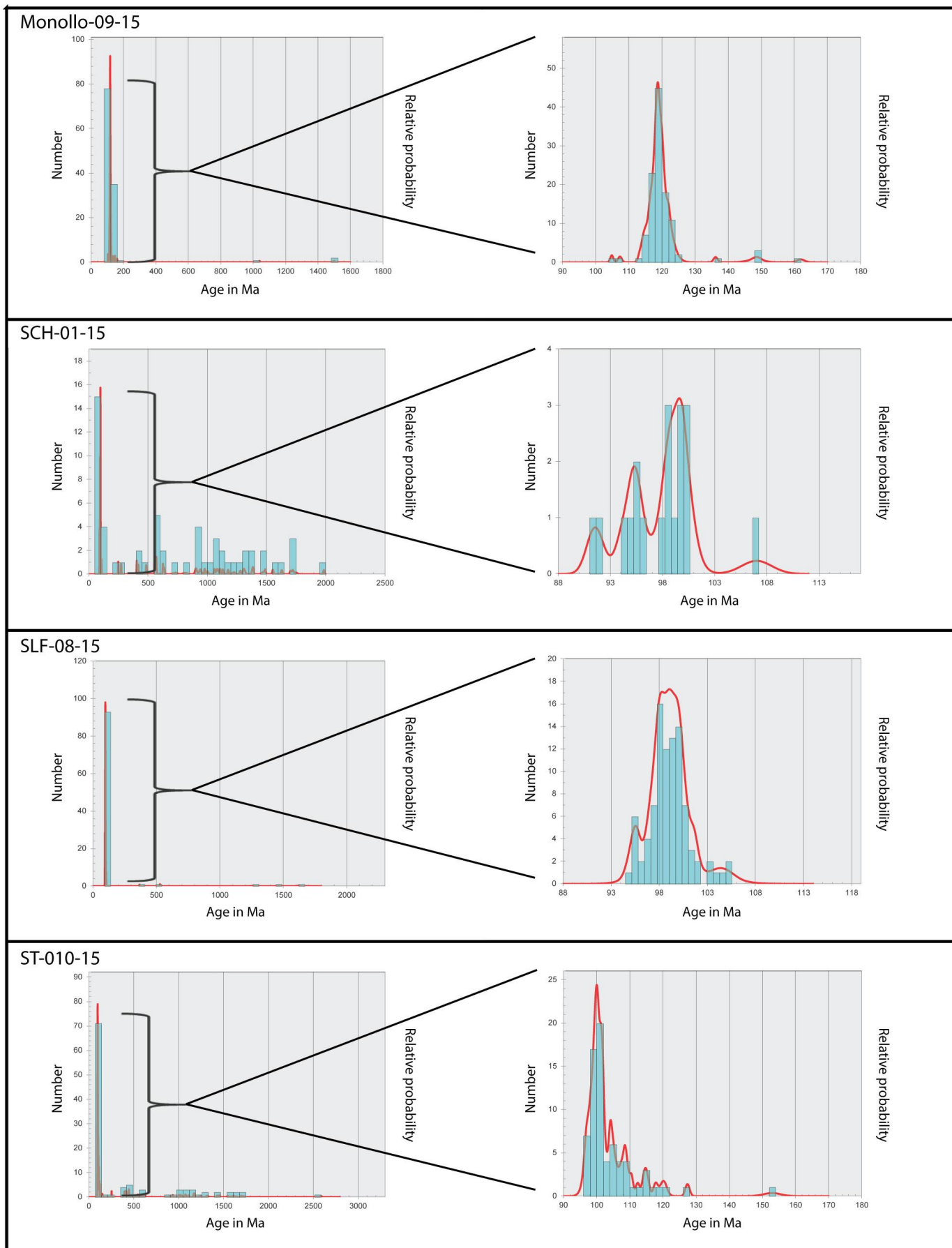


Figure 4.3.4a: Probability density plots of samples between 80 Ma and 2500 Ma with exploded views of youngest peaks. Produced in ISOPLOT with bin size of 40.

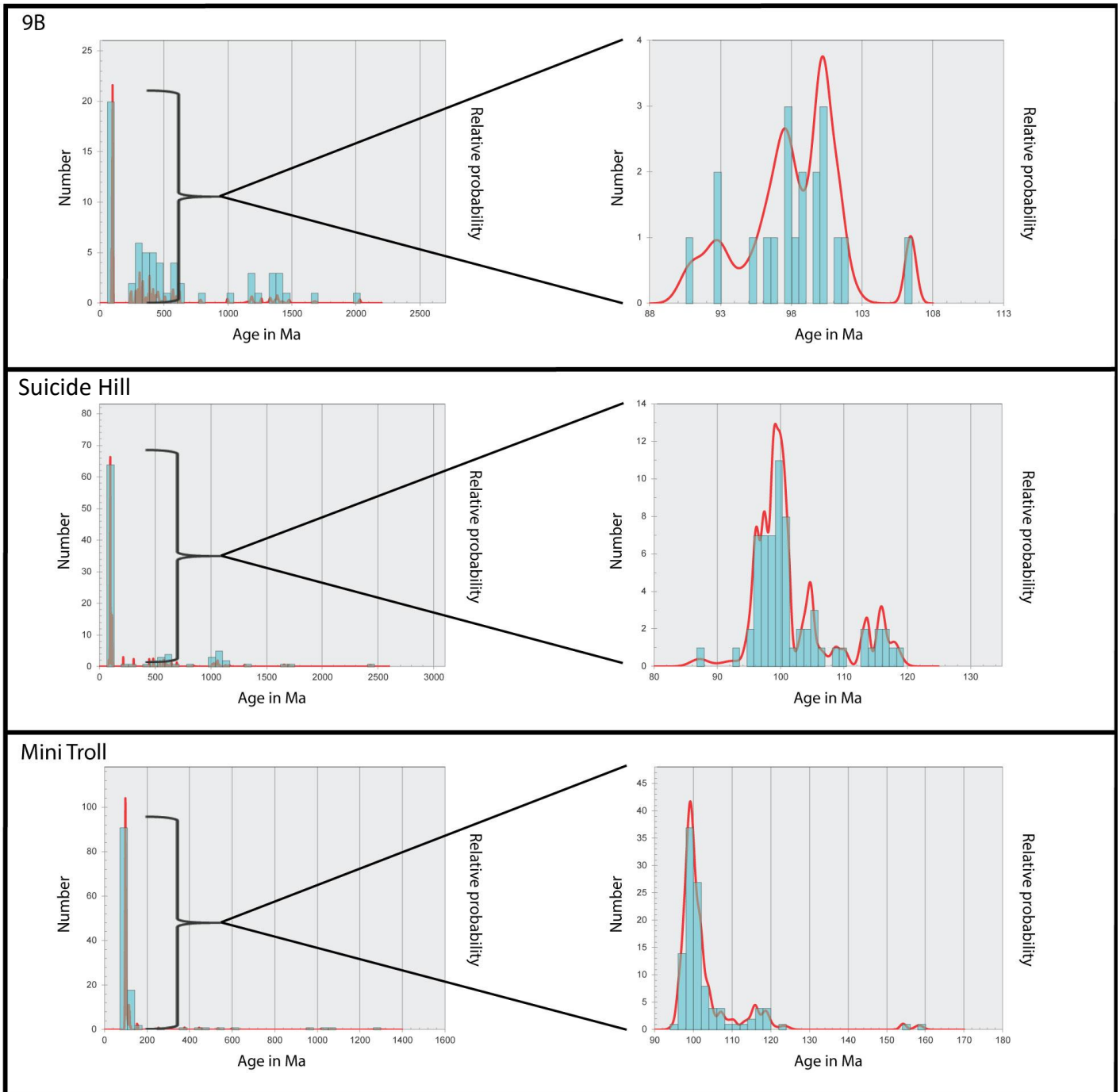


Figure 4.3.4b: Probability density plots of samples between 80 Ma and 2500 Ma with exploded views of youngest peaks. Produced in ISOPLOT with bin size of 40.

4.3.1 Sample Descriptions

4.3.1.1 9B

Sample 9B was collected from the middle Mussentuchit, and shows a representative (handpicked) population of zircon grains, which predominantly (95%) consist of magmatic grains exhibiting pristine, magmatic oscillatory zoning. A small proportion (5%) of the grains exhibited homogenous sector zoning, associated with metamorphism, and approximately 20% of grains exhibited relict textures, evident from the high angle truncation and difference in luminosity under CL-imaging (Fig. 4.3.3). Grains vary in size between 30 μm and 120 μm with the majority (60%) between 70 μm and 90 μm . Zircon crystals appear as euhedral, angular to sub-rounded grains, with a moderate amount of microfracturing, and the common inclusions of other minerals such as quartz. Typical morphological types within the representative population of sample 9B include P1-P2, S2-S7, and R1-R3. Sample 9B yielded 90 analysable zircons with 64 zircons falling within the 15% discordancy inclusion criteria. Core analysis was conducted on 23% of the samples with 77% representing rim analysis. The largest population within the sample, 31% ($n=20$), occurs at the Cenomanian age of 93.9 – 100 Ma, with subordinate populations of 26.5% ($n=17$) occurring around the Middle to Lower Devonian (380 – 410 Ma), 9.38% ($n=6$) around the late Neoproterozoic (541 – 635 Ma) and 7.8% ($n=5$) occurring around the early Mesoproterozoic (1350-1500 Ma) (Fig. 4.3.4b; 4.3.5). A single grain of the Paleoproterozoic age (2045 Ma) is also present. Analysis of the sample yielded the following youngest age signatures: YSG at 91 (± 1.5) Ma; YPP at 97 Ma; YDZ at 90.5 (+2.5 – 3.6) Ma; YC1 σ (+3) at 92 (± 1.4) Ma; YC2 σ (+3) at 92 (± 2.2) Ma; weighted mean (10) at 95.7 (± 1.8) Ma; TuffZirc age at 96.6 (+1.3 – 3.8) Ma through a coherent group of 9 out of 10 grains (Table 4.3.8).

Table 4.3.1: Pb/U data for sample 9B. ²⁰⁶Pb/²³⁸U ratio used for age calculations.

9B				RATIOS										AGES (Ma)			Conc.	
Analysis	U [ppm] ^a	Pb [ppm] ^b	Th/U ^a	²⁰⁶ Pb/ ²⁰⁴ Pb	²⁰⁷ Pb/ ²³⁵ U ^b	2 σ^d	²⁰⁶ Pb/ ²³⁸ U ^b	2 σ^d	rho ^e	²⁰⁷ Pb/ ²⁰⁶ Pb ^b	2 σ^d	Pb ²³² 2 σ	²⁰⁶ Pb/ ²³⁸ U	2 σ	²⁰⁷ Pb/ ²⁰⁶ Pb	2 σ	%	
A_301.FIN2	339	102	0.73	410	0.0998	0.0075	0.0142	0.0003	0.0154	0.0498	0.0035	96	7	90.9	2	200	150	94
A_233.FIN2	329	83	0.54	70	0.1025	0.0073	0.0145	0.0003	0.0263	0.0522	0.0039	99	7	92.6	2	270	150	94
A_283.FIN2	673	69	0.23	500	0.0988	0.0062	0.0145	0.0002	0.1278	0.0491	0.0028	96	6	92.8	2	150	110	97
A_245.FIN2	1257	240	0.44	3300	0.1101	0.0089	0.0149	0.0004	0.2769	0.0527	0.0047	106	8	95.2	2	290	190	90
A_306.FIN2	418	130	0.80	-50	0.1068	0.0073	0.0151	0.0003	0.0323	0.0510	0.0037	103	7	96.3	2	210	140	94
A_263.FIN2	349	80	0.53	20	0.1033	0.0057	0.0151	0.0002	0.0434	0.0502	0.0030	100	5	96.6	1	190	120	97
A_227.FIN2	487	219	1.06	320	0.1048	0.0040	0.0152	0.0002	0.1676	0.0502	0.0020	101	4	97.5	1	188	81	96
A_234.FIN2	590	240	1.00	50	0.1049	0.0039	0.0153	0.0002	0.1018	0.0491	0.0018	101	4	97.7	1	150	75	97
A_255.FIN2	397	121	0.70	210	0.1050	0.0130	0.0153	0.0005	0.2333	0.0491	0.0066	101	12	97.9	3	140	270	97
A_218.FIN2	390	70	0.38	50	0.1052	0.0091	0.0153	0.0004	0.1809	0.0515	0.0055	101	8	98.1	2	230	200	97
A_237.FIN2	337	56	0.39	360	0.1093	0.0097	0.0154	0.0006	0.0682	0.0511	0.0048	105	9	98.6	4	230	190	94
A_288.FIN2	289	63	0.48	6	0.1031	0.0056	0.0155	0.0003	0.0808	0.0491	0.0026	101	5	98.9	2	180	85	98
A_314.FIN2	453	167	0.88	430	0.1082	0.0039	0.0156	0.0001	0.0514	0.0502	0.0018	104	4	99.8	1	188	74	96
A_257.FIN2	457	129	0.76	120	0.1140	0.0110	0.0156	0.0003	0.0197	0.0524	0.0051	109	10	99.9	2	270	200	92
A_256.FIN2	538	99	0.43	-120	0.1091	0.0034	0.0157	0.0001	0.1291	0.0500	0.0016	105	3	100.3	1	192	65	96
A_248.FIN2	394	97	0.55	70	0.1161	0.0046	0.0157	0.0002	0.0062	0.0526	0.0021	111	4	100.4	1	293	85	90
A_220.FIN2	572	171	0.68	180	0.1108	0.0045	0.0157	0.0002	0.0483	0.0503	0.0022	107	4	100.4	1	192	86	94
A_273.FIN2	1280	297	0.52	1480	0.1110	0.0040	0.0158	0.0002	0.6212	0.0505	0.0017	107	4	101.3	1	205	68	95
A_219.FIN2	501	142	0.68	630	0.1069	0.0051	0.0159	0.0003	0.4958	0.0490	0.0020	103	5	101.6	2	133	80	99
A_250.FIN2	569	102	0.38	-520	0.1130	0.0030	0.0167	0.0001	0.0533	0.0489	0.0013	109	3	106.4	1	141	54	98
A_264.FIN2	324	113	0.30	440	0.3089	0.0086	0.0381	0.0008	0.5165	0.0584	0.0014	273	7	241.1	5	517	54	88
A_277.FIN2	736	370	0.34	1100	0.3429	0.0091	0.0390	0.0007	0.6247	0.0633	0.0013	299	7	246.5	4	711	45	82
A_249.FIN2	549	86	0.05	400	0.3762	0.0088	0.0443	0.0011	0.5186	0.0629	0.0016	324	7	279.2	7	686	56	86
A_246.FIN2	570	78	0.01	620	0.4030	0.0120	0.0448	0.0011	0.6861	0.0659	0.0015	343	9	282.2	7	793	45	82
A_228.FIN2	365	482	1.09	1110	0.3890	0.0100	0.0476	0.0005	0.8002	0.0578	0.0016	333	8	299.7	3	509	63	90
A_293.FIN2	691	758	0.65	1120	0.4479	0.0092	0.0494	0.0008	0.6951	0.0655	0.0010	375	7	310.9	5	777	32	83
A_307.FIN2	846	304	0.19	90000	0.4210	0.0056	0.0495	0.0004	0.2364	0.0613	0.0008	356	4	311.5	2	644	29	87
A_278.FIN2	297	302	0.63	940	0.4750	0.0120	0.0505	0.0006	0.5417	0.0680	0.0015	394	8	317.5	4	850	44	81
A_310.FIN2	507	585	0.62	1690	0.4440	0.0130	0.0526	0.0011	0.7304	0.0608	0.0012	372	9	330.5	7	624	41	89
A_266.FIN2	861	428	0.31	580	0.4548	0.0084	0.0534	0.0008	0.3399	0.0616	0.0010	380	6	335.1	5	643	35	88
A_261.FIN2	276	338	0.75	440	0.4620	0.0120	0.0535	0.0008	0.4516	0.0624	0.0015	385	8	335.8	5	657	50	87
A_270.FIN2	731	452	0.22	680	0.5520	0.0180	0.0574	0.0013	0.5988	0.0699	0.0018	445	12	359.9	8	908	49	81
A_289.FIN2	222	147	0.39	590	0.5020	0.0130	0.0608	0.0008	0.2186	0.0595	0.0016	412	9	380.5	5	554	59	92
A_217.FIN2	642	254	0.21	400	0.5057	0.0069	0.0620	0.0004	0.1501	0.0588	0.0009	417	5	387.9	2	555	33	93
A_267.FIN2	274	234	0.33	880	0.5690	0.0130	0.0624	0.0008	0.6027	0.0658	0.0012	456	8	390.1	5	781	39	86
A_238.FIN2	413	271	0.41	900	0.5510	0.0160	0.0644	0.0008	0.2118	0.0611	0.0018	445	11	402.2	5	628	63	90
A_284.FIN2	478	662	0.85	-80	0.5340	0.0130	0.0668	0.0005	0.2572	0.0571	0.0012	434	8	417.0	3	481	47	96
A_271.FIN2	392	156	0.21	-820	0.5550	0.0230	0.0703	0.0010	0.3088	0.0563	0.0022	448	15	437.8	6	443	87	98
A_295.FIN2	245	175	0.38	-390	0.5620	0.0210	0.0717	0.0012	0.0550	0.0565	0.0024	452	14	446.4	8	450	98	99
A_223.FIN2	946	90	0.12	-40	0.6310	0.0130	0.0731	0.0010	0.0411	0.0621	0.0012	495	8	454.5	6	660	38	92
A_260.FIN2	702	360	0.19	1260	0.6880	0.0130	0.0740	0.0014	0.7732	0.0671	0.0009	530	8	459.8	9	833	28	87
A_286.FIN2	491	394	0.26	700	0.7550	0.0400	0.0782	0.0036	0.8905	0.0709	0.0015	565	24	484.0	21	949	45	86
A_222.FIN2	143	215	0.66	-230	0.6620	0.0290	0.0823	0.0012	0.0760	0.0588	0.0026	514	18	509.5	7	524	98	99
A_247.FIN2	71	215	0.94	-10	0.9400	0.0410	0.0923	0.0016	0.3284	0.0752	0.0033	674	22	569.3	10	1036	85	84
A_236.FIN2	87	125	0.57	-150	0.7660	0.0250	0.0929	0.0009	0.0917	0.0594	0.0019	575	14	572.6	6	550	70	100
A_296.FIN2	333	408	0.30	690	1.0450	0.0540	0.0945	0.0053	0.9430	0.0806	0.0017	711	27	579.0	31	1197	38	81
A_258.FIN2	161	197	0.50	-240	0.8130	0.0220	0.0971	0.0013	0.6226	0.0596	0.0017	603	12	597.3	8	568	63	99
A_235.FIN2	84	147	0.61	-260	0.8430	0.0280	0.1004	0.0011	0.1423	0.0608	0.0020	618	16	616.9	6	594	72	100
A_269.FIN2	132	307	0.88	910	0.8590	0.0170	0.1016	0.0007	0.1008	0.0611	0.0013	629	10	623.8	4	616	45	99
A_280.FIN2	567	1660	0.74	1000	1.5340	0.0330	0.1298	0.0024	0.9181	0.0853	0.0007	941	13	786.0	14	1320	17	84
A_231.FIN2	272	794	0.58	290	2.1190	0.0320	0.1673	0.0019	0.7102	0.0910	0.0010	1152	11	997.0	11	1442	20	87
A_311.FIN2	274	704	0.40	3200	2.6700	0.0980	0.1969	0.0065	0.9479	0.0972	0.0014	1309	28	1156.0	35	1568	25	88
A_276.FIN2	109	242	0.32	390	2.9530	0.0830	0.2018	0.0028	0.4749	0.1078	0.0026	1393	21	1185.0	15	1764	41	85
A_232.FIN2	115	360	0.58	150	2.2330	0.0680	0.2023	0.0026	0.2484	0.0807	0.0024	1189	21	1187.0	14	1204	59	100
A_230.FIN2	233	792	0.59	1700	2.4920	0.0410	0.2161	0.0019	0.4233	0.0840	0.0013	1269	12	1261.0	10	1288	29	99
A_224.FIN2	1060	1520	0.12	1650	3.5970	0.0980	0.2299	0.0065	0.8320	0.1118	0.0013	1539	22	1330.0	34	1823	21	86
A_291.FIN2	187	293	0.28	2400	2.7190	0.0450	0.2293	0.0024	0.6354	0.0850	0.0011	1331	12	1330.0	12	1309	25	100
A_244.FIN2	63	217	0.54	-220	2.9480	0.0860	0.2368	0.0026	0.1605	0.0890	0.0025	1391	23	1370.0	14	1402	58	98
A_298.FIN2	85	305	0.62	350	2.9410	0.0460	0.2394	0.0019	0.3104	0.0883	0.0014	1390	12	1383.5	10	1383	29	100
A_221.FIN2	236	592	0.39	-500	3.2250	0.0400	0.2408	0.0022	0.7987	0.0956	0.0008	1462	10	1390.0	12	1537	17	95
A_304.FIN2	129	421	0.40	360	4.6000	0.1100	0.2474	0.0054	0.9167	0.1336	0.0013	1740	20	1422.0	28	2146	17	82
A_281.FIN2	180	632	0.53	0	3.3470	0.0610	0.2576	0.0027	0.0016	0.0940	0.0020	1491	14	1477.0	14	1503	40	99
A_226.FIN2	94	363	0.53	-700	4.2000	0.1100	0.2971	0.0049	0.4081	0.1031	0.0024	1671	21	1677.0	25	1675	45	100
A_302.FIN2	280	1640	0.61	22000	6.3790	0.0750	0.3697	0.0028	0.5675	0.1262	0.0012	2029	10	2028.0	13	2045	16	100

Legend

Cretaceous Upper	Jurassic	Permian	Devonian	Ordovician	Precambrian
------------------	----------	---------	----------	------------	-------------

Cretaceous Lower	Triassic	Carboniferous	Silurian	Cambrian
------------------	----------	---------------	----------	----------

4.3.1.2 Suicide Hill

Sample Suicide Hill was collected from the Suicide Hill fossil quarry, stratigraphically located within the upper middle portions of the Mussentuchit Member (Fig. 4.3.8). A representative (handpicked) population of zircon grains from the sample consisted of 95% magmatic grains exhibiting pristine, magmatic oscillatory zoning. A small proportion (5%) of the grains exhibited homogenous sector zoning, associated with metamorphism, and approximately 20% of grains exhibited relict textures, evident from the high angle truncation and difference in luminosity under CL-imaging (Fig. 4.3.3). Limited occurrences (1%) of convolute zoning is noted within the grains along fracture paths. Grains varied in size between 50 μm and 120 μm with the majority (75%) averaging around 100 μm . Zircon crystals appear as euhedral, angular to sub-rounded grains, with a large amount of microfracturing present within the grains. Typical morphological types within the representative population of sample Suicide Hill include P1-P2 and S8-S9. Suicide Hill yielded 119 analysable zircons, with 92 zircons falling within the 10% discordancy inclusion criteria. Core analysis was conducted on 20% of the samples with 80% representing rim analysis. The largest population within the sample, 57.61% (n=53), shows a Cenomanian age of 93.9 – 100 Ma, with subordinate populations of 10.87% (n=10) occurring at an Aptian age of 115-120 Ma, 4.35% (n=4) occurring around the Middle to Lower Devonian (380 – 410 Ma), 6.52% (n=6) around the late Neoproterozoic (541 - 635 Ma), and 9.78% (n=9) occurring around the Late Mesoproterozoic (1035-1125 Ma) (Fig. 4.3.4b; 4.3.5). A single grain of Neoproterozoic age (2617 Ma) is also present. Analysis of the sample yielded the following youngest age signatures: YSG at 87.54 (\pm 4.5) Ma; YPP at 99.7 Ma; YDZ at 87.54 (+5.4 – 6.2) Ma; YC1 σ (+3) at 93.5 (\pm 1.5) Ma; YC2 σ (+3) at 93.5 (\pm 2.4) Ma; weighted mean (10) at 95.7 (\pm 1.0) Ma; TuffZirc age at 96.6 (+1.3 –3.8) Ma through a coherent group of 9 out of 10 grains. It is suspected that the 87.54 Ma age may be due to lead loss experienced by grain

A₄₃₁.FIN2, and may, therefore, be erroneous. As such, the 2nd YSG age at 92.5 (± 4.5) Ma can be considered the more probable YSG age (Table 4.3.8).

Table 4.3.2: Pb/U data for sample Suicide Hill. ²⁰⁶Pb/²³⁸U ration used for age calculations.

Suicide Hill				RATIOS											AGES [Ma]				Conc.
Analysis	U [ppm] ^a	Pb [ppm] ^b	Th/U ^c	206/204	²⁰⁷ Pb/ ²³⁵ U ^d	2 σ ^d	²⁰⁶ Pb/ ²³⁸ U ^e	2 σ ^e	rho ^c	²⁰⁷ Pb/ ²⁰⁶ Pb	2 σ ^f	²⁰⁷ Pb/ ²³⁵ U	2 σ ^g	²⁰⁶ Pb/ ²³⁸ U	2 σ ^h	²⁰⁷ Pb/ ²⁰⁶ Pb	2 σ ⁱ	%	
A_431.FIN2	797	139	0.41	630	0.0968	0.0092	0.0136	0.0004	0.5804	0.0556	0.0040	93	9	87.2	3	420	160	94	
A_319.FIN2	415	76	0.34	-140	0.1018	0.0089	0.0145	0.0006	0.3461	0.0540	0.0047	98	9	92.5	4	470	150	94	
A_331.FIN2	511	162	0.77	570	0.1045	0.0054	0.0148	0.0002	0.0660	0.0506	0.0027	101	5	94.8	1	200	110	94	
A_334.FIN2	271	69	0.62	100	0.1019	0.0041	0.0150	0.0002	0.0371	0.0497	0.0021	99	4	95.7	1	167	83	97	
A_360.FIN2	677	118	0.40	30	0.1110	0.0045	0.0150	0.0002	0.0693	0.0532	0.0023	107	4	95.9	1	311	93	90	
A_384.FIN2	355	68	0.48	90	0.1034	0.0041	0.0150	0.0002	0.0486	0.0497	0.0020	100	4	96.0	1	179	79	96	
A_437.FIN2	593	102	0.44	130	0.1062	0.0057	0.0150	0.0002	0.1420	0.0512	0.0029	102	5	96.2	1	220	110	94	
A_350.FIN2	428	157	0.94	130	0.1031	0.0033	0.0150	0.0001	0.1094	0.0496	0.0016	99	3	96.2	1	169	63	97	
A_396.FIN2	601	362	1.45	210	0.1091	0.0072	0.0151	0.0003	0.0098	0.0522	0.0035	105	7	96.5	2	260	140	92	
A_356.FIN2	139	72	1.27	-16	0.1064	0.0071	0.0151	0.0003	0.0118	0.0509	0.0035	102	7	96.5	2	220	140	94	
A_366.FIN2	1301	330	0.67	-270	0.1052	0.0047	0.0151	0.0003	0.4005	0.0499	0.0020	102	4	96.8	2	182	87	95	
A_438.FIN2	628	136	0.53	-310	0.1066	0.0040	0.0152	0.0002	0.1917	0.0513	0.0020	103	4	97.3	1	239	79	95	
A_362.FIN2	738	125	0.44	-24000	0.1040	0.0130	0.0152	0.0004	0.1365	0.0498	0.0064	101	12	97.3	2	160	250	96	
A_348.FIN2	908	350	0.97	240	0.1023	0.0024	0.0152	0.0001	0.1946	0.0485	0.0011	99	2	97.3	1	129	46	99	
A_426.FIN2	813	188	0.61	-660	0.1111	0.0050	0.0152	0.0002	0.2395	0.0526	0.0023	107	5	97.4	1	289	95	91	
A_388.FIN2	716	99	0.31	430	0.1047	0.0039	0.0152	0.0002	0.2033	0.0494	0.0018	101	4	97.5	1	161	74	97	
A_333.FIN2	402	90	0.55	80	0.1043	0.0034	0.0153	0.0001	0.1547	0.0494	0.0016	101	3	97.8	1	157	63	97	
A_324.FIN2	351	76	0.47	80	0.1106	0.0063	0.0153	0.0002	0.0781	0.0517	0.0031	106	6	97.9	2	240	120	92	
A_394.FIN2	932	193	0.52	-110	0.1108	0.0053	0.0154	0.0003	0.1723	0.0520	0.0026	107	5	98.2	2	270	110	92	
A_365.FIN2	351	74	0.48	90	0.1039	0.0043	0.0154	0.0002	0.0746	0.0491	0.0021	100	4	98.5	1	142	81	98	
A_400.FIN2	1281	450	0.89	980	0.1033	0.0021	0.0154	0.0001	0.1945	0.0487	0.0010	100	2	98.6	1	138	42	99	
A_358.FIN2	317	82	0.57	140	0.1049	0.0043	0.0154	0.0002	0.0559	0.0494	0.0020	101	4	98.8	1	155	80	98	
A_351.FIN2	852	184	0.53	20	0.1042	0.0023	0.0155	0.0001	0.0401	0.0485	0.0011	101	2	99.0	1	135	46	98	
A_379.FIN2	335	99	0.69	-40	0.1093	0.0055	0.0155	0.0002	0.2376	0.0507	0.0024	105	5	99.0	2	220	98	94	
A_370.FIN2	545	100	0.46	-40	0.1054	0.0030	0.0155	0.0001	0.0054	0.0494	0.0015	102	3	99.1	1	164	59	98	
A_325.FIN2	372	115	0.79	340	0.1096	0.0039	0.0155	0.0002	0.1585	0.0510	0.0018	105	4	99.2	1	221	71	94	
A_380.FIN2	1139	351	0.83	-310	0.1091	0.0047	0.0155	0.0002	0.1344	0.0509	0.0023	105	4	99.2	1	223	94	94	
A_316.FIN2	573	139	0.59	830	0.1078	0.0043	0.0155	0.0002	0.0990	0.0501	0.0021	104	4	99.2	1	189	84	96	
A_422.FIN2	496	120	0.60	-20	0.1049	0.0031	0.0155	0.0001	0.0425	0.0494	0.0016	101	3	99.4	1	161	63	98	
A_397.FIN2	839	79	0.22	-190	0.1079	0.0023	0.0156	0.0002	0.3730	0.0499	0.0015	104	2	99.5	1	194	54	96	
A_427.FIN2	482	87	0.45	-940	0.1041	0.0056	0.0156	0.0002	0.1453	0.0480	0.0026	100	5	99.6	1	110	110	99	
A_339.FIN2	797	203	0.59	-900	0.1092	0.0035	0.0156	0.0002	0.0809	0.0504	0.0017	105	3	99.8	1	201	69	95	
A_393.FIN2	845	136	0.40	-130	0.1055	0.0031	0.0156	0.0001	0.1673	0.0484	0.0014	102	3	99.9	1	131	59	98	
A_361.FIN2	544	155	0.65	140	0.1074	0.0034	0.0156	0.0002	0.0035	0.0498	0.0016	103	3	100.1	1	175	66	97	
A_420.FIN2	532	156	0.68	-10	0.1047	0.0029	0.0156	0.0001	0.0238	0.0489	0.0014	101	3	100.1	1	145	57	99	
A_359.FIN2	459	90	0.42	-120	0.1080	0.0036	0.0157	0.0002	0.0721	0.0496	0.0018	104	3	100.2	1	169	74	96	
A_364.FIN2	409	100	0.59	150	0.1076	0.0042	0.0157	0.0002	0.0100	0.0494	0.0020	104	4	100.3	1	154	77	97	
A_403.FIN2	398	128	0.76	-20	0.1101	0.0053	0.0157	0.0002	0.0219	0.0506	0.0026	106	5	100.4	2	200	100	95	
A_330.FIN2	559	130	0.55	410	0.1110	0.0054	0.0157	0.0002	0.0125	0.0504	0.0025	107	5	100.6	1	200	100	94	
A_408.FIN2	994	301	0.74	-120	0.1042	0.0026	0.0157	0.0001	0.0337	0.0483	0.0013	101	2	100.6	1	118	53	100	
A_413.FIN2	287	40	0.31	70	0.1072	0.0044	0.0158	0.0002	0.0435	0.0494	0.0020	103	4	100.8	1	153	79	98	
A_335.FIN2	970	257	0.62	760	0.1056	0.0031	0.0158	0.0001	0.0280	0.0480	0.0015	102	3	100.8	1	103	61	99	
A_421.FIN2	332	87	0.59	150	0.1110	0.0045	0.0158	0.0002	0.0318	0.0515	0.0022	107	4	101.0	1	228	84	95	
A_373.FIN2	631	196	0.73	60	0.1070	0.0031	0.0159	0.0001	0.1723	0.0488	0.0014	103	3	101.4	1	135	56	98	
A_382.FIN2	768	190	0.58	80	0.1039	0.0024	0.0159	0.0001	0.0166	0.0476	0.0012	100	2	101.4	1	89	48	101	
A_404.FIN2	882	163	0.43	210	0.1143	0.0062	0.0161	0.0004	0.2261	0.0514	0.0030	110	6	103.2	2	240	120	94	
A_345.FIN2	899	473	1.21	230	0.1142	0.0048	0.0162	0.0002	0.1746	0.0504	0.0021	110	4	103.6	1	202	83	95	
A_385.FIN2	380	111	0.75	-20	0.1099	0.0098	0.0163	0.0003	0.0017	0.0487	0.0044	106	9	104.1	2	120	170	99	
A_402.FIN2	413	70	0.40	-30	0.1115	0.0043	0.0163	0.0002	0.0400	0.0496	0.0030	107	4	104.3	1	172	77	97	
A_390.FIN2	545	81	0.35	0	0.1116	0.0032	0.0164	0.0001	0.0388	0.0493	0.0014	107	3	104.8	1	158	58	98	
A_326.FIN2	452	123	0.63	540	0.1160	0.0044	0.0164	0.0002	0.2969	0.0508	0.0019	111	4	104.8	1	221	76	94	
A_391.FIN2	151	23	0.31	16	0.1163	0.0082	0.0165	0.0003	0.0873	0.0510	0.0036	111	8	105.3	2	220	140	95	
A_320.FIN2	434	111	0.61	-810	0.1185	0.0082	0.0167	0.0003	0.0214	0.0511	0.0036	113	8	106.6	2	220	140	94	
A_357.FIN2	947	169	0.40	330	0.1126	0.0025	0.0170	0.0002	0.2565	0.0482	0.0011	108	2	108.7	1	112	45	100	
A_372.FIN2	224	35	0.53	109	0.1143	0.0054	0.0172	0.0002	0.0757	0.0484	0.0023	109	5	110.1	1	114	89	101	
A_407.FIN2	243	71	0.60	40	0.1228	0.0050	0.0177	0.0002	0.1361	0.0506	0.0021	117	5	112.9	1	190	79	96	
A_337.FIN2	1229	560	0.95	360	0.1230	0.0027	0.0178	0.0002	0.3294	0.0501	0.0010	118	3	113.4	1	189	43	96	
A_381.FIN2	1262	327	0.52	-320	0.1233	0.0020	0.0178	0.0001	0.3416	0.0504	0.0008	118	2	113.8	1	209	36	97	
A_349.FIN2	1110	424	0.86	-510	0.1249	0.0039	0.0181	0.0002	0.2733	0.0493	0.0015	119	4	115.6	1	170	64	97	
A_353.FIN2	211	96	0.97	370	0.1271	0.0057	0.0181	0.0002	0.0305	0.0500	0.0022	121	5	115.9	1	192	85	96	
A_354.FIN2	266	75	0.51	690	0.1258	0.0077	0.0182	0.0003	0.0750	0.0499	0.0031	120	7	116.1	2	170	120	97	
A_332.FIN2	433	100	0.48	100	0.1254	0.0038	0.0182	0.0002	0.1308	0.0497	0.0015	120	3	116.1	1	177	61	97	
A_323.FIN2	390	128	0.69	140	0.1280	0.0062	0.0185	0.0002	0.1076	0.0494	0.0024	122	6	117.9	2	154	95	97	
A_374.FIN2	472	166	0.81	30	0.1261	0.0093	0.0185	0.0003	0.0927	0.0491	0.0036	120	8	118.4	2	140	140	98	

A_395.FIN2	646	1351	2.32	-100	0.2557	0.0051	0.0341	0.0003	0.3572	0.0541	0.0011	232	4	216.3	2	358	43	93
A_340.FIN2	475	1282	2.10	-1900	0.3602	0.0097	0.0492	0.0004	0.0040	0.0533	0.0015	313	8	309.3	3	324	61	99
A_389.FIN2	392	565	0.78	300	0.5561	0.0075	0.0721	0.0004	0.1878	0.0559	0.0007	448	5	448.9	2	437	30	100
A_409.FIN2	343	278	0.40	30	0.6110	0.0094	0.0781	0.0004	0.1271	0.0571	0.0009	483	6	484.7	3	480	35	100
A_423.FIN2	536	119	0.10	-1600	0.6310	0.0130	0.0789	0.0007	0.2507	0.0578	0.0012	496	8	489.3	4	508	45	99
A_346.FIN2	297	166	0.23	380	0.7180	0.0120	0.0881	0.0006	0.1571	0.0589	0.0010	548	7	544.4	3	548	35	99
A_430.FIN2	161	259	0.60	-110	0.7760	0.0200	0.0931	0.0011	0.2375	0.0613	0.0015	582	11	573.7	7	636	54	99
A_341.FIN2	208	373	0.72	-950	0.7730	0.0140	0.0937	0.0006	0.0673	0.0597	0.0011	580	8	577.3	4	567	41	100
A_369.FIN2	73	168	0.93	300	0.8130	0.0220	0.0971	0.0009	0.0512	0.0609	0.0018	601	12	597.2	5	598	63	99
A_419.FIN2	94	167	0.53	120	0.8810	0.0290	0.0997	0.0018	0.6728	0.0641	0.0016	636	16	612.0	11	715	52	96
A_401.FIN2	150	268	0.68	-90	0.8970	0.0470	0.1047	0.0019	0.2317	0.0617	0.0032	648	25	642.0	11	630	110	99
A_392.FIN2	74	445	2.16	-20	0.9030	0.0290	0.1056	0.0011	0.0957	0.0625	0.0021	650	15	647.2	6	641	74	100
A_415.FIN2	218	469	0.77	-470	0.9730	0.0160	0.1141	0.0008	0.2545	0.0622	0.0010	690	8	696.5	5	664	35	101
A_428.FIN2	105	193	0.45	180	1.4540	0.0800	0.1396	0.0038	0.4377	0.0756	0.0037	906	33	842.0	21	1088	85	93
A_424.FIN2	175	314	0.39	-700	1.7920	0.0420	0.1699	0.0017	0.1698	0.0776	0.0018	1041	15	1011.4	10	1136	44	97
A_418.FIN2	807	694	0.16	1600	1.9510	0.0260	0.1720	0.0022	0.6861	0.0821	0.0008	1098	9	1023.0	12	1246	20	93
A_344.FIN2	121	466	0.87	780	1.7670	0.0350	0.1730	0.0015	0.1784	0.0742	0.0015	1031	13	1028.7	8	1042	39	100
A_439.FIN2	526	1164	0.48	2400	1.9570	0.0340	0.1771	0.0026	0.7395	0.0797	0.0010	1100	12	1051.0	14	1188	24	96
A_435.FIN2	200	485	0.57	2100	1.8340	0.0240	0.1778	0.0014	0.3851	0.0750	0.0009	1057	8	1054.9	7	1065	23	100
A_429.FIN2	47	69	0.32	30	1.8450	0.0550	0.1784	0.0022	0.1315	0.0760	0.0024	1062	20	1058.0	12	1068	62	100
A_434.FIN2	469	983	0.47	-104000	1.8480	0.0160	0.1792	0.0008	0.3562	0.0753	0.0006	1062	6	1063.2	4	1074	15	100
A_355.FIN2	60	296	1.07	630	1.9070	0.0450	0.1817	0.0018	0.3020	0.0757	0.0017	1081	16	1075.9	10	1066	46	100
A_436.FIN2	297	880	0.50	2200	2.2180	0.0480	0.1921	0.0026	0.5557	0.0854	0.0017	1185	15	1133.0	14	1318	38	96
A_367.FIN2	136	145	0.24	1300	2.2240	0.0710	0.1982	0.0030	0.3281	0.0811	0.0026	1187	23	1166.0	16	1232	55	98
A_425.FIN2	158	880	0.94	-70	2.6140	0.0480	0.2247	0.0022	0.1509	0.0864	0.0017	1303	14	1306.0	11	1340	37	100
A_405.FIN2	340	281	0.12	700	4.1300	0.0310	0.2934	0.0020	0.4873	0.1018	0.0007	1660	6	1658.0	10	1655	13	100
A_336.FIN2	167	404	0.28	2500	5.4090	0.0650	0.3011	0.0029	0.7392	0.1299	0.0011	1884	10	1698.0	14	2093	15	90
A_414.FIN2	325	3935	1.09	-500	12.1780	0.0850	0.4584	0.0028	0.7281	0.1929	0.0010	2617	7	2432.0	12	2766	8	93

Legend									
Cretaceous Upper	Jurassic	Permian	Devonian	Ordovician	Precambrian				
Cretaceous Lower	Triassic	Carboniferous	Silurian	Cambrian					

4.3.1.3 Mini Troll

Sample Mini Troll was collected from the Mini Troll fossil quarry, stratigraphically located within the middle portions of the Mussentuchit Member (Fig. 4.3.2). A representative (handpicked) population of zircon grains from the sample consisted of 90% magmatic grains exhibiting pristine, magmatic oscillatory zoning. A limited proportion (10%) of the grains exhibited homogenous sector zoning, associated with metamorphism, and approximately 25% of grains exhibited relict textures, evident from the high angle truncation and difference in luminosity under CL-imaging. Limited occurrences (1%) of convolute zoning is noted within the grains along fracture paths. Grains varied in size between 20 μm and 150 μm with the majority (60%) between 100 μm and 130 μm . Zircon crystals appear as euhedral, angular to sub-rounded grains with notably high aspect ratios and moderate amounts of microfracturing. Typical morphological types within the representative population of the Mini Troll sample include P1-P2, S6-S9, and R1-R2. Mini Troll yielded 129 analysable zircons, with 121 zircons falling within the 10% discordancy inclusion criteria. Core analysis was conducted on 15% of the samples with 85% representing rim analysis. The largest population within the sample, 79.34% (n=96), shows a Cenomanian age of 93.9 – 100 Ma, with subordinate populations of 10.74% (n=13) occurring at an Aptian age of 115-120 Ma, 2.48% (n=3) occurring around the Middle to Lower Devonian (380 – 410 Ma), and 2.48% (n=3) occurring around the Late Mesoproterozoic (1035-1125 Ma) (Fig. 4.3.4b; 4.3.5). Analysis of the sample yielded the following youngest age signatures: YSG at 96.1 (\pm 1.1) Ma; YPP at 99.8 Ma; YDZ at 93.958 (+1.5 – 5) Ma; YC1 σ (+3) at 96.1 (\pm 1.3) Ma; YC2 σ (+3) at 96.1 (\pm 1.9) Ma; weighted mean (10) at 96.8 (\pm 1.0) Ma; TuffZirc age at 97.1 (+0.5 – 0.9) Ma through a coherent group of 10 grains (Table 4.3.8).

Table 4.3.3: Pb/U data for sample Mini Troll. $^{206}\text{Pb}/^{238}\text{U}$ ratios used for age calculations.

Mini Troll				RATIOS								AGES [Ma]						Conc.
Analys	U [ppm] ^a	Pb [ppm] ^b	Th/U ^a	$^{206}\text{Pb}/^{238}\text{U}$ ^b	$^{207}\text{Pb}/^{235}\text{U}$ ^b	2σ ^d	$^{206}\text{Pb}/^{235}\text{U}$ ^b	2σ ^d	rho ^c	$^{207}\text{Pb}/^{206}\text{Pb}$ ^a	2σ ^d	$^{207}\text{Pb}/^{235}\text{U}$	2σ	$^{206}\text{Pb}/^{238}\text{U}$	2σ	$^{207}\text{Pb}/^{206}\text{Pb}$	2σ	%
A_170.FIN2	412	115	0.80	-10	0.1071	0.0078	0.0150	0.0004	0.1696	0.0516	0.0036	103	7	95.7	2	260	140	93
A_169.FIN2	753	106	0.42	250	0.1022	0.0027	0.0150	0.0002	0.2182	0.0492	0.0013	99	3	96.2	1	158	53	97
A_163.FIN2	751	186	0.80	430	0.0995	0.0029	0.0150	0.0002	0.2679	0.0484	0.0014	96	3	96.2	1	120	58	100
A_198.FIN2	336	98	0.60	160	0.1038	0.0093	0.0151	0.0004	0.0879	0.0504	0.0047	100	9	96.8	3	170	170	97
A_167.FIN2	394	86	0.65	51	0.0998	0.0038	0.0152	0.0002	0.1021	0.0480	0.0019	96	4	97.0	1	125	77	101
A_235.FIN2	361	134	0.99	410	0.1117	0.0068	0.0152	0.0003	0.1736	0.0530	0.0032	107	6	97.1	2	280	120	91
A_134.FIN2	1144	259	0.48	1080	0.1061	0.0044	0.0152	0.0003	0.2762	0.0502	0.0018	102	4	97.2	2	208	80	95
A_223.FIN2	273	64	0.70	-44	0.1052	0.0061	0.0152	0.0002	0.2270	0.0502	0.0028	101	6	97.3	2	180	100	96
A_195.FIN2	441	138	0.58	300	0.1030	0.0033	0.0153	0.0002	0.0248	0.0493	0.0017	99	3	97.5	1	151	65	98
A_260.FIN2	315	126	0.83	300	0.1127	0.0085	0.0153	0.0004	0.1510	0.0541	0.0045	108	8	97.6	3	310	160	90
A_154.FIN2	425	51	0.39	180	0.1096	0.0087	0.0153	0.0005	0.3283	0.0524	0.0040	105	8	97.6	3	270	150	93
A_129.FIN2	786	337	0.90	280	0.1051	0.0049	0.0153	0.0003	0.2423	0.0504	0.0023	101	5	97.6	2	197	91	96
A_181.FIN2	1220	244	0.45	410	0.1026	0.0026	0.0153	0.0002	0.3050	0.0489	0.0012	99	2	97.7	1	139	49	99
A_184.FIN2	987	209	0.45	750	0.1044	0.0034	0.0153	0.0003	0.2089	0.0504	0.0018	101	3	97.8	2	202	72	97
A_171.FIN2	239	112	1.33	270	0.1044	0.0052	0.0153	0.0002	0.0603	0.0497	0.0026	100	5	97.9	2	163	97	98
A_177.FIN2	1199	317	0.66	0	0.1120	0.0120	0.0153	0.0006	0.0423	0.0535	0.0062	108	11	98.0	4	310	230	91
A_166.FIN2	219	39	0.51	100	0.1092	0.0077	0.0154	0.0004	0.1124	0.0516	0.0037	105	7	98.2	2	270	150	94
A_264.FIN2	574	181	0.65	390	0.1062	0.0051	0.0154	0.0003	0.4346	0.0503	0.0022	102	5	98.2	2	199	89	96
A_179.FIN2	399	129	0.75	220	0.1049	0.0056	0.0154	0.0003	0.1087	0.0497	0.0026	101	5	98.2	2	180	100	97
A_164.FIN2	750	103	0.41	510	0.1032	0.0031	0.0154	0.0002	0.2625	0.0488	0.0015	100	3	98.2	1	133	58	99
A_202.FIN2	146	34	0.46	37	0.1104	0.0087	0.0154	0.0004	0.1288	0.0525	0.0041	106	8	98.4	2	250	150	93
A_225.FIN2	540	147	0.84	160	0.1073	0.0047	0.0154	0.0003	0.2538	0.0509	0.0022	103	4	98.4	2	218	88	95
A_214.FIN2	520	116	0.63	-1200	0.1040	0.0046	0.0154	0.0002	0.2019	0.0494	0.0022	100	4	98.4	2	148	84	98
A_180.FIN2	335	89	0.59	70	0.1072	0.0048	0.0154	0.0003	0.1586	0.0513	0.0024	103	4	98.5	2	220	90	96
A_252.FIN2	404	181	0.94	23	0.1037	0.0042	0.0154	0.0002	0.1550	0.0484	0.0019	100	4	98.5	1	129	77	99
A_133.FIN2	292	51	0.36	290	0.1050	0.0056	0.0154	0.0003	0.1047	0.0501	0.0027	101	5	98.6	2	180	110	98
A_238.FIN2	350	58	0.44	70	0.1113	0.0074	0.0154	0.0003	0.1370	0.0528	0.0036	107	7	98.7	2	270	130	93
A_261.FIN2	1288	716	1.68	1600	0.1080	0.0051	0.0154	0.0003	0.2208	0.0510	0.0024	104	5	98.7	2	224	97	95
A_258.FIN2	1165	500	0.90	730	0.1081	0.0035	0.0155	0.0003	0.2922	0.0508	0.0016	104	3	98.8	2	219	66	95
A_212.FIN2	951	189	0.54	1140	0.1056	0.0033	0.0154	0.0002	0.2100	0.0502	0.0016	102	3	98.8	1	189	67	97
A_190.FIN2	1734	392	0.42	910	0.1061	0.0038	0.0155	0.0003	0.2127	0.0503	0.0019	102	4	98.9	2	199	79	97
A_160.FIN2	901	137	0.48	240	0.1047	0.0027	0.0155	0.0002	0.3677	0.0494	0.0012	101	3	98.9	1	159	51	98
A_270.FIN2	960	214	0.45	1240	0.1070	0.0026	0.0155	0.0002	0.3650	0.0501	0.0011	103	2	99.0	1	194	45	96
A_199.FIN2	586	229	0.72	680	0.1063	0.0036	0.0155	0.0002	0.2423	0.0499	0.0016	102	3	99.0	1	175	63	97
A_246.FIN2	1553	610	1.18	9700	0.1058	0.0020	0.0155	0.0002	0.4633	0.0496	0.0008	102	2	99.0	1	177	37	97
A_231.FIN2	212	32	0.42	2	0.1091	0.0059	0.0155	0.0003	0.0581	0.0518	0.0029	105	6	99.1	2	230	110	94
A_189.FIN2	208	56	0.51	53	0.1065	0.0066	0.0155	0.0003	0.1554	0.0502	0.0031	102	6	99.1	2	160	110	97
A_203.FIN2	859	155	0.37	190	0.1039	0.0031	0.0155	0.0002	0.3307	0.0484	0.0013	101	3	99.2	1	127	55	99
A_142.FIN2	515	131	0.70	-770	0.1067	0.0052	0.0155	0.0003	0.4400	0.0500	0.0022	103	5	99.3	2	173	85	97
A_267.FIN2	919	886	3.04	1260	0.1060	0.0035	0.0155	0.0002	0.2499	0.0499	0.0016	102	3	99.3	1	179	66	97
A_251.FIN2	973	205	0.43	220	0.1093	0.0047	0.0155	0.0003	0.4116	0.0511	0.0020	105	4	99.4	2	232	80	94
A_205.FIN2	994	355	0.82	860	0.1055	0.0031	0.0156	0.0002	0.3819	0.0496	0.0014	102	3	99.4	1	169	55	97
A_162.FIN2	218	51	0.71	12	0.1050	0.0052	0.0155	0.0003	0.1475	0.0490	0.0024	101	5	99.4	2	152	96	99
A_233.FIN2	357	57	0.43	96	0.1111	0.0059	0.0156	0.0003	0.1089	0.0518	0.0027	107	5	99.5	2	250	100	93
A_256.FIN2	760	234	0.58	540	0.1094	0.0042	0.0156	0.0002	0.2033	0.0516	0.0020	105	4	99.5	2	251	80	95
A_161.FIN2	422	71	0.52	83	0.1033	0.0040	0.0156	0.0002	0.2547	0.0482	0.0018	100	4	99.6	2	104	71	100
A_248.FIN2	536	167	0.66	680	0.1085	0.0037	0.0156	0.0002	0.2432	0.0505	0.0017	104	3	99.7	1	195	66	96
A_220.FIN2	761	175	0.65	330	0.1086	0.0037	0.0156	0.0003	0.1556	0.0511	0.0019	105	3	99.8	2	225	74	96
A_226.FIN2	1126	286	0.81	790	0.1053	0.0025	0.0156	0.0002	0.4264	0.0489	0.0010	102	2	99.8	1	145	44	98
A_176.FIN2	579	128	0.54	180	0.1108	0.0061	0.0156	0.0003	0.4126	0.0522	0.0026	108	6	99.9	2	280	100	92
A_149.FIN2	310	51	0.48	234	0.1063	0.0044	0.0156	0.0002	0.0676	0.0498	0.0022	103	4	99.9	1	167	83	97
A_132.FIN2	453	113	0.50	150	0.1063	0.0034	0.0156	0.0002	0.0744	0.0494	0.0016	102	3	99.9	1	163	65	98
A_271.FIN2	1590	672	1.40	1100	0.1114	0.0040	0.0156	0.0003	0.2850	0.0518	0.0018	107	4	100.0	2	264	77	93
A_263.FIN2	264	57	0.40	19	0.1113	0.0055	0.0156	0.0003	0.1324	0.0519	0.0026	107	5	100.0	2	237	98	94
A_273.FIN2	522	158	0.70	650	0.1060	0.0052	0.0156	0.0003	0.1718	0.0489	0.0023	102	5	100.0	2	153	96	98
A_165.FIN2	591	71	0.36	370	0.1091	0.0055	0.0156	0.0003	0.2780	0.0510	0.0024	105	5	100.1	2	224	98	95
A_168.FIN2	318	110	1.09	180	0.1109	0.0071	0.0157	0.0003	0.1271	0.0519	0.0034	106	7	100.2	2	250	130	94
A_250.FIN2	474	160	0.72	230	0.1104	0.0066	0.0157	0.0004	0.1180	0.0516	0.0035	106	6	100.2	2	230	130	94
A_130.FIN2	610	199	0.64	260	0.1027	0.0032	0.0157	0.0002	0.2603	0.0475	0.0014	99	3	100.2	1	96	59	101
A_249.FIN2	536	302	1.18	130	0.1108	0.0058	0.0157	0.0003	0.0647	0.0513	0.0027	106	5	100.3	2	240	110	94
A_239.FIN2	985	225	0.55	470	0.1101	0.0031	0.0157	0.0002	0.2008	0.0506	0.0015	106	3	100.4	2	217	62	95
A_143.FIN2	462	111	0.71	1500	0.1037	0.0078	0.0157	0.0004	0.3741	0.0490	0.0037	100	7	100.4	3	130	140	101

A_145.FIN2	269	45	0.46	260	0.1106	0.0071	0.0157	0.0003	0.0458	0.0517	0.0034	106	7	100.5	2	230	130	95
A_137.FIN2	721	176	0.58	-360	0.1141	0.0075	0.0157	0.0004	0.3974	0.0521	0.0027	109	7	100.6	2	290	120	92
A_259.FIN2	580	112	0.38	40	0.1095	0.0047	0.0157	0.0002	0.3133	0.0507	0.0021	105	4	100.6	2	214	82	96
A_237.FIN2	731	121	0.41	2090	0.1079	0.0039	0.0157	0.0002	0.3211	0.0498	0.0016	104	4	100.6	1	178	65	97
A_244.FIN2	237	72	0.69	-100	0.1060	0.0056	0.0157	0.0003	0.0479	0.0491	0.0027	102	5	100.6	2	119	99	99
A_158.FIN2	833	159	0.59	120	0.1091	0.0053	0.0158	0.0004	0.0405	0.0505	0.0027	106	5	101.2	2	220	110	95
A_265.FIN2	507	144	0.57	190	0.1085	0.0042	0.0159	0.0003	0.1551	0.0499	0.0020	105	4	101.4	2	176	79	97
A_254.FIN2	189	64	0.60	205	0.1069	0.0056	0.0159	0.0003	0.1250	0.0490	0.0026	103	5	101.4	2	132	98	99
A_194.FIN2	439	99	0.39	170	0.1058	0.0042	0.0159	0.0002	0.1734	0.0484	0.0019	102	4	101.5	1	113	75	100
A_247.FIN2	609	131	0.44	2400	0.1068	0.0032	0.0159	0.0002	0.2666	0.0486	0.0014	103	3	101.6	1	124	58	99
A_131.FIN2	463	197	0.85	160	0.1109	0.0059	0.0159	0.0003	0.2827	0.0509	0.0026	106	5	101.7	2	210	100	96
A_136.FIN2	681	183	0.59	2700	0.1096	0.0034	0.0159	0.0002	0.2191	0.0502	0.0015	106	3	101.7	1	187	62	96
A_201.FIN2	328	74	0.45	210	0.1079	0.0053	0.0159	0.0003	0.2907	0.0495	0.0024	104	5	101.7	2	149	92	98
A_187.FIN2	835	206	0.49	400	0.1097	0.0036	0.0159	0.0002	0.2283	0.0503	0.0016	106	3	101.8	1	198	67	96
A_148.FIN2	486	98	0.61	150	0.1092	0.0050	0.0159	0.0003	0.1878	0.0502	0.0022	105	5	101.8	2	193	89	97
A_197.FIN2	802	435	1.05	430	0.1092	0.0033	0.0159	0.0002	0.2625	0.0499	0.0015	105	3	101.8	1	187	60	97
A_222.FIN2	511	78	0.46	-40	0.1081	0.0059	0.0159	0.0003	0.1819	0.0497	0.0027	104	5	101.8	2	190	110	98
A_159.FIN2	750	176	0.68	200	0.1106	0.0056	0.0160	0.0004	0.0580	0.0509	0.0028	106	5	102.0	3	240	120	96
A_135.FIN2	482	285	1.27	430	0.1062	0.0037	0.0160	0.0002	0.0561	0.0484	0.0017	102	3	102.4	1	122	70	100
A_266.FIN2	494	110	0.42	460	0.1092	0.0035	0.0160	0.0002	0.1693	0.0495	0.0016	105	3	102.5	1	158	65	98
A_144.FIN2	597	73	0.32	1240	0.1064	0.0028	0.0160	0.0002	0.1879	0.0489	0.0014	103	3	102.6	1	142	57	100
A_227.FIN2	389	121	0.82	250	0.1102	0.0045	0.0161	0.0002	0.1000	0.0499	0.0021	106	4	102.7	1	169	80	97
A_178.FIN2	771	146	0.40	220	0.1073	0.0033	0.0162	0.0002	0.1916	0.0479	0.0014	103	3	103.6	1	110	59	100
A_230.FIN2	756	207	0.82	130	0.1187	0.0055	0.0163	0.0003	0.4934	0.0531	0.0022	114	5	103.9	2	308	86	91
A_156.FIN2	467	58	0.36	240	0.1084	0.0038	0.0163	0.0002	0.2908	0.0487	0.0017	104	4	103.9	1	127	66	100
A_157.FIN2	644	129	0.60	610	0.1121	0.0052	0.0163	0.0003	0.3303	0.0502	0.0023	108	5	104.1	2	203	92	97
A_224.FIN2	436	63	0.38	210	0.1117	0.0042	0.0163	0.0002	0.2034	0.0502	0.0019	108	4	104.2	2	189	76	97
A_155.FIN2	576	80	0.40	320	0.1095	0.0045	0.0164	0.0003	0.2990	0.0493	0.0020	105	4	104.7	2	157	81	99
A_210.FIN2	808	117	0.36	570	0.1087	0.0039	0.0164	0.0003	0.1816	0.0486	0.0018	105	4	104.7	2	125	73	100
A_268.FIN2	385	91	0.41	170	0.1196	0.0059	0.0167	0.0003	0.4554	0.0512	0.0024	114	5	106.8	2	246	96	93
A_245.FIN2	387	103	0.55	510	0.1131	0.0048	0.0168	0.0002	0.1393	0.0491	0.0021	109	4	107.1	2	141	82	99
A_236.FIN2	770	183	0.50	1180	0.1181	0.0042	0.0168	0.0003	0.4197	0.0509	0.0017	113	4	107.5	2	230	72	95
A_196.FIN2	166	48	0.43	230	0.1221	0.0096	0.0169	0.0006	0.1345	0.0543	0.0050	117	9	107.8	4	320	180	92
A_204.FIN2	260	55	0.41	126	0.1188	0.0051	0.0171	0.0003	0.1249	0.0505	0.0022	114	5	109.3	2	203	85	96
A_182.FIN2	459	196	0.80	360	0.1158	0.0038	0.0173	0.0002	0.1924	0.0485	0.0016	111	3	110.6	1	139	65	100
A_183.FIN2	274	103	0.69	180	0.1244	0.0068	0.0177	0.0003	0.2013	0.0519	0.0029	119	6	113.2	2	260	110	95
A_269.FIN2	233	90	0.69	27	0.1329	0.0079	0.0179	0.0004	0.0293	0.0539	0.0033	126	7	114.1	3	330	130	90
A_188.FIN2	80	18	0.36	51	0.1310	0.0120	0.0182	0.0005	0.0022	0.0528	0.0050	124	11	115.9	3	230	170	93
A_186.FIN2	839	347	0.72	340	0.1290	0.0067	0.0182	0.0003	0.2364	0.0515	0.0025	123	6	116.0	2	250	100	94
A_253.FIN2	396	123	0.53	90	0.1240	0.0042	0.0182	0.0002	0.0758	0.0491	0.0016	118	4	116.0	2	163	69	98
A_192.FIN2	388	149	0.61	220	0.1221	0.0047	0.0182	0.0002	0.2290	0.0488	0.0018	117	4	116.0	2	129	72	99
A_262.FIN2	124	29	0.37	100	0.1320	0.0140	0.0183	0.0006	0.1856	0.0527	0.0055	125	12	116.7	4	240	200	93
A_255.FIN2	327	78	0.37	310	0.1235	0.0050	0.0185	0.0002	0.1789	0.0486	0.0020	118	5	118.3	2	118	77	100
A_232.FIN2	64	13	0.43	3	0.1320	0.0110	0.0186	0.0005	0.0758	0.0528	0.0047	125	10	118.8	3	200	160	95
A_272.FIN2	569	211	0.66	250	0.1264	0.0040	0.0186	0.0002	0.1474	0.0486	0.0015	121	4	119.1	2	131	61	98
A_147.FIN2	321	76	0.54	-30	0.1321	0.0097	0.0187	0.0005	0.3786	0.0516	0.0035	127	8	119.6	3	230	130	94
A_228.FIN2	165	31	0.40	110	0.1349	0.0096	0.0194	0.0004	0.1154	0.0508	0.0036	129	9	123.6	3	200	140	96
A_217.FIN2	1603	254	0.29	990	0.1648	0.0026	0.0242	0.0003	0.3947	0.0492	0.0007	155	2	154.2	2	160	32	100
A_193.FIN2	536	204	0.44	390	0.1698	0.0052	0.0249	0.0004	0.1761	0.0501	0.0016	159	5	158.3	2	186	63	100
A_229.FIN2	351	304	1.01	440	0.2930	0.0140	0.0403	0.0008	0.3507	0.0531	0.0024	260	11	254.8	5	304	93	98
A_151.FIN2	658	943	1.25	1010	0.4665	0.0094	0.0603	0.0008	0.3948	0.0565	0.0011	388	7	377.2	5	467	43	97
A_221.FIN2	188	186	0.63	750	0.5570	0.0140	0.0716	0.0009	0.3167	0.0565	0.0014	449	9	445.5	5	441	51	99
A_150.FIN2	283	511	1.14	500	0.5830	0.0200	0.0733	0.0014	0.3929	0.0574	0.0018	465	13	456.2	8	478	70	98
A_191.FIN2	138	250	0.60	450	0.6960	0.0240	0.0865	0.0013	0.2739	0.0587	0.0021	536	15	535.0	8	519	75	100
A_153.FIN2	368	757	1.00	2900	0.8240	0.0180	0.0976	0.0014	0.3411	0.0609	0.0013	609	10	600.2	8	617	46	99
A_215.FIN2	116	560	1.37	2300	1.5910	0.0320	0.1605	0.0018	0.3539	0.0720	0.0014	963	13	999.0	10	963	40	100
A_218.FIN2	118	257	0.60	430	1.7600	0.0350	0.1719	0.0019	0.4669	0.0742	0.0013	1027	13	1022.0	10	1029	37	100
A_146.FIN2	127	227	0.46	1250	1.8900	0.1200	0.1804	0.0033	0.7827	0.0763	0.0038	1065	31	1068.0	18	1042	59	100
A_185.FIN2	100	401	0.57	-10	2.7530	0.0850	0.2211	0.0056	0.6106	0.0911	0.0024	1339	23	1287.0	29	1438	48	96

Legend

Cretaceous Upper	Jurassic	Permian	Devonian	Ordovician	Precambrian
Cretaceous Lower	Triassic	Carboniferous	Silurian	Cambrian	

4.3.1.4 Monollo-09-15

Sample Monollo-09-15 was collected from the Hard-Boiled Jack fossil quarry, previously excavated by the Oklahoma Museum of Natural History and is stratigraphically located within the lower portions of the Mussentuchit Member (Fig. 4.3.2). A representative (handpicked) population of zircon grains from the sample consisted of more than 95% magmatic grains exhibiting pristine, magmatic oscillatory zoning (Fig. 4.3.3). Almost none (<1%) of the grains exhibited homogenous sector zoning associated with metamorphism. Relict textures were also very limited, with only approximately 5% of the representative grains exhibiting the typical high angle truncation and differential luminosity associated with relict grain textures. Grains varied in size between 50 μm and 300 μm with the majority (70%) between 70 μm and 90 μm . Zircon crystals appeared as very euhedral, angular to sub-angular grains with only modest amounts of microfracturing. Typical morphological types within the representative population of the Monollo-09-15 sample include P2, S6-S9, and R1-R2. Monollo-09-15 yielded 122 analysable zircons, with 117 zircons falling within the 10% discordancy inclusion criteria. Core analysis was conducted on 10% of the samples with 90% representing rim analysis. The sample shows a single population of 91% ($n=107$) at an Aptian age of 115-120 Ma, with no other populations consisting of more than 2 grains present (Fig. 4.3.4a; 4.3.5). A single oldest grain of Mesoproterozoic age (1498 Ma) is also present. Analysis of the sample yielded the following youngest age signatures: YSG at 105 (± 0.9) Ma; YPP at 119.8 Ma; YDZ at 105.17 ($+1.7 - 2.3$) Ma; YC1 σ ($+3$) at 108.6 (± 1.3) Ma; YC2 σ ($+3$) at 108.6 (± 105) Ma; weighted mean (10) at 112.1 (± 2.9) Ma; TuffZirc age at 114.9 ($+0.4 - 0.9$) Ma through a coherent group of 8 out of 10 grains (Table 4.3.8).

Table 4.3.4: Pb/U data for sample Monollo-09-15. ²⁰⁶Pb/²³⁸U ratio used for age calculations.

Monollo				RATIOS								AGES [Ma]				Conc.		
Analysis	U [ppm] ^a	Pb [ppm] ^a	Th U ^a	²⁰⁶ Pb/ ²⁰⁴ Pb	²⁰⁷ Pb/ ²³⁵ U ^b	2 σ ^d	²⁰⁶ Pb/ ²³⁸ U ^c	2 σ ^d	rho ^e	²⁰⁷ Pb/ ²³⁶ Pb ^f	2 σ ^d	²⁰⁷ Pb/ ²³⁵ U	2 σ	²⁰⁶ Pb/ ²³⁸ U	2 σ	²⁰⁷ Pb/ ²³⁵ U	2 σ	%
A_169.FIN2	789	126.3	0.343473	51.5	0.1113	0.0025	0.01641	0.00014	0.057636	0.0492	0.0012	107	2.3	105.0	0.9	154	48	98
A_236.FIN2	476	183	0.77521	25.5	0.1153	0.0035	0.01681	0.00018	0.15364	0.0501	0.0016	111	3.2	107.4	1.1	186	62	97
A_140.FIN2	541.9	151.3	0.5704	18.42	0.1201	0.003	0.01773	0.00015	0.18949	0.0487	0.0012	115.6	2.7	113.3	0.92	143	50	98
A_177.FIN2	648.9	135	0.411311	34.5	0.121	0.0033	0.01786	0.00015	0.10311	0.0491	0.0013	115.8	3	114.1	0.98	160	56	99
A_162.FIN2	520	330	1.313462	39.8	0.1217	0.0033	0.0179	0.00017	0.30713	0.0492	0.0014	116.5	3	114.4	1.1	160	58	98
A_164.FIN2	211	82.1	0.780569	17.3	0.1209	0.005	0.01799	0.00022	0.11325	0.049	0.002	115.4	4.5	114.9	1.4	136	76	100
A_160.FIN2	209.6	72.5	0.692748	17.6	0.1265	0.0068	0.01801	0.00028	0.17391	0.0507	0.0027	120.6	6.1	115.0	1.8	210	110	95
A_156.FIN2	329.3	93.5	0.558457	28	0.119	0.0032	0.018	0.00016	0.16934	0.0477	0.0013	114.3	3	115.0	1	99	54	101
A_183.FIN2	264.2	80.9	0.577593	13.21	0.1194	0.0051	0.01805	0.00022	0.057482	0.0483	0.0021	114	4.6	115.3	1.4	107	80	101
A_258.FIN2	323.2	87.8	0.5362	20.1	0.1229	0.0098	0.01813	0.0004	0.38679	0.0493	0.0036	122	12	115.8	2.6	220	290	95
A_193.FIN2	199	82.3	0.763819	13.5	0.1246	0.0076	0.01817	0.00029	0.14803	0.0497	0.0029	118.6	6.8	116.1	1.9	160	110	98
A_268.FIN2	394	115.9	0.63198	22.1	0.1258	0.0054	0.0182	0.00026	0.1797	0.0504	0.0023	120.1	4.9	116.2	1.6	198	91	97
A_184.FIN2	599.9	148.5	0.489915	27.8	0.1237	0.0046	0.0182	0.0002	0.090465	0.0495	0.0019	118.2	4.1	116.2	1.3	172	75	98
A_230.FIN2	623	154.7	0.486356	35	0.1232	0.0031	0.01819	0.00018	0.3007	0.0493	0.0012	117.8	2.8	116.2	1.2	153	49	99
A_142.FIN2	329.1	132.1	0.863567	14.7	0.1273	0.0069	0.01824	0.00034	0.10528	0.0505	0.0036	121.3	7.9	116.5	2.2	200	140	96
A_221.FIN2	534.3	107.6	0.393225	28.6	0.1229	0.0032	0.01824	0.00015	0.063327	0.0494	0.0013	117.5	2.9	116.5	0.96	164	54	99
A_163.FIN2	107.6	53	0.957249	7.47	0.128	0.012	0.01829	0.00049	0.08158	0.0511	0.0053	121	11	116.8	3.1	190	290	97
A_152.FIN2	196.1	50.6	0.537481	15.4	0.1286	0.0084	0.01831	0.00028	0.072328	0.0508	0.0033	122.3	7.5	116.9	1.8	230	130	96
A_245.FIN2	493.5	178	0.704357	27.5	0.1269	0.0044	0.01832	0.00019	0.14984	0.0503	0.0017	121	3.9	117.0	1.2	192	68	97
A_159.FIN2	537	145.1	0.561266	45.3	0.1264	0.0041	0.01832	0.0002	0.055669	0.0501	0.0018	120.7	3.7	117.0	1.3	198	74	97
A_155.FIN2	247.5	122.7	0.962828	20.6	0.1244	0.0044	0.01832	0.00017	0.078659	0.0492	0.0018	118.7	3.9	117.0	1.1	144	69	99
A_251.FIN2	275.2	64.7	0.421948	14.21	0.1275	0.0064	0.01833	0.00028	0.081174	0.0506	0.0026	121.5	5.8	117.1	1.8	200	100	96
A_200.FIN2	309	101.7	0.618123	17.4	0.1255	0.0051	0.01834	0.0003	0.003359	0.05	0.0022	119.7	4.6	117.1	1.9	188	86	98
A_260.FIN2	857	112	0.238623	48.2	0.132	0.014	0.01835	0.00049	0.024581	0.0525	0.0056	126	12	117.2	3.1	300	230	93
A_174.FIN2	655	178	0.546565	35	0.127	0.012	0.01839	0.00063	0.36296	0.0501	0.0045	122	11	117.5	4	180	180	96
A_185.FIN2	598	113.5	0.361204	27.9	0.1249	0.0059	0.0184	0.00027	0.27215	0.0493	0.0023	119.2	5.4	117.5	1.7	157	92	99
A_198.FIN2	2075	445.8	0.416482	118.4	0.1251	0.0019	0.0184	0.00013	0.21292	0.04963	0.00075	119.7	1.7	117.6	0.81	173	33	98
A_150.FIN2	183.1	66.4	0.699618	14.31	0.1243	0.0044	0.01842	0.00019	0.024006	0.049	0.0018	119.1	4	117.6	1.2	136	71	99
A_252.FIN2	293.3	46.5	0.30924	17.7	0.1243	0.0081	0.01842	0.00028	0.073704	0.049	0.0032	118.5	7.3	117.6	1.8	160	130	99
A_272.FIN2	316.1	71.2	0.430244	16.7	0.1291	0.0092	0.01843	0.0004	0.32107	0.0507	0.0034	123	8.2	117.7	2.5	210	140	96
A_227.FIN2	189.5	65.4	0.614776	10.2	0.131	0.015	0.01846	0.00078	0.16943	0.0521	0.0062	125	14	117.9	5	250	240	94
A_157.FIN2	222.8	140.7	1.208259	19.19	0.1273	0.0049	0.01846	0.00023	0.029889	0.0501	0.002	121.3	4.4	117.9	1.4	180	79	97
A_264.FIN2	625.8	136.1	0.424736	41.1	0.1238	0.0026	0.01847	0.00014	0.066111	0.0486	0.0011	118.4	2.3	118.0	0.89	130	44	100
A_205.FIN2	359.9	211.1	1.071964	25.6	0.1287	0.0082	0.01847	0.00035	0.078445	0.052	0.0037	122.7	7.4	118.0	2.2	260	140	96
A_145.FIN2	451.8	133.3	0.582116	24.9	0.1245	0.0038	0.01848	0.00017	0.19925	0.0486	0.0015	119	3.4	118.0	1.1	127	61	99
A_196.FIN2	480.7	186.7	0.788642	29.2	0.1258	0.0051	0.01849	0.00025	0.010649	0.0494	0.002	120.1	4.6	118.1	1.6	166	84	98
A_266.FIN2	810	232.7	0.57284	44.3	0.1254	0.0028	0.0185	0.00014	0.23234	0.0491	0.0011	119.8	2.5	118.2	0.88	150	45	99
A_143.FIN2	399.6	237.9	1.248749	17.53	0.1283	0.0047	0.01852	0.00022	0.10018	0.0503	0.0019	122.4	4.2	118.3	1.4	199	79	97
A_195.FIN2	684	90.5	0.241374	42.2	0.1252	0.0032	0.01853	0.00015	0.034564	0.0494	0.0013	119.6	2.9	118.4	0.92	160	53	99
A_136.FIN2	173.7	49.9	0.524467	2.888	0.13	0.01	0.01854	0.00034	0.027258	0.0506	0.0041	123	9.3	118.4	2.2	180	150	96
A_154.FIN2	187	93	0.986631	13.7	0.1267	0.005	0.01853	0.00024	0.16613	0.0494	0.002	120.8	4.5	118.4	1.5	174	81	98
A_257.FIN2	706	159.6	0.46983	44.7	0.1254	0.0038	0.01854	0.0002	0.21749	0.049	0.0015	119.8	3.4	118.4	1.2	143	62	99
A_254.FIN2	238.3	48.4	0.373898	15.59	0.1247	0.0047	0.01853	0.00021	0.018759	0.0491	0.0019	119	4.2	118.4	1.3	145	76	99
A_186.FIN2	1106	238.2	0.412297	49.7	0.1253	0.0027	0.01854	0.00015	0.10128	0.0492	0.0011	119.7	2.4	118.4	0.97	160	47	99
A_146.FIN2	369	139.2	0.780488	22.3	0.1294	0.005	0.01858	0.00021	0.2892	0.0508	0.0019	123.3	4.5	118.6	1.3	212	77	96
A_217.FIN2	946	220.2	0.454228	56	0.1236	0.0027	0.01858	0.00016	0.18475	0.0483	0.001	118.2	2.5	118.6	1	127	46	100
A_187.FIN2	971	209	0.416066	48.1	0.1257	0.0031	0.01858	0.00016	0.24104	0.0492	0.0012	120.1	2.7	118.7	0.99	151	49	99
A_247.FIN2	253.6	90	0.663249	15.5	0.1268	0.0071	0.01858	0.00039	0.057011	0.0498	0.0029	120.9	6.4	118.7	2.4	170	120	98
A_214.FIN2	309.8	63.4	0.393157	22	0.1249	0.0039	0.01859	0.00016	0.21704	0.0493	0.0016	119.3	3.5	118.7	1	161	63	99
A_218.FIN2	351.6	75	0.394767	24	0.1247	0.0038	0.01859	0.00019	0.030537	0.049	0.0015	119.1	3.5	118.7	1.2	153	64	100
A_147.FIN2	239.1	90.2	0.735675	16.47	0.1298	0.0047	0.01861	0.00018	0.078358	0.0504	0.0018	123.5	4.2	118.8	1.1	193	72	96
A_179.FIN2	388	102.6	0.539691	16.4	0.1292	0.0079	0.0186	0.00029	0.1886	0.0507	0.0031	122.9	7.1	118.8	1.8	200	120	97
A_209.FIN2	1709	498	0.580456	132.4	0.1285	0.0033	0.01859	0.00016	0.36873	0.0504	0.0012	122.6	2.9	118.8	1	206	51	97
A_232.FIN2	475.4	160.5	0.645982	31.2	0.1278	0.0049	0.0186	0.00022	0.002378	0.0501	0.002	121.9	4.4	118.8	1.4	186	80	97
A_201.FIN2	1492	313.1	0.41555	94.5	0.1248	0.0028	0.01861	0.00015	0.22877	0.0489	0.0011	119.3	2.5	118.9	0.95	143	45	100
A_148.FIN2	199	79.4	0.809045	13.62	0.1285	0.0065	0.01863	0.00028	0.078924	0.0502	0.0027	122.5	5.9	119.0	1.8	190	110	97
A_144.FIN2	550.8	127.9	0.490559	29.2	0.1278	0.0036	0.01863	0.00022	0.064583	0.0495	0.0015	122	3.2	119.0	1.4	167	61	98
A_182.FIN2	1737	1424	1.519862	77.3	0.1263	0.0028	0.01863	0.00018	0.38078	0.0494	0.001	120.7	2.5	119.0	1.2	162	44	99
A_216.FIN2	258	65	0.464729	16.35	0.1234	0.0044	0.01863	0.00019	0.048499	0.0486	0.0018	117.8	4	119.0	1.2	127	73	101
A_153.FIN2	876	374	0.884703	63.8	0.1263	0.0025	0.01865	0.00015	0.15974	0.0489	0.00096	120.7	2.2	119.1	0.93	142	41	99
A_170.FIN2	534	72	0.255993	38.1	0.1263	0.003	0.01865	0.00015	0.000478	0.0491	0.0012	120.6	2.7</					

A_263.FIN2	546.1	115.7	0.427577	32.7	0.1333	0.0084	0.01868	0.0004	0.32906	0.0517	0.0031	126.8	7.5	119.3	2.6	260	130	94
A_267.FIN2	253.1	47.3	0.377716	14.24	0.1297	0.0061	0.01868	0.00028	0.13093	0.0505	0.0024	123.5	5.5	119.3	1.8	203	98	97
A_223.FIN2	648	247.4	0.766975	35.3	0.1298	0.0068	0.01869	0.0003	0.026716	0.0504	0.0028	123.7	6.1	119.4	1.9	200	110	97
A_271.FIN2	310.9	80.5	0.498231	18.53	0.1245	0.0041	0.01873	0.00018	0.06922	0.0485	0.0016	119.3	3.6	119.6	1.2	121	63	100
A_253.FIN2	792	157.6	0.377778	54.5	0.1279	0.0034	0.01874	0.00019	0.27449	0.0494	0.0013	122	3.1	119.7	1.2	163	54	98
A_204.FIN2	392.7	61	0.286224	28.4	0.127	0.0046	0.01875	0.0002	0.066708	0.0496	0.0019	121.1	4.2	119.7	1.2	164	76	99
A_219.FIN2	512.4	110.8	0.399688	33.4	0.1258	0.0033	0.01875	0.00015	0.23922	0.0488	0.0012	120.5	2.9	119.7	0.97	140	51	99
A_233.FIN2	371.4	190	0.76979	20.2	0.1312	0.0093	0.01875	0.00044	0.25634	0.0511	0.0035	124.9	8.3	119.8	2.8	230	140	96
A_265.FIN2	354	81.2	0.435028	20	0.1277	0.0096	0.01876	0.00045	0.1814	0.0507	0.0028	124.5	7.2	119.8	2.8	220	120	96
A_149.FIN2	206.8	48	0.454062	13.63	0.1297	0.0042	0.01876	0.00023	0.34268	0.0506	0.0017	123.9	3.9	119.8	1.4	208	67	97
A_189.FIN2	507.8	120.9	0.460614	26.9	0.1288	0.0046	0.01876	0.0002	0.16255	0.05	0.0018	122.8	4.1	119.8	1.2	191	72	98
A_219.FIN2	317.5	85.3	0.506457	19.88	0.1285	0.0047	0.01876	0.0002	0.042947	0.0496	0.0018	122.4	4.2	119.8	1.3	169	73	98
A_190.FIN2	384.5	122.1	0.59948	22.6	0.1275	0.0043	0.01875	0.00018	0.093429	0.0494	0.0017	121.5	3.8	119.8	1.2	165	67	99
A_220.FIN2	536.7	151.6	0.516303	24.7	0.1259	0.0033	0.01878	0.00018	0.082718	0.0489	0.0013	120.2	3	119.9	1.2	144	53	100
A_188.FIN2	782	163	0.407928	42.7	0.1285	0.0043	0.01881	0.00023	0.29582	0.0497	0.0016	122.6	3.8	120.1	1.4	171	66	98
A_210.FIN2	559	67.6	0.214311	42.8	0.1257	0.0035	0.01881	0.00015	0.1079	0.0486	0.0013	120	3.1	120.1	0.98	138	55	100
A_149.FIN2	961	200.6	0.391467	55.6	0.1269	0.0026	0.01881	0.00013	0.43408	0.04925	0.00095	121.5	2.3	120.1	0.82	161	41	99
A_242.FIN2	274.6	59.3	0.394392	15.8	0.1305	0.0047	0.01883	0.00021	0.035897	0.0508	0.0019	124.6	4.3	120.2	1.3	205	74	96
A_237.FIN2	680.6	173.2	0.454452	43.1	0.1272	0.0036	0.01883	0.00019	0.31547	0.0491	0.0013	121.4	3.3	120.3	1.2	143	58	99
A_219.FIN2	271	62.7	0.431734	14.91	0.1272	0.0052	0.01884	0.00018	0.25127	0.0492	0.002	121.1	4.7	120.3	1.1	145	77	99
A_197.FIN2	656	131.6	0.370732	42.8	0.124	0.003	0.01885	0.00016	0.19853	0.048	0.0011	118.5	2.7	120.4	0.98	103	47	102
A_248.FIN2	768.6	185	0.510018	49.2	0.1301	0.0088	0.01886	0.00027	0.41044	0.0501	0.0031	123.8	7.8	120.4	1.7	180	120	97
A_166.FIN2	271.3	85.7	0.618872	22.3	0.131	0.013	0.01888	0.00048	0.2207	0.0503	0.0046	124	11	120.6	3	190	180	97
A_175.FIN2	1050	184	0.333181	59.8	0.1271	0.0024	0.01889	0.00014	0.010841	0.0489	0.001	121.4	2.2	120.7	0.89	142	42	99
A_203.FIN2	416	92.9	0.41274	27.4	0.1278	0.0038	0.01892	0.00017	0.21558	0.049	0.0014	121.8	3.5	120.8	1.1	154	59	99
A_250.FIN2	402.1	201.1	0.971649	23.9	0.1272	0.0037	0.01895	0.00018	0.25476	0.0487	0.0014	121.3	3.4	121.0	1.2	131	58	100
A_249.FIN2	508	136.2	0.503937	29.4	0.1267	0.003	0.01894	0.00017	0.001632	0.0486	0.0012	121	2.7	121.0	1.1	134	52	100
A_238.FIN2	437	117.9	0.50389	25.9	0.1247	0.0037	0.01896	0.00022	0.17515	0.0479	0.0014	119.1	3.3	121.1	1.4	101	57	102
A_208.FIN2	382.7	220	1.124902	26.6	0.131	0.011	0.01903	0.00042	0.008991	0.0502	0.0041	124.5	9.5	121.5	2.7	190	170	98
A_222.FIN2	905	257	0.551381	49.6	0.1271	0.0029	0.01904	0.00015	0.056672	0.0487	0.0012	121.7	2.5	121.6	0.96	140	49	100
A_212.FIN2	311.9	52.3	0.325425	26.4	0.1299	0.0053	0.01905	0.00021	0.25415	0.0499	0.0019	123.6	4.7	121.6	1.3	172	77	98
A_178.FIN2	337.8	50.2	0.26791	21.6	0.1322	0.0048	0.01907	0.0002	0.13179	0.0504	0.0018	125.7	4.3	121.8	1.3	191	72	97
A_231.FIN2	545	148.5	0.496697	30.3	0.1302	0.0038	0.0191	0.00022	0.003577	0.0497	0.0015	124.1	3.4	122.0	1.4	174	64	98
A_228.FIN2	1314	336.9	0.467428	79.4	0.1289	0.0022	0.01912	0.00013	0.31073	0.04907	0.0008	123	2	122.1	0.84	149	34	99
A_213.FIN2	201.9	61.8	0.547598	14.31	0.1342	0.005	0.01912	0.00023	0.002425	0.0517	0.0021	127.4	4.5	122.1	1.5	234	79	96
A_151.FIN2	55.8	37.8	1.114695	4.82	0.132	0.011	0.01914	0.00047	0.13169	0.0522	0.0048	128	11	122.2	2.9	200	160	95
A_137.FIN2	272	97.2	0.732153	5.4	0.1277	0.0074	0.01913	0.00031	0.067572	0.0485	0.003	121.7	6.7	122.2	2	160	130	100
A_212.FIN2	532.6	152	0.536988	27.5	0.135	0.0093	0.01918	0.0004	0.17487	0.0513	0.0035	128.4	8.3	122.5	2.5	280	160	95
A_181.FIN2	354	50	0.265537	18.8	0.1327	0.0054	0.01919	0.00025	0.11695	0.0504	0.0021	126.1	4.8	122.5	1.6	193	80	97
A_224.FIN2	1533	738	0.936725	96	0.1306	0.0029	0.01918	0.00017	0.30966	0.0496	0.001	124.6	2.6	122.5	1.1	164	47	98
A_211.FIN2	386	125.9	0.637906	30.8	0.134	0.0095	0.01932	0.0004	0.22091	0.0507	0.0035	127.3	8.5	123.3	2.5	210	140	97
A_180.FIN2	338	45.6	0.238757	19.15	0.1313	0.0048	0.01933	0.00021	0.079683	0.0495	0.0018	124.9	4.3	123.4	1.4	157	73	99
A_239.FIN2	274	88.2	0.629562	16.7	0.1316	0.0065	0.01934	0.0003	0.003118	0.0495	0.0025	125.2	5.8	123.5	1.9	170	100	99
A_215.FIN2	203.6	33.5	0.327603	14	0.136	0.012	0.01948	0.00042	0.059088	0.051	0.0044	129	10	124.4	2.6	210	170	96
A_256.FIN2	814	638	1.418919	51.5	0.1331	0.0073	0.01954	0.00045	0.28452	0.0495	0.0027	126.8	6.6	124.7	2.9	170	110	98
A_141.FIN2	548	70.7	0.225	23.63	0.1465	0.0035	0.02135	0.00019	0.26558	0.0493	0.0011	138.7	3.1	136.2	1.2	159	48	98
A_192.FIN2	44	54.1	1.802273	3.4	0.167	0.024	0.02323	0.00083	0.053429	0.0551	0.0083	153	21	148.0	5.3	220	280	97
A_165.FIN2	123.2	87.7	1.215909	11.8	0.164	0.025	0.02328	0.00068	0.22261	0.0516	0.0083	153	22	148.3	4.3	220	310	97
A_171.FIN2	364.4	220.7	1.038419	31	0.163	0.01	0.02333	0.00036	0.013776	0.0508	0.0083	153.2	8.9	148.7	2.3	240	140	97
A_255.FIN2	414	192	0.676329	34.1	0.177	0.0063	0.02544	0.00035	0.079715	0.0505	0.0019	165.2	5.4	161.9	2.2	207	76	98
A_194.FIN2	278	320.5	0.242806	139.9	1.778	0.021	0.1749	0.0011	0.43929	0.07401	0.00076	1036	7.5	1039.2	6.3	1038	21	100
A_226.FIN2	192.2	601.8	0.448491	149.2	3.807	0.038	0.2614	0.0019	0.61046	0.10601	0.00086	1593	8.1	1496.8	9.7	1729	15	94
A_161.FIN2	192	672	0.491146	272	3.397	0.057	0.262	0.0032	0.58253	0.0937	0.0013	1503	13	1500.0	16	1498	26	100

Legend

Cretaceous Upper	Jurassic	Permian	Devonian	Ordovician	Precambrian
Cretaceous Lower	Triassic	Carboniferous	Silurian	Cambrian	

4.3.1.5 SCH-01-15

Sample SCH-01-15 was collected from the *Siats meekerorum* holotype locality, stratigraphically located within the upper portions of the Mussentuchit Member (Fig. 4.3.2). A representative (handpicked) population of zircon grains from the sample consisted of 90% magmatic grains exhibiting pristine, magmatic oscillatory zoning. A limited proportion (10%) of the grains exhibited homogenous sector zoning, associated with metamorphism, and approximately 15% of grains exhibited relict textures, evident from the high angle truncation and difference in luminosity under CL-imaging. Grains varied in size between 20 μm and 120 μm with the majority (70%) averaging around 60-70 μm . Zircon crystals appear as weathered euhedral, sub-angular rounded grains, with 20% showing inclusions of other minerals and limited amounts of microfracturing. Typical morphological types within the representative population of sample SCH-01-15 include S6-S12. SCH yielded 72 analysable zircons, with 59 zircons falling within the 10% discordancy inclusion criteria. Core analysis was conducted on 10% of the samples with 90% representing rim analysis. The largest population within the sample, 32% (n=19), shows a Cenomanian age of 93.9 – 100 Ma, with subordinate populations of 5.% (n=3), occurring around the Middle to Lower Devonian (380 – 410 Ma), 11.86% (n=7) around the late Neoproterozoic (541 - 635 Ma), 11.8% (n=7) occurring around the Late Mesoproterozoic (1035-1125 Ma), 7.8% (n=5) occurring around the early Mesoproterozoic (1350-1500 Ma), and 5.08% (n=3) occurring around the Late Paleoproterozoic (1600-1800) (Fig. 4.3.4a; 4.3.5). A single grain of Middle Paleoproterozoic age (1986 Ma) is also present. Analysis of the sample yielded the following youngest age signatures: YSG at 91 (± 1.5) Ma; YPP at 96 Ma; YDZ at 90.5 (+2.6 – 2.6) Ma; YC1 σ (+3) at 92.6 (± 1.3) Ma; YC2 σ (+3) at 92.6 (± 2.0) Ma; weighted mean (10) at 95.2 (± 1.7) Ma; TuffZirc age at 95.3 (+2.8 – 3.5) Ma through a coherent group of 9 out of 10 grains (Table 4.3.8).

Table 4.3.5: Pb/U data for sample SCH-01-15. $^{206}\text{Pb}/^{238}\text{U}$ ratio used for age calculations.

SCH-01-15				RATIOS								AGES [Ma]					Conc.	
Analysis	U [ppm] ^a	Pb [ppm] ^b	Th/U ^a	206/204	$^{207}\text{Pb}/^{235}\text{U}^b$	2 σ^d	$^{206}\text{Pb}/^{238}\text{U}^b$	2 σ^d	rho ^c	$^{207}\text{Pb}/^{206}\text{Pb}$	2 σ^d	$^{207}\text{Pb}/^{235}\text{U}$	2 σ	$^{206}\text{Pb}/^{238}\text{U}$	2 σ	$^{207}\text{Pb}/^{206}\text{Pb}$	2 σ	%
A_385.FIN2	256	75	0.74	16	0.0954	0.0066	0.0143	0.0002	0.0514	0.0486	0.0033	92	6	91.3	2	110	130	99
A_398.FIN2	159	32	0.47	10	0.0986	0.0061	0.0144	0.0003	0.0470	0.0502	0.0032	95	6	91.8	2	180	120	97
A_397.FIN2	517	138	0.65	29	0.0992	0.0046	0.0147	0.0002	0.2783	0.0492	0.0023	97	5	94.1	1	152	93	97
A_353.FIN2	829	674	2.22	37	0.0999	0.0035	0.0149	0.0002	0.1932	0.0487	0.0017	97	3	95.1	1	134	72	98
A_340.FIN2	569	190	0.89	18	0.1049	0.0070	0.0149	0.0004	0.0659	0.0514	0.0038	101	6	95.3	2	240	150	94
A_359.FIN2	825	402	1.31	47	0.1014	0.0032	0.0149	0.0002	0.0695	0.0495	0.0016	98	3	95.3	1	163	66	97
A_336.FIN2	144	43	0.70	4	0.1040	0.0056	0.0150	0.0002	0.0112	0.0497	0.0026	100	5	95.8	1	170	100	96
A_399.FIN2	436	96	0.61	24	0.1060	0.0091	0.0153	0.0004	0.0872	0.0505	0.0045	102	9	98.1	3	210	180	96
A_361.FIN2	81	26	0.70	5	0.1061	0.0077	0.0154	0.0003	0.0816	0.0513	0.0038	102	7	98.2	2	200	140	96
A_403.FIN2	508	183	0.93	26	0.1052	0.0048	0.0154	0.0002	0.3475	0.0498	0.0023	101	4	98.5	1	173	91	97
A_360.FIN2	143	22	0.38	8	0.1089	0.0099	0.0154	0.0003	0.1146	0.0519	0.0049	104	9	98.7	2	240	180	95
A_351.FIN2	367	78	0.51	16	0.1042	0.0052	0.0154	0.0002	0.2670	0.0495	0.0024	100	5	98.8	1	158	93	98
A_372.FIN2	340	74	0.53	25	0.1065	0.0048	0.0156	0.0002	0.0487	0.0495	0.0022	103	4	99.5	1	171	90	97
A_396.FIN2	664	192	0.77	33	0.1053	0.0065	0.0156	0.0004	0.0470	0.0494	0.0033	102	6	99.5	2	160	130	98
A_339.FIN2	566	189	0.80	19	0.1040	0.0030	0.0156	0.0001	0.0989	0.0484	0.0014	100	3	99.8	1	128	60	100
A_418.FIN2	76	22	0.67	7	0.1075	0.0074	0.0156	0.0003	0.0066	0.0512	0.0037	104	7	100.0	2	170	130	97
A_363.FIN2	223	50	0.45	14	0.1099	0.0083	0.0157	0.0003	0.0302	0.0501	0.0044	106	8	100.3	2	180	170	95
A_401.FIN2	587	217	0.91	34	0.1062	0.0043	0.0157	0.0002	0.2936	0.0491	0.0019	102	4	100.4	1	155	78	98
A_355.FIN2	590	194	0.65	34	0.1142	0.0090	0.0167	0.0005	0.3851	0.0497	0.0044	110	8	107.0	3	180	180	98
A_405.FIN2	211	484	2.30	29	0.2840	0.0130	0.0394	0.0006	0.0601	0.0525	0.0024	253	10	249.1	4	282	97	98
A_391.FIN2	740	301	0.35	125	0.3160	0.0130	0.0435	0.0007	0.3493	0.0527	0.0021	278	10	274.7	4	302	89	99
A_378.FIN2	309	116	0.22	79	0.4952	0.0089	0.0650	0.0005	0.2345	0.0554	0.0010	408	6	405.8	3	406	39	100
A_345.FIN2	346	379	0.64	53	0.5170	0.0120	0.0671	0.0008	0.2202	0.0562	0.0014	424	9	418.5	5	446	55	99
A_373.FIN2	416	227	0.25	139	0.6230	0.0120	0.0782	0.0008	0.1683	0.0577	0.0012	491	8	485.2	5	506	47	99
A_380.FIN2	434	542	0.51	178	0.7420	0.0130	0.0904	0.0010	0.2899	0.0594	0.0010	563	8	558.1	6	578	40	99
A_388.FIN2	224	418	0.81	77	0.7350	0.0200	0.0909	0.0010	0.2419	0.0588	0.0016	558	12	560.7	6	533	61	100
A_413.FIN2	106	274	0.99	58	0.7560	0.0490	0.0918	0.0019	0.1184	0.0598	0.0041	571	28	566.0	11	580	150	99
A_362.FIN2	364	429	0.51	129	0.7550	0.0160	0.0921	0.0009	0.3311	0.0597	0.0012	571	10	567.9	5	575	46	99
A_409.FIN2	257	407	0.66	119	0.7590	0.0120	0.0927	0.0007	0.2323	0.0594	0.0009	572	7	571.5	4	573	35	100
A_375.FIN2	260	312	0.45	116	0.8540	0.0130	0.1020	0.0007	0.2578	0.0608	0.0009	626	7	626.3	4	618	32	100
A_354.FIN2	170	355	0.81	49	0.8700	0.0240	0.1036	0.0011	0.2994	0.0609	0.0016	634	13	635.6	7	619	58	100
A_337.FIN2	245	381	0.56	48	1.0790	0.0410	0.1199	0.0052	0.1382	0.0657	0.0037	743	20	730.0	30	790	110	98
A_334.FIN2	145	262	0.59	11	1.2500	0.1100	0.1348	0.0062	0.2667	0.0676	0.0060	821	52	815.0	35	830	190	99
A_338.FIN2	313	360	0.29	100	1.4480	0.0240	0.1506	0.0022	0.4902	0.0704	0.0010	908	10	904.0	12	936	31	100
A_419.FIN2	200	371	0.42	174	1.4580	0.0670	0.1509	0.0039	0.5600	0.0702	0.0029	912	28	906.0	22	931	83	99
A_365.FIN2	262	204	0.20	165	1.5370	0.0440	0.1570	0.0058	0.5724	0.0734	0.0020	944	18	939.0	32	1015	55	99
A_335.FIN2	43	64	0.34	11	1.5570	0.0660	0.1573	0.0023	0.0137	0.0721	0.0032	947	27	942.0	13	933	99	99
A_381.FIN2	90	178	0.46	65	1.6320	0.0330	0.1639	0.0015	0.2469	0.0717	0.0014	979	13	978.4	8	971	41	100
A_341.FIN2	34	89	0.61	15	1.7000	0.0730	0.1678	0.0027	0.0605	0.0739	0.0035	1001	28	1000.0	15	979	98	100
A_382.FIN2	357	1004	0.57	254	2.0390	0.0210	0.1790	0.0016	0.2414	0.0824	0.0010	1128	7	1061.1	9	1253	24	94
A_393.FIN2	68	266	0.80	53	1.9130	0.0630	0.1828	0.0033	0.0927	0.0766	0.0023	1083	22	1082.0	18	1098	63	100
A_416.FIN2	187	436	0.54	185	1.9310	0.0540	0.1835	0.0027	0.2942	0.0766	0.0022	1090	19	1086.0	15	1101	56	100
A_367.FIN2	308	393	0.20	174	2.3650	0.0510	0.1875	0.0016	0.5747	0.0917	0.0016	1231	15	1107.8	9	1445	32	90
A_402.FIN2	226	645	0.55	175	2.0650	0.0360	0.1918	0.0017	0.3119	0.0781	0.0013	1136	12	1131.3	9	1141	34	100
A_350.FIN2	64	94	0.28	41	2.1770	0.0460	0.2001	0.0019	0.2071	0.0790	0.0017	1172	15	1176.0	10	1156	42	100
A_347.FIN2	192	492	0.49	126	2.6700	0.1600	0.2092	0.0045	0.2468	0.0931	0.0064	1318	42	1224.0	24	1480	120	93
A_414.FIN2	405	438	0.21	630	2.5440	0.0390	0.2196	0.0025	0.6267	0.0837	0.0010	1284	11	1279.0	13	1288	24	100
A_369.FIN2	39	163	0.75	33	2.6460	0.0560	0.2247	0.0021	0.1942	0.0856	0.0018	1308	16	1306.0	11	1315	40	100
A_392.FIN2	61	266	0.75	60	2.6870	0.0500	0.2267	0.0027	0.4561	0.0864	0.0015	1322	14	1316.0	14	1333	35	100
A_346.FIN2	113	260	0.39	77	2.9130	0.0370	0.2388	0.0020	0.4010	0.0885	0.0011	1385	10	1380.0	11	1391	24	100
A_364.FIN2	158	803	0.80	150	2.9410	0.0370	0.2402	0.0017	0.4406	0.0889	0.0010	1392	10	1387.3	9	1397	22	100
A_394.FIN2	162	487	0.51	151	3.2680	0.0720	0.2559	0.0042	0.3919	0.0929	0.0020	1472	17	1469.0	22	1480	42	100
A_386.FIN2	203	546	0.42	215	3.3370	0.0400	0.2597	0.0020	0.3941	0.0932	0.0010	1489	10	1488.0	10	1489	20	100
A_357.FIN2	176	745	0.60	172	3.7730	0.0390	0.2725	0.0020	0.3764	0.1007	0.0011	1588	9	1553.0	10	1636	19	98
A_383.FIN2	87	334	0.54	107	3.9590	0.0580	0.2874	0.0023	0.4549	0.0999	0.0013	1623	12	1628.0	11	1616	25	100
A_349.FIN2	78	450	0.81	76	4.3850	0.0700	0.3025	0.0027	0.3396	0.1049	0.0016	1706	13	1703.0	13	1706	28	100
A_390.FIN2	150	260	0.23	176	4.4440	0.0500	0.3061	0.0024	0.5140	0.1055	0.0011	1720	10	1721.0	12	1719	19	100
A_412.FIN2	76	294	0.58	114	4.6400	0.1700	0.3109	0.0056	0.0625	0.1071	0.0036	1754	30	1744.0	27	1741	63	99
A_356.FIN2	85	317	0.43	111	6.0810	0.0610	0.3603	0.0024	0.3879	0.1223	0.0012	1986	9	1983.0	11	1991	17	100

Legend

Cretaceous Upper	Jurassic	Permian	Devonian	Ordovician	Precambrian
Cretaceous Lower	Triassic	Carboniferous	Silurian	Cambrian	

4.3.1.6 ST-010-15







Sample ST-010-15 was collected from the Stormy Theropod fossil quarry, which is stratigraphically located within the middle portions of the Mussentuchit Member (Fig. 4.3.2). A representative (handpicked) population of zircon grains from the sample consisted of 90% magmatic grains exhibiting pristine, magmatic oscillatory zoning. A limited proportion (10%) of the grains exhibited homogenous sector zoning, associated with metamorphism, and approximately 20% of grains exhibited relict textures, evident from the high angle truncation and difference in luminosity under CL-imaging. Grains varied in size between 30 μm and 150 μm with the majority (80%) averaging around 70-80 μm . Zircon crystals appear as euhedral, angular to rounded grains, with moderate amounts of microfracturing. A notable portion of grains, approximately 30%, exhibited inclusions of mineral such as quartz. Grains additionally exhibited a moderate amount of convolute zoning, typically concentrated around microfracture paths. Typical morphological types within the representative population of sample ST-010-15 include P1-P2, S7-S10, and R1 to R2. ST-010-15 yielded 120 analysable zircons, with 109 zircons falling within the 10% discordancy inclusion criteria. Core analysis was conducted on 10% of the samples with 90% representing rim analysis. The largest population within the sample, 56.88% (n=62), shows a Cenomanian age of 93.9 – 100 Ma, with subordinate populations of 8.26% (n=9) occurring at an Aptian age of 115-120 Ma, 8.26% (n=9) occurring around the Middle to Lower Devonian (380 – 410 Ma), 2.75% (n=3) around the late Neoproterozoic (541 - 635 Ma), 5.5% (n=6) occurring around the Late Mesoproterozoic (1035-1125 Ma), 2.75% (n=3) occurring around the early Mesoproterozoic (1350-1500 Ma), and 2.75% (n=3) occurring around the Late Paleoproterozoic (1600-1800) (Fig. 4.3.4a; 4.3.5). A single grain of Neoproterozoic age (2643 Ma) is also present. Analysis of the sample yielded the following youngest age signatures: YSG at 96 (\pm 2.6) Ma; YPP at 100 Ma; YDZ at 94.83 (+1.7 – 4.6) Ma; YC1 σ (+3) at 96.6 (\pm 1.6) Ma; YC2 σ (+3) at 96.6 (\pm 2.3)

Ma; weighted mean (10) at 97.5 (± 0.5) Ma; TuffZirc age at 97.3 (+0.9 –0.7) Ma through a coherent group of 10 grains (Table 4.3.8).

Table 4.3.6: Pb/U data for sample ST-10-15. ²⁰⁶Pb/²³⁸U ration used for age calculations.

ST-010-15					RATIOS							AGES [Ma]				Conc.		
Analysis	U [ppm] ^a	Pb [ppm] ^a	Th/U ^a	206/204	²⁰⁷ Pb/ ²³⁵ U ^b	2 σ ^d	²⁰⁶ Pb/ ²³⁸ U ^b	2 σ ^d	rho ^c	²⁰⁷ Pb/ ²⁰⁶ Pb ^a	2 σ ^d	²⁰⁷ Pb/ ²³⁵ U	2 σ	²⁰⁶ Pb/ ²³⁸ U	2 σ	²⁰⁷ Pb/ ²⁰⁶ Pb	2 σ	%
A_066.FIN2	300	148	1.10	13	0.1049	0.0073	0.0150	0.0004	0.0528	0.0513	0.0031	101	7	96.2	3	220	120	95
A_123.FIN2	281	31	0.29	10	0.1048	0.0064	0.0151	0.0003	0.0346	0.0504	0.0032	101	6	96.6	2	210	130	96
A_130.FIN2	362	121	0.80	16	0.1004	0.0055	0.0151	0.0003	0.0074	0.0490	0.0028	98	5	96.8	2	130	110	99
A_122.FIN2	869	104	0.26	25	0.1021	0.0044	0.0151	0.0002	0.1637	0.0488	0.0020	99	4	96.9	1	137	84	98
A_047.FIN2	387	62	0.38	12	0.1029	0.0044	0.0152	0.0002	0.0852	0.0497	0.0022	100	4	97.1	1	160	86	97
A_102.FIN2	541	192	0.88	31	0.1047	0.0044	0.0152	0.0002	0.2069	0.0498	0.0023	101	4	97.4	1	173	94	97
A_014.FIN2	401	115	0.70	10	0.1046	0.0058	0.0153	0.0003	0.1133	0.0496	0.0029	101	5	97.9	2	160	110	97
A_113.FIN2	526	147	0.68	20	0.1042	0.0039	0.0153	0.0002	0.0095	0.0492	0.0019	100	4	98.1	1	146	76	98
A_032.FIN2	888	193	0.54	35	0.1034	0.0031	0.0153	0.0002	0.0840	0.0492	0.0016	100	3	98.1	1	150	68	98
A_076.FIN2	371	107	0.69	11	0.1085	0.0067	0.0154	0.0003	0.1482	0.0506	0.0032	104	6	98.7	2	200	120	95
A_065.FIN2	311	68	0.49	14	0.1061	0.0048	0.0154	0.0002	0.1351	0.0504	0.0024	102	4	98.7	1	185	91	97
A_057.FIN2	333	74	0.50	11	0.1053	0.0042	0.0154	0.0002	0.1067	0.0496	0.0021	102	4	98.7	1	169	83	97
A_038.FIN2	446	115	0.60	16	0.1056	0.0044	0.0155	0.0002	0.0493	0.0495	0.0021	102	4	98.8	1	163	85	97
A_062.FIN2	298	133	0.91	8	0.1060	0.0075	0.0155	0.0003	0.2905	0.0497	0.0034	102	7	98.9	2	190	140	97
A_049.FIN2	337	71	0.47	9	0.1056	0.0040	0.0155	0.0002	0.3013	0.0497	0.0019	102	4	99.3	1	169	74	98
A_083.FIN2	607	151	0.55	39	0.1054	0.0032	0.0155	0.0002	0.2326	0.0491	0.0015	102	3	99.4	1	156	64	98
A_012.FIN2	326	86	0.58	14	0.1060	0.0046	0.0156	0.0002	0.0773	0.0492	0.0021	102	4	99.5	1	164	87	98
A_110.FIN2	565	174	0.75	31	0.1053	0.0030	0.0156	0.0001	0.1506	0.0490	0.0014	102	3	99.6	1	142	57	98
A_021.FIN2	535	206	0.96	23	0.1074	0.0054	0.0156	0.0003	0.0009	0.0502	0.0026	104	5	99.6	2	190	110	96
A_086.FIN2	575	298	1.29	36	0.1064	0.0037	0.0156	0.0002	0.0190	0.0499	0.0019	103	4	99.6	1	179	79	97
A_127.FIN2	473	88	0.47	21	0.1039	0.0088	0.0156	0.0005	0.0668	0.0485	0.0043	100	8	99.6	3	110	170	100
A_041.FIN2	377	60	0.36	12	0.1064	0.0042	0.0156	0.0002	0.1582	0.0492	0.0021	103	4	99.8	1	168	87	97
A_007.FIN2	322	106	0.79	9	0.1074	0.0039	0.0156	0.0002	0.0040	0.0500	0.0020	104	4	99.9	1	184	78	96
A_111.FIN2	639	126	0.48	33	0.1049	0.0054	0.0156	0.0002	0.0736	0.0493	0.0028	101	5	99.9	2	150	110	99
A_085.FIN2	773	167	0.49	45	0.1086	0.0033	0.0157	0.0002	0.1470	0.0502	0.0016	105	3	100.1	1	196	64	96
A_118.FIN2	938	125	0.32	44	0.1050	0.0027	0.0157	0.0001	0.1994	0.0487	0.0012	101	2	100.2	1	130	51	99
A_044.FIN2	569	92	0.37	18	0.1071	0.0033	0.0157	0.0002	0.0373	0.0493	0.0016	103	3	100.2	1	164	66	97
A_120.FIN2	441	73	0.39	19	0.1062	0.0044	0.0157	0.0002	0.0578	0.0492	0.0021	103	4	100.2	1	161	86	98
A_074.FIN2	646	200	0.71	34	0.1042	0.0028	0.0157	0.0001	0.1374	0.0481	0.0013	101	3	100.4	1	109	54	100
A_043.FIN2	513	83	0.35	17	0.1079	0.0039	0.0157	0.0002	0.0907	0.0494	0.0018	104	4	100.6	1	170	72	97
A_089.FIN2	162	43	0.59	10	0.1120	0.0100	0.0157	0.0005	0.4787	0.0525	0.0048	107	9	100.7	3	260	180	94
A_080.FIN2	451	85	0.43	27	0.1061	0.0036	0.0157	0.0001	0.1176	0.0488	0.0017	102	3	100.7	1	133	67	99
A_046.FIN2	476	92	0.42	17	0.1070	0.0054	0.0158	0.0002	0.1867	0.0496	0.0025	103	5	100.9	1	170	100	98
A_018.FIN2	523	122	0.54	26	0.1070	0.0029	0.0158	0.0001	0.2064	0.0492	0.0013	103	3	101.0	1	152	55	98
A_019.FIN2	479	222	1.01	27	0.1075	0.0040	0.0158	0.0002	0.2868	0.0496	0.0018	104	4	101.2	1	172	73	98
A_094.FIN2	624	141	0.55	39	0.1079	0.0042	0.0158	0.0002	0.0426	0.0491	0.0021	104	4	101.3	1	147	87	97
A_100.FIN2	572	130	0.51	41	0.1054	0.0026	0.0158	0.0001	0.1280	0.0481	0.0012	102	2	101.3	1	114	50	100
A_030.FIN2	152	51	0.77	9	0.1093	0.0062	0.0159	0.0002	0.0469	0.0501	0.0028	105	6	101.6	2	160	110	97
A_048.FIN2	642	104	0.37	20	0.1076	0.0038	0.0159	0.0002	0.0253	0.0493	0.0019	104	4	101.6	1	151	76	98
A_004.FIN2	608	197	0.75	8	0.1066	0.0038	0.0159	0.0002	0.2131	0.0488	0.0017	103	4	101.6	1	134	69	99
A_006.FIN2	740	154	0.49	26	0.1080	0.0039	0.0159	0.0003	0.1752	0.0496	0.0018	104	4	101.7	2	172	76	98
A_129.FIN2	897	133	0.33	41	0.1065	0.0026	0.0159	0.0001	0.2860	0.0484	0.0011	103	2	101.8	1	126	47	99
A_132.FIN2	472	70	0.29	24	0.1046	0.0036	0.0159	0.0002	0.0178	0.0478	0.0018	101	3	101.9	1	92	70	101
A_054.FIN2	1084	158	0.33	35	0.1075	0.0025	0.0159	0.0001	0.1850	0.0487	0.0012	104	2	101.9	1	135	49	98
A_072.FIN2	155	28	0.40	6	0.1104	0.0052	0.0161	0.0002	0.0576	0.0501	0.0024	106	5	102.6	1	175	93	97
A_121.FIN2	1066	205	0.45	47	0.1086	0.0045	0.0161	0.0003	0.5526	0.0493	0.0020	105	4	102.9	2	150	81	98
A_029.FIN2	471	114	0.53	26	0.1129	0.0037	0.0162	0.0002	0.0858	0.0506	0.0017	108	3	103.4	1	205	70	95
A_013.FIN2	1152	235	0.43	35	0.1175	0.0059	0.0162	0.0005	0.0729	0.0529	0.0031	113	5	103.8	3	320	130	92
A_035.FIN2	605	106	0.38	31	0.1093	0.0031	0.0163	0.0001	0.1594	0.0485	0.0013	105	3	104.1	1	115	52	99
A_091.FIN2	362	97	0.59	26	0.1114	0.0038	0.0163	0.0002	0.1068	0.0499	0.0018	108	3	104.2	1	173	70	97
A_022.FIN2	463	99	0.45	22	0.1093	0.0032	0.0163	0.0001	0.0969	0.0485	0.0014	105	3	104.2	1	130	59	99
A_020.FIN2	750	301	0.93	37	0.1101	0.0029	0.0164	0.0001	0.2026	0.0485	0.0012	106	3	104.9	1	129	53	99
A_016.FIN2	443	209	1.05	20	0.1125	0.0043	0.0165	0.0002	0.1672	0.0492	0.0018	108	4	105.2	1	151	73	97
A_115.FIN2	798	128	0.34	47	0.1119	0.0041	0.0165	0.0002	0.4663	0.0494	0.0017	108	4	105.5	2	157	71	98
A_131.FIN2	322	79	0.52	15	0.1128	0.0057	0.0166	0.0002	0.2015	0.0491	0.0024	108	5	106.1	2	149	96	98
A_125.FIN2	1882	448	0.55	68	0.1172	0.0063	0.0167	0.0003	0.3915	0.0506	0.0024	113	6	106.7	2	210	100	95
A_134.FIN2	529	233	0.98	18	0.1147	0.0038	0.0168	0.0002	0.0178	0.0494	0.0017	110	3	107.5	1	156	69	98

A_055.FIN2	1147	104	0.19	37	0.1163	0.0039	0.0169	0.0002	0.0135	0.0499	0.0018	112	4	107.7	1	177	75	97
A_025.FIN2	362	90	0.52	24	0.1141	0.0039	0.0170	0.0002	0.2305	0.0486	0.0016	110	4	108.5	1	140	65	99
A_060.FIN2	330	59	0.37	14	0.1147	0.0039	0.0170	0.0002	0.0358	0.0490	0.0018	110	4	108.6	1	147	71	99
A_024.FIN2	252	127	1.02	14	0.1123	0.0040	0.0171	0.0002	0.1046	0.0478	0.0017	108	4	109.2	1	93	68	101
A_026.FIN2	246	65	0.49	13	0.1134	0.0052	0.0172	0.0002	0.1542	0.0480	0.0022	109	5	109.7	1	101	88	101
A_108.FIN2	884	266	0.65	49	0.1169	0.0026	0.0173	0.0002	0.2996	0.0490	0.0011	112	2	110.6	1	147	44	98
A_009.FIN2	418	182	0.95	16	0.1173	0.0040	0.0176	0.0002	0.0746	0.0485	0.0017	113	4	112.4	1	139	71	100
A_058.FIN2	711	102	0.26	27	0.1231	0.0042	0.0179	0.0002	0.1109	0.0496	0.0017	118	4	114.5	1	165	71	97
A_045.FIN2	286	60	0.42	10	0.1224	0.0051	0.0179	0.0002	0.0500	0.0498	0.0022	117	5	114.5	1	163	83	98
A_081.FIN2	452	290	1.33	30	0.1247	0.0050	0.0181	0.0002	0.0416	0.0500	0.0020	119	5	115.4	1	182	81	97
A_042.FIN2	366	161	0.85	14	0.1286	0.0045	0.0184	0.0002	0.0769	0.0505	0.0018	123	4	117.8	1	200	71	96
A_073.FIN2	111	64	1.01	5	0.1296	0.0090	0.0188	0.0004	0.1937	0.0510	0.0035	123	8	119.9	2	220	130	97
A_075.FIN2	125	30	0.45	7	0.1322	0.0071	0.0188	0.0003	0.1430	0.0514	0.0030	125	6	120.3	2	200	110	96
A_023.FIN2	269	106	0.69	17	0.1339	0.0042	0.0200	0.0002	0.1917	0.0487	0.0015	127	4	127.4	1	129	61	100
A_090.FIN2	321	103	0.39	31	0.1690	0.0210	0.0240	0.0008	0.2658	0.0511	0.0062	158	18	152.9	5	210	240	97
A_010.FIN2	173	163	0.86	18	0.2891	0.0094	0.0404	0.0004	0.1901	0.0520	0.0017	257	7	255.5	2	255	64	100
A_106.FIN2	151	82	0.32	39	0.4840	0.0120	0.0638	0.0005	0.0810	0.0552	0.0015	401	8	398.4	3	387	57	99
A_084.FIN2	296	446	0.80	59	0.4960	0.0130	0.0645	0.0007	0.2147	0.0558	0.0015	409	9	402.7	4	425	60	99
A_078.FIN2	326	306	0.52	63	0.5030	0.0120	0.0656	0.0006	0.1848	0.0551	0.0012	413	8	409.5	4	401	50	99
A_082.FIN2	264	259	0.54	62	0.5063	0.0091	0.0663	0.0005	0.2909	0.0552	0.0010	415	6	413.5	3	400	39	100
A_031.FIN2	96	234	1.32	22	0.5210	0.0130	0.0676	0.0006	0.0644	0.0559	0.0015	424	9	421.4	4	417	57	99
A_011.FIN2	107	335	1.56	20	0.5230	0.0310	0.0681	0.0015	0.1610	0.0561	0.0034	425	21	424.8	9	420	130	100
A_028.FIN2	154	214	0.71	23	0.5370	0.0200	0.0695	0.0013	0.1317	0.0554	0.0020	436	13	433.2	8	427	87	99
A_116.FIN2	262	263	0.51	60	0.5550	0.0130	0.0721	0.0008	0.1656	0.0560	0.0013	447	8	448.4	5	422	51	100
A_053.FIN2	369	1288	1.76	53	0.5620	0.0100	0.0723	0.0006	0.1507	0.0562	0.0010	452	7	449.7	4	442	41	100
A_087.FIN2	263	441	0.69	105	0.7220	0.0140	0.0886	0.0011	0.3644	0.0591	0.0011	551	8	547.2	7	558	40	99
A_064.FIN2	398	610	0.56	109	0.7850	0.0270	0.0943	0.0019	0.0232	0.0605	0.0024	588	16	581.0	11	607	90	99
A_077.FIN2	116	203	0.70	27	0.8330	0.0390	0.0993	0.0048	0.1645	0.0612	0.0037	615	21	610.0	28	630	130	99
A_069.FIN2	275	361	0.47	55	0.8750	0.0380	0.1024	0.0019	0.0858	0.0621	0.0028	637	21	628.0	11	660	100	99
A_098.FIN2	62	300	1.21	37	1.5150	0.0670	0.1515	0.0039	0.1422	0.0727	0.0035	934	27	909.0	22	980	100	97
A_119.FIN2	107	95	0.20	47	1.6180	0.0420	0.1565	0.0015	0.4194	0.0756	0.0020	975	16	936.9	8	1058	51	96
A_063.FIN2	68	485	1.59	33	1.7040	0.0390	0.1678	0.0014	0.5076	0.0736	0.0016	1006	15	999.7	8	1017	42	99
A_059.FIN2	182	335	0.41	73	1.7440	0.0250	0.1717	0.0014	0.3683	0.0734	0.0010	1023	9	1021.1	8	1015	27	100
A_117.FIN2	278	321	0.23	150	1.7970	0.0490	0.1755	0.0021	0.3834	0.0740	0.0019	1043	18	1042.0	12	1032	51	100
A_027.FIN2	251	955	0.86	133	1.9010	0.0260	0.1822	0.0017	0.3499	0.0753	0.0010	1081	9	1078.7	9	1074	27	100
A_093.FIN2	52	178	0.73	41	1.9180	0.0850	0.1833	0.0035	0.1198	0.0757	0.0036	1084	30	1085.0	19	1060	100	100
A_092.FIN2	186	141	0.14	163	2.0140	0.0310	0.1888	0.0018	0.4347	0.0774	0.0011	1119	10	1114.5	10	1125	28	100
A_051.FIN2	64	120	0.36	29	2.1590	0.0450	0.1988	0.0021	0.2346	0.0786	0.0016	1165	15	1168.0	11	1142	42	100
A_033.FIN2	180	542	0.57	116	2.2000	0.0330	0.1997	0.0016	0.4195	0.0795	0.0011	1179	10	1173.5	9	1178	27	100
A_008.FIN2	209	542	0.49	87	2.1980	0.0250	0.2007	0.0015	0.3750	0.0796	0.0009	1179	8	1178.7	8	1181	22	100
A_128.FIN2	223	599	0.50	115	2.7310	0.0430	0.2136	0.0029	0.5353	0.0924	0.0011	1334	12	1247.0	15	1468	22	93
A_126.FIN2	155	304	0.32	109	2.6700	0.1000	0.2256	0.0067	0.6378	0.0840	0.0027	1316	28	1310.0	34	1283	64	100
A_068.FIN2	152	641	0.63	96	3.0620	0.0540	0.2277	0.0034	0.8204	0.0975	0.0011	1421	14	1324.0	18	1572	21	93
A_079.FIN2	180	444	0.39	161	3.1190	0.0390	0.2488	0.0022	0.6376	0.0910	0.0010	1437	10	1432.0	11	1442	22	100
A_107.FIN2	216	539	0.38	183	3.3640	0.0370	0.2540	0.0018	0.3925	0.0956	0.0010	1496	9	1458.7	9	1538	20	98
A_095.FIN2	121	400	0.50	141	3.6210	0.0620	0.2718	0.0029	0.0130	0.0964	0.0015	1553	14	1549.0	15	1550	30	100
A_015.FIN2	161	992	0.93	111	3.8200	0.1600	0.2790	0.0052	0.3480	0.0995	0.0039	1594	33	1586.0	26	1606	71	99
A_124.FIN2	74	188	0.34	56	4.2130	0.0720	0.2843	0.0027	0.2843	0.1071	0.0018	1673	14	1612.0	14	1737	32	96
A_097.FIN2	177	1328	0.96	233	4.0180	0.0610	0.2891	0.0049	0.5229	0.1009	0.0017	1637	12	1637.0	24	1637	31	100
A_114.FIN2	269	419	0.21	212	4.3070	0.0540	0.3015	0.0029	0.5355	0.1030	0.0011	1695	10	1698.0	14	1678	20	100
A_109.FIN2	275	1639	0.83	313	4.3920	0.0730	0.3067	0.0038	0.5120	0.1033	0.0015	1710	14	1724.0	19	1681	27	101
A_017.FIN2	91	936	0.90	133	12.5000	0.1400	0.4939	0.0045	0.6234	0.1833	0.0016	2643	10	2587.0	19	2681	15	98

Legend											
Cretaceous Upper		Jurassic		Permian		Devonian		Ordovician		Precambrian	
Cretaceous Lower		Triassic		Carboniferous		Silurian		Cambrian			

4.3.1.7 SLF-08-15

Sample SLF-08-15 was collected from the Scared Little Fatty fossil quarry, which is stratigraphically located within the upper portions of the Mussentuchit Member (Fig. 4.3.2). A representative (handpicked) population of zircon grains from the sample consisted of 95% magmatic grains exhibiting pristine, magmatic oscillatory zoning. A very limited proportion (5%) of the grains exhibited homogenous sector zoning, associated with metamorphism, and approximately 15% of grains exhibited relict textures, evident from the high angle truncation and difference in luminosity under CL-imaging. Grains varied in size between 20 μm and 120 μm with the majority (80%) averaging around 100 μm . Zircon crystals appear as euhedral, sub-angular to rounded grains, with moderate amounts of microfracturing. A notable portion of grains, approximately 20%, exhibited inclusions of mineral such as quartz. Grains exhibited a limited amount of convolute zoning, restricted to a small number of grains, concentrated around microfracture paths. Typical morphological types within the representative population of sample SLF-08-15 include P1-P3, S6-S12, and R2 to R3. SLF-08-15 yielded 105 analysable zircons, with 98 zircons falling within the 10% discordancy inclusion criteria. Core analysis was conducted on 10% of the samples with 90% representing rim analysis. The largest population within the sample, 94.9% ($n=93$), shows a Cenomanian age of 93.9 – 100 Ma, with no further age populations consisting of more than a single zircon (Fig. 4.3.4a; 4.3.5). A single grain of Late Paleoproterozoic age (1623 Ma) is also present. Analysis of the sample yielded the following youngest age signatures: YSG at 94.93 (± 0.91) Ma; YPP at 98 Ma; YDZ at 93.667 ($+1.1 - 7.6$) Ma; YC1 σ (+3) at 95.1 (± 1.2) Ma; YC2 σ (+3) at 95.1 (± 1.7) Ma weighted mean (10) at 95.5 (± 0.4) Ma; TuffZirc age at 95.6 ($+0.5 - 0.3$) Ma through a coherent group of 10 grains (Table 4.3.8).

Table 4.3.7: Pb/U data for sample SLF-08-15. $^{206}\text{Pb}/^{238}\text{U}$ ratios used for age calculations.

SLF-08-15				RATIOS								AGES [Ma]				Conc.		
Analysis	U [ppm] ^a	Pb [ppm] ^a	Th/U ^a	$^{206}\text{Pb}/^{238}\text{U}^b$	$2\sigma^d$	$^{207}\text{Pb}/^{235}\text{U}^b$	$2\sigma^d$	ρ^c	$^{207}\text{Pb}/^{206}\text{Pb}$	$2\sigma^d$	$^{207}\text{Pb}/^{235}\text{U}$	2σ	$^{86}\text{Pb}/^{235}\text{U}$	2σ	$^{107}\text{Pb}/^{206}\text{Pb}$	2σ	%	
A_322.FIN2	717	183	0.64	39	0.0994	0.0028	0.0148	0.0001	0.1213	0.0487	0.0014	96	3	94.9	1	141	60	99
A_330.FIN2	297	101	0.86	21	0.1018	0.0046	0.0149	0.0002	0.0046	0.0496	0.0023	98	4	95.3	1	166	91	97
A_297.FIN2	642	97	0.40	31	0.1090	0.0120	0.0149	0.0003	0.4961	0.0536	0.0064	105	11	95.5	2	330	250	91
A_245.FIN2	1007	330	0.81	55	0.1007	0.0032	0.0149	0.0002	0.0323	0.0490	0.0016	97	3	95.5	1	146	69	98
A_295.FIN2	665	139	0.52	35	0.1009	0.0026	0.0149	0.0001	0.2293	0.0491	0.0012	98	2	95.5	1	150	51	98
A_310.FIN2	541	162	0.76	31	0.1014	0.0034	0.0149	0.0002	0.0866	0.0492	0.0016	98	3	95.6	1	150	65	98
A_317.FIN2	1388	380	0.65	72	0.1078	0.0051	0.0150	0.0002	0.6042	0.0530	0.0025	104	5	95.8	1	268	77	92
A_258.FIN2	930	342	1.00	63	0.1065	0.0080	0.0150	0.0006	0.4349	0.0517	0.0035	103	7	95.9	4	260	150	93
A_251.FIN2	989	238	0.62	43	0.1073	0.0071	0.0150	0.0005	0.2313	0.0521	0.0034	103	7	96.1	3	280	140	93
A_286.FIN2	792	181	0.64	32	0.1014	0.0054	0.0151	0.0003	0.1419	0.0490	0.0026	98	5	96.5	2	150	110	98
A_318.FIN2	642	94	0.34	31	0.1055	0.0073	0.0151	0.0005	0.1946	0.0509	0.0037	102	7	96.8	3	220	150	95
A_305.FIN2	720	163	0.56	43	0.1018	0.0026	0.0151	0.0001	0.1647	0.0488	0.0012	98	2	96.9	1	136	51	99
A_280.FIN2	693	106	0.37	35	0.1012	0.0026	0.0152	0.0001	0.3060	0.0483	0.0012	98	2	96.9	1	123	50	99
A_227.FIN2	721	123	0.41	26	0.1041	0.0026	0.0152	0.0001	0.1545	0.0496	0.0012	100	2	97.2	1	167	50	97
A_268.FIN2	691	164	0.57	40	0.1029	0.0027	0.0152	0.0001	0.0735	0.0490	0.0013	99	3	97.3	1	147	55	98
A_306.FIN2	866	187	0.56	47	0.1060	0.0052	0.0152	0.0003	0.1158	0.0504	0.0026	102	5	97.4	2	200	100	95
A_228.FIN2	313	60	0.47	14	0.1028	0.0037	0.0152	0.0002	0.0871	0.0491	0.0018	99	3	97.5	1	140	72	98
A_301.FIN2	639	106	0.39	31	0.1021	0.0024	0.0153	0.0001	0.1346	0.0485	0.0012	99	2	97.7	1	127	48	99
A_298.FIN2	798	119	0.41	32	0.1052	0.0057	0.0153	0.0003	0.2090	0.0499	0.0028	102	5	97.7	2	180	120	96
A_256.FIN2	748	120	0.40	44	0.1007	0.0022	0.0153	0.0001	0.1464	0.0478	0.0011	97	2	97.7	1	98	45	100
A_311.FIN2	677	101	0.36	19	0.1032	0.0085	0.0153	0.0005	0.2764	0.0492	0.0039	100	8	97.8	3	140	170	98
A_247.FIN2	378	86	0.56	20	0.1000	0.0031	0.0153	0.0002	0.1710	0.0476	0.0015	97	3	97.8	1	85	61	101
A_289.FIN2	732	122	0.43	34	0.1049	0.0055	0.0153	0.0003	0.3097	0.0499	0.0026	101	5	97.9	2	190	110	97
A_299.FIN2	681	176	0.61	35	0.1018	0.0025	0.0153	0.0001	0.2499	0.0483	0.0012	98	2	97.9	1	117	51	100
A_244.FIN2	850	171	0.49	46	0.1029	0.0023	0.0153	0.0001	0.1678	0.0488	0.0011	99	2	98.0	1	142	47	99
A_326.FIN2	665	116	0.40	40	0.1084	0.0066	0.0153	0.0003	0.1714	0.0515	0.0034	104	6	98.0	2	240	140	94
A_288.FIN2	376	72	0.48	17	0.1042	0.0045	0.0153	0.0002	0.2273	0.0494	0.0021	100	4	98.0	1	152	82	98
A_287.FIN2	623	103	0.41	31	0.1031	0.0026	0.0153	0.0001	0.1295	0.0489	0.0013	100	2	98.0	1	141	52	99
A_231.FIN2	655	106	0.38	30	0.1075	0.0029	0.0153	0.0001	0.1339	0.0508	0.0014	104	3	98.1	1	211	56	95
A_237.FIN2	916	220	0.58	48	0.1016	0.0022	0.0153	0.0001	0.0430	0.0482	0.0011	98	2	98.1	1	113	47	100
A_230.FIN2	615	100	0.38	27	0.1055	0.0037	0.0153	0.0002	0.0064	0.0502	0.0019	102	3	98.1	1	192	78	96
A_319.FIN2	194	52	0.64	11	0.1064	0.0074	0.0154	0.0004	0.1576	0.0506	0.0035	102	7	98.2	3	200	140	96
A_285.FIN2	496	90	0.42	29	0.1042	0.0036	0.0154	0.0002	0.0715	0.0497	0.0019	101	3	98.2	1	167	75	98
A_264.FIN2	902	275	0.77	48	0.1026	0.0023	0.0154	0.0001	0.1794	0.0485	0.0011	99	2	98.2	1	126	46	99
A_291.FIN2	580	89	0.37	31	0.1028	0.0028	0.0154	0.0001	0.2041	0.0485	0.0014	99	3	98.3	1	134	56	99
A_320.FIN2	517	87	0.40	28	0.1017	0.0030	0.0154	0.0001	0.0539	0.0479	0.0014	99	3	98.3	1	112	59	100
A_312.FIN2	857	218	0.63	51	0.1024	0.0028	0.0154	0.0001	0.1662	0.0483	0.0014	99	3	98.5	1	121	58	100
A_304.FIN2	537	103	0.42	24	0.1045	0.0048	0.0154	0.0002	0.0679	0.0493	0.0024	101	4	98.6	2	153	99	98
A_307.FIN2	605	164	0.68	30	0.1031	0.0043	0.0154	0.0002	0.1573	0.0486	0.0020	100	4	98.6	1	129	84	99
A_234.FIN2	828	131	0.38	35	0.1060	0.0041	0.0154	0.0002	0.0279	0.0499	0.0019	102	4	98.7	1	181	79	97
A_300.FIN2	623	101	0.40	33	0.1032	0.0024	0.0154	0.0001	0.1814	0.0485	0.0011	100	2	98.8	1	127	47	99
A_303.FIN2	253	69	0.65	12	0.1084	0.0094	0.0155	0.0004	0.0479	0.0513	0.0048	104	9	98.8	2	200	170	95
A_294.FIN2	814	126	0.40	43	0.1042	0.0039	0.0155	0.0002	0.3276	0.0490	0.0018	101	4	98.8	1	142	72	98
A_327.FIN2	522	122	0.57	38	0.1031	0.0032	0.0155	0.0002	0.0248	0.0488	0.0016	99	3	98.8	1	135	64	99
A_255.FIN2	1004	193	0.47	62	0.1023	0.0023	0.0155	0.0001	0.2603	0.0482	0.0011	99	2	98.9	1	109	45	100
A_221.FIN2	1077	332	0.79	28	0.1022	0.0020	0.0155	0.0001	0.1858	0.0480	0.0009	99	2	99.0	1	108	40	100
A_259.FIN2	699	111	0.37	43	0.1035	0.0028	0.0155	0.0001	0.1325	0.0486	0.0013	100	3	99.0	1	125	53	99
A_316.FIN2	894	266	0.69	51	0.1053	0.0049	0.0155	0.0003	0.0538	0.0493	0.0023	102	5	99.0	2	164	99	97
A_262.FIN2	1193	326	0.76	64	0.1031	0.0031	0.0155	0.0002	0.0850	0.0485	0.0016	100	3	99.1	1	131	69	100
A_324.FIN2	968	256	0.60	66	0.1037	0.0020	0.0155	0.0001	0.2532	0.0486	0.0010	100	2	99.1	1	127	42	99
A_250.FIN2	861	225	0.66	55	0.1075	0.0062	0.0155	0.0003	0.2388	0.0504	0.0028	104	6	99.2	2	200	110	96
A_229.FIN2	544	88	0.38	26	0.1061	0.0031	0.0155	0.0001	0.0695	0.0497	0.0015	102	3	99.2	1	170	59	97
A_246.FIN2	331	83	0.61	20	0.1087	0.0064	0.0155	0.0003	0.1475	0.0508	0.0030	104	6	99.3	2	200	110	95
A_223.FIN2	587	86	0.34	19	0.1086	0.0029	0.0155	0.0001	0.2143	0.0508	0.0014	105	3	99.4	1	223	56	95
A_252.FIN2	708	119	0.43	47	0.1069	0.0043	0.0155	0.0002	0.1559	0.0501	0.0020	103	4	99.4	1	190	85	97
A_284.FIN2	869	222	0.70	39	0.1037	0.0063	0.0156	0.0003	0.3146	0.0486	0.0029	100	6	99.4	2	130	120	99
A_267.FIN2	879	373	1.08	55	0.1048	0.0027	0.0156	0.0001	0.1018	0.0490	0.0013	101	3	99.5	1	146	52	98
A_276.FIN2	574	170	0.78	27	0.1053	0.0034	0.0156	0.0002	0.0325	0.0494	0.0017	101	3	99.6	1	158	69	98
A_218.FIN2	737	111	0.38	7	0.1080	0.0047	0.0156	0.0002	0.0785	0.0505	0.0023	104	4	99.6	1	209	94	96
A_271.FIN2	470	101	0.50	28	0.1049	0.0030	0.0156	0.0002	0.1207	0.0488	0.0014	101	3	99.6	1	142	58	99
A_220.FIN2	682	101	0.36	16	0.1041	0.0035	0.0156	0.0002	0.0060	0.0486	0.0017	100	3	99.6	1	125	68	99
A_235.FIN2	499	78	0.37	25	0.1040	0.0034	0.0156	0.0001	0.1619	0.0483	0.0015	100	3	99.7	1	118	62	100
A_282.FIN2	411	60	0.33	22	0.1095	0.0080	0.0156	0.0004	0.3582	0.0513	0.0035	105	7	99.8	3	230	130	95
A_219.FIN2	1063	310	0.71	20	0.1043	0.0025	0.0156	0.0001	0.2600	0.0485	0.0011	101	2	99.9	1	123	46	99

A_279.FIN2	589	93	0.37	32	0.1046	0.0028	0.0156	0.0001	0.1814	0.0484	0.0013	101	3	100.0	1	128	53	99
A_257.FIN2	694	113	0.38	33	0.1058	0.0042	0.0156	0.0002	0.1723	0.0491	0.0019	102	4	100.0	1	146	79	98
A_281.FIN2	2228	473	0.57	126	0.1054	0.0033	0.0156	0.0002	0.2158	0.0491	0.0015	102	3	100.0	1	148	64	98
A_239.FIN2	631	94	0.37	36	0.1090	0.0100	0.0156	0.0005	0.2083	0.0507	0.0047	105	9	100.1	3	210	180	96
A_313.FIN2	807	240	0.71	41	0.1047	0.0025	0.0157	0.0001	0.1375	0.0485	0.0012	101	2	100.1	1	129	49	99
A_328.FIN2	716	159	0.52	51	0.1054	0.0024	0.0157	0.0001	0.2277	0.0488	0.0011	102	2	100.1	1	143	46	99
A_265.FIN2	749	154	0.49	45	0.1058	0.0030	0.0157	0.0002	0.0200	0.0489	0.0015	102	3	100.2	1	147	61	98
A_226.FIN2	770	111	0.36	27	0.1081	0.0041	0.0157	0.0003	0.0492	0.0502	0.0018	104	4	100.3	2	193	77	96
A_277.FIN2	578	173	0.67	31	0.1073	0.0067	0.0157	0.0004	0.1180	0.0497	0.0032	103	6	100.3	2	170	130	97
A_325.FIN2	499	84	0.34	34	0.1066	0.0063	0.0157	0.0003	0.0317	0.0488	0.0029	103	6	100.3	2	160	120	98
A_238.FIN2	1140	365	0.82	63	0.1049	0.0026	0.0157	0.0002	0.0421	0.0486	0.0013	101	2	100.3	1	130	53	99
A_314.FIN2	328	114	0.84	20	0.1075	0.0044	0.0157	0.0002	0.0723	0.0499	0.0021	104	4	100.4	1	174	80	97
A_236.FIN2	698	125	0.43	41	0.1064	0.0029	0.0157	0.0002	0.0156	0.0494	0.0015	103	3	100.4	1	162	60	98
A_272.FIN2	378	108	0.63	26	0.1078	0.0080	0.0157	0.0003	0.1444	0.0501	0.0040	104	7	100.5	2	170	150	97
A_269.FIN2	610	192	0.71	42	0.1066	0.0048	0.0157	0.0002	0.2771	0.0491	0.0021	103	4	100.5	1	143	82	98
A_254.FIN2	610	92	0.36	41	0.1059	0.0042	0.0157	0.0002	0.0731	0.0490	0.0019	102	4	100.5	1	142	79	99
A_315.FIN2	259	71	0.65	15	0.1078	0.0047	0.0157	0.0002	0.0731	0.0499	0.0022	104	4	100.6	1	172	87	97
A_248.FIN2	277	80	0.68	15	0.1034	0.0092	0.0158	0.0005	0.2802	0.0476	0.0038	100	9	100.8	3	140	180	101
A_233.FIN2	680	96	0.35	34	0.1068	0.0039	0.0158	0.0002	0.1955	0.0485	0.0016	103	4	101.3	1	136	72	98
A_266.FIN2	1070	285	0.65	57	0.1079	0.0038	0.0159	0.0002	0.0533	0.0494	0.0018	104	4	101.6	1	162	76	98
A_302.FIN2	1146	331	0.68	62	0.1057	0.0020	0.0159	0.0001	0.2937	0.0483	0.0009	102	2	101.6	1	116	38	100
A_283.FIN2	808	182	0.49	50	0.1059	0.0024	0.0159	0.0001	0.1648	0.0484	0.0011	102	2	101.7	1	122	45	100
A_242.FIN2	744	254	0.70	51	0.1124	0.0081	0.0159	0.0004	0.0591	0.0514	0.0037	108	7	101.8	2	240	150	94
A_296.FIN2	283	76	0.53	17	0.1200	0.0150	0.0161	0.0010	0.7035	0.0576	0.0079	114	13	103.2	6	430	260	91
A_225.FIN2	624	138	0.54	23	0.1140	0.0170	0.0162	0.0006	0.0161	0.0514	0.0080	109	16	103.5	4	230	320	95
A_270.FIN2	440	65	0.29	28	0.1102	0.0047	0.0163	0.0002	0.3588	0.0491	0.0019	106	4	104.0	2	147	79	98
A_260.FIN2	389	85	0.43	29	0.1146	0.0064	0.0163	0.0007	0.0071	0.0509	0.0023	110	6	104.3	4	229	95	95
A_290.FIN2	2091	300	0.31	114	0.1138	0.0060	0.0164	0.0004	0.2264	0.0506	0.0027	109	6	104.9	3	210	120	96
A_292.FIN2	539	188	0.73	30	0.1101	0.0038	0.0164	0.0003	0.1117	0.0487	0.0018	106	4	105.1	2	129	72	99
A_289.FIN2	421	233	0.33	106	0.4360	0.0130	0.0588	0.0008	0.0321	0.0539	0.0018	367	9	368.5	5	352	73	100
A_321.FIN2	333	145	0.20	97	0.8860	0.0110	0.0855	0.0006	0.6046	0.0581	0.0008	529	7	528.8	4	521	32	100
A_224.FIN2	215	785	0.63	102	2.7650	0.0700	0.2164	0.0055	0.8131	0.0926	0.0014	1343	19	1262.0	29	1481	30	94
A_253.FIN2	719	1191	0.28	688	3.2350	0.0510	0.2550	0.0041	0.3839	0.0923	0.0015	1465	12	1464.0	21	1471	31	100
A_273.FIN2	70	463	0.97	69	3.9390	0.0600	0.2857	0.0028	0.0976	0.1004	0.0018	1622	13	1620.0	14	1623	33	100

Legend									
Cretaceous Upper	Jurassic	Permian	Devonian	Ordovician	Precambrian				
Cretaceous Lower	Triassic	Carboniferous	Silurian	Cambrian					

Table 4.3.8: Summary of youngest age matrices for the seven samples.

Analysis	Samples						
	Suicide Hill	Mini Troll	9B	Monollo-09-15	SCH-01-15	ST-010-15	SLF-08-15
YSG	Age	87.5 (+ 4.5) Ma	96.1 (+ 1.1) Ma	91.0 (+ 1.5) Ma	105.0 (+ 0.9) Ma	96.0 (+ 2.6) Ma	94.9 (+ 0.9) Ma
YPP	Age	99.7 Ma	99.8 Ma	97.0 Ma	119.8 Ma	100.0 Ma	98.0 Ma
YDZ	Age	87.0 Ma	93.9 Ma	90.5 Ma	105.2 Ma	94.8 Ma	93.7 Ma
	Range	+5.4-6.2 Ma	+1.5-5.0 Ma	+2.5-3.6 Ma	+1.7-2.3 Ma	+1.7-4.6 Ma	+1.1-7.6 Ma
	Confidence	95%	95%	95%	95%	95%	95%
YC1σ	Final Age	93.5 + 1.5 Ma (1.6%)	96.1 + 1.3 Ma (1.4%)	92.0 + 1.4 Ma (1.5%)	108.6 + 1.3 Ma (1.2%)	92.6 + 1.3 Ma (1.4%)	95.1 + 1.2 Ma (1.3%)
	Weighted Mean Age	93.5 + 1.1 Ma (1.1%)	96.1 + 0.8 Ma (0.8%)	92.0 + 1.0 Ma (1.1%)	108.6 + 0.6 Ma (0.5%)	92.6 + 0.8 Ma (0.9%)	95.1 + 1.2 Ma (1.3%)
	Systematic Error	1.1%	1.1%	1.1%	1.1%	1.1%	1.1%
	MSWD	12.6	0.1	1.7	87.7	4.7	0.1
YC2σ	Final Age	93.5 + 2.4 Ma (2.5%)	96.1 + 1.9 Ma (1.9%)	92.0 + 2.2 Ma (2.4%)	108.6 + 1.6 Ma (1.5%)	92.6 + 2.0 Ma (2.1%)	95.1 + 1.7 Ma (1.8%)
	Weighted Mean Age	93.5 + 2.1 Ma (2.3%)	96.1 + 1.5 Ma (1.6%)	92.0 + 2.2 Ma (2.1%)	108.6 + 1.1 Ma (1.0%)	92.6 + 1.7 Ma (1.8%)	95.1 + 1.4 Ma (1.4%)
	Systematic Error	1.10%	1.10%	1.10%	1.10%	1.10%	1.10%
	MSWD	3.2	0	0.4	21.9	1.2	0.1
Weighted Average	Age	95.7 + 1.0 Ma (1.1%)	96.8 + 1.0 Ma (1.0%)	95.7 + 1.8 Ma (1.9%)	112.1 + 2.9 Ma (2.6%)	95.2 + 1.7 Ma (1.7%)	95.5 + 0.4 Ma (0.5%)
	Confidence	95%	95%	95%	95%	95%	95%
	Rejected	0	0	0	0	0	0
	MSWD	1.3	0.2	9.7	51	9.9	0.4
	Probability	0.2	0.9	0	0	0	0.9
TuffZirc	Age	95.9 + 0.6 - 3.5 Ma	97.1 + 0.5 - 0.9 Ma	96.6 + 1.3 - 3.8 Ma	114.9 + 0.4 - 0.9 Ma	95.3 + 2.8 - 3.5 Ma	95.6 + 0.5 - 0.3 Ma
	Confidence	97.9%	97.9%	96.1%	93.0%	96.1%	97.9%
	Total Coherent Grains	10 of 10	10 of 10	9 of 10	8 of 10	9 of 10	10 of 10

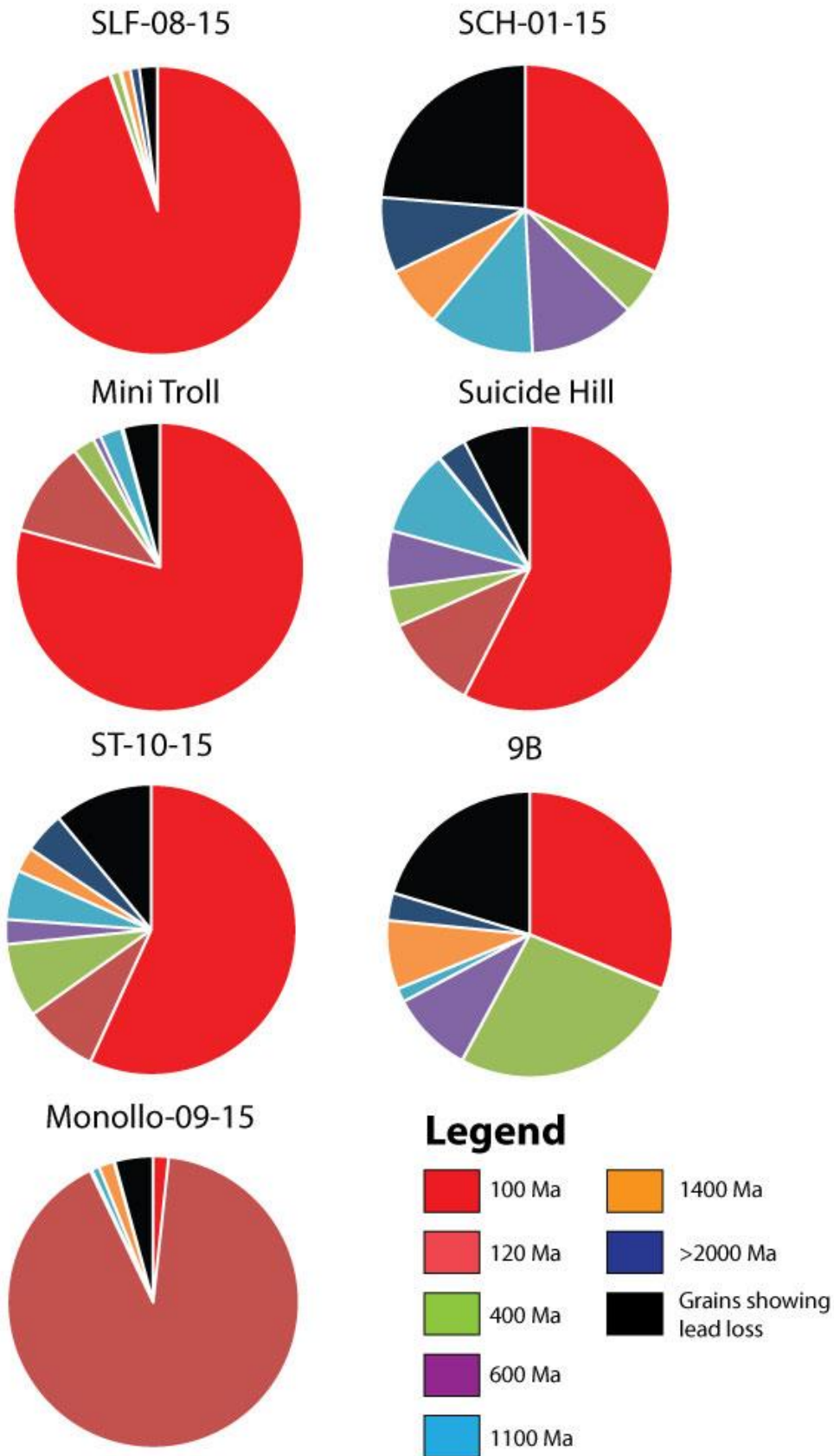


Figure 4.3.5: Pie Diagram showing portions of grains within successive age populations per sample.

4.3.2 Detrital Zircon Age Population

Within all the samples taken from the Cedar Mountain Formation, numerous distinct age populations ($n \geq 3$) could be discerned, recording many of the orogenic and intrusive events which occurred during the formation of Western North America (Fig. 4.3.4a,b). Many zircons, however, yielded ages which do not fall within any of the specific age populations, but rather form a continuous spread of singular ages between populations. This is the result of lead loss processes, most likely through microfracturing and diagenic alteration, resulting in zircons exhibiting an age younger than that of actual formation (Anderson, 2013).

The populations derived from the zircons can be broken into three main age groups with further subdivisions within each group. These groups include signatures from the formation of the Proterozoic basement rocks, the formation of the Cordilleran Fold Belt and the subsequent later stage orogenesis on the western portions of North America.

The oldest notable age signatures occur during the Paleoproterozoic. Typically representing core analyses, these age clusters represent zircons derived from the basement metamorphosed rocks of the Mojave province (Fig. 4.3.6, A) (Van Schmus *et al.*, 1993; Strickland *et al.*, 2013; Wooden *et al.*, 2013). These signatures are associated with (1) the initial formation of the Mojave supracrustal gneisses (2300–2000 Ma), (2) deformation following the Ivanpah Orogeny (1700 Ma), and (3) intrusion of multiple granitic bodies within the province (1400 – 1300 Ma) (Wooden & Miller, 1990; Van Schmus *et al.*, 1993; Strickland *et al.*, 2013). These rocks were later uplifted and reworked following the southern portions of the Grenville Orogeny occurring during the amalgamation of Rodinia and forming the Unkar Group sediments around 1200 until 1000 Ma (Mosher, 1998; Dickenson, 2004). Northwesterly flowing rivers deposited reworked basement sediments from the Mojave gneisses, Ivanpah provinces, and sediments from the Grenville Orogeny south of the Canadian shield.

The younger grouping of signatures records the initial assembly of the Cordilleran Fold Belt and spans from the Late Neoproterozoic to Early Triassic, (400 Ma, 360 Ma, and 250 Ma) (Dickenson, 2004, 2006). The Neoproterozoic (600 Ma) signature is derived from synrift deposits formed south of the trans-Idaho discontinuity via easterly input from the Transcontinental arc into the Cordilleran miogeocline (Prave, 1999; Dickinson, 2004) (Fig. 4.3.6, B). This sedimentary succession was later deformed via obduction of the Roberts Mountain allochthon by the Antler Orogeny during the Devonian (400-350 Ma) (Fig. 4.3.6, C) (Dickinson, 1983, 2004, 2006). Sediments from the obducted allochthon and Antler Orogeny was captured within the Havallah Basin via west to east flowing rivers from the Quensnell and Yukon-Tanana terranes. Subsequent deformation of the Roberts Mountains occurred during the Sonoma Orogeny, which straddles the Permian-Triassic boundary (260-235 Ma) and represents the sedimentary source into the Triassic Havallah Foreland Basin (Fig. 4.3.6, D) (Dickinson, 2004).

The youngest grouping of age signatures records the latter part of the Cordilleran evolution spanning the Upper Jurassic to Upper Cretaceous. Tectonism during this time was marked by the formation of the Nevadan Orogeny following accretion of the Wrangellia Terrane onto the Cordilleran Arc During the Late Jurassic (160-145 Ma) (Schweickert *et al.*, 1984; Albino, 1992; Blakey & Ranney, 2018). This led to the sedimentation into the associated Morrison Basin within the Western Interior Basin, resulting in a notable peak of detrital zircon grains during this period (Fig. 4.3.6, E). The largest detrital zircon signature ($n > 500$) occurs during the Cretaceous, which coincides with the development of the Sevier Orogeny (Heller *et al.*, 1986; Yingling & Heller, 1992; DeCelles *et al.*, 1995). This peak shows a distinct subdivision into Aptian (118 Ma), Cenomanian (99 Ma), and Turonian (94 Ma) age clusters, recording multiple stages of orogenesis during the formation of the Sevier Fold Belt (Fig. 4.3.6, F). These different stages are characterized by the Canyon Range

Thrust, occurring around 140 Ma, and the Pavant Thrust, occurring around 110 Ma to 90 Ma (DeCelles & Coogan, 2006). The large detrital zircon peak is temporally concurrent with the Pavant Thrust of the Sevier Orogeny, representing the main sedimentary input for the Mussentuchit Member of the Cretaceous Cedar Mountain Formation (DeCelles, 2004; DeCelles & Coogan, 2006). Age peaks during the Pavant thrusts are, in themselves, quite varied as the Pavant thrusts are comprised of multiple tectonic events. Specifically, Pavant thrusting initiated during the Albian, recorded by the 110 Ma peak, with subsequent sheet breakup and duplexing during the Cenomanian and Turonian, recorded by the 98 Ma and 94 Ma peaks (DeCelles & Coogan, 2006).

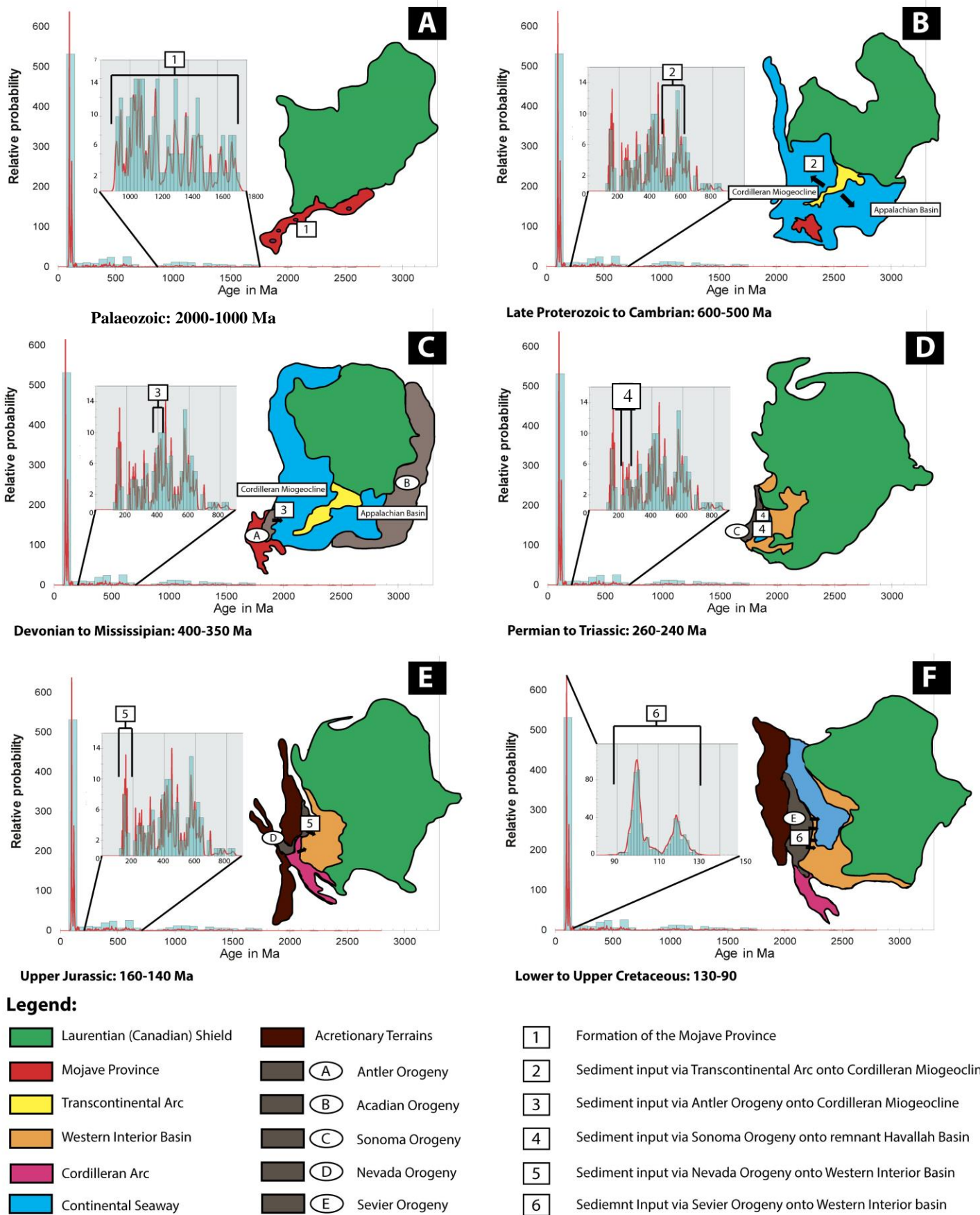


Figure 4.3.6: Figure shows evolution of North America with specific focus on the western margin. A-F notes various points of evolution during the amalgamation of various terrains.

4.3.3 Kolmogorov-Smirnov Test

Similar sediment source probability analysis utilized the Kolmogorov-Smirnov Test, which tests the dissimilarity in cumulative density functions across multiple samples. Samples, which passed the test with a similarity coefficient (p) of higher than 0.05, are seen to have a higher probability of sharing the similar source terrains. All the samples were tested simultaneously against each other for the entire suite of age populations in addition to analysing only the youngest age domains (Table 4.3.9, A, B).

When analysing the full suite of representative age domains, only samples ST-010-15 and sample Suicide Hill show a coupled p of higher than 0.05 between the two samples. Samples SLF-08-15 and 9B show the next highest coupled p -value between samples, followed by the coupled p -value of samples Suicide Hill and Mini Troll. These samples, however, do not show a coupled p -value higher than 0.05, which indicates a low statistical probability of a shared source region. Samples Monollo-09-15 and SLF-08-15 show zero probability of shared sediment provenance to any other samples (Table 4.3.9, A).

Cumulative density plots illustrate a shared trend followed by all but two samples from 90 Ma until 100 Ma, from which point large deviations in these cumulative density trends start occurring (Fig. 4.3.7). The trends of four of these samples converge around 600-700 Ma, exhibiting only moderate variation in signatures between the samples at this point. The trends in the cumulative probability curves diverge again until a second convergence of all but two trends around 1250-1300 Ma.

Table 4.3.9: (A) Probability values of all samples following Kolmogorov-Smirnov test. Note that only Suicide Hill and St-010-15 show a possible genetic relationship. Samples highlighted in light blue show a slight probability of a shared source, however statistically a very low probability. (B) Shows table constructed from youngest age peaks. Following this, only sample Monollo-09-15 shows no genetic links to any other samples.

A							
K-S P-values using error in the CDF							
	9B	Suicide Hill	Mini Troll	Monollo	SCH-01-15	SLF-08-15	ST-010-15
9B		0.000	0.000	0.000	0.035	0.000	0.000
Suicide Hill	0.000		0.015	0.000	0.000	0.000	0.352
Mini Troll	0.000	0.015		0.000	0.000	0.008	0.000
Monollo	0.000	0.000	0.000		0.000	0.000	0.000
SCH-01-15	0.035	0.000	0.000	0.000		0.000	0.000
SLF-08-15	0.000	0.000	0.008	0.000	0.000		0.000
ST-010-15	0.000	0.352	0.000	0.000	0.000	0.000	

B							
K-S P-values using error in the CDF							
	9B	Suicide Hill	Mini Troll	Monollo	SCH-01-15	SLF-08-15	ST-010-15
9B		0.377	0.122	0.000	1.000	0.651	0.022
Suicide Hill	0.377		0.655	0.000	0.223	0.034	0.130
Mini Troll	0.122	0.655		0.000	0.076	0.003	0.255
Monollo	0.000	0.000	0.000		0.000	0.000	0.000
SCH-01-15	1.000	0.223	0.076	0.000		0.268	0.003
SLF-08-15	0.651	0.034	0.003	0.000	0.268		0.000
ST-010-15	0.022	0.130	0.255	0.000	0.003	0.000	

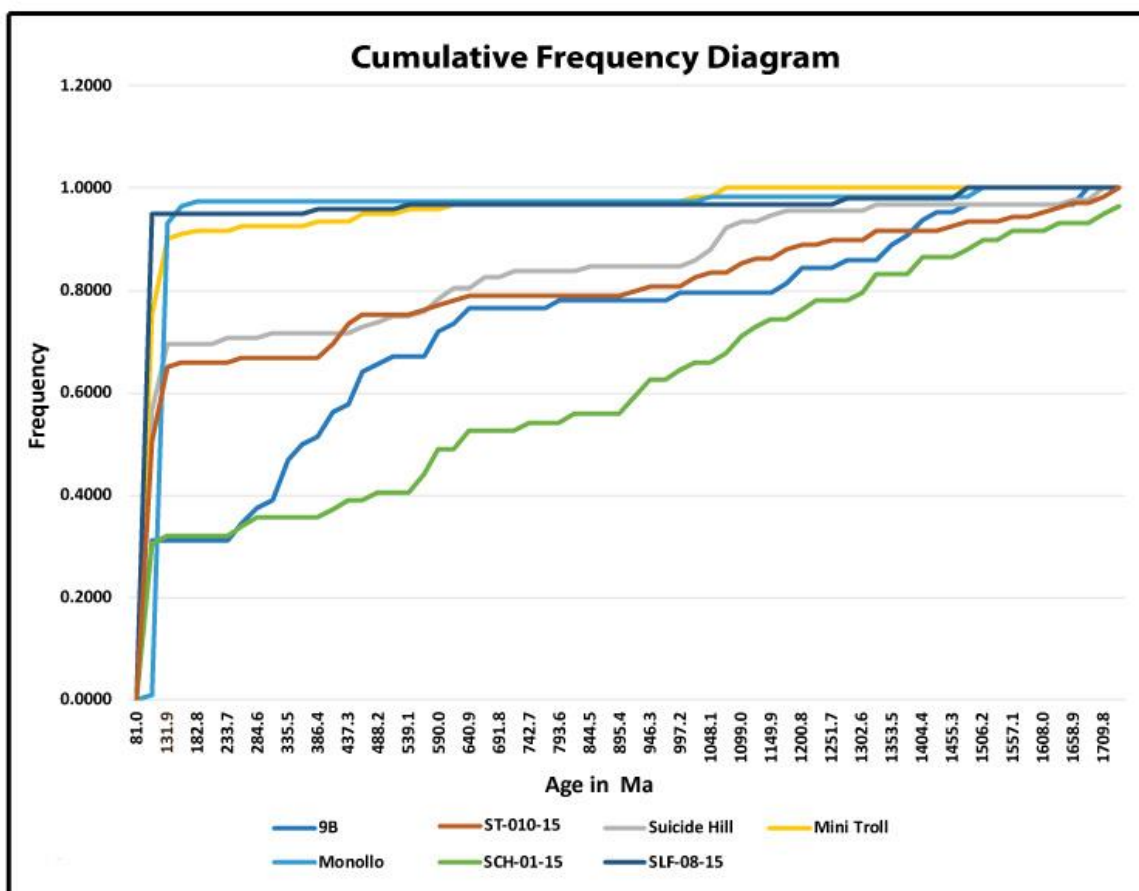


Figure 4.3.7: Figure shows the Cumulative Probability plots for all sample zircon populations. Most samples show little to no correlation with population, save for ages at which age populations occur.

Considering the strong correlation at younger ages (Fig. 4.3.7), all samples were additionally analysed with the Kolmogorov-Smirnoff test for all ages under 150 Ma, thereby elucidating on the genetic relationships of the younger zircon assemblages. The results from this younger population test yielded more usable relationships; only sample Monollo-09-15 shows a coupled p -value of zero with any other sample (Table 4.3.9B). The other six samples, however, showed several relationships of coupled p -values greater than 0.5. Samples which showed coupled p -values lower than 0.05 include: 9B with ST-010-15; Suicide Hill with SLF-08-15; Mini Troll with SLF-08-15; SCH-01-15 with ST-010-15; SLF-08-15 with ST-010-15; SLF-08-15 with Suicide Hill, Mini Troll, and ST-010-15; and ST-010-15 with 9B, SCH-015, and SLF-08-15.

The cumulative density plot further elucidates on the relationships between these younger age populations. From the cumulative density plot, samples 9B, SCH-01-15, and SLF-08-15 showed a shared cumulative probability trend while samples Mini Troll, ST-010-15, and Suicide Hill showed a different shared trend (Fig. 4.3.8). Sample Monollo-09-15 shows its own distinct distribution pattern removed from the other samples. These shared trends diverge from each other around 96 Ma, 99 Ma, 115 Ma, and 120 Ma. Additional KS analysis was conducted between samples of each shared trend, which showed p -values of more than 0.05 (Table 4.3.10).

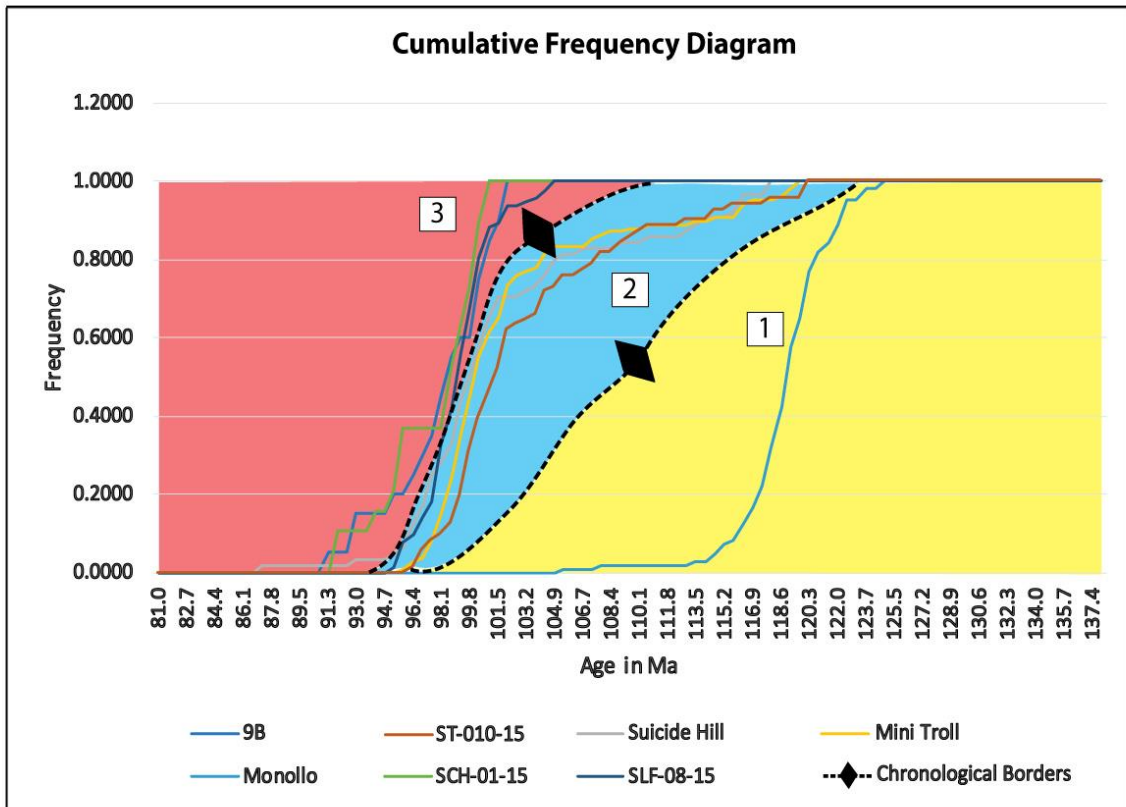


Figure 4.3.8: Figure shows the Cumulative Probability plots for only the youngest fractions of each sample. Note the genetic relationships between samples suggest three distinct age domains.

Table 4.3.10: Genetic probability values of samples Following K-S test in age domains 2 and 3 showing high probability of genetic relationship.

K-S P-values using error in the CDF			
	Suicide Hill	Mini-Troll	ST-010-15
Suicide Hill		0.648	0.147
Mini-Troll	0.648		0.289
ST-010-15	0.147	0.289	

K-S P-values using error in the CDF			
	9B	SCH-01-15	SLF-08-15
9B		0.999	0.650
SCH-01-15	0.999		0.268
SLF-08-15	0.650	0.268	

4.3.4 Youngest Maximum Depositional Ages for the Mussentuchit Member

From the seven collected samples, two are restricted to the upper Mussentuchit, four were collected from the middle portions of the Mussentuchit, and one is limited to the basal Mussentuchit units. By averaging the ages obtained from six of the seven methodologies described above, these ages can be utilized to draw inferences as to the youngest maximum depositional (YMD) age of each of the sampled units (Fig. 4.3.9).

For this study, we are limited to one sample that was collected from the lower portion of the lower Mussentuchit (± 5.0 m above the basal contact with the underlying Ruby Ranch Member). The sample was collected from the Chicago Field Museum's fossil locality, Hard Boiled Jack. The averaged YMD age based on six different analysis indicates an age of ± 110.8 Ma (Upper Albian). This study finds that, as a whole, the youngest maximum depositional age is quite reserved when compared to overlying sediments. While this may be a depositional bias, the amount of grains ($n=117$) strongly indicates the age of 110.8 to be a supported youngest maximum depositional (YMD) age.

Samples collected from the Suicide Hill (Suicide Hill), Mini Troll (Mini Troll), and Stormy Theropod (ST-010-15) fossil quarries, as well as sample 9B, are restricted to the middle portions of the Mussentuchit stratigraphy. The averaged YMD age based on six different analysis indicates an age of 95.1 Ma for Suicide Hill, 95.3 Ma for 9B, 96.63 Ma for Mini Troll, and 97.03 Ma for ST-010-15. By analysing the zircons within these four samples as a single representative sample, the YMD age for the middle portions of the Mussentuchit is interpreted to be ± 95.6 Ma ($n=389$).

Samples collected from the upper third of the Mussentuchit Member stratigraphy include the *Siats meekerorum* holotype locality (SCH-01-15) and the Chicago Field Museum's Scared Little Fatty fossil quarry (SLF-08-15). The averaged YMD age based on six different analysis indicates an age of 93.43 Ma for SCH-01-15, and 95.47 Ma for SLF-08-

15. By analysing the zircons within these two samples as a single representative sample, the YMD age for the upper portions of the Mussentuchit is interpreted to be ± 94.45 Ma (n=157).

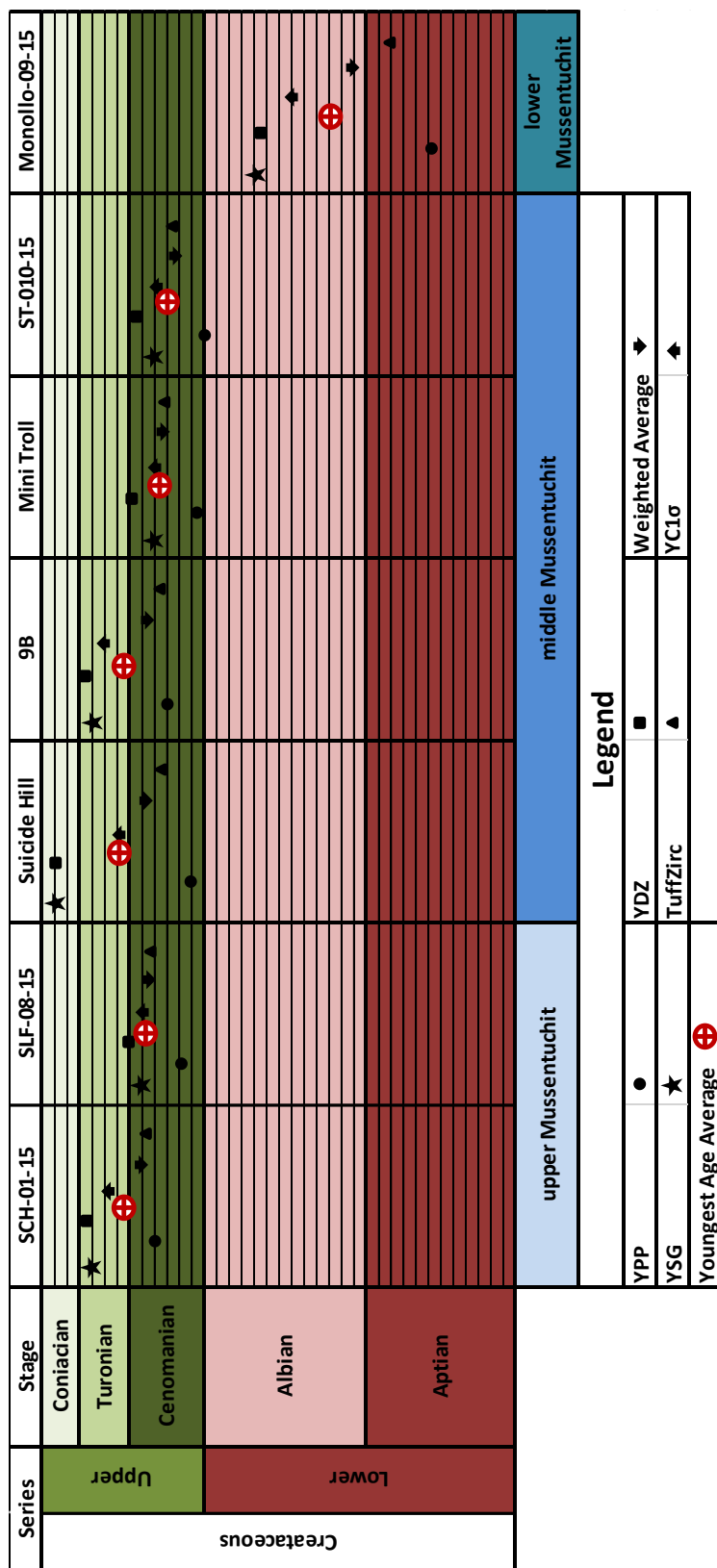


Figure 4.3.9: Figure showing a graphical representation of youngest ages along with averaged youngest age.

5. Discussion

This study sought to generate a framework by which newly discovered fossil assemblages from the Mussentuchit Member of the Cedar Mountain Formation can be rigorously contextualized within the western flank of the San Rafael Swell near Capitol Reef, Central Utah. Regionally, environmental change can be attributed to continental-scale Kiowa-Skull Creek and Greenhorn transgressive cycles of the Western Interior Seaway (WIS) (Kauffman & Caldwell, 1993; Obradovich, 1993; Oboh-Ikuenobe *et al.*, 2008; Suarez *et al.*, 2012). These transgressions are currently linked to the local-regional scale tectonism in the later stages of the Sevier Orogeny, which formed in response to accretionary tectonism on the western continental margin (Currie, 2002; DeCelles, 2004; De Celles & Coogan, 2006; Dickenson & Gehrels, 2008; Lawton, 2010). Sedimentological and geochronological results from this study indicate that deposition of the Mussentuchit initiated during the Cenomanian (± 97 Ma) in response to tectonism, which occurred in Albian (± 110.92 Ma) time. Deposition continued at least into the Turonian (± 93.43 Ma) with marginal marine conditions persisting at Mussentuchit Wash until this time. A distinct change in sedimentation patterns occurs between the upper and lower Mussentuchit around ± 95.6 Ma. This indicates a sudden shift in the tectonic regime, coinciding with a change in the development of the Western Interior Seaway during this time. To better understand these environmental shifts, this study synthesized high-resolution environmental and temporal models following the unofficial subdivision of the Mussentuchit Member into the lower and upper Mussentuchit.

5.1 Deposition of the Mussentuchit Member

The Mussentuchit Member is locally underlain by the Ruby Ranch Member, which shares numerous sedimentological similarities with the overlying member unit. (Suarez *et al.*, 2012; Kirkland *et al.*, 2017). Consisting predominantly of variegated mudstones, interbedded sandstone, and numerous calcisol horizons, the Ruby Ranch Member is interpreted to

represent the distal portions of a vast, alluvial floodplain depositing within an arid climatic setting (Garrison, 2007; Ludvigson *et al.*, 2015; Kirkland *et al.*, 2016). Radiometric dating of $^{206}\text{Pb}/^{238}\text{U}$ and $^{40}\text{Ar}/^{39}\text{Ar}$ isotopes, along with chemo-stratigraphic calcium carbonate profiles, have succinctly placed the deposition of the Ruby Ranch Member within the Early to Middle Albian, ± 107 Ma (Kirkland *et al.*, 2017). Deposition of the Ruby Ranch Member has accordingly been attributed to the Kiowa-Skull Creek Transgression of the Mowry Seaway in response to the initiation of the Canyon Range Thrust and later Pavant thrusting within the Sevier orogenic belt (DeCelles & Coogan, 2006; Suarez *et al.*, 2012; Sprinkel *et al.*, 2012).

Though the Ruby Ranch and Mussentuchit members appear quite similar, this study found key variations in both the palaeoenvironment and tectonic controls between these two units. Furthermore, this study identified a distinct change in sedimentation patterns within the Mussentuchit Member itself. Fine-grained, rhythmically interbedded silts and muds (FA1) form a major sediment type within the lower Mussentuchit and, resultantly, hosts all other lithological features. These other lithologies include palaeosol horizons (FA2), coarse-grained, gravelly lenses (FA3), finely laminated silty lenses (FA4), and cross-bedded sandstones (FA5). The rhythmically interbedded mud and silt couplets of FA1 represent large tidal mudflats, which expand across the field area, similar to the tidal mudflats found at the modern-day Ganges-Brahmaputra and Changjiang deltas (Goodbred & Saito, 2011). Further similarities to these deltas include FA2, which represent inter-channel mounds or tidal bars of stable sediment within the delta (Ryu *et al.*, 2002; Chakrabarti, 2005; Dalrymple & Choi, 2007). The gravelly silts of FA3 represent crevasse splays, resulting from major flooding events. The finely laminated silty lenses of FA4 are interpreted to represent muddy infilled abandoned channels or oxbow lakes, similar to the lacustrine and palustrine features previously reported by Garrison *et al.* (2007) and Ludvigson *et al.* (2015) (Wolfe *et al.*, 2006; Erskine *et al.*, 1992; Citterio & Piegay, 2009). FA5 represents channel deposits, which incise

into the muddy substrate and preserve numerous palaeocurrent indicators (Allen, 1963; Nadon, 1994; Miall, 1985, 1996; Lang *et al.*, 2004; Fielding, 2006; Gibling, 2006; Nichols & Fisher, 2007; Miall, 2014). Palaeocurrents derived from structures within FA5 are indicative of multi-modal flow in northeasterly and easterly directions. These agree with the flow direction of Cenomanian timed river systems reported by Suarez *et al.* (2012). Accordingly, the channels of FA5 in the lower Mussentuchit form the distal portions of the large river systems which fed from south-western highlands in the Sevier Mountains into the Western Interior Seaway. The varying current direction reflects deposition within sinuous intertidal channels, typically associated with the supratidal portion of a tide-dominated delta (Dalrymple *et al.*, 1992). From the co-occurrence of the above-mentioned facies assemblages, this study interprets the lower Mussentuchit as depositing within the supratidal portions of a laterally extensive, flat-lying tidal delta, similar to the Ganges-Brahmaputra and Changjiang deltas (Bhattacharya, 1992; Orton & Reading, 1993; Olariu & Bhattacharya, 2006; Nichols & Fisher, 2007; Dalrymple & Choi, 2007; Dalrymple, 2010; Goodbred & Saito, 2011).

The topmost portions of the lower Mussentuchit show a notable increase in palaeosol development. This is interpreted to represent a series of short-lived depositional hiatuses resulting in increased palaeosol development during the end of the lower Mussentuchit sedimentation (Massini *et al.*, 2010; Sorenson, 2011; Lepre, 2017). Renewed sediment influx from the Sevier Orogeny led to the subsequent deposition of the overlying upper Mussentuchit.

The upper Mussentuchit shows the same facies associations as the lower Mussentuchit, namely FA1, FA2, FA3, FA4, and FA5, with the addition of the ephemeral water bodies of FA6. The most notable difference between the upper and lower Mussentuchit is the relative proportions with which the facies associations occur. FA1 silts and muds dominate this succession, comprising the majority of the sediments found within the upper

Mussentuchit. This is followed by thinly bedded palaeosols of FA2 and fine silts of FA4. FA3 is present as thinly bedded lenticular units. The sandstones of FA5 occur very sporadically and only as thin, fine-grained silty ribbons. FA6 is present only within the topmost portions of the upper Mussentuchit as small, lenticular units representing ephemeral, saltmarsh-like water bodies (Wolfe *et al.*, 2006; Chen *et al.*, 2015). The slight increase in abandoned channels indicates a higher sediment input within the upper Mussentuchit, suggesting a slightly stronger terrestrial signature than in the lower Mussentuchit. Palaeocurrent indicators taken from FA5 indicated multi-directional flow similar to that of the lower Mussentuchit, with a slight drop in sinuosity. This, indicates current flow associated with the intertidal to subtidal portion of tidal deltas (Klein, 1970; Amajor, 1984; Dalrymple *et al.*, 1992; Dalrymple & Choi, 2007; Dalrymple, 2010). Furthermore, palaeocurrent indicators from the upper Mussentuchit show a more easterly current direction as opposed to the lower Mussentuchit. This indicates that the upper Mussentuchit was deposited in response to a slightly different river system than the one identified by Suarez *et al.* (2012). This is attributed to a shift in the relative position of the highlands in the Sevier Mounitan range to a more northern position due to thrust reactivation. Though the upper Mussentuchit shows numerous similarities to the lower Mussentuchit, an overall finer grain size, marked dominance of FA1 and more linear palaeocurrents indicate a slightly different depositional environment. This study, therefore, interprets the upper Mussentuchit to represent the sub-tidal to intertidal portions of a marine-dominated tidal flat (Bhattacharya, 1992; Orton & Reading; 1993; Olariu & Bhattacharya, 2006; Nichols & Fisher, 2007; Dalrymple & Choi, 2007).

Though also distal deposits, these palaeoenvironmental interpretations differ from previous authors, which interpreted the Mussentuchit to represent cyclic lacustrine and palustrine deposits within a humid, distal distributive to terminal floodplain delta (Garrison *et*

al., 2007; Ludvigson *et al.*, 2015; Holmes, 2017; Kirkland *et al.*, 2017). Previous studies by Kirkland *et al.* (2017) have, however, noted that the Mussentuchit Member does not follow a typical layer cake stratigraphic pattern. Variations in sedimentation occurring at similar stratigraphic heights commonly reflect geographic variations in the depositional environment. Therefore, the Mussentuchit sedimentary succession at the study area is interpreted to record the palaeogeographic position of a coastal embayment within a distal distributive to terminal floodplain delta, similar to the Changjiang delta of eastern China (Goodbred & Saito, 2011), see Figure 5.1.

Radiometric dating of detrital zircon assemblages greatly aided in adding temporal context to the environmental evolution of the Mussentuchit Member. Considering the distal nature of the depositional environment, sediments will naturally preserve detrital zircon signatures from multiple orogenies throughout the tectonic assembly of the Cordilleran Fold Belt (Finzel, 2017). All the detrital zircon samples, however, showed a robust youngest detrital zircon age signature, ranging between ± 93.43 and ± 110.92 Ma. Radiometric dating of the basal-most Monollo-09-15 sample yielded an Early Albian age of ± 110.92 Ma, averaged from six youngest depositional age matrices. The absolute youngest age for this sample is ± 105 Ma, derived from the youngest single zircon age. These Albian ages are complemented by $^{206}\text{Pb}/^{238}\text{U}$ isotope results reported by Sorensen (2011) and Holmes (2017), which dated basal Mussentuchit units at ± 105 Ma. Detrital zircon ages, however, represent only the youngest maximum age of deposition and do not record the actual time of deposition. The Cenomanian (96.7 Ma to 98.38 Ma) $^{40}\text{Ar}/^{39}\text{Ar}$ isotope ages reported by Cifelli, (1997), Garrison *et al.* (2007), and Kirkland *et al.* (2017) are more likely to represent the actual depositional age. The detrital zircon age data is, however, still useful as it represents the formation of the lower Mussentuchit's sediment source terrain. Considering the average age bracket of ± 110.92 (+4-5) Ma, the source terrain of the lower Mussentuchit is interpreted to

be associated with the initiation of Pavant thrusting within the Sevier Fold Belt (DeCelles & Cooper, 2006). This source terrain is similar to that of the underlying upper Ruby Ranch Member, indicating a genetic relationship in the sediments characterizing the Ruby Ranch/Mussentuchit transition. Furthermore, the sedimentary succession of the lower Mussentuchit is only slightly different than that of the upper Ruby Ranch, indicating that the lower Mussentuchit deposited within a similar late underfilled phase as the Ruby Ranch Member, during the early Cenomanian (Yang, 2011) (Fig. 5.1). The difference in sedimentation style between the Ruby Ranch and Mussentuchit members is, therefore, not due to different tectonic controls, but rather only to a change in the depositional environment brought on by the underfilled/filled phase transition during the initiation of the Greenhorn Transgression. This would account for the gradational nature of the member contacts as well as the absence of distinctive higher order bounding surfaces between members.

Detrital zircon assemblages preserved directly above the notable palaeosol horizons record the start of deposition for the upper Mussentuchit and, hence, the timing of the environmental shift between the lower and upper Mussentuchit. Samples taken from the base of the upper Mussentuchit include ST-010-15 and Mini Troll, which yielded ages of ± 96.5 Ma and ± 96.0 Ma, respectively. This agrees with the younger $^{40}\text{Ar}/^{39}\text{Ar}$ ages of ± 96.7 Ma reported by Garrison *et al.* (2007) and Kirkland *et al.* (2017). More importantly, these results indicate that deposition of the upper Mussentuchit occurred in response to a more recent orogenic event than that of the lower Mussentuchit. This orogenic event is related specifically to the fault reactivation and duplexing of the Pavant Sheet during the overfilled phase of the Greenhorn Transgression (DeCelles & Cooper, 2006). Sample SCH-01-15 was taken from one of the stratigraphically highest ash layers in the Mussentuchit and yielded an age of ± 93.43 Ma. This age is much younger than has been previously reported, however, this may

be due to the youngest portions of the Mussentuchit Member only being preserved at the type section present at Mussentuchit Wash (Kirkland *et al.*, 2017).

This youngest maximum depositional age fits within the timing of the Greenhorn Transgression of the epi-continental Mowry seaway (Oboh-Ikuenobe *et al.*, 2008). The laterally extensive sedimentation packages and the up-section increase of terrestrial influences of the upper Mussentuchit resulted from flat-lying, shallow sea deposition within the filled-overfilled phase of the Sevier Foreland Basin (Yang, 2011). This overfilled phase of the basin occurred closely after the final stages of the Pavant Sheet duplexing event, placing the overfilled phase during the Turonian (DeCelles & Googen, 2006), see Figure 5.1.

The deposition of the Mussentuchit Member within the underfilled and overfilled stages of the Sevier Foreland Basin resulted in an aggradational to a slight progradational sequence stacking pattern. This specific stacking pattern is, however, only limited to the Mussentuchit Member. When the Cedar Mountain Formation is viewed in its entirety, it exhibits a retrogradational sequence stacking pattern (Arthur & Sageman, 2004). Additionally, Oboh-Ikuenobe *et al.* (2008) suggested a number of small transgressive-regressive cycles occurring during the start of the Greenhorn Transgression at a similar time as the deposition of the Mussentuchit Member. It is therefore interpreted that the aggradational sequence stacking pattern of the Mussentuchit Member is linked to sediment input from the Pavant fault reactivation matching, and briefly outpacing accommodation space brought on by fluctuating global sea levels (Haq *et al.*, 1987; Arthur & Sageman, 2004). Data for this interpretation is, however, limited as the majority of the Mussentuchit Member appears to only be preserved up until just above the middle Mussentuchit (Sorensen, 2011; Holmes, 2017). Refining the sequence stacking pattern of the Mussentuchit Member at other localities may, therefore, aid in defining more evidence of progradation within the Mussentuchit as a function of fluctuating global sea levels.

The long-lived nature of Pavant thrusting and stable sedimentation enabled highly resolved environmental and temporal contextualization for multiple fossil preservation sites at Mussentuchit Wash. The Fortunate Son fossil quarry is situated near the base of the lower Mussentuchit and is associated with numerous palaeosols and silty lenses, indicating an environmental position within the supratidal portion of the tidal flat. Additionally, the Monollo-09-15 sample, also situated within the basal Mussentuchit, is dated at an average age of ± 110.92 Ma. This suggests that fossil preservation within the lower Mussentuchit occurred no later than the Late Albian. Both the Mini Troll and Suicide Hill fossil quarries are located within the upper Mussentuchit, suggesting preservation at these sites occurred within the inter-tidal portions of a tidal mudflat. Sample Mini Troll was taken from the Mini Troll fossil quarry and was dated at an average age of ± 96.00 Ma with a youngest single zircon age of ± 93.95 Ma. This indicates a preservational age no older than the Late Cenomanian. Sample Suicide Hill was taken from the Suicide Hill fossil quarry and exhibited an average age of ± 94.10 Ma with a youngest single zircon age of ± 92.50 Ma, indicating deposition no earlier than the Turonian.

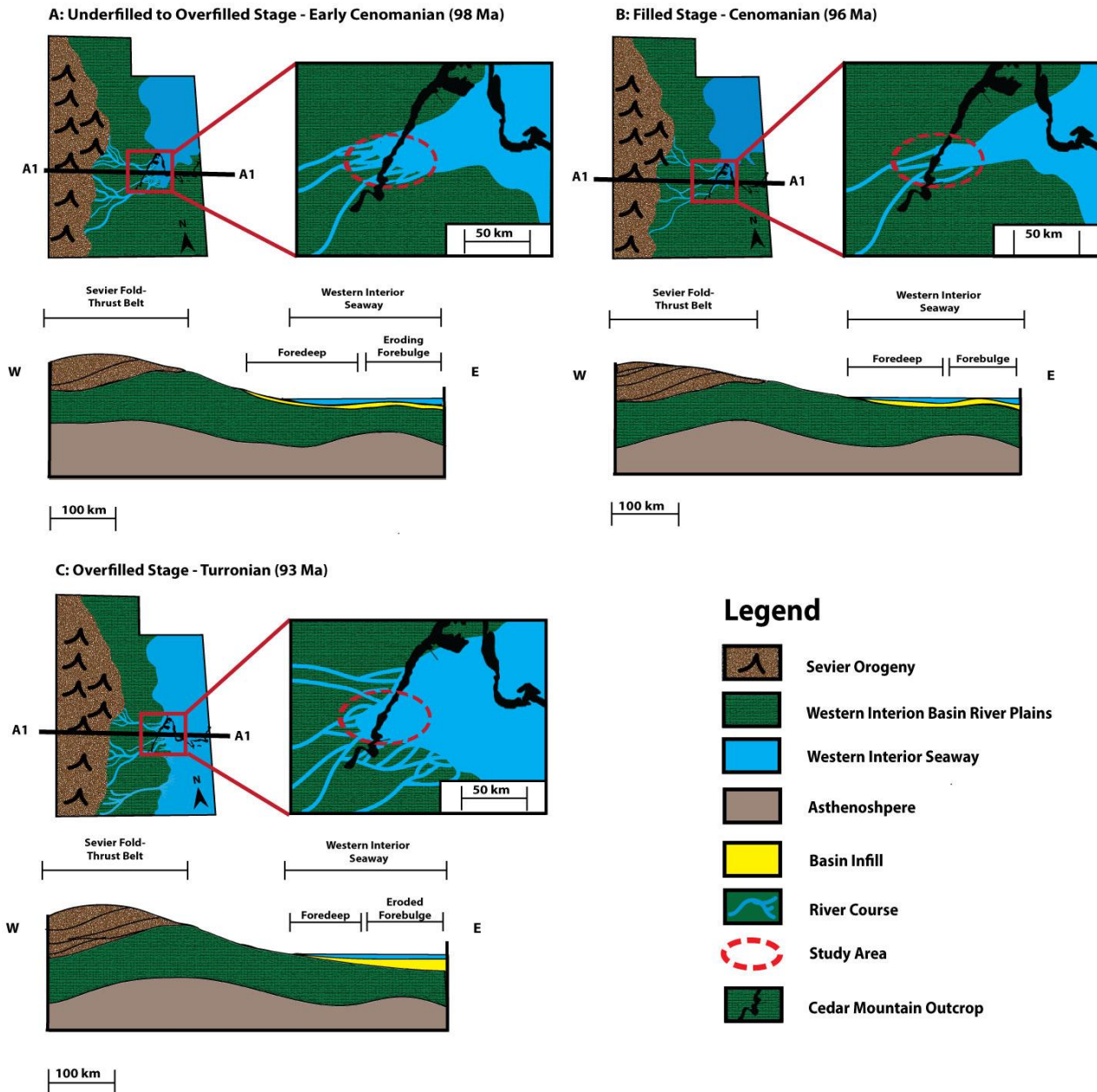


Figure 5.1: Diagram illustrating the development of the coastal embayment at the study area in response to various filled stages of the Western Interior Basin. Specifically, (1) the late underfilled to filled stage during the Early Cenomanian showing initial formation of the embayment, (2) the filled to early overfilled stage of the Late Cenomanian showing a partially filled embayment, and (3) the overfilled stage of the Turonian, showing reinvigoration of the embayment.

6. Conclusion

This study aimed to contextualize a section of the Mussentuchit Member stratigraphy located on the western flank of the San Rafael Swell, within rigorous temporal, environmental, and stratigraphic frameworks. This was done to elucidate the environmental context of the newly emerging fossil assemblages from this area. This was achieved through the combination of traditional field-based stratigraphical and facies analysis and modern $^{206}\text{Pb}/^{238}\text{U}$ isotope geochronology of detrital zircon assemblages. These techniques enabled the study to create highly resolved 3-dimensional palaeoenvironmental, temporal and depositional models. The creation and analysis of these frameworks resulted in the following conclusions:

- 1) The stratigraphy of the Mussentuchit Member at the study locality on the western flank of the San Rafael Swell exhibits limited stratigraphic variation, with the average thickness of the unit and its stratigraphic position remaining constant throughout. The only exception to this is some slight structural deformation in the western portions of the study area, present as open monoclines and minor faulting. From lithological analyses, distinct differences in sedimentation type distinguish the Mussentuchit from the underlying Ruby Ranch Member and overlying Naturita Formation.
- 2) Palaeoenvironmental reconstructions indicate that deposition of the Mussentuchit Member at the study area occurred within the supra- to subtidal portions of a distal deltaic mudflat, similar to the modern-day Ganges-Brahmaputra lower delta plain of southern India, or the Changjiang Delta of eastern China. By combining this interpretation with findings in the literature, this study interprets that the sediments at the study area preserve the palaeogeographic position of a coastal embayment.

- 3) Detailed facies analysis illustrated a distinct environmental transition between the lower and upper Mussentuchit from a supratidal to a more inter-subtidal environment. This transition is marked by notably developed palaeosol horizons, indicating a depositional hiatus during this environmental transition.
- 4) Through a combination of geochronological results with west to east palaeocurrent indicators, this study showed that the Mussentuchit Member was deposited in response to the Pavant thrusting stage of the Sevier Orogeny. Specifically, lower Mussentuchit deposition occurred during Cenomanian time (± 98 Ma), sourcing sediment formed during the initial Pavant thrusting during ± 110.92 Ma. This was followed by deposition of the upper Mussentuchit in reaction to the internal breakup and duplexing of the Pavant Sheet during ± 95.6 Ma to ± 93 Ma.
- 5) Deposition of the Mussentuchit occurred as a result from multiple transgressive cycles. The lower and middle Mussentuchit was deposited during the late underfilled to filled stage of the Albian aged Western Interior Basin during the initial stages of the Greenhorn Transgression. The upper Mussentuchit was deposited during the early to late overfilled stage of the Cenomanian aged Western Interior Basin in response to the continuation of the Greenhorn Transgression. The palaeosols marking the transition between the two stratigraphic intervals are indicative of a depositional hiatus, effectively marking a pause in the sea level rise associated with the Greenhorn Transgression.
- 6) Through the combination of facies, stratigraphical and geochronological analysis, it was possible to place three fossil quarry sites at Mussentuchit Wash within their respective environmental and temporal frameworks across the Mussentuchit Wash tidal delta. These include:

- (I) The Fortunate Son fossil quarry, which is located within the supratidal portion of the tidal delta, and is situated within a portion of the sedimentary succession dated at an Albian average youngest maximum depositional age of ± 110.92 Ma and a youngest single zircon age of ± 105 Ma.
- (II) The Mini Troll fossil quarry, which is preserved within the intertidal facies of the tidal delta and dated at a Cenomanian average youngest maximum depositional age of ± 96.63 Ma and youngest single zircon age of ± 93.95 Ma.
- (III) The Suicide Hill fossil quarry, which is preserved within the intertidal mudflats of the tidal delta, with a Turonian averaged youngest maximum depositional age of ± 95.1 Ma and a youngest single zircon age of ± 93.45 Ma.

This study was able to place the sediments at a specific area within the western flank of the San Rafael Swell within detailed temporal and palaeoenvironmental models, greatly increasing the resolution of the environmental interpretations of the area. This enabled the study to not only add much-needed context to already existing fossil quarries, but also to build a geological framework for future fossil assemblages which will emerge from these sediments.

References

- Adams, C.J., Campbell, H.J. and Griffin, W.L., 2007. Provenance comparisons of Permian to Jurassic tectonostratigraphic terranes in New Zealand: perspectives from detrital zircon age patterns. *Geological Magazine*, 144(04), pp.701-729.
- Allen J. R., 1970, Studies in fluvial sedimentation: a comparison of fining-upward cyclothems, with special reference to coarse-member composition and interpretation: *Journal of Sedimentary Petrology*. 40, pp. 298-323.
- Allen, J.R.L., 1963, Asymmetrical ripple marks and the origin of waterlaid cosets of cross-strata: Liverpool-Manchester. *Geological Journal*. 3, pp. 187-235.
- Amajor, L.C., 1984. Sedimentary facies analysis of the ajali sandstone (upper cretaceous), southern Benue Trough. *Journal of Mining and Geology*, 21, pp.171-176.
- Andersen, T., 2013. Age, Hf isotope and trace element signatures of detrital zircons in the Mesoproterozoic Eriksfjord sandstone, southern Greenland: are detrital zircons reliable guides to sedimentary provenance and timing of deposition?. *Geological Magazine*, 150(3), pp.426- 440.
- Andreae, M.O., Barnard, W.R. and Ammons, J.M., 1983. The biological production of dimethylsulfide in the ocean and its role in the global atmospheric sulfur budget. *Ecological Bulletins*, pp.167-177.
- Arens, N.C. and Harris, E.B., 2015. Paleoclimatic reconstruction for the Albian–Cenomanian transition based on a dominantly angiosperm flora from the Cedar Mountain Formation, Utah, USA. *Cretaceous Research*. 53, pp.140-152
- Armstrong, R.L., 1968, Sevier Orogenic Belt in Nevada and Utah: *Geological Society of America, Bulletin*. 79, p. 429–458.

- Aubrey, W.M., 1998. 1. Sedimentology and Stratigraphy - A Newly Discovered, Widespread Fluvial Facies and Unconformity Marking the Upper Jurassic/Lower Cretaceous Boundary, Colorado Plateau. *Modern Geology*, 22(1), pp.209-234.
- Bhattacharya, J.P., 1992. Deltas. In *In: Facies Models*), pp. 157-177. Geological Association of America.
- Bird, J., 2005, September. New finds at the Price River II site, Cedar Mountain Formation in eastern Utah. In *Journal of Vertebrate Paleontology*. 25, pp. 37A-37A
- Bjerrum, C.J., And Dorsey, R.J., 1995, Tectonic controls on deposition of Middle Jurassic strata in a retroarc foreland basin, Utah–Idaho trough, Western Interior, United States: *Tectonics* 14,p. 962–978.
- Blakey, R.C. and Ranney, W.D., 2018. The Antler Orogeny and the First Suspect Terrane: Middle Devonian to Late Pennsylvanian: Ca. 400–300 Ma. In *Ancient Landscapes of Western North America* (pp. 73-82). Springer, Cham.
- Brenner, R.L., 1983, Late Jurassic tectonic setting and paleogeography of Western Interior, North America, in Reynolds, M.W., and Dolly, E.D., eds., Mesozoic Paleogeography of West-Central United States: *SEPM, Rocky Mountain Section*, p. 119–132.
- Britt, B.B., Stadtman, K.L., Scheetz, R.D. and McIntosh, J.S., 1997. Camarasaurid and titanosaurid sauropods from the Early Cretaceous Dalton Wells Quarry (Cedar Mountain Formation), Utah. *Journal of Vertebrate Paleontology*, 17(3), p.34A.
- Buck, B.J. and Van Hoesen, J.G., 2002. Snowball morphology and SEM analysis of pedogenic gypsum, southern New Mexico, USA. *Journal of Arid Environments*, 51(4), pp.469-487.

- Burggraaf, A.J.P. and Shipton, W.A., 1982. Estimates of Frankia growth under various pH and temperature regimes. *Plant and Soil*, 69(2), pp.135-147.
- Caillaud, A., Blanpied, C. and Delvaux, D., 2017. The Upper Jurassic Stanleyville Group of the eastern Congo Basin: An example of perennial lacustrine system. *Journal of African Earth Sciences*, 132, pp.80-98.
- Carpenter, K. and Cifelli, R., 2016. A possible juvenile ceratopsoid ilium from the Cenomanian of central Utah, U.S.A.. *Cretaceous Research*. 60. pp.167-175..
- Carpenter, K., J. Bartlett, J. Bird, and R. Barrick. 2008: Ankylosaurs from the Price River Quarries, Cedar Mountain Formation (Lower Cretaceous), east-central Utah. *Journal of Vertebrate Paleontology* 28, pp.1089–1101.
- Carpenter, K., DiCroce, T., Gilpin, D., Kinneer, B., Sanders, F., Tidwell, V. and Shaw, A., 2002, May. Origins of the Early and “Middle” Cretaceous dinosaurs of North America: implications for plate tectonics. In *Proceedings of the International Symposium on new concepts in global tectonics* 289, pp. 308
- Carpenter, K., Kirkland, J.I., Burge, D. and Bird, J., 2001. Disarticulated skull of a new primitive ankylosaurid from the Lower Cretaceous of eastern Utah. *The armored dinosaurs*, pp.211-238.
- Carpenter, K., Kirkland, J.I., Burge, D. and Bird, J., 1999. Ankylosaurs (Dinosauria: Ornithischia) of the Cedar Mountain Formation, Utah, and their stratigraphic distribution. *Vertebratepaleontology in Utah*, 99(1), pp.243-251.
- Cawood, P.A., Hawkesworth, C.J. and Dhuime, B., 2012. Detrital zircon record and tectonic setting. *Geology*, 40(10), pp.875-878.
- Cawood, P.A., Nemchin, A.A., Freeman, M. and Sircombe, K., 2003. Linking source and sedimentary basin: detrital zircon record of sediment flux along a modern river system and

implications for provenance studies. *Earth and Planetary Science Letters*, 210(1), pp.259-268.

Chakrabarti, A., 2005. Sedimentary structures of tidal flats: a journey from coast to inner estuarine region of eastern India. *Journal of Earth System Science*, 114(3), pp.353-368.

Chart, G.R.C., 1991. The Geological Society of America Rock-Color Chart with genuine Munsell Color chips. *Printed by Munsell Color USA*.

Chen, C.T.A., Lin, C.M., Huang, B.T. and Chang, L.F., 1996. Stoichiometry of carbon, hydrogen, nitrogen, sulfur and oxygen in the particulate matter of the western North Pacific marginal seas. *Marine Chemistry*, 54(1-2), pp.179-190.

Chinnery, B.J., Lipka, T.R., Kirkland, J.I., Parrish, J.M. and Brett-Surman, M.K., 1998. Neoceratopsian teeth from the Lower to middle Cretaceous of North America. Lower and Middle Cretaceous Terrestrial Ecosystems. *New Mexico Museum of Natural History and Science Bulletin*, 14, pp.297-302.

Chure, D.J. and Greenhalgh, B., 2006, September. A new titanosauriform sauropod with abundant skull material from the Cedar Mountain Formation, Dinosaur National Monument. *In Journal of Vertebrate Paleontology*. 26 (3), pp. 50A-50A.

Cifelli, R. L., J. E. Cohen, and B. M. Davis. 2016: New tribosphenic mammals from the Mussentuchit Local Fauna (Cedar Mountain formation, Cenomanian), Utah, USA. *Palaeontologia Polonica* 67, pp. 67–81.

Cifelli, R.L., Nydam, R.L., Gardner, J.D., Weil, A., Eaton, J.G., Kirkland, J.I., & Madsen, S.K., 1999. Medial Cretaceous vertebrates from the Cedar Mountain Formation, Emery County, Utah: the Mussentuchit local fauna. *Vertebrate paleontology in Utah*, 99(1), pp. 219-242.

- Cifelli, R.L., Kirkland, J.I., Weil, A., Deino, A.L. and Kowallis, B.J., 1997. High-precision $^{40}\text{Ar}/^{39}\text{Ar}$ geochronology and the advent of North America's Late Cretaceous terrestrial fauna. *Proceedings of the National Academy of Sciences*, 94(21), pp.11163-11167.
- Cifelli, R.L., and Muizon, C. de, 1997, Dentition and jaw of Kokopellia juddi, a primitive marsupial or near marsupial from the medial Cretaceous of Utah: *Journal of Mammalian Evolution*. 4, pp. 241-258.
- Citterio, A. and Piégay, H., 2009. Overbank sedimentation rates in former channel lakes: characterization and control factors. *Sedimentology*, 56(2), pp.461-482.
- Cluzel, D., Adams, C.J., Maurizot, P. and Meffre, S., 2011. Detrital zircon records of Late Cretaceous syn-rift sedimentary sequences of New Caledonia: An Australian provenance questioned. *Tectonophysics*, 501(1), pp.17-27.
- Cooper, J.A.G., 2001. Geomorphological variability among microtidal estuaries from the wave-dominated South African coast. *Geomorphology*, 40(1), pp.99-122.
- Corfu, F., Hanchar, J.M., Hoskin, P.W. and Kinny, P., 2003. Atals of Zircon Textures. *Reviews in mineralogy and geochemistry*, 53(1), pp.469-500
- Cowan, E.J., 1992. The large-scale architecture of the fluvial Westwater Canyon Member, Morrison Formation (Upper Jurassic), San Juan Basin, New Mexico. *SEPM Special Publications*
- Cowan, D.S., And Bruhn, R.L., 1992, Late Jurassic to Early Cretaceous geology of the U.S. Cordillera, in Burchfiel, B.C., Lipman, P.W., and Zoback, M.L., eds., The Cordilleran Orogen: Conterminous U.S.: *Geological Society of America, The Geology of North America*. G-3, p. 169–203.
- Craig, L. C. 1981: Lower Cretaceous rocks, southwestern Colorado and southeastern Utah. Geology of the Paradox basin: *Rocky Mtn. Assoc. Geol. Guidebook*, 1981 Field Conference

- Craig, L.C., Ekren, E.B., Housr, F.N., Shawe, D.R., Simmons, G.C. and Katich Jr, P.J., 1961. Dakota Group of Colorado Plateau [Discussion]: American Association of Petroleum Geologists. *Bulletin*, 45, pp.1582-1592
- Currie, B.S., 2002, Structural Configuration of the Early Cretaceous Cordilleran Foreland-Basin System and Sevier Thrust Belt, Utah and Colorado: *The Journal of Geology*. 110, pp. 697–718.
- Currie, P.J., 1998. Possible evidence of gregarious behaviour in tyrannosaurids. *Gaia*, 15, pp. 271-277.
- Curtis, C.D., 1980. Diagenetic alteration in black shales. *Journal of the Geological Society*, 137(2), pp.189-194.
- Dalrymple, R.W. 2010. Tidal depositional systems. *Facies Models* 4. 201-231.
- Dalrymple, R.W. and Choi, K., 2007. Morphologic and facies trends through the fluvial–marine transition in tide-dominated depositional systems: a schematic framework for environmental and sequence-stratigraphic interpretation. *Earth-Science Reviews*, 81(3), pp.135-174.
- Dalrymple, R.W., Zaitlin, B.A., Boyd, R., 1992. Estuarine facies models: conceptual basis and stratigraphic implications. *Journal of Sedimentary Petrology* 62, 1130–1146.
- Dayvault, R.D., and Hatch, H.S., 2005, Cycads from the Upper Jurassic and Lower Cretaceous rocks of southeastern Utah: *Rocks and Minerals*. 80(6), pp. 412-432.
- DeCelles, P.G., 2004. Late Jurassic to Eocene evolution of the Cordilleran thrust belt and foreland basin system, western USA. *American Journal of Science*, 304(2), pp. 105-168.
- DeCelles, P.G. and Coogan, J.C., 2006. Regional structure and kinematic history of the Sevier fold-and-thrust belt, central Utah. *Geological Society of America Bulletin*, 118(7-8), pp.841-864.

- DeCelles, P.G. and Currie, B.S., 1996. Long-term sediment accumulation in the Middle Jurassic–early Eocene Cordilleran retroarc foreland-basin system. *Geology*, 24(7), pp.591-594.
- DeCelles, P.G., Lawton, T.F. and Mitra, G., 1995. Thrust timing, growth of structural culminations, and synorogenic sedimentation in the type Sevier orogenic belt, western United States. *Geology*. 23(8), pp.699-702.
- DeCourten, F.L., 1991. New data on Early Cretaceous dinosaurs from the Long Walk quarry and tracksite, Emery County, Utah. *Utah Geological Association*
- Díez-Canseco, D., Arz, J.A., Benito, M.I., Díaz-Molina, M. and Arenillas, I., 2014. Tidal influence in redbeds: a palaeoenvironmental and biochronostratigraphic reconstruction of the Lower Tremp Formation (South-Central Pyrenees, Spain) around the Cretaceous/Paleogene boundary. *Sedimentary Geology*, 312, pp.31-49.
- Dickinson, W.R., 2006. Geotectonic evolution of the Great Basin. *Geosphere*, 2(7), pp.353-368.
- Dickinson, W.R., 2004. Evolution of the North American cordillera. *Annu. Rev. Earth Planet. Sci.*, 32, pp.13-45.
- Dickinson, W.R. and Gehrels, G.E., 2009. Use of U–Pb ages of detrital zircons to infer maximum depositional ages of strata: a test against a Colorado Plateau Mesozoic database. *Earth and Planetary Science Letters*, 288(1), pp.115-125.
- Dickinson, W.R. and Gehrels, G.E., 2008. Sediment delivery to the Cordilleran foreland basin: Insights from U-Pb ages of detrital zircons in Upper Jurassic and Cretaceous strata of the Colorado Plateau. *American Journal of Science*, 308(10), pp.1041-1082.
- Dickinson, W.R., 1983, Cretaceous sinistral strike slip along Nacimiento fault in coastal California: *American Association of Petroleum Geologists Bulletin*, 67, pp. 624–645.

- DiCroce, T., and Kenneth Carpenter, K., 2001, New ornithopod from the Cedar Mountain Formation (Lower Cretaceous) of eastern Utah, in Tanke, D.H., and Carpenter, K., (eds.), *Mesozoic vertebrate life*: Bloomington, Indiana University Press, p. 183-196.
- Eaton, J.G., 1990, Stratigraphic revision of Campanian (Upper Cretaceous) rocks in the Henry Basin, Utah: *Rocky Mountain Geologist*, 27, pp. 27-38.
- Eaton, J.G. and Cifelli, R.L., 2001. Multituberculata mammals from near the Early-Late Cretaceous boundary, Cedar Mountain Formation, Utah. *Acta Palaeontologica Polonica*, 46(4).
- Eberth, D.A., Britt, B.B., Scheetz, R., Stadtman, K.L. and Brinkman, D.B., 2006. Dalton Wells: Geology and significance of debris-flow-hosted dinosaur bonebeds in the Cedar Mountain Formation (Lower Cretaceous) of eastern Utah, USA. *Palaeogeography, Palaeoclimatology, Palaeoecology*, 236(3), pp.217-245.
- Eberth, D.A. and Miall, A.D., 1991. Stratigraphy, sedimentology and evolution of a vertebrate-bearing, braided to anastomosed fluvial system, Cutler Formation (Permian-Pennsylvanian), North-central New Mexico. *Sedimentary Geology*, 72(3-4), pp.225-252.
- Elder, W.P. and Kirkland, J.I., 1994. Cretaceous paleogeography of the southern Western Interior region. Rocky Mountain Section. *SEPM Special Publications*
- Erskine, W., McFadden, C. and Bishop, P., 1992. Alluvial cutoffs as indicators of former channel conditions. *Earth Surface Processes and Landforms*, 17(1), pp.23-37.
- Fielding, C.R., 2006. Upper flow regime sheets, lenses and scour fills: extending the range of architectural elements for fluvial sediment bodies. *Sedimentary Geology*, 190(1), pp.227-240.
- Fedo, C.M., Sircombe, K.N. and Rainbird, R.H., 2003. Detrital zircon analysis of the sedimentary record. *Reviews in Mineralogy and Geochemistry*, 53(1), pp.277-303.

- Frei, D. and Gerdes, A., 2009. Precise and accurate in situ U–Pb dating of zircon with high sample throughput by automated LA-SF-ICP-MS. *Chemical Geology*, 261(3), pp.261-270.
- Galloway, W.E., 1975. Process framework for describing the morphologic and stratigraphic evolution of deltaic depositional systems.
- Galton, P. M., and J. A. Jensen. 1979. Remains of ornithopod dinosaurs from the Lower Cretaceous of North America. *Brigham Young University Geology Studies*, 25(part1) pp 1-10
- Garrison, J.R., Brinkman, D., Nichols, D.J., Layer, P., Burge, D., Thayn, D., 2007. A multidisciplinary study of the Lower Cretaceous Cedar Mountain Formation, Mussentuchit Wash, Utah: a determination of the paleoenvironment and paleoecology of the *Eolambia caroljonesa* dinosaur quarry. *Cretaceous Research*, 28(3), 461-494.
- Gerdes, A. and Zeh, A., 2006. Combined U–Pb and Hf isotope LA-(MC-) ICP-MS analyses of detrital zircons: comparison with SHRIMP and new constraints for the provenance and age of an Armorican metasediment in Central Germany. *Earth and Planetary Science Letters*, 249(1), pp.47-61.
- Gibling, M.R., 2006. Width and thickness of fluvial channel bodies and valley fills in the geological record: a literature compilation and classification. *Journal of sedimentary Research*, 76(5), pp.731-770.
- Goodbred, S.L. and Saito, Y., 2012. Tide-dominated deltas. In *Principles of Tidal Sedimentology* pp. 129-149. Springer, Dordrecht
- Gradstein, F.M., Ogg, J.G., and Smith, A.G., 2004, *A geologic time scale 2004*: Cambridge University Press, pp. 589

- Grant, C.D. and Blackmore, A.V., 1991. Self mulching behavior in clay soils-Its definition and measurement. *Soil Research*, 29(2), pp.155-173.
- Greenhalgh, B.W., Britt, B.B., And Kowallis, B.J., 2006, New U-Pb age control for the lower Cedar Mountain Formation and an evaluation of the Morris Formation/Cedar Mountain Formation Boundary, Utah: *Geological Society of American Abstracts with Programs*,. 38, (7), pp. 52
- Harris, P.T., Hughes, M.G., Baker, E.K., Dalrymple, R.W. and Keene, J.B., 2004. Sediment transport in distributary channels and its export to the pro-deltaic environment in a tidally dominated delta: Fly River, Papua New Guinea. *Continental Shelf Research*, 24(19), pp.2431-2454.
- Heller, P.L., Dueker, K. and McMillan, M.E., 2003. Post-Paleozoic alluvial gravel transport as evidence of continental tilting in the US Cordillera. *Geological Society of America Bulletin*,115(9), pp.1122-1132.
- Heller, P.L., and Paola, C., 1989, The paradox of Lower Cretaceous gravels and the initiation of thrusting in the Sevier orogenic belt: *Geological Society of America, Bulletin*, v. 101, p. 864–875.
- Heller, P.L., Bowdler, S.S., Chambers, H.P., Coogan, J.C., Hagen, E.S., Shuster, M.W., Winslow, N.S. and Lawton, T.F., 1986. Time of initial thrusting in the Sevier orogenic belt, Idaho-Wyoming and Utah. *Geology*, 14(5), pp.388-391.
- Hokanson, W.H., 2011. Identifying Complex Fluvial Sandstone Reservoirs Using Core, Well Log, and 3D Seismic Data: Cretaceous Cedar Mountain and Dakota Formations, Southern Uinta Basin, Utah.
- Holmes, A.D., 2017. Sedimentology and Taphonomy of the Abydosaurus mcintoshi Quarry, (Naturita Formation, Early Cretaceous, Latest Albian), Dinosaur National Monument, Utah.

- Horton, B.K., Constenius, K.N. and DeCelles, P.G., 2004. Tectonic control on coarse-grained foreland- basin sequences: An example from the Cordilleran foreland basin, Utah. *Geology*, 32(7), pp.637-640.
- Hunt, G. J., Lawton T. F., Kirkland J. I., Sprinkel, D.A., Yonkee, W.A. and Chidsey, T.C. 2011: Detrital zircon U-Pb geochronological provenance of Lower Cretaceous strata, foreland basin, Utah. *Sevier thrust belt: northern and central Utah and adjacent areas: Utah Geological Association, Publication*, 40 pp. 193–211.
- Imlay, R.W., 1980. Jurassic paleobiogeography of the conterminous United States in its continental setting (No. 1062). US Govt. Print. Off.
- Ireland, T.R. and Williams, I.S., 2003. Considerations in zircon geochronology by SIMS. *Reviews in Mineralogy and Geochemistry*, 53(1), pp.215-241.
- Jackson, S.E., Pearson, N.J., Griffin, W.L. and Belousova, E.A., 2004. The application of laser ablation- inductively coupled plasma-mass spectrometry to in situ U–Pb zircon geochronology. *Chemical Geology*, 211(1), pp.47-69
- Jangid, K., Whitman, W.B., Condrón, L.M., Turner, B.L. and Williams, M.A., 2013. Soil bacterial community succession during long- term ecosystem development. *Molecular ecology*, 22(12), pp.3415-3424.
- Jones, J.V., Connelly, J.N., Karlstrom, K.E., Williams, M.L. and Doe, M.F., 2009. Age, provenance, and tectonic setting of Paleoproterozoic quartzite successions in the southwestern United States. *Geological Society of America Bulletin*, 121(1-2), pp.247-264.
- Johnston, S., Gehrels, G., Valencia, V. and Ruiz, J., 2009. Small-volume U–Pb zircon geochronology by laser ablation-multicollector-ICP-MS. *Chemical Geology*, 259(3), pp.218-229.

- Kauffman, E.G. and Caldwell, W.G.E., 1993. The Western Interior Basin in space and time. Evolution of the Western Interior Basin: *Geological Association of Canada, Special Paper*, 39, pp.1-30.
- Kirkland, 2005. Utah's newly recognized dinosaur record from the Early Cretaceous Cedar Mountain Formation: *Utah Geological Survey, Survey Notes*, 33(1), pp. 1-5.
- Kirkland, J. I. 1998. A new hadrosaurid from the upper Cedar Mountain Formation (Albian-Cenomanian: Cretaceous) of eastern Utah—the oldest known hadrosaurid (lambeosaurine?); pp. 283-295 in S. G. Lucas, J. I. Kirkland, and J. W. Estep (eds.), Lower and Middle Cretaceous Terrestrial Ecosystems. *New Mexico Museum of Natural History and Science Bulletin*, 14.
- Kirkland, J.I., 1992. Dinosaurs define a two-fold Lower Cretaceous zonation of the Cedar Mountain Formation, central Utah. In *Geological Society of America, Abstracts with Programs*, 24, pp. 22
- Kirkland, J. I., and S. K. Madsen. 2007: The Lower Cretaceous Cedar Mountain Formation, eastern Utah: the view up an always interesting learning curve. Field guide to geologic excursions in southern Utah. Geological Society of America, Rocky Mountain Section 2007 *Annual Meeting*, Dixie State College, St. George, Utah, May 7-9, 2007 35: pp1–108.
- Kirkland, J.I., Suarez, M., Suarez, C. and Hunt-Foster, R., 2017. The Lower Cretaceous in East-Central Utah—The Cedar Mountain Formation and its Bounding Strata. *Geology of the Intermountain West*, 3, pp.101-228.
- Kirkland, J.I., Zanno, L.E., Sampson, S.D., Clark, J.M., DeBlieux, D.D., 2005. A primitive therizinosauroid dinosaur from the Early Cretaceous of Utah. *Nature*, 435(7038), 84-87.

- Kirkland, J.I., Cifelli, R.L., Britt, B.B., Burge, D.L., DeCourten, F.L., Eaton, J.G., Parrish, J.M., 1999. Distribution of vertebrate faunas in the Cedar Mountain Formation, east-central Utah. *Vertebrate Paleontology in Utah: Utah Geological Survey Miscellaneous Publication*, 1 pp. 201-217.
- Kirkland, J.I., Britt, B., Burge, D.L., Carpenter, K., Cifelli, R., DeCourten, F., Eaton, J., Hasiotis, S., Lawton, T., 1997. Lower to middle Cretaceous dinosaur faunas of the central Colorado Plateau: a key to understanding 35 million years of tectonics, sedimentology, evolution, and biogeography. *Brigham Young University Geology Studies*, 42, pp. 69-104.
- Kirkland, J.I., Burge, D., and Gaston, R. 1993. A large dromaeosaur (Theropod) from the Lower Cretaceous of eastern Utah. *Hunteria*, 2, pp. 2–16.
- Klein, G.D., 1970. Tidal origin of a Precambrian Quartzite--the lower fine-grained quartzite (Middle Dalradian) of Islay, Scotland. *Journal of Sedimentary Research*, 40(3).
- Košler, J., Fonneland, H., Sylvester, P., Tubrett, M. and Pedersen, R.B., 2002. U–Pb dating of detrital zircons for sediment provenance studies—a comparison of laser ablation ICPMS and SIMS techniques. *Chemical Geology*, 182(2), pp.605-618.
- Kowallis, B.J., Christiansen, E.H., Deino, A.L., Peterson, F., Turner, C.E., Kunk, M.J. and Obradovich, J.D., 1998. The age of the Morrison Formation. *Modern Geology*, 22(1-4), pp.235-260.
- Kowallis, B.J., Christiansen, E.H. and Deino, A.L., 1991. Age of the Brushy Basin Member of the Morrison Formation, Colorado Plateau, western USA. *Cretaceous Research*, 12(5), pp.483-493.
- Larson, R.L., 1995. The mid-Cretaceous superplume episode. *Scientific American*, 272(2), pp.82-86.
- Larson, R.L., 1991. Geological consequences of superplumes. *Geology*, 19(10), pp.963-966.

- Lang, S.C., Payenberg, T.H.D., Reilly, M.R.W., Hicks, T., Benson, J. and Kassan, J., 2004. Modern analogues for dryland sandy fluvial-lacustrine deltas and terminal splay reservoirs. *The APPEA Journal*, 44(1), pp.329-356.
- Lawton, T.F., 1994, Tectonic setting of Mesozoic sedimentary basin, Rocky Mountain region, United States, in Caputo, M.V., Peterson, J.S., and Franczyk, K.J., eds., Mesozoic Systems of the Rocky Mountain Region, U.S.A.: *SEPM, Rocky Mountain Section*, p. 1–25.
- Lawton, T.F. and Bradford, B.A., 2011. Correlation and provenance of Upper Cretaceous (Campanian) fluvial strata, Utah, USA, from zircon U-Pb geochronology and petrography. *Journal of Sedimentary Research*, 81(7), pp.495-512.
- Lawton, T.F., Hunt, G.J., Gehrels, G.E., 2010. Detrital zircon record of thrust belt unroofing in Lower Cretaceous synorogenic conglomerates, central Utah. *Geology* 38, pp. 463-466.
- Lawton, T.F., Pollock, S.L., and Robinson, R.A., 2003, Integrating sandstone petrology and nonmarine sequence stratigraphy: Application to the Late Cretaceous fluvial systems of southwestern Utah, U.S.A.: *Journal of Sedimentary Research*, 73, pp. 389–406.
- Lease, R.O., Burbank, D.W., Gehrels, G.E., Wang, Z. and Yuan, D., 2007. Signatures of mountain building: Detrital zircon U/Pb ages from northeastern Tibet. *Geology*, 35(3), pp.239-242.
- Leckie, D.A., And Smith, D.G., 1992, Regional setting, evolution, and depositional cycles of the Western Canada Foreland Basin, in Macqueen, R.W., and Leckie, D.A., eds., Foreland Basins and Fold Belts: *American Association of Petroleum Geologists, Memoir* 55, pp. 9–46.
- Lepre, C.J., 2017. Crevasse- splay and associated depositional environments of the hominin-bearing lower Okote Member, Koobi Fora Formation (Plio- Pleistocene), Kenya. *The Depositional Record*.

- Litwin, R.J., Turner, C.E. and Peterson, F., 1998. 4. Palynology and Paleobotany-Palynological Evidence on the age of the Morrison Formation, Western Interior Us. *Modern Geology*, 22(1), pp.297-320.
- Lloyd, T.G., Davis, K.E., Pisani D., Tarver, J. E., Ruta, M., Sakamoto M., Hone D. W. E., Jennings R. And Benton M. J., 2008. Dinosaurs and the Cretaceous Revolution. *Proceedings of the Royal Society*, 275, pp. 2483-2490
- Love, L.G., 1967. Early diagenetic iron sulphide in recent sediments of the Wash (England). *Sedimentology*, 9(4), pp.327-352.
- Ludwig, K.R., 2004. Isoplot/Ex: a geochronological toolkit for Microsoft Excel. Version 3. Berkeley, Berkeley Geochronology Center Publ. 4.
- Ludvigson, G.A., Joeckel, R.M., Murphy, L.R., Stockli, D.F., Gonzalez, L.A., Suarez, C.A., Kirkland, J.I., Al-Suwaidi, A., 2015 The emerging terrestrial record of Aptian-Albian global change. *Cretaceous Research*, 56, pp. 1-24
- Ludvigson, G.A., Joeckel, R.M., González, L.A., Gulbranson, E.L., Rasbury, E.T., Hunt, G.J., Kirkland, J.I. and Madsen, S., 2010. Correlation of Aptian-Albian carbon isotope excursions in continental strata of the Cretaceous foreland basin, eastern Utah, USA. *Journal of Sedimentary Research*, 80(11), pp.955-974.
- Ludvigson, G.A., González, L.A., Joeckel, R.M., Al-Suwaidi, A., Kirkland, J.I., and Madsen, S., 2006, Terrestrial paleoclimatic impacts of an Aptian-Albian carbon cycle perturbation [abs.]: American Geophysical Union, Fall Meeting Program, PP41B-1196, Thursday-Friday Detailed Session Program, p. 25.
- Ludvigson, G.A., González, L.A., Kirkland, J.I., and Joeckel, R.M., 2002, The terrestrial stable isotopic record of Aptian-Albian OAE1b in palustrine carbonates of the Cedar Mountain

- Formation, Utah – Implications for continental paleohydrology [abs.]: Program Abstracts, International Workshop on Cretaceous Climate and Ocean Dynamics, Florissant, CO, July 14-18, 2002, pp. 54.
- MacEachern, J.A., Bann, K.L., Hampson, G.J., Steel, R.J., Burgess, P.M. and Dalrymple, R.W., 2008. The role of ichnology in refining shallow marine facies models. In Recent advances in models of siliciclastic shallow-marine stratigraphy. *SEPM Special Publication*. 90, pp. 73-116
- Mack, G.H., James, W.C. and Monger, H.C., 1993. Classification of paleosols. *Geological Society of America Bulletin*, 105(2), pp.129-136.
- Martinus, A.W. and Gowland, S., 2011. Tide-influenced fluvial bedforms and tidal bare deposits (Late Jurassic Lourinhã Formation, Lusitanian Basin, Western Portugal). *Sedimentology*, 58, pp.285-324.
- Massini, J.G., Jacobs, B.F. and Tabor, N.J., 2010. Paleobotany and sedimentology of late Oligocene terrestrial strata from the northwestern Ethiopian Plateau. *Palaeontol Electron*, 13(1), pp.1-51.
- Mazumder, R. and Arima, M., 2005. Tidal rhythmites and their implications. *Earth-Science Reviews*, 69(1-2), pp.79-95.
- McCarthy, T.S., Ellery, W.N. and Stanistreet, I.G., 1992. Avulsion mechanisms on the Okavango fan, Botswana: the control of a fluvial system by vegetation. *Sedimentology*, 39(5), pp.779-795.
- Mcgookey, D.P., Haun, J.D., Hale, L.A., Goodell, H.G., Mccubbin, D.G., Weimer, R.J., and Wulf, G.R., 1972, Cretaceous System, in Mallory, M.M., ed., *Geologic Atlas of the Rocky Mountain Region: Rocky Mountain Association of Geologists*, p. 190–228.
- Miall, A. D., 2014. The facies and architecture of fluvial systems. In *Fluvial Depositional Systems* (pp. 9-68). Springer International Publishing.

- Miall, A.D., 2010. Alluvial deposits. In: James, N.P., Dalrymple, R.W. (Eds.), *Facies Models 4*. Queen's University, Kingston, Canada, pp. 105-138
- Miall, A.D., 1996. The geology of fluvial deposits. *Sedimentary facies, basin analysis, and petroleum geology*.
- Miall, A.D., 1985. Architectural-element analysis, a new method of facies analysis applied to fluvial deposits: *Earth Science Reviews*, 22; 261-308.
- Miall, A.D., 1977. A review of the braided-river depositional environment: *Earth Science Reviews*, 13, pp. 1-62.
- Miall, A. D., O. Catuneanu, B. K. Vakarelov, and R. Post. 2008: Chapter 9 The Western Interior Basin. *Sedimentary Basins of the World* 5 pp. 329–362.
- Milán, J., L. M. Chiappe, D. B. Loope, J. I. Kirkland, and M. G. Lockley. 2015: First report on dinosaur tracks from the burro canyon formation, San Juan County, Utah, USA -evidence of a diverse, hitherto unknown lower cretaceous dinosaur fauna. *Annales Societatis Geologorum Poloniae* 85, pp. 515–525.
- Mosher, S., 1998. Tectonic evolution of the southern Laurentian Grenville orogenic belt. *Geological Society of America Bulletin*, 110(11), pp.1357-1375.
- Nadon, G.C., 1994. The genesis and recognition of anastomosed fluvial deposits: data from the St. Mary River Formation, southwestern Alberta, Canada. *Journal of Sedimentary Research*, 64(4).
- Nasdala, L., Corfu, F., Valley, J.W., Spicuzza, M.J., Wu, F.Y., Li, Q.L., Yang, Y.H., Fisher, C., Münker, C., Kennedy, A.K. and Reiners, P.W., 2016. Zircon M127–A Homogeneous Reference Material for SIMS U–Pb Geochronology Combined with Hafnium, Oxygen and,

Potentially, Lithium Isotope Analysis. *Geostandards and Geoanalytical Research*, 40(4), pp.457-475

Nelson, D.R., 2001. *Compilation of geochronology data, 2000*. Geological Survey of Western Australia.

Nichols, G.J. and Fisher, J.A., 2007. Processes, facies and architecture of fluvial distributary system deposits. *Sedimentary Geology*, 195(1), pp.75-90.

Oboh-Ikuenobe, F., Holbrook, J.M., Scott, R.W., Akins, S.L., Evetts, M.J., Benson, D.G. and Pratt, L.M., 2008. Anatomy of Epicontinental Flooding: Late Albian-Early Cenomanian of the Southern US Western Interior Basin. Geological Association of Canada.

Obradovich, J.D., 1993. A Cretaceous time scale. *Evolution of the Western Interior Basin*, 39, pp.379-396.

Olariu, C. and Bhattacharya, J.P., 2006. Terminal distributary channels and delta front architecture of river-dominated delta systems. *Journal of sedimentary research*, 76(2), pp.212-233.

Pal, D.K., 2017. Clay and Other Minerals in Soils and Sediments as Evidence of Climate Change. In *A Treatise of Indian and Tropical Soils*. Springer International Publishing. (pp. 115-125).

Pang, M., and Nummedal, D., 1995, Flexural subsidence and basement tectonics of the Cretaceous Western Interior basin, United States: *Geology*, 23, pp. 173–176.

Pipiringos, G.N. and O'Sullivan, R.B., 1978. Principal unconformities in Triassic and Jurassic rocks, western interior United States; a preliminary survey (No. 1035-A). United States Government Printing Office.

Prave, A.R., 1999. Two diamictites, two cap carbonates, two $\delta^{13}\text{C}$ excursions, two rifts: the Neoproterozoic Kingston Peak Formation, Death Valley, California. *Geology*, 27(4), pp.339-342.

- Pupin, J.P., 1980. Zircon and granite petrology. *Contributions to Mineralogy and Petrology*, 73(3), pp.207-220.
- Rainbird, R.H., Hamilton, M.A. and Young, G.M., 2001. Detrital zircon geochronology and provenance of the Torridonian, NW Scotland. *Journal of the Geological Society*, 158(1), pp.15-27.
- Reading, H.G. and Collinson, J.D., 1996. Clastic coasts. *Sedimentary environments: processes, facies and stratigraphy*, pp.154-231.
- Retallack, G.J., 2008. Cambrian paleosols and landscapes of South Australia*. *Australian Journal of Earth Sciences*, 55(8), pp.1083-1106.
- Retallack, G.J., 2001. *Soils of the past*. Blackwell, Oxford. 600 pp.
- Retallack, G.J., 1988. Field recognition of paleosols. *Geological Society of America Special Papers*, 216, pp.1-20.
- Robinson, A.C., Ducea, M. and Lapen, T.J., 2012. Detrital zircon and isotopic constraints on the crustal architecture and tectonic evolution of the northeastern Pamir. *Tectonics*, 31(2).
- Roca, X., Nadon, G.C., 2007. Tectonic control on the sequence stratigraphy of nonmarine retroarc foreland basin fills: Insights from the Upper Jurassic of central Utah, USA. *Journal of Sedimentary Research*, 77(3), 239-255.
- Ryu, J.H., Won, J.S. and Min, K.D., 2002. Waterline extraction from Landsat TM data in a tidal flat: a case study in Gomso Bay, Korea. *Remote Sensing of Environment*, 83(3), pp.442-456.
- Schweickert, R.A., Bogen, N.L., Girty, G.H., Hanson, R.E. and Merguerian, C., 1984. Timing and structural expression of the Nevadan orogeny, Sierra Nevada, California. *Geological Society of America Bulletin*, 95(8), pp.967-979.

- Saleeby, J.B., and Busby-Spera, C.J., 1992, Early Mesozoic tectonic evolution of the western U.S. Cordillera, in Burchfiel, B.C., Lipman, P.W., and Zoback, M.L., eds., The Cordilleran Orogen: Conterminous U.S.: Geological Society of America, *The Geology of North America*. G-3, p. 107–168.
- Schudack, M.E., Turner, C.E. and Peterson, F., 1998. Biostratigraphy, paleoecology and biogeography of charophytes and ostracodes from the Upper Jurassic Morrison Formation, Western Interior, USA. *Modern Geology*, 22(1), pp.1-4.
- Sláma, J., Košler, J., Condon, D.J., Crowley, J.L., Gerdes, A., Hanchar, J.M., Horstwood, M.S. A., Morris, G.A., Nasdala, L., Norberg, N., Schaltegger, U., Schoene, B., Tubrett, M.N., Whitehouse, M.J., 2008. Plešovice zircon—a new natural reference material for U–Pb and Hf isotopic microanalysis. *Chemical Geology* 249, pp. 1–35.
- Sorensen, A.E.M., 2011. Geologic mapping of exhumed, mid-Cretaceous paleochannel complexes near Castle Dale, Emery County, Utah: On the correlative relationship between the Dakota Sandstone and the Mussentuchit Member of the Cedar Mountain Formation.
- Sprinkel, D.A., Madsen, S.K., Kirkland, J.I., Waanders, G.L. and Hunt, G.J., 2012. Cedar Mountain and Dakota formations around Dinosaur National Monument: evidence of the first incursion of the Cretaceous Western Interior Seaway into Utah. *Utah Geological Survey*. 143.
- Steiner, M.B., 1998, Age, correlation, and tectonic implications of Morrison Formation paleomagnetic data, including rotation of the Colorado Plateau: *Modern Geology* 22, pp. 261– 281.
- Steiner, M.B., Lucas, S.G., And Shoemaker, E.M., 1994, Correlation and age of the Upper Jurassic Morrison Formation from magnetostratigraphic analysis, in Caputo, M.V., Peterson, J.S., and Franczyk, K.J., eds., *Mesozoic Systems of the Rocky Mountain Region, U.S.A.: SEPM, Rocky Mountain Section*, pp. 315–330.

- Stokes, W.L., 1952. Lower Cretaceous in Colorado Plateau. *AAPG Bulletin*, 36(9), 1766-17
- Stokes, W.L., 1944. Morrison Formation and related deposits in and adjacent to the Colorado Plateau. *Geological Society of America Bulletin*, 55(8), pp. 951-992.
- Stott, D.F., 1993, Evolution of Cretaceous foredeeps: a comparative analysis along the length of the Canadian Rocky Mountains, in Caldwell, W.G.E., and Kauffman, E.G., eds., Evolution of the Western Interior Basin: *Geological Association of Canada, Special Paper* 39, pp. 131–150.
- Strickland, A., Wooden, J.L., Mattinson, C.G., Ushikubo, T., Miller, D.M. and Valley, J.W., 2013. Proterozoic evolution of the Mojave crustal province as preserved in the Ivanpah Mountains, southeastern California. *Precambrian Research*, 224, pp.222-241.
- Suarez, C.A., González, L.A., Ludvigson, G.A., Kirkland, J.I., Cifelli, R.L. and Kohn, M.J., 2013. Multi-taxa isotopic investigation of paleohydrology in the Lower Cretaceous Cedar Mountain Formation, eastern Utah, USA: deciphering effects of the Nevadaplano Plateau on regional climate. *Journal of Sedimentary Research*, 84(11), pp.975-987.
- Suarez, C.A., González, L.A., Ludvigson, G.A., Cifelli, R.L. and Tremain, E., 2012. Water utilization of the Cretaceous Mussentuchit Member local vertebrate fauna, Cedar Mountain Formation, Utah, USA: Using oxygen isotopic composition of phosphate. *Palaeogeography, Palaeoclimatology, Palaeoecology*, 313, pp.78-92.
- Suarez, M.B., Suarez, C.A., Kirkland, J.I., González, L.A., Grandstaff, D.E. and Terry, D.O., 2007. Sedimentology, stratigraphy, and depositional environment of the Crystal Geyser Dinosaur Quarry, east-central Utah. *Palaios*, 22(5), pp.513-527.
- Suarez, C.A., Suarez, M.B., Terry, D.O. and Grandstaff, D.E., 2007. Rare earth element geochemistry and taphonomy of the Early Cretaceous Crystal Geyser Dinosaur Quarry, east-central Utah *Palaios*, 22(5), pp.500-512.

- Tidwell, V., Carpenter, K. and Meyer, S., 2001. New titanosauriform (Sauropoda) from the poison strip member of the cedar mountain formation (Lower Cretaceous), Utah. *Mesozoic vertebrate life*, 137, pp.165.
- Tidwell, V., Carpenter, K. and Brooks, W., 1999. New sauropod from the Lower Cretaceous of Utah, USA. *Oryctos*, 2, pp.21-37.
- Tschudy, R.H., Tschudy, B.D. and Craig, L.C., 1984. Palynological evaluation of Cedar Mountain and Burro Canyon formations, Colorado Plateau (No. 1281).
- Turner, C.E. and Peterson, F., 2004. Reconstruction of the Upper Jurassic Morrison Formation extinct ecosystem—a synthesis. *Sedimentary Geology*, 167(3), pp.309-355.
- Trujillo, K. C., B. J. Kowallis, D. A. Sprinkel, and B. J. Kowallis. 2016: Recalibrated legacy $^{40}\text{Ar}/^{39}\text{Ar}$ ages for the Upper Jurassic Morrison Formation, Western interior, USA. *Geology of the intermountain west* .2(1), pp. 1-8
- Trujillo, K.C., Chamberlain, K.R. and Strickland, A., 2006, May. Oxfordian U/Pb ages from SHRIMP analysis for the Upper Jurassic Morrison Formation of southeastern Wyoming with implications for biostratigraphic correlations. *In Geological Society of America Abstracts with Programs* 3896), p. 7).
- Tucker, R.T., Roberts, E.M., Darlington, V. and Salisbury, S.W., 2017. Investigating the stratigraphy and palaeoenvironments for a suite of newly discovered mid-Cretaceous vertebrate fossil localities in the Winton Formation, Queensland, Australia. *Sedimentary Geology*. 358, pp. 210-229
- Tucker, R.T., Roberts, E.M., Hu, Y., Kemp, A.I. and Salisbury, S.W., 2013. Detrital zircon age constraints for the Winton Formation, Queensland: contextualizing Australia's Late Cretaceous dinosaur faunas. *Gondwana Research*, 24(2), pp.767-779.
- Vail, P.R., Mitchum Jr., R.M., Thompson III, S., 1977. Seismic stratigraphy and global

changes of sea level, part 3: relative changes of sea level from coastal onlap. In:

Payton, C.E. (Ed.), *Seismic Stratigraphy — Applications to Hydrocarbon Exploration*.

Memoir, vol. 26. American Association of Petroleum Geologists, pp. 63–81.

Van Schmus, W.R., M.E. Bickford, and K.C. Condie, 1993. Early Proterozoic crustal evolution, in J.C. Reed et al., (eds.) *Precambrian: Conterminous U.S., Decade of North American Geology*, C-2 pp. 270-281, Geological Society of America., Boulder, Colorado.

Warren, D., and Carpenter, K., 2004, A large nodosaurid ankylosaur from the Cedar Mountain Formation of Utah [abs.]: *Journal of Vertebrate Paleontology*, v. 24, supplement to no. 3, p. 126A.

Wolanski, E. and Gibbs, R.J., 1995. Flocculation of suspended sediment in the Fly River estuary, Papua New Guinea. *Journal of Coastal Research*, pp.754-762.

Wolfe, B.B., Hall, R.I., Last, W.M., Edwards, T.W., English, M.C., Karst- Riddoch, T.L., Paterson, A. And Palmini, R., 2006. Reconstruction of multi- century flood histories from oxbow lake sediments, Peace- Athabasca Delta, Canada. *Hydrological Processes*, 20(19), pp.4131-4153.

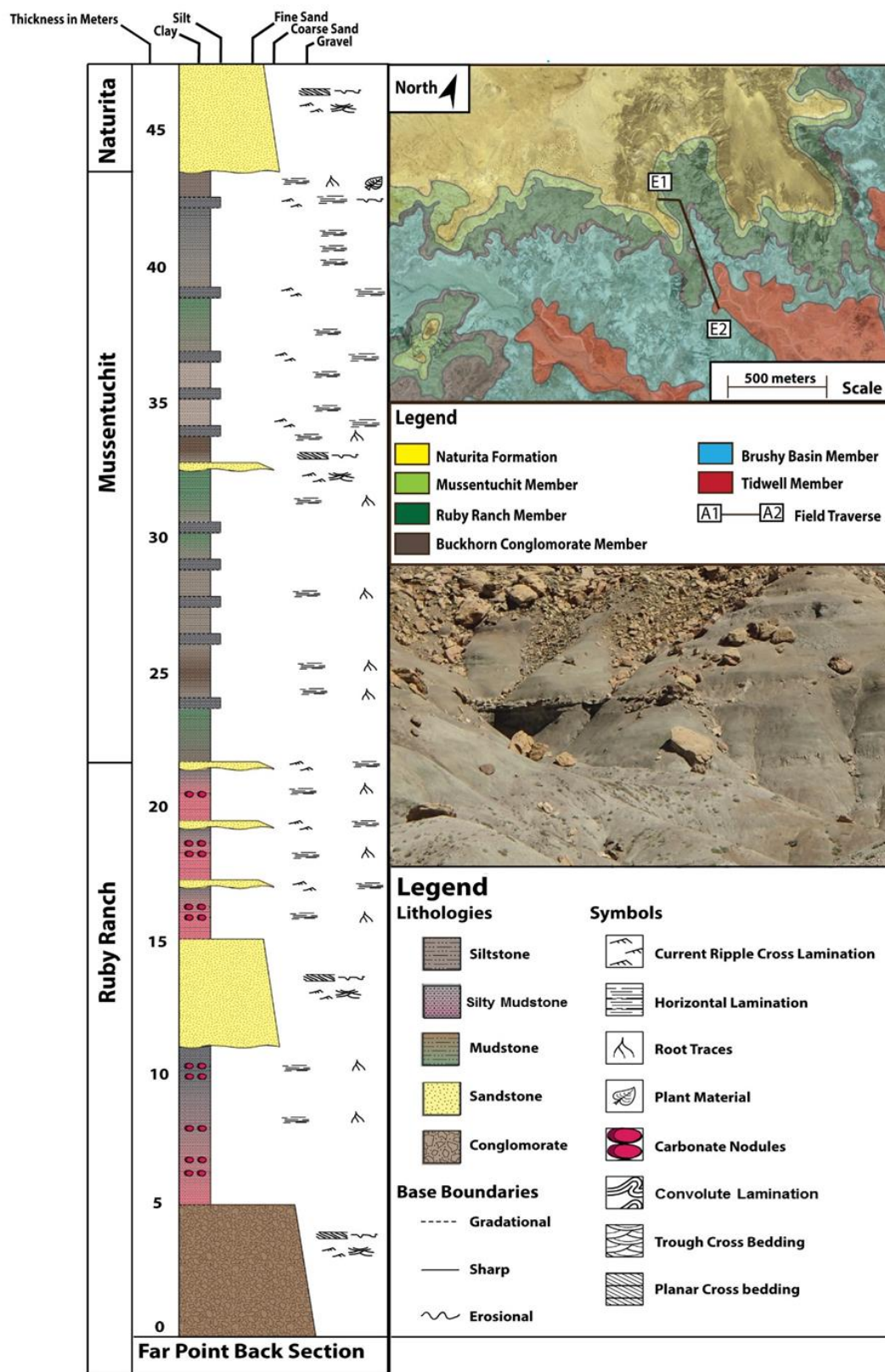
Wooden, J.L., Barth, A.P. and Mueller, P.A., 2013. Crustal growth and tectonic evolution of the Mojave crustal province: Insights from hafnium isotope systematics in zircons. *Lithosphere*, 5(1), pp. 17-28.

Wooden, J.L. and Miller, D.M., 1990. Chronologic and isotopic framework for Early Proterozoic crustal evolution in the eastern Mojave Desert region, SE California. *Journal of Geophysical Research: Solid Earth*, 95(B12), pp. 20133-20146.

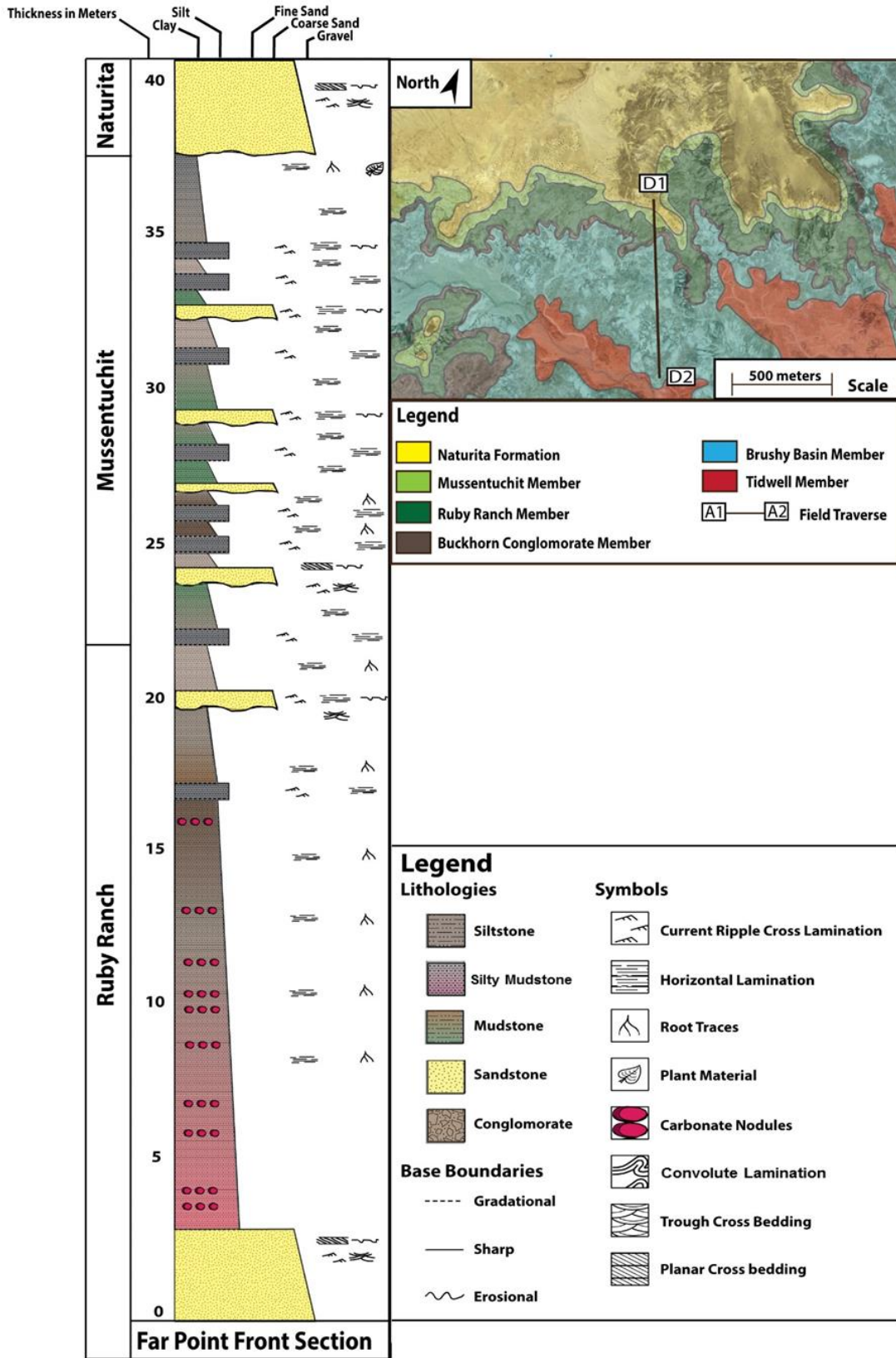
Yang, Y., 2011. Tectonically-driven underfilled–overfilled cycles, the Middle Cretaceous in the northern Cordilleran foreland basin. *Sedimentary Geology*, 233(1-4), pp.15-27.

- Yingling, V.L., 1987. Timing of initiation of the Sevier orogeny: Morrison and Cedar Mountain formations and Dakota Sandstone, east-central Utah [Unpublished M.S. Thesis]: University of Wyoming, 169 p.
- Yingling, V.L., And Heller, P.L., 1992, Timing and record of foreland sedimentation during the initiation of the Sevier orogenic belt in central Utah: *Basin Research*, 4, pp. 279–290.
- Young, R.G., 1965. Type Section of Naturita Formation: GEOLOGICAL NOTES. *AAPG Bulletin*, 49(9), pp.1512-1516.
- Young, R.G., 1960, Dakota Group of Colorado Plateau: *AAPG Bulletin*, 44, pp. 156–194.
- Zanno, L.E., 2006. The pectoral girdle and forelimb of the primitive therizinosauroid *Falcarius utahensis* (Theropoda, Maniraptora): analyzing evolutionary trends within Therizinosauroidea. *Journal of Vertebrate Paleontology*, 26(3), pp.636-650.
- Zanno, L. E., and P. J. Makovicky. 2013: Neovenatorid theropods are apex predators in the Late Cretaceous of North America. *Nature communications* 4, pp.2827.

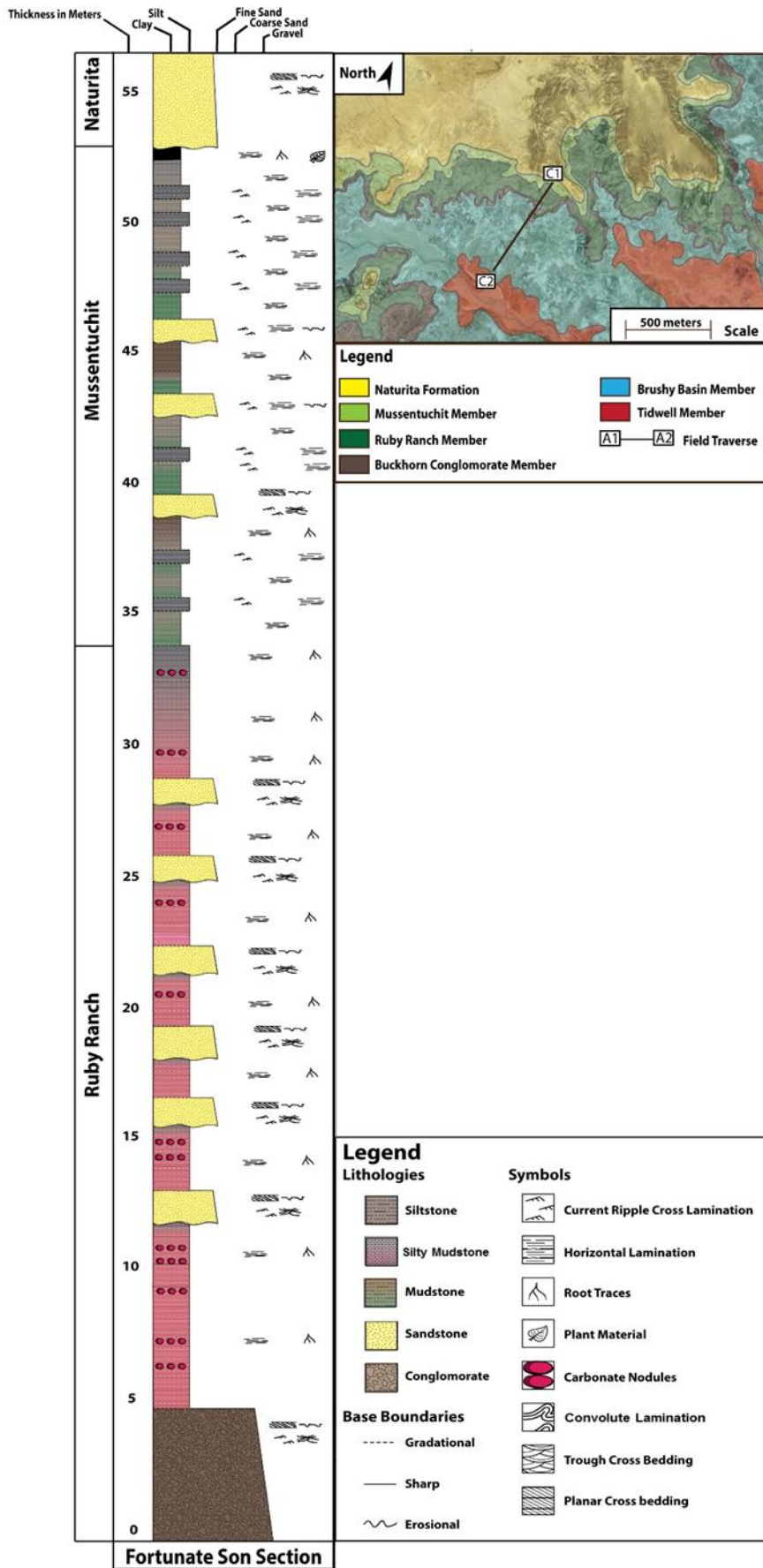
Appendix: Stratigraphic columns of field transects



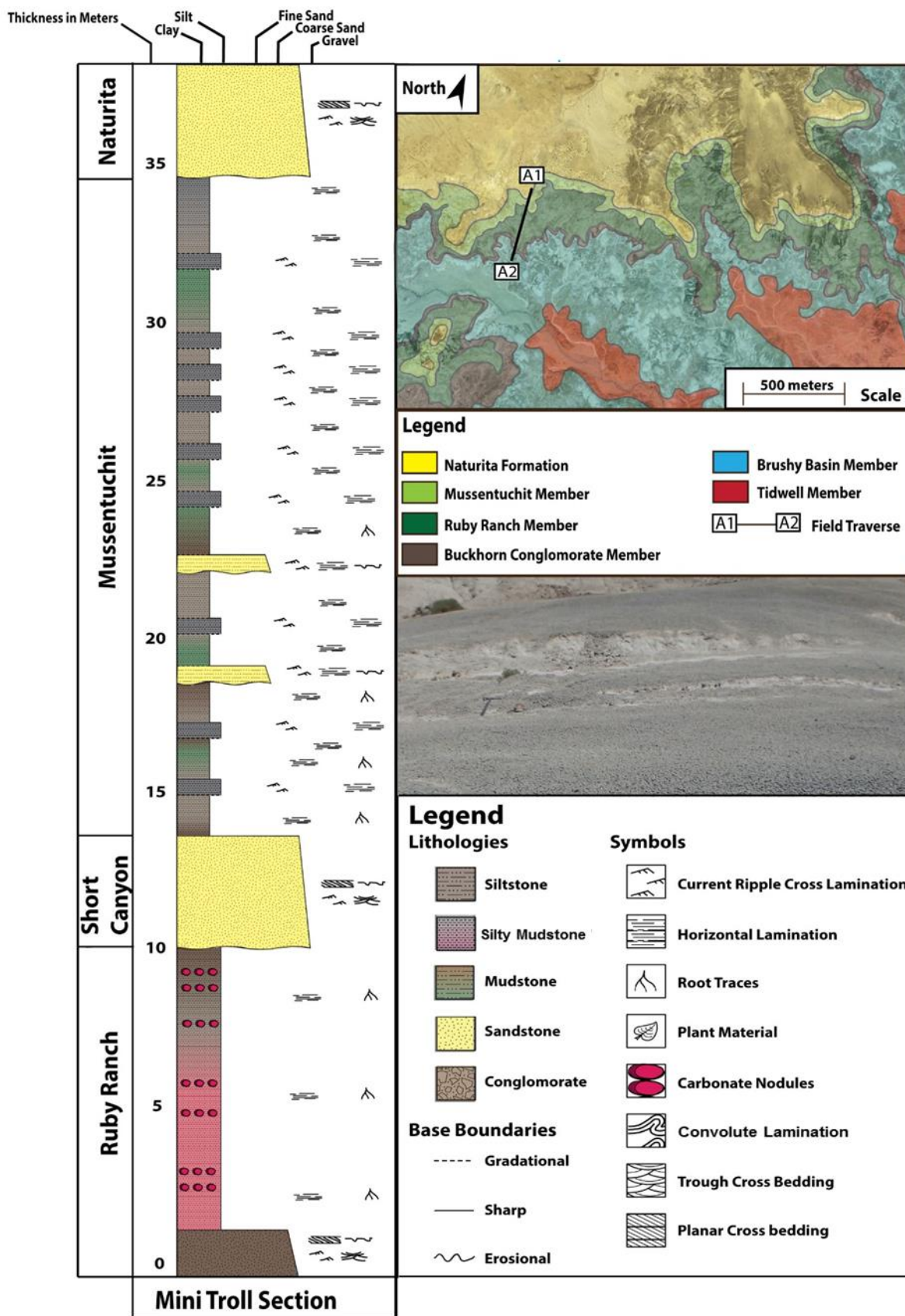
Map modified from Google Earth ESRI Satellite Image



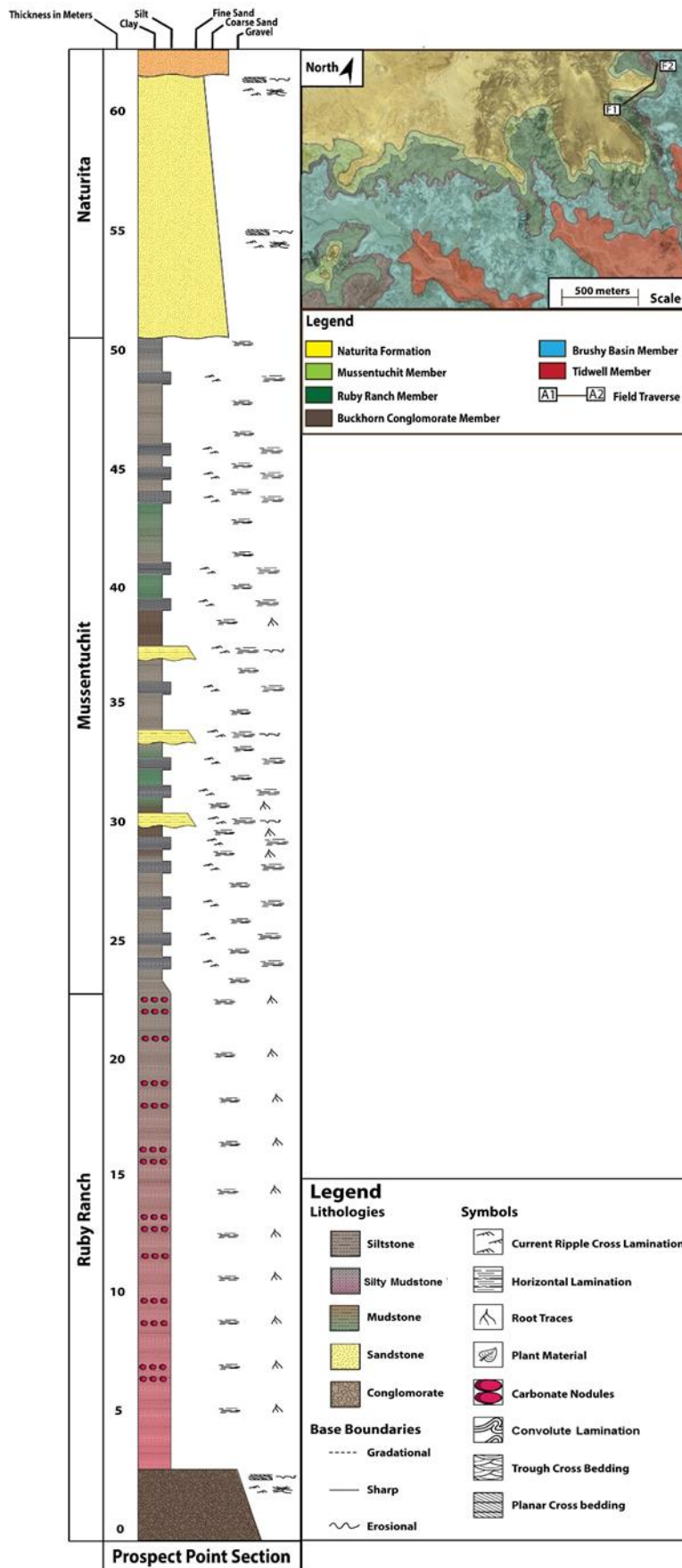
Map modified from Google Earth ESRI Satellite Image



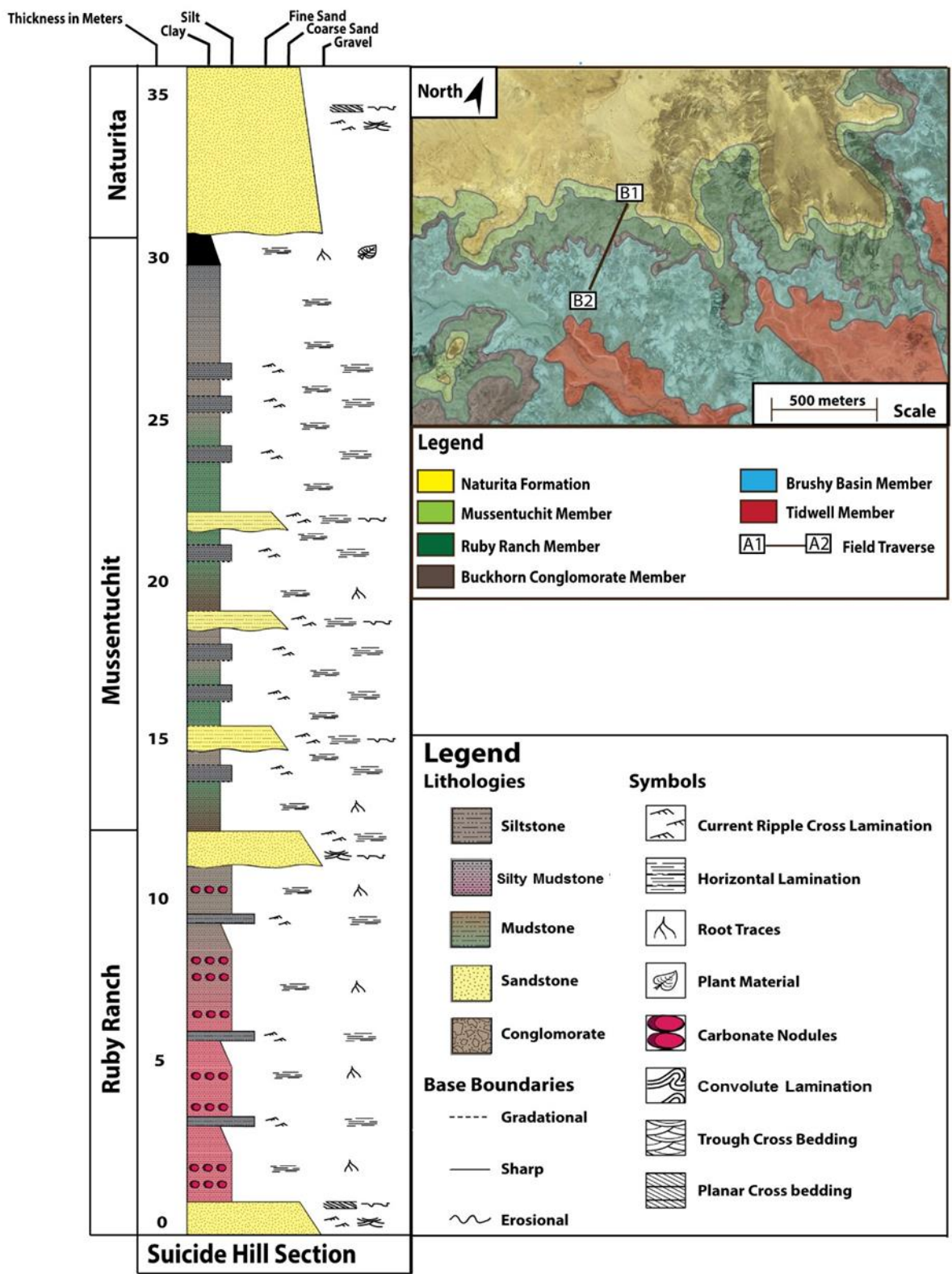
Map modified from Google Earth ESRI Satellite Image



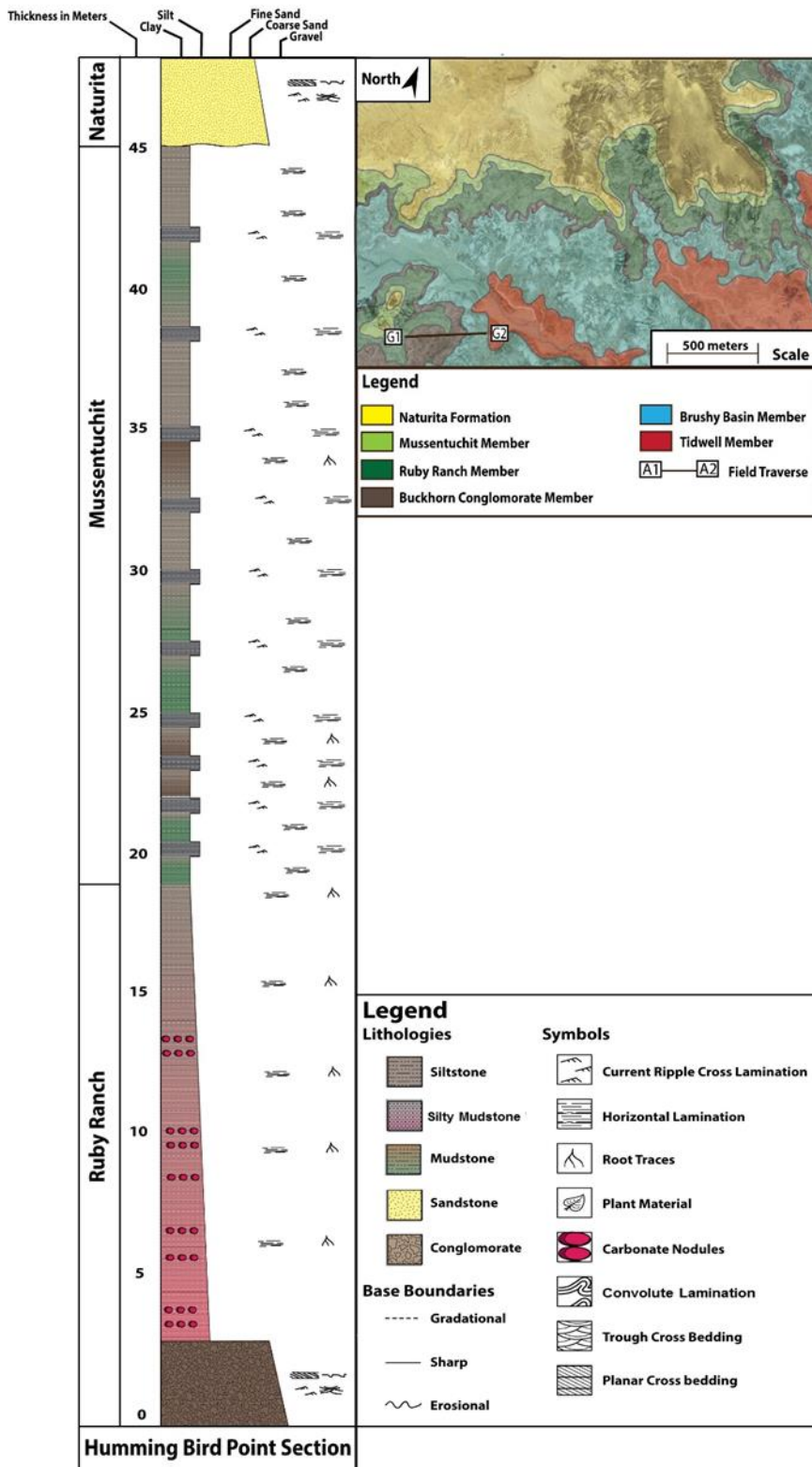
Map modified from Google Earth ESRI Satellite Image



Map modified from Google Earth ESRI Satellite Image



Map modified from Google Earth ESRI Satellite Image



Map modified from Google Earth ESRI Satellite Image